UNIVERSITA' DEGLI STUDI DI MILANO
FACOLTA' DI SCIENZE DEL FARMACO
Department of Pharmaceutical Sciences
PhD Course in Pharmaceutical Sciences (XXXI Cycle)

Unnatural amino acids as synthetic tools for the preparation of complex molecular architectures

CHIM/06

Coordinator: Prof. Giancarlo ALDINI

Tutor: Prof. Maria Luisa GELMI

Co-tutor: Prof. Francesca CLERICI

PhD Thesis of:

Silvia Alice LOCARNO

R11418

Academic year 2017/2018

Acknowledgements

Firstly, I would like to thank my research supervisors Professors Maria Luisa Gelmi and Francesca Clerici for their mentorship.

The research presented here has also benefited from collaborations. I am grateful to Professor Cristina Lenardi and Dr. Simona Argentiere who provided me the opportunity to join their team at Fondazione Unimi and for their suggestions. I would also like to acknowledge Dr. Daniela Maggioni for helpful discussions and Dr. Raffaella Soave for crystallographic data.

I wish to address a particular thank to all the members of DISFARM, Organic chemistry section labs, who have been a great intellectual resource and have made it fun to come to work, with a special thanks to Dr. Sara Pellegrino for her helpful advice and continuous support over these years.

My sincere thanks go to Professor Alexander Bittner, who welcomed me into his team at CIC nanoGUNE (Donostia, Spain) and to all his wonderful group, who made me feel at home.

Unnatural amino acids as synthetic tools for the preparation of complex molecular architectures

By

Silvia Alice Locarno

Under the Supervision of

Professors Maria Luisa Gelmi and Francesca Clerici

Abstract

Self-assembly is the process by which an organized structure spontaneously is formed from individual components, as a result of specific, local interactions between the units.

In recent years, peptide-based self-assembled structures have emerged as a powerful approach for developing soft and hybrid materials due to their biocompatibility, biodegradability and easily tuning properties of the final structure.

The introduction of non-natural amino acids into a peptide backbone imparts additional features such as reduced conformational flexibility, high tendency to adopt a well-defined secondary structure and enhanced metabolic stability.

My PhD thesis is focused on the synthesis of ultrashort peptides containing non-natural scaffolds which are able to self-assemble and form supramolecular structures. The thesis is divided into three chapters, each one reports a project regarding the synthesis and chemical characterization of scaffolds which can be inserted in peptide sequences and exploited for developing soft or hybrid materials by self-assembly.

The first chapter concerns the supramolecular assemblies of spherical shape obtained from different peptides containing $C^{\alpha,\alpha}$-tetrasubstituted amino acids. Firstly, the results on a pentapeptide containing norbornene amino acid is reported (work published on RSC Advances). Then, the simplification of this structure is reported until obtaining a pentapeptide containing Ala-Aib motif only. The ability of this peptide to form aggregates that can be exploited for the encapsulation of hydrophobic molecules has been studied. As a proof of concept the well-known curcumin molecule has been used. The interaction of

the drug molecules with peptide aggregates has been studied using the absorption and the intrinsic fluorescence emission of curcumin.

Starting from this peptide, it is also possible to develop peptide-ligands which stabilize gold nanoparticles in aqueous solution. The stability of nanoparticles has been studied using DLS and UV-vis spectroscopy.

The second chapter reports on a $\beta^{2,3}$-diarylamino acid, developed in our group, which is non-natural analogous of the dipeptide Phe-Phe. This amino acid has been used to develop hybrid antifouling film which has been characterized using different techniques (contact angles values, QCM-D). The third chapter concerns the preparation of an original heterocyclic scaffold to be inserted into a peptide backbone and its exploitation for the formation of soft materials by the way of an "induced assembly". The electrospinning technique allowed the formation of electrospun nanofibers from these non-natural peptide-based small molecules and their characterization with several techniques (SEM, AFM, FT-IR, Raman) is reported.

Table of contents

Abbreviations

$[\alpha]_D$	specific rotation at 589 nm
Abs	absorbance
Ac_5c	aminocyclopentanecarboxylic acid
AFM	atomic force microscopy
Aib	2-aminoisobutyric acid
Ala	alanine
AuNPs	gold nanoparticles
Boc	tert-butoxycarbonyl
bs	broad singlet
CD	circular dichroism
COSY	correlation spectroscopy
Cys	cysteine
d	doublet
DCE	1,2-Dichloroethene
DCM	dichloromethane
DCU	dicyclohexylurea
dd	doublet of doublets
DIC	N,N′-diisopropylcarbodiimide
DIPEA	N,N-Diisopropylethylamine
DLS	dynamic light scattering
DMAP	4-dimethylaminopyridine
DMF	N,N-dimethylformamide
DMSO	dimethyl sulfoxide
DOPA	3,4-dihydoxy-Lphenyalanine
EDC	1-ethyl-3-(3-dimethylaminopropyl)carbodiimide

EEDQ	N-ethoxycarbonyl-2-ethoxy-1,2-dihydroquinoline
eq	molar equivalent
ESI-MS	electrospray ionization-mass spectrometry
FBS	foetal bovine serum
Fmoc	fluorenylmethyloxycarbonyl
FT-IR	fourier transform infrared
Gly	glycine
HBTU	hexafluorophosphate benzotriazole tetramethyl uronium
HFIP	hexafluoroisopropanol
HMBA	4-(hydroxymethyl)benzoic acid
HMBC	heteronuclear multiple-bond correlation
HOBt	1-hydroxybenzotriazole
HPLC	high-performance liquid chromatography
HSQC	heteronuclear single-quantum correlation
IR	infrared spectroscopy
J	coupling constant
Leu	leucine
m	multiplet
MBHA	4-methylbenzhydrylamine
mCPBA	metachloperbenzoic acid
MNE	magnetic non-equivalence
mp	melting point
NMP	N-methyl-2-pyrrolidone
NMR	nuclear magnetic resonance
NOE	nuclear overhauser effect
NOESY	nuclear overhauser effect spectroscopy

NRB	norbornene
nrb	norbornane
o.n.	overnight
PdI	polydispersity index
QCM-D	quartz crystal microbalance with dissipation
R_f	retention factor
ROESY	rotating frame nuclear overhauser effect spectroscopy
rt	room temperature
s	singlet
SAM	self-assembled monolayer
SEM	scanning electron microscopy
SPPS	solid phase peptide synthesis
t	triplet
tBu	tert-butyl
TEA	trimethylamine
TEM	transmission electron microscopy
TFA	trifluoroacetic acid
TFE	trifluoroethanol
THF	tetrahydrofuran
TIS	triisopropylsilane
TLC	thin layer chromatography
TW80	Tween80®
UV	ultraviolet light
Val	Valine
VT-NMR	variable temperature NMR
Δ	chemical shift

General introduction

Introduction

Amino acids are the building blocks of peptides and proteins. During the evolution, Nature has optimized their structures to carry out a lot of functions in several biological processes. They are indeed able to induce a high molecular complexity starting from relatively simple molecules, being at the molecular basis of the living world. The sequence of side chains determines the unique properties of a particular protein or peptide, including its biological function and its specific three-dimensional structure. Each of the side groups has a certain "personality" which contributes to this task. The wide range of fascinating supramolecular architectures found in nature, from DNA double helices to protein folding, inspires scientists to create similar artificial systems by using the building blocks of life, in order to develop smart materials for several medical and biological applications, such as biomolecular devices, biosensors, and hybrid catalysts. These molecules are called foldamers, a term to describe any synthetic oligomers that fold into well-defined three-dimensional structures.[1] In most cases, thermodynamically stable structures are formed through intermolecular interactions that involve both the assembling subunits and the surrounding solvent molecules.[2] Several foldamer families including unnatural-peptides,[3] peptoids,[4] azapeptides,[5] oligoureas,[6] aromatic oligoamides,[7] hybrids of these, and many others have been synthesized, and each backbone displays distinct secondary structures. These non-natural synthetic oligomers follow different folding rules and thus form secondary structures that are different from natural building blocks. For this reason, foldamers can acquire properties not found in natural compounds.[8]. Among all organic building blocks, peptides are one of the most promising that imitate the structural behaviour of biological molecules, due to their biocompatibility, chemical diversity and resemblance to proteins. Their diversity is further enriched by the introduction of non-proteinogenic amino acids into the peptide backbone. Moreover, due to their well-defined conformation it is possible to precisely modify the spatial arrangements of functional groups on foldamers in a predictable way. During the past decade, peptides have gained a wide range of applications in medicine and biotechnology, and therapeutic peptide research is also currently experiencing a renaissance for commercial reasons. Notwithstanding this interest, naturally occurring peptides are often not directly suitable for use as convenient therapeutics because they have intrinsic weaknesses, such as rapid degradation in vivo by proteolytic enzymes[9] and unfavourable pharmacokinetic profile.[10] The problem of poor biostability is overcome by

almost all foldamers, as most proteases do not effectively recognize peptide backbones that deviate from natural ones. Regarding the issue of cell permeability, appropriately designed sequences can be subject to active cellular uptake Consequently, peptide materials containing different unnatural amino acid sequences can be designed to serve a variety of biological functions and, depending on the solvent and the environmental conditions, hydro- and organo-gels, nanoarchitectures, vesicles and micelles have been obtained.[11]

This PhD work is mainly focused on the synthesis and the study of self-assembled unnatural peptides, for developing smart soft- or hybrid-materials of submicron size with potential use in several applications ranging from nanotechnology to biotechnology.

Self-assembled peptides

Self-assembly is an autonomous process of organization of molecular units into ordered structures as a result of intramolecular/intermolecular interactions.[12] This process is mediated through non-covalent interactions, including van der Waals, electrostatic, hydrogen bonding and π-stacking interactions (Fig. 1).

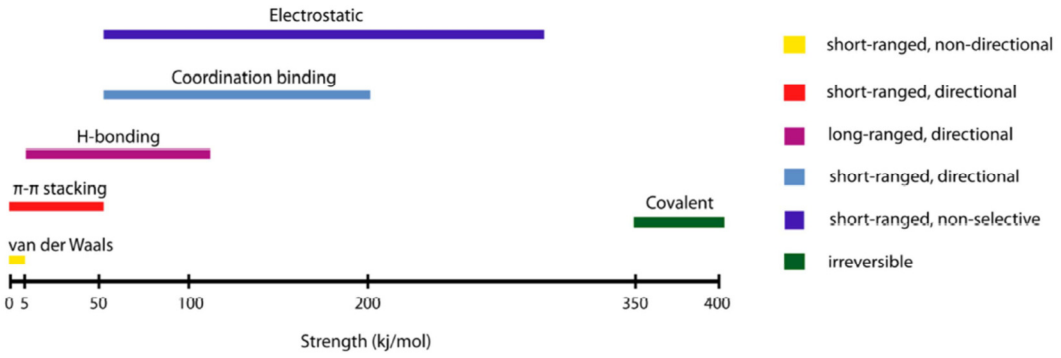

Figure 1. Strength and properties of the noncovalent interactions involved in self-assembly (adapted from [13])

While nonpolar amino acids, aliphatic (e.g. alanine, leucine, valine) and aromatic (e.g. tyrosine, phenylalanine), are mainly subjected to hydrophobic interactions and π–π stacking, respectively, polar amino acids interact mainly with hydrogen bonding or electrostatic interactions depending on whether they have uncharged (e.g. serine, asparagine) or charged (e.g. lysine, histidine, glutamic acid) residues[13]. In addition to

individual amino acids, the peptide backbone itself provides considerable stability through hydrogen bonds. Although these interactions are individually weak, their multiple cooperative action can allow the formation of stable assemblies and also stabilize the secondary structure. Moreover, the surrounding environment (e.g. pH, solvent, temperature) may significantly influence the outcome of biomolecular self-assembly.

In nature, the most straightforward and well-known example of self-assembled structure is the lipid cellular membrane, which consists of lipid bilayers that are arranged with the hydrophobic tails, interacting with each other inside the membrane, and hydrophilic groups exposed to the intra- and extracellular aqueous environments.

The fabrication of new materials that mimic biological systems is becoming a subject of major interest. In particular, self-assembled peptide structures have demonstrated considerable potential as biomaterials and as drug-delivery systems, in tissue engineering, for imaging tools, energy storage, biomineralization and membrane protein stabilization.[14]

The common strategy employed for generation of self-assembled materials is the "bottom up" approach, in which molecules arrange themselves into ordered structures by exploiting physical or chemical interactions between the units to find the lowest-energy configuration.

The simplest peptide block for the self-assembly is diphenylalanine peptide (L-Phe-L-Phe) which forms a tubular structure with a length of 100 μm and longer through the formation of hydrogen bonding as well as π–π stacking of aromatic residues. Phe-Phe motif is one of the most versatile building blocks for self-assembly since small changes to its chemical structure are sufficient to obtain different morphologies (Fig. 2). Moreover, the assembly of each compound can be driven toward distinct structures by varying the experimental conditions.[15] The result of this self-assembly process is obtaining soft materials, which are materials that can be easily deformed by thermal stresses or thermal fluctuations also at room temperature. Soft materials include liquids, polymers, foams, gels, colloids, granular materials, as well as most biological materials.

Another self-assembly approach allows the formation of the so-called "Self-Assembled Monolayers" (SAMs) based on self-assembly of constituent molecules, such as lipids, thiols and silanes. For SAMs, synthetic chemistry and artificial precursors are used only to construct the basic building blocks, and weaker intermolecular bonds such as van der Waals bonds are involved in arranging and binding up the blocks together into a structure.[16] This strategy is also used for producing hybrid materials which combine two or more materials to attribute new properties not offered by any material on its own.

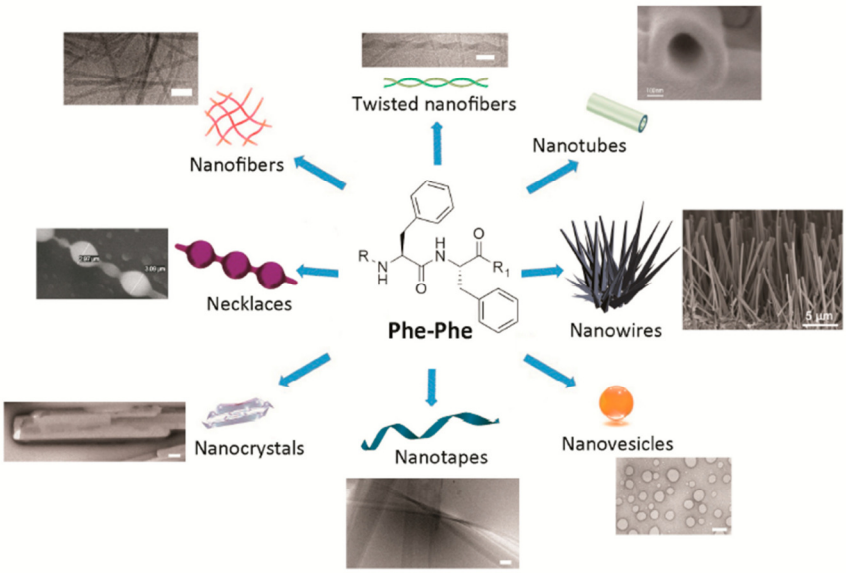

Figure 2. Different morphologies of self-assembles Phe-Phe motif. Scale bars = 100 nm, unless otherwise stated on the image(adapted from [15])

Aim of the thesis

This PhD thesis regards the synthesis and exploitation of known and new unnatural self-assembled peptides for developing soft and hybrid materials with potential applications in biological and medical fields.

The thesis is divided in three chapters, each one based on the synthesis of peptides containing unnatural amino acids or synthetic scaffold.

The first chapter is divided in three parts. Part I reports on the synthesis and chemical characterization of unnatural pentapeptides containing different C^{α}-tetrasubstituted amino acids in position 2 and different substitutions at C-terminus. The interesting feature of these compounds is their ability to produce, in water, supramolecular assemblies of spherical shape that have been exploited for developing both soft (part II) and hybrid (part III) materials, opening the way for several applications.

In Part II, the simplest peptide described in Part I has been used to propose a carrier-system for hydrophobic molecules. The encapsulation process has been analysed and verified with several techniques, using curcumin as model molecule. In Part III, after the addition of thiol group into the previously described peptide sequences, the effect on the

stabilization of gold nanoparticles (AuNPs) through the formation of SAMs has been studied and the hybrid system has been characterized. The use of peptides as small ligands for cancer targeting and selective cancer therapy has been suggested as a powerful approach. In addition, Joule heating by metal nanoparticles under radiofrequency fields opens up their application in photothermal therapy.

Another example of hybrid material is given in chapter 2 which is focused on $\beta^{2,3}$-diaryl-amino acids for the preparation of a α/β-peptide. The insertion of the DOPA amino acid has allowed immobilizing this compound on different surfaces, forming a "Teflon-like" film for antifouling applications.

Chapter 3 differs from the others because reports a self-assembly mechanism which is not spontaneous, but induced by electric forces. In this chapter electrospinning technique has been exploited for producing fibers from small molecules, in particular from pyrazole-isothiazole derivatives. This part of the thesis was performed during an internship at CIC nanoGUNE in Bittner group.

References

[1] a) S. H. Gellman, *Accounts of Chemical Research* **1998**, *31*, 173-180; b) C. M. Goodman, S. Choi, S. Shandler, W. F. DeGrado, *Nature Chemical Biology* **2007**, *3*, 252-262.

[2] N. Stephanopoulos, J. H. Ortony, S. I. Stupp, *Acta Materialia* **2013**, *61*, 912-930.

[3] a) D. Seebach, J. Gardiner, *Accounts of Chemical Research* **2008**, *41*, 1366-1375; b) D. Seebach, D. F. Hook, A. Glattli, *Biopolymers* **2006**, *84*, 23-37.

[4] K. Kirshenbaum, A. E. Barron, R. A. Goldsmith, P. Armand, E. K. Bradley, K. T. V. Truong, K. A. Dill, F. E. Cohen, R. N. Zuckermann, *Proceedings of the National Academy of Sciences of the United States of America* **1998**, *95*, 4303-4308.

[5] A. Salauen, M. Potel, T. Roisnel, P. Gall, P. Le Grel, *Journal of Organic Chemistry* **2005**, *70*, 6499-6502.

[6] A. Violette, M. C. Averlant-Petit, V. Semetey, C. Hemmerlin, R. Casimir, R. Graff, M. Marraud, J.-P. Briand, D. Rognan, G. Guichard, *Journal of the American Chemical Society* **2005**, *127*, 2156-2164.

[7] I. Huc, *European Journal of Organic Chemistry* **2004**, 17-29.

[8] S. H. Yoo, H.-S. Lee, *Accounts of Chemical Research* **2017**, *50*, 832-841.

[9] a) B. Geueke, K. Namoto, D. Seebach, H.-P. E. Kohler, *Journal of Bacteriology* **2005**, *187*, 5910-5917; b) J. V. Schreiber, J. Frackenpohl, F. Moser, T. Fleischmann, H.-P. E. Kohler, D. Seebach, *ChemBioChem* **2002**, *3*, 424-432.

[10] F. Heitz, M. C. Morris, G. Divita, *British Journal of Pharmacology* **2009**, *157*, 195-206.

[11] F. Clerici, A. Contini, M. L. Gelmi, D. Pocar, *Tetrahedron* **2003**, *59*, 9399–9408.

[12] J.-M. Lehn, *Proceedings of the National Academy of Sciences of the United States of America* **2002**, *99*, 4763-4768.

[13] M. S. Ekiz, G. Cinar, M. A. Khalily, M. O. Guler, *Nanotechnology* **2016**, *27*, 402002/402001-402002/402037.

[14] D. Mandal, A. Nasrolahi Shirazi, K. Parang, *Organic & Biomolecular Chemistry* **2014**, *12*, 3544-3561.

[15] S. Marchesan, A. V. Vargiu, K. E. Styan, *Molecules* **2015**, *20*, 19775-19788.

[16] T. Zohrabi, N. Habibi, *International Journal of Peptide Research and Therapeutics* **2015**, *21*, 423-431.

Chapter 1

Ala-Aib peptide oligomers

Part I

Introduction

C^{α}-tetrasubstituted amino acids

C^{α}-tetrasubstituted amino acids represent a wide class of non-proteinogenic amino acids with well recognized folding induction ability.[1] The introduction of amino acids belonging to this class into peptide backbones represents a versatile approach to reduce conformational flexibility, to induce high tendency to adopt a well-defined secondary structure and enhanced metabolic stability.[2]

α-Amino isobutyric acid (Aib) is the achiral prototype of this class. This compound is similar to alanine, but possesses an additional methyl group on the α-carbon instead of a hydrogen. It is therefore achiral (Fig. 1.1.1). It is a non-proteinogenic amino acid naturally wide spread, especially in peptides produced by microbes. For example, in some fungi Aib is produced as a precursor to peptides, some of which exhibit antibiotic properties, such as alamethicin, antiamoebin and emerimicin, which produce voltage-gated channels in lipid membranes.[3] Recently, Aib has been found as a metabolite of skeleton muscle. In fact, its concentration increases by exercise and it is considered a protective factor against metabolic disorder since it can induce brown fat function.[4] Moreover, it was confirmed its compatibility with ribosomal elongation of the peptide chain.[5]

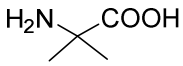

Figure 1.1.1. Molecular structure of α-amino isobutyric acid (Aib)

Experimental evidences indicate that Aib and many other achiral and chiral amino acids of this class are conformationally restricted and strong promoters of folded and, particularly, helical structure.[6]

The classification of amino acids on the base of their conformational preference is described by the ϕ, ω and ψ angles (Fig. 1.1.2) of the Ramachandran plot which has become a standard tool used in determining protein structure and in defining secondary structure.[7] Conformational analysis of Aib shows that the presence of geminal methyl groups on α-carbon induce a marked conformational restriction. Helical structures of 3_{10} (ϕ = ±57°; ψ =±30°) and α (ϕ = ±63°; ψ =±42°) types are more stable than fully extended

structures (ϕ = ψ =180°). On the other hand, the difference in energy between 3_{10}- and α-helical structures is small.[1] Furthermore, the ability of Aib to induce β-turn conformation has been demonstrated for a tripeptide.[8]

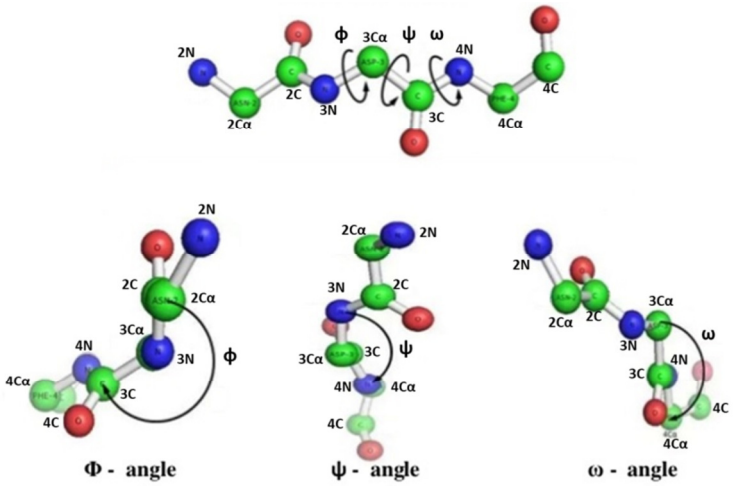

Figure 1.1.2. Main chain torsional angles

Many analogues of Aib have been exploited in order to design sequences with a predictable structure and impart novel functionalities. In particular, the group of Cα-tetrasubstituted residues in which the quaternary α-carbon forms part of a ring such as the achiral 1-aminocycloalkane-1-carboxylic acids (Ac_nc, where n indicates the number of carbon atoms in the cycloalkane ring[9]), has been the object of extensive investigation.[10]
For several years, my research group have developed synthetic strategies for the preparation of many cyclic Cα-tetrasubstituted achiral and chiral amino acids (Fig. 1.1.3) and some of them have been inserted in short peptide sequences in order to induce a stable helical structure.[11]

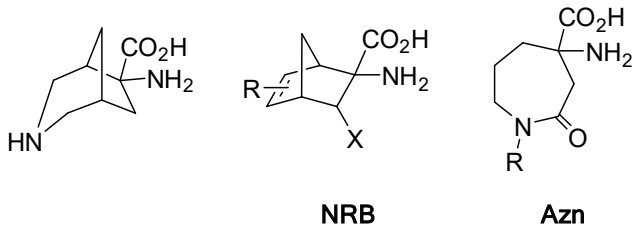

Figure 1.1.3. Examples of cyclic Cα-tetra substituted amino acids developed in our group

The presence of a constrained structure induced by C^{α}-tetrasubstituted amino acids is extremely efficient in stabilize specific secondary structures of the peptides and thus in driving the self-assembly. One example is the study conducted on *Degarelix,* a gonadotropin-releasing hormone (GnRH) peptide antagonist that, depending on the residue in position 7, is able to self-assemble in spherical nanostructures finding application as drug delivery system.[12] Peptides containing Ac_nc amino acids are able to form stable vesicles and act as long active compounds. Another example is the new method developed by Gatto and co-workers to build a peptide self-assembled monolayer (SAMs) on gold nanoparticles exploiting only helix-helix macrodipole interactions induced by residues such as Aib, 4-aminopiperidine-4-carboxylic acid (Api) and Cα-methyl norvaline (L-(αMe)Nva).[13]

Aim of the project

The first part of this chapter is focused on the preparation of two diastereoisomeric pentapeptides AcAla-NRB-Ala-Aib-AlaNH_2 **1'** and **1''** (Fig. 1.1.4), containing in position 2 two enantiomers of the unnatural constrained Norbornene amino acid (NRB) and the self-assembling studies on these compounds. These short peptides resulted insoluble in organic solvent except methanol and DMSO but completely soluble in water despite they are made of hydrophobic non polar amino acids. Self-assembly experiments have shown that peptides **1'** and **1''** are only apparently soluble in water, but, in real, they form supramolecular assemblies of spherical shape both individually and in mixture. This work is published on *RCS Advances*.[14]

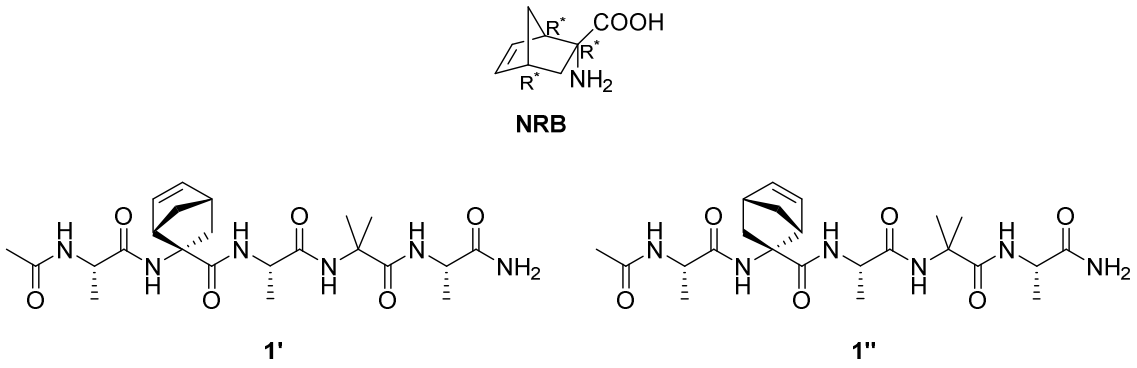

Figure 1.1.4. Molecular structure of NRB, peptides **1'** and **1''**

The numerous advantages of using peptides as building blocks of complex architectures are well-known. In particular, spherical (micelles and vesicle-like) architectures appear very attractive due to their promising applications in biomedicine and nanotechnology as drug delivery systems. Therefore, as a development of this study, in order to increase the applicability of such system, simplified analogues of compounds **1'** and **1''** (table 1.1.1) were designed, i.e. peptides **2'/2''**, **3**, **4**. For this purpose, NRB scaffold was substituted with other C^{α}-tetrasubstituted amino acids (norbornane, Ac_5c, Aib) some of them commercially available. The resulting peptides have shown the same solubility of peptides **1'** and **1''** and the same self-assemble ability. The simplest synthesized peptide which is able to self-assemble in water, contains only Ala and Aib residues (peptide **4**). Since Clayden and co-workers reported that also the choice of C- and N-terminus functionalities can affect the propensity of the peptides to aggregate,[15] the simplicity of peptide **4** was exploited, designing compounds with the same sequence but different substitutions at C-terminus (table 1.1.1, peptides **5**, **6**, **7**) and evaluate their influence on chemical structure and morphology.

Compound	Sequence
1'/1''	Ac-A-**NRB**-A-Aib-A-$CONH_2$
2'/2''	Ac-A-**nrb**-A-Aib-A-$CONH_2$
3	Ac-A-**Ac_5c**-A-Aib-A-$CONH_2$
4	Ac-A-**Aib**-A-Aib-A-**$CONH_2$**
5	Ac-A-Aib-A-Aib-A-**COOMe**
6	Ac-A-Aib-A-Aib-A-**CONHMe**
7	Ac-A-Aib-A-Aib-A-**COOH**

Table 1.1.1. Synthesized peptides (NRB = norbornene, nrb = norbornane)

The simplest system, formed only by Ala and Aib residues, is a very well-studied motif in the literature since it predisposes the peptides to exhibit preference for both α- as well as 3_{10}-helical backbone which are important secondary structure in proteins. In the following paragraph, an overview of the main studied aspects of Ala-Aib motif is reported due to its implication in this project. It is interesting to note that all peptides reported in the literature, containing only Ala and Aib residues, have methoxylated C-terminus and little is

published on the structural influence of different C-terminal groups. Therefore, it can be interesting to find innovative applications for Ala-Aib containing peptides and, on the other hand, to fill the gap on these compounds with different carboxylic groups.

Literature overview of Ala-Aib containing peptides

In 1983, Balaram and Vijayan described the folded conformation in $CDCl_3$ and DMSO on pentapeptide and heptapeptide with general structure Boc-Ala-(Aib-Ala)$_n$-OMe (n=2, 3). The NMR data suggested that pentapeptide favours 3_{10}-helical conformation, stabilized by 4←1 H-bonding both in $CDCl_3$ and DMSO. In contrast, the heptapeptide showed evidence of conformational changes on going from a relatively non-polar solvent like $CDCl_3$ to a polar solvent like DMSO. In particular, in DMSO one of the 4←1 H-bonds involving an Ala NH group is loosened, since the Ala-Aib β-turn is partially broken.[16]

Another important factor that influences the conformational preference of Aib containing peptides is the length. Benedetti and co-workers in 1990 solved the X-ray diffraction structures of peptides with general formula pBrBz-(Aib-Ala)$_n$-OMe (n=5, 6) and they found that the hexapeptide (n=3) is a complete 3_{10}-helix in crystal state with four 1←4 intramolecular N-H · · ·O=CH-bonds, while the octapeptide (n=4) has an α-helical structure with four 1←5 H-bonds. This study represents the first experimental proof for a 3_{10}→α-helix conversion in the crystal state induced by peptide backbone lengthening only.[17] The same authors also demonstrated that when the number of repeating dipeptide units exceeds three, the -(Aib-Ala)$_n$- peptides preferentially fold into an α-helical structure and the helix is initiated by the Aib residue at the N-terminus.[18] The critical chain length for conformational transition from the 3_{10}- to α-helix should therefore be 7. Afterwards, the preferentially conformations adopted by Aib-rich oligopeptides were extensively investigated in solid state and in several organic solvents. Few years later, in 1993, Imanishi group from Osaka University, reported on the conformation of oligopeptides having longer chain length than eight, with the general formula Boc-(Ala-Aib)$_n$-OMe (n=4, 6, 8), the sequence of which is opposite to pBrBz-(Aib-Ala)$_4$-OMe. In this case the octapeptide showed hydrogen bonds of 1←4 type, indicating a completely 3_{10}-helical structure which is in contrast to α-helix preference of pBrBz-(Aib-Ala)$_4$-OMe. The reason for the different behaviour was found, as in the previous case, in the different polarity of crystallization solvent, in fact the crystal of Boc-(Ala-Aib)$_4$-OMe was grown in a less polar medium than pBrBz-(Aib-Ala)$_4$-OMe. The different polarities of solvents resulted in a 3_{10}-

helix of the former and α-helix of the latter.[19] This strengthened the idea that the solvent has a strong influence due to differences in dielectric constant and relative stabilities of hydrogen bonds on structural preference. In particular, the stability of α-helical structure increases with the dielectric constant of the solvent. Another aspect that affects the overall propensity of Aib-based peptides in crystals is the choice of protection group at N-terminus. Winter, Jung and co-workers reported the structure of crystallized Ac-Ala-Aib-Ala-OMe and Boc-Ala-Aib-Ala-OMe. In the first peptide, dihedral angles suggested that the central Aib adopts a 3_{10}-like conformation while in the Boc-peptide the authors identified a distorted β-turn.[20]

Finally, the behaviour of Aib-rich oligopeptides in water became of interest. In 2007 Schweitzer-Stenner studied the structural impact of an individual Aib residue in an Ala context of short peptides in water and Aib's influence on the conformation of nearest-neighbour residues. They investigated the structure of three blocked Aib-containing tripeptides, namely Ac-Aib-Ala-Ala-OMe, Ac-Ala-Aib-Ala-OMe and Ac-Ala-Ala-Aib-OMe in aqueous solution and they found that all peptides adopted multiple conformation. Ala showed polyproline II helix (PPII) propensity, but its conformational equilibrium was shifted towards helical conformations in Ac-Aib-Ala-Ala-OMe, indicating that Aib can induce helical conformations of neighbouring residues positioned towards the C-terminal direction of the peptide.[21] In 2011 Toniolo and co-workers reported a series of N-terminally acetylated, C-terminally methoxylated Ala-Aib oligopeptides, characterized only by alternative Aib and Ala residues, from the dimer to the nonamer level They found that the critical main-chain lengths for 3_{10}- and α-helices, in aqueous solution are six and eight residues, respectively, while dimer, trimer, tetramer and pentamer have an unordered conformation.[22] The same authors reported that the undecapeptide Z-$(Ala)_3$-$(Aib\text{-}Ala)_4$-OMe is able to form self-assembled structures of spherical shape in water.[23] This peptide maintains in water the same helical conformations that it has in organic solvents. The authors hypothesized that the hydrophobic parts of the sequence, mainly the aromatic functionalities of the Z groups, are located in the internal part of the aggregate interacting through non covalent interaction (π/π stacking). Polar groups are, in turn, pointed toward the aqueous environment so a network able to arrange in a spherical aggregate is hypothesized (fig. 1.1.6). This is the first example of a class of N- and C-terminally protected, hydrophobic peptides able to give ordered water aggregates and this finding opens the way of use such system in the fields of biomedicine and material science.

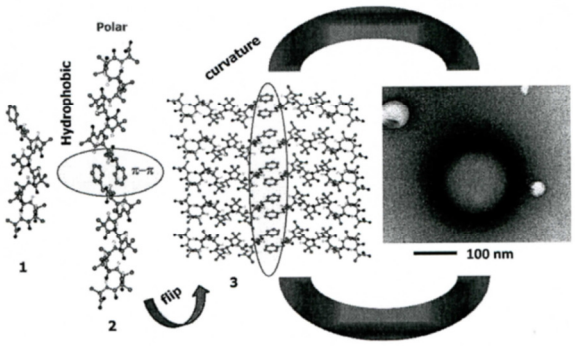

Figure 1.1.6. Tentative explanation for the aggregates formation[23]

Result and discussion

Synthesis

The synthesis of peptide **1'** and **1''** is reported in Scheme 1.1.1.

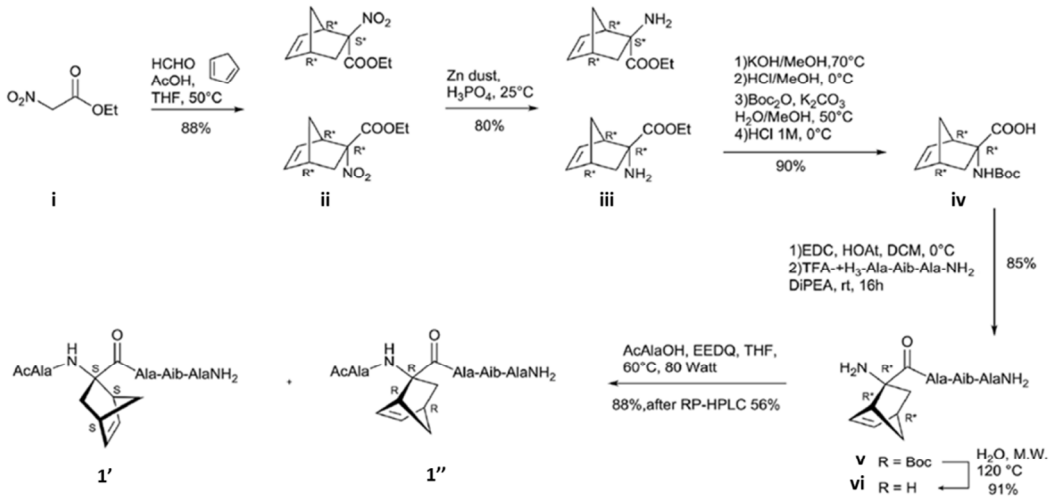

Scheme 1.1.1. Synthetic scheme of peptides **1'** and **1''**[14]

NRB nitroesters (**ii**, yield 88%) were prepared in gram scale using a modified multicomponent protocol described by Carrol.[24] Then, nitroesters **ii** were reduced with

an excess of Zn dust in H_3PO_4 (1 M in THF) affording the respective amines (**iii**, 80% yields) that were easily separated by flash chromatography. Hydrolysis of (1R*,2R*,4R*)-NRB amine (KOH 6 eq, MeOH, 70°C for 24 h, then HCl/MeOH, 0°C) gave the free NRB amino acid (90% overall yields) which was Boc-protected (Boc_2O, K_2CO_3, H_2O/MeOH) and purified by precipitation from reaction mixture with HCl 1 M at 0°C, affording compound **iv**. Compound **iv** is, then, coupled with tripeptide H-Ala-Aib-Ala-NH_2, which was previously prepared by a linear Boc chemistry solution strategy recently reported by our research group (scheme 1.1.2),[25] using HOAt (1.1 eq), EDC (1.1 eq), in DCM, 25°C, overnight.

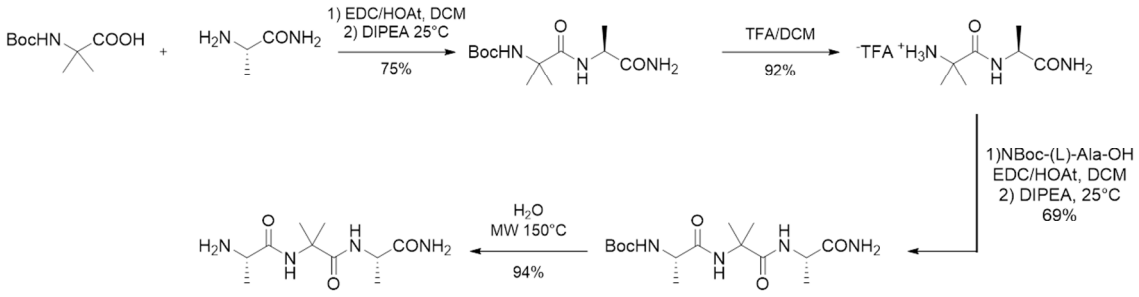

Scheme 1.1.2. Synthetic scheme of tripeptide H-Ala-Aib-Ala-NH_2

The obtained tetrapeptides (**v**) were purified by precipitation in DCM/hexane in satisfactory yield (85%) as diastereoisomeric mixture and then they were Boc-deprotected with TFA but the recovery of the free amine was very hard due to their high water solubility. To overcome this problem, we used the microwave assisted Boc deprotection in water (150°C, 20 min, 80 watt) affording the respective amine (**vi**, 91% yield). The diastereoisomeric mixture of the two tetrapeptides (**vi**) was then coupled with Ac-Ala-OH. To avoid the high trend of racemization of the acetylated alanine under standard coupling condition, the microwave assisted reaction was performed with EEDQ (1.1 eq) as coupling reagent in absence of base (THF, 60°C, 80 watt). The two diasteroisomers **1'** and **1''** were precipitated from the reaction mixture in pure form with Et_2O (88% yield) and separated by HPLC.

The synthesis of the pentapeptides **1'** and **1''**, however, is chemically complex, needs a lot of synthetic steps and it couldn't be transferred in solid phase. In order to increase the applicability of this interesting system, the sequence has been modified and the peptide structure has been simplified. Moreover, the modification of the C-terminus is also studied. All synthesized compounds are shown in figure 1.1.5.

The first modification to the original structure consisted in the saturation of the norbornene double bond affording a more flexible scaffold (compounds **2'** and **2''**). Then, the NRB amino acid is replaced with Ac_5c amino acid (peptide **3**) because it is known from the literature that Ac_nc amino acids are able to form stable vesicles.[12] Finally, NRB amino acid is replaced with Aib (peptide **4**) which is the simplest compound of C^{α}-tetrasubstituted amino acids class and it is a strong promoter of folded and, particularly, helical conformations. Peptides **5**, **6** and **7** are analogues of peptide **4** with different groups at C-terminus, in particular methyl ester, methyl-amide and carboxylic acid, respectively.

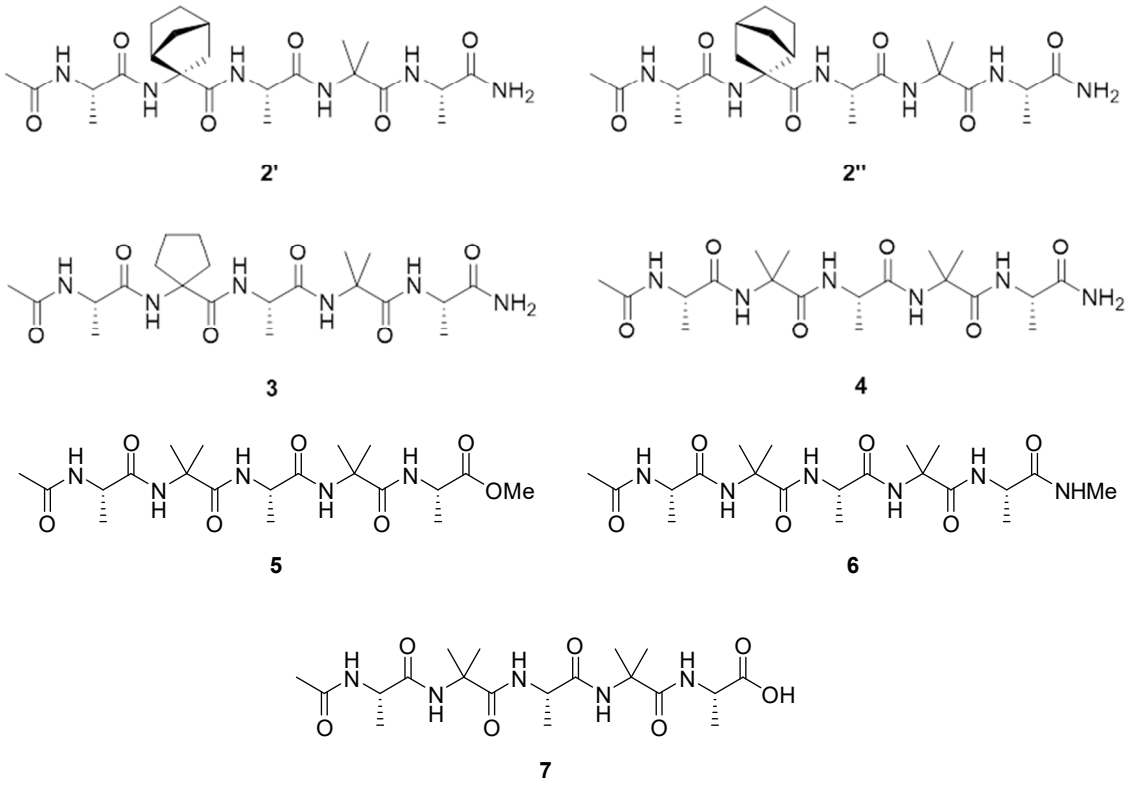

Figure 1.1.5. Molecular structure of peptides **2'/2''**, **3** and **4**

Peptides **2'** and **2''** were synthesized from peptides **1'** and **1''** respectively, by catalytic reduction of double bond (H_2, Pd/C, MeOH, 25°C, 1 atm, overnight).

The other peptides, from **3** to **7**, were synthesized in solid phase, using: i) Rink Amide resin to afford the $CONH_2$ terminus peptides **3** and **4**, ii) HMBA-AM resin to afford COOMe terminus peptide **5**, iii) 2-chlorotritylchloride resin to afford COOH terminus (peptide **7**). Peptide **6** was synthesized treating peptide **5** with 33 wt % methylamine solution in

ethanol affording the CONHMe terminus (see Experimental part for the description of the procedure).

Chemical characterization – conformational analysis

NMR experiments (^{1}H, ^{13}C, COSY, NOESY, ROESY, HSQC, HMBC) were performed for a complete characterization of all synthesized peptides. The choice of the solvent for these analyses was crucial, since the peptides seemed soluble only in water, methanol and DMSO, while in acetonitrile the solubility was very low. Each of these solvents has not proved sufficiently suitable to completely study the secondary structures of peptides. In particular, water and methanol are able to exchange their deuterium (D) atoms with the amide proton making the NOESY structural analysis impossible to be performed[26]; $DMSO_{d6}$ is usually used to destructure the peptide through the strong H bond interaction with the amide protons, while CD_3CN gave incomplete C^{13}-NMR and NOESY data due to the small amount of product in solution. To overcome these problems, we used a mixture of D_2O-H_2O 10%-90% and CD_3OH, but both of them required the signal suppression of the solvent.

The characterization of peptides was reported **1'** and **1"** on the article published on *RCS Advances.*[14] Below, a summary of the principal signals of **1'** and **1"** is given.

First of all, $^{3}J_{NH-H\alpha}$ coupling constants of alanine residues were evaluated. Average values of $^{3}J_{NH-H\alpha}$ have been computed by different groups, from crystal structure and in solution state, for each peptide secondary structure (α-helix: 3.9-4.8 Hz, 3_{10}-helix: 4.2-5.6 Hz, β-sheet: 8.5-9.7)[27]

$^{3}J_{NH-H\alpha}$ values in CD_3OH and H_2O/D_2O for **1'** and **1''** showed that Ala1 and Ala3 have typical values of helical backbone in CD_3OH in both peptides.

	Ala1 $^{3}J_{NH-H\alpha}$ (Hz)	Ala3 $^{3}J_{NH-H\alpha}$ (Hz)	Ala5 $^{3}J_{NH-H\alpha}$ (Hz)
1' CD_3OH	5.00	5.10	7.31
1' H_2O/D_2O	5.68	5.58	6.48
1'' CD_3OH	4.21	-	6.87
1'' H_2O/D_2O	5.10	5.16	6.51

Table 1.1.2. $^{3}J_{NH-H\alpha}$ values (Hz) for Ala1, Ala3, Ala5 of peptides **1'** and **1''** in CD_3OH and H_2O/D_2O

In H_2O/D_2O a moderate increase of $^3J_{NH-H\alpha}$ was observed underlining a contribution of the extended unfolded conformation to helical backbone structure (Table 1.1.2). The helical structure was confirmed by the NOE signals in NOESY and ROESY experiments in CD_3OH and H_2O/D_2O ($N,N_{i,\ i+\ 1}$ (s), $C_\alpha H_i–NH_{i+1}$ (s) and $C_\alpha H_{i–NHi+3}$ (m/w)). In peptide **1'**, the formation of 3_{10}-helix was supported by $C^\alpha H_i$-NH_{i+2} signals. A similar behaviour was found for peptide **1''**, even if many NH signals were overlapped. The experiment in H_2O/D_2O for peptides **1'** and **1''** showed that the helical conformation is less stable than in methanol and a helix/random coil transition was observed. The experiment at variable temperature in CD_3OH (Fig. 1.1.7) showed that the most stable part was the C-terminus with the lowest values of $\Delta\delta/\Delta T$ for one NH of $CONH_2$, highlighting the importance of the primary amide in the helix stabilization. Interestingly, the ppb/K NHs values of peptide **1''**, are lower with respect to those of peptide **1'** indicating a more stable helix secondary structure. A different behaviour was found in H_2O/D_2O where higher $\Delta\delta/\Delta T$ values were detected for all NHs except for the second primary amide of **1''**which we hypothesized involved in a H-bond.

A further confirmation of stable asymmetric secondary structure comes from the evaluation of the magnetic non-equivalence (MNE) of the signals related to the diastereotopic methyl groups of Aib4 in ^{13}C NMR spectrum.[16] The MNE is an important data in order to verify the presence of secondary structure: when its value is higher than 0.5-0.8, the MNE is not due to a close stereocenter but is generated by molecular conformation. The MNE has been extrapolated from HSQC experiments in CD_3CN, CD_3OD and D_2O. The values reported in table 1.1.3 demonstrate that in CD_3CN and CD_3OD both peptides present a stable asymmetric secondary structure in solution that fit with the 3_{10}-helix previously postulated by VT-NMR. The same analysis in D_2O gave very low values (0,24 for **1'** and 0,85 for **1''**). Taking in account that chiral residues of Ala3 and Ala5 could induce an MNE in Aib4 not higher than 0.5 ppm we could hypothesize the absence of stable helix asymmetric secondary structure in **1'** and a small contribution in **1''**, in favour of a transition helix/random coil structure.

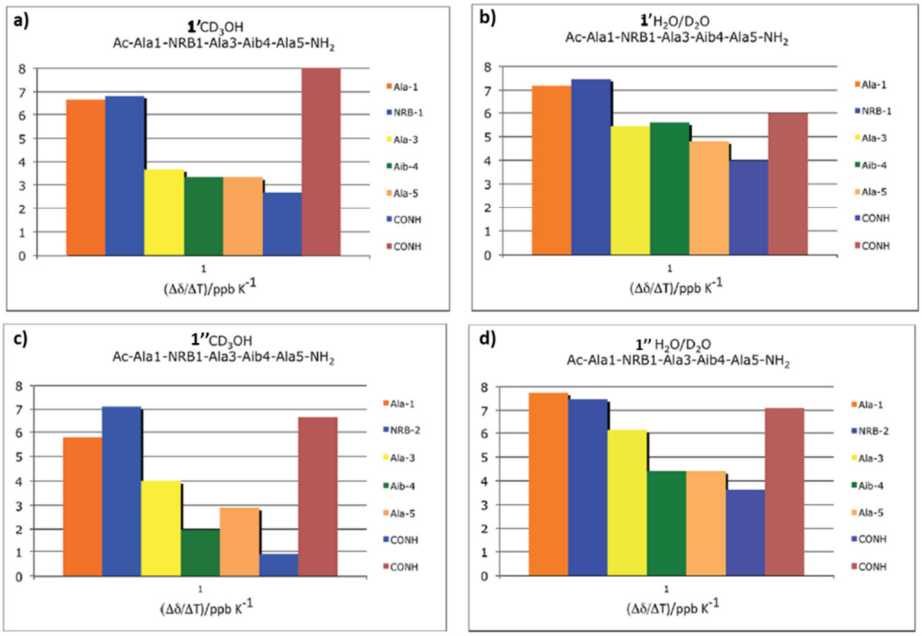

Figure 1.1.7. Temperature dependence of amide chemical shift (Δδ/ΔT 273–300 K) of peptide **1'** in a) CD_3OH and b) H_2O/D_2O and of peptide **1''** in c) CD_3OH and d) H_2O/D_2O

The comparison with MNE values reported in literature for differently capped $(Ala\text{-}Aib)_2$-Ala pentamers corroborates the hypothesis that primary amides at C-terminus together with N-terminal acetyl group strongly stabilized helix conformation in organic solvent.[28] Norbornene also play an important role in such stabilization as observed in a previously published computational model[19, 29] and, basing on the magnitude of MNE in CD_3CN, it seems to be the best helix inducer among the unnatural constrained amino acids synthesized in our group referring to the same model peptide.[30]

Solvent	**Peptide 1'**		**Peptide 1''**	
	Aib4 δ	**MNE δ**	**Aib4 δ**	**MNE δ**
CD_3CN	26.22-22.92	3.38	26.50-22.81	3.69
CD_3OD	25.15-23.21	1.94	25.59-22.80	2.79
D_2O	24.22-23.97	0.25	24.50-23.65	0.85

Table 1.1.3. Chemical shift in ppm of Aib-4 in peptide **1'** and **1''** and NME

The absolute stereochemistry of norbornene scaffold was assigned taking into account the long range spatial proximity between NH of Ala5 and specific protons of norbornene ring.

Peptide **1'** shows a spatial proximity between Ala5NH-NRB2H3 but no proximity between Ala5NH-NRB2H1 that, as expected, is detected in compound **1''**. As a further confirmation, peptide **1'** shows a very intense NOE between Ala3NH-NRB2H1 and signals of very low intensity between Ala3NH-NRB2H3 and Ala3NH-NRB2H7. Peptide **1''** does not present any Ala3NH-NRB2H7 cross peak but NOEs, comparable in intensity, between Ala3NH-NRB2H1 and Ala3NH-NRB2H3. Finally, the NOE between Ala5Hβ-NRB2H1 is suitable only for **1''** (Fig. 1.1.8). As a result, the S- and R- stereochemistry was assigned to norbornene scaffold in peptide **1'** and **1''**, respectively (fig. 1.1.9).

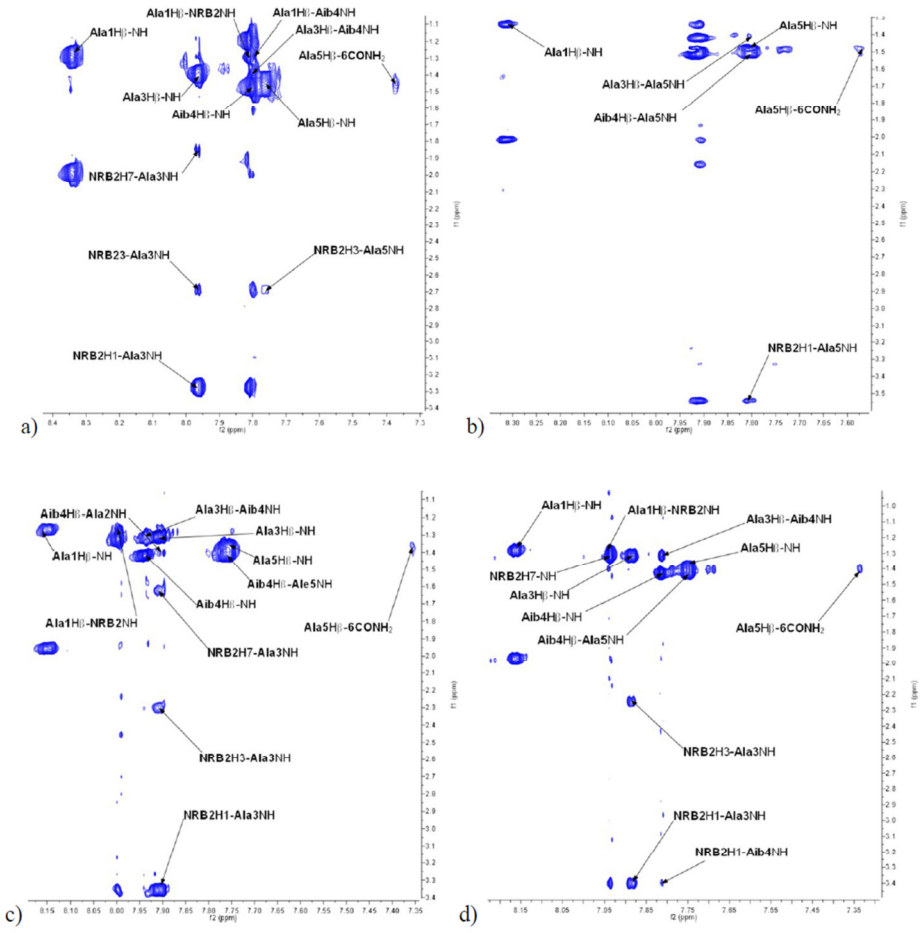

Figure 1.1.8. NOESY experiment analysis of a) peptide **1'** in CD_3OH; b) ROESY experiment analysis of peptide **1''** CD_3OH. c) NOESY experiment analysis of peptide **1'** in H_2O/D_2O d) NOESY experiment analysis peptide **1''** in H_2O/D_2O [14]

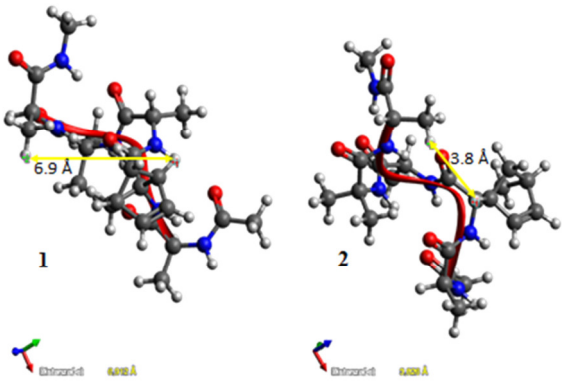

Figure 1.1.9. S- and R- stereochemistry assigned to norbornene scaffold

Chemical characterization – conformational analysis of simplified analogues

A complete NMR characterization of peptide **2'/2''**, **3** and **4** was performed in order to compare their secondary structure with that of peptides **1'/1''** and verify their similarity. The NMR analysis of peptides **2'** and **2''** gave good spectra only in acetonitrile since the compounds don't give good signals in methanol and water. The analysis in CD_3OH and H_2O/D_2O is referred to peptides **3** and **4**.

To obtain detailed information on the conformational preferences, 2D-NOESY and ROESY experiments at different mixing times, were performed in CD_3OH and H_2O/D_2O. The analysis showed a complete set of NH_i,NH_{i+1} NOE cross peaks which are characteristic of a helical conformation for both peptides **3** and **4** (Fig. 1.1.10).

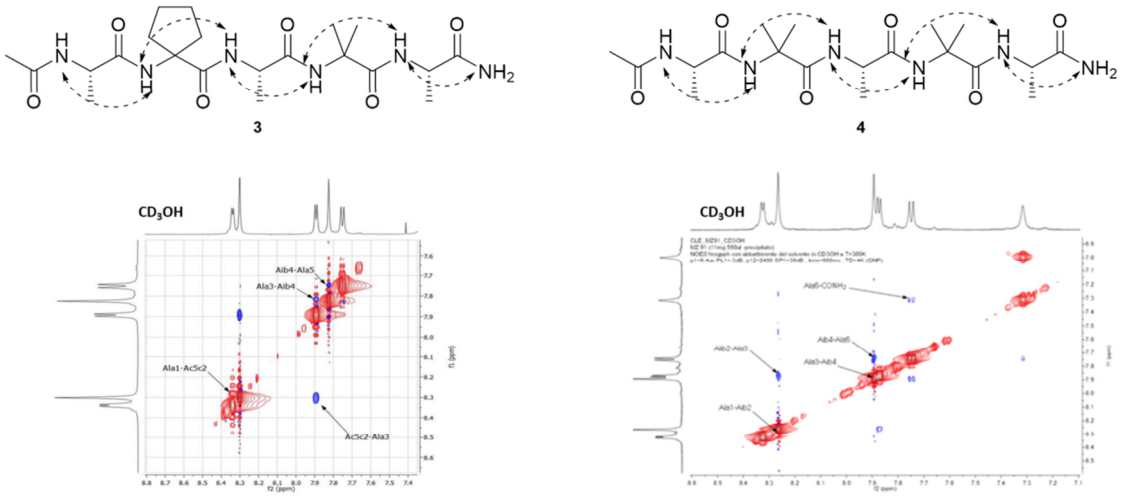

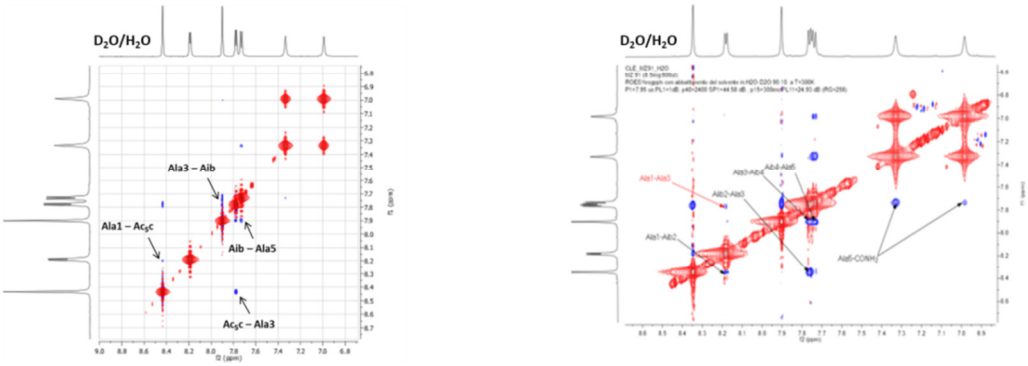

Figure 1.1.10. NOESY experiments analysis of N_i, N_{i+1} region in CD_3OH for peptides **3** and **4**

The analysis of $C^{\alpha}H$-NH region allowed to identify in CD_3OH strong $C^{\alpha}H_i$-NH_{i+1} (Ala1-Ac_5c NH for **3** or Ala1-Aib2 NH for **4**; Ala3-Aib4NH; Ala5- $CONH_2$ for both) and $C^{\alpha}H_i$-NH_{i+3} diagnostic signals (Ala1-Aib4 NH and Ala3-CONH2 for both **3** and **4**) characterizing the helical structure. $C^{\alpha}H_i$-NH_{i+2} signals between Ala1-Ala3 NH and Ala3-Ala5 NH confirmed the formation of a 3_{10}-helix for both peptides **3** and **4**. Moreover, compound **4** exhibited a weak effect between Ala1 and CONH. The experiment in H_2O/D_2O showed the same $C^{\alpha}H_i$-NH_{i+1} cross peaks for peptide **4** so these data confirmed the formation of a helical structure but the less intensity of the signals in H_2O/D_2O compared to CD_3OH indicates a less stable helix secondary structure. On the other hand, in peptide **3**, only $C^{\alpha}H_i$-NH_{i+1} signals (Ala1-Ac_5c NH and Ala3-Aib NH) were observed indicated a less stable secondary structure (Fig. 1.1.11).

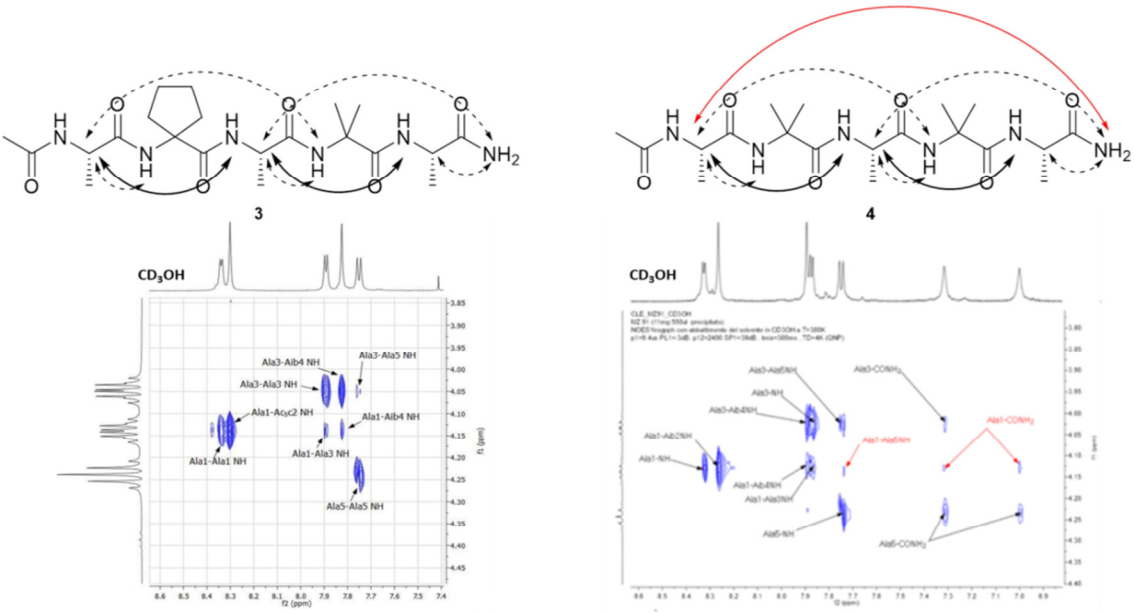

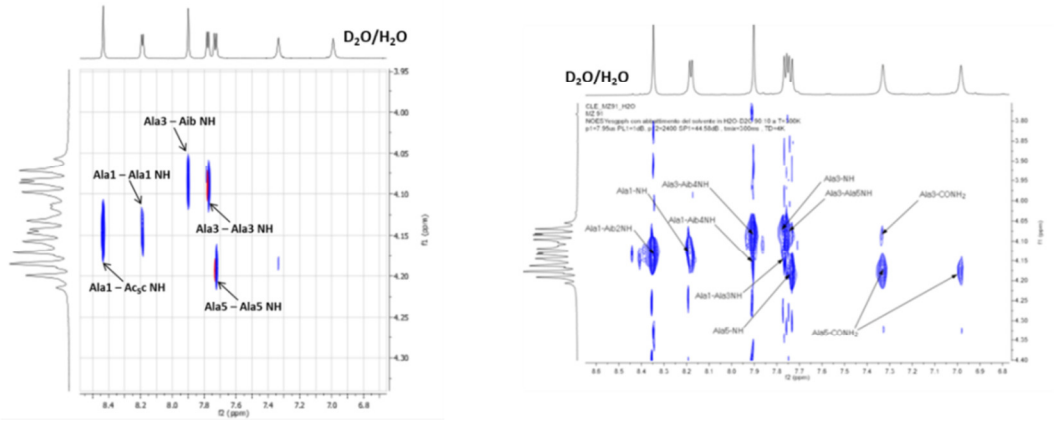

Figure 1.1.11. NOESY experiments analysis of $C^{\alpha}H$-NH region in CD_3OH for peptides **3** and **4**

Further evidence of the helical conformation is given by $C^{\alpha}H_i$-C^{β}_{i+3} cross peaks between Ala1-Aib4 clearly evident in CD_3OH but not in H_2O/D_2O (Fig. 1.1.12).

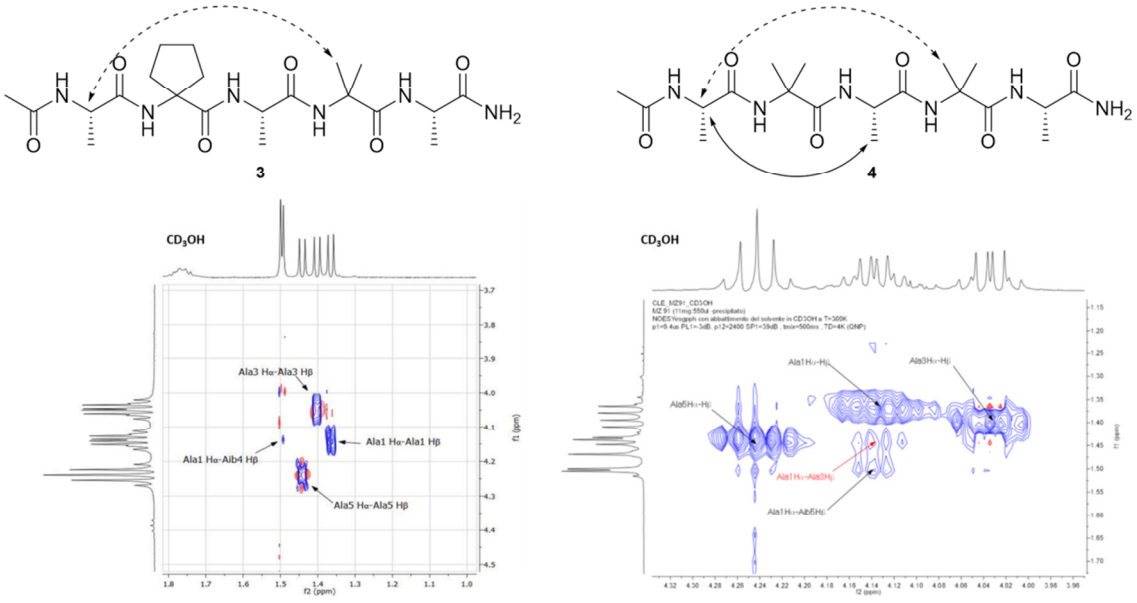

Figure 1.1.12. NOESY experiments analysis of $C^{\alpha}H$-C^{β} region in CD_3OH for peptides **3** and **4**

Confirmation that C-terminus is the most stable part in both peptides was given estimating the temperature dependence of amide chemical shift ($\Delta\delta/\Delta T$, 273–300 K) as shown in figure 1.1.13. In CD_3OH, $\Delta\delta/\Delta T$ NH values of Ala3, Aib4, Ala5 are around 4.0 ppb/K. The lowest value of $\Delta\delta/\Delta T$ is attributed to one NH of $CONH_2$, this means that, effectively, the most stable part is amide at C-terminus. On the other hand, the other NHs (Ala1, Aib2 or

Ac_5c at N-terminus and the other NH proton of the primary amide) are not involved in any intramolecular H-bond (Δδ/ΔT 6–8 ppb/K).

A different behaviour was found in H_2O/D_2O (Fig. 1.1.13c,d) where higher Δδ/ΔT values were detected for all NHs. Moreover it is interesting to notice that in water the differences between the two primary amide protons Δδ/ΔT values are smaller than in methanol. Especially one of the two primary amides of peptides **3** and **4** with a values of 4 ppb/K seems to be involved in a H-bond but it's not possible to determinate the inter- or intra-molecular nature of that bond.

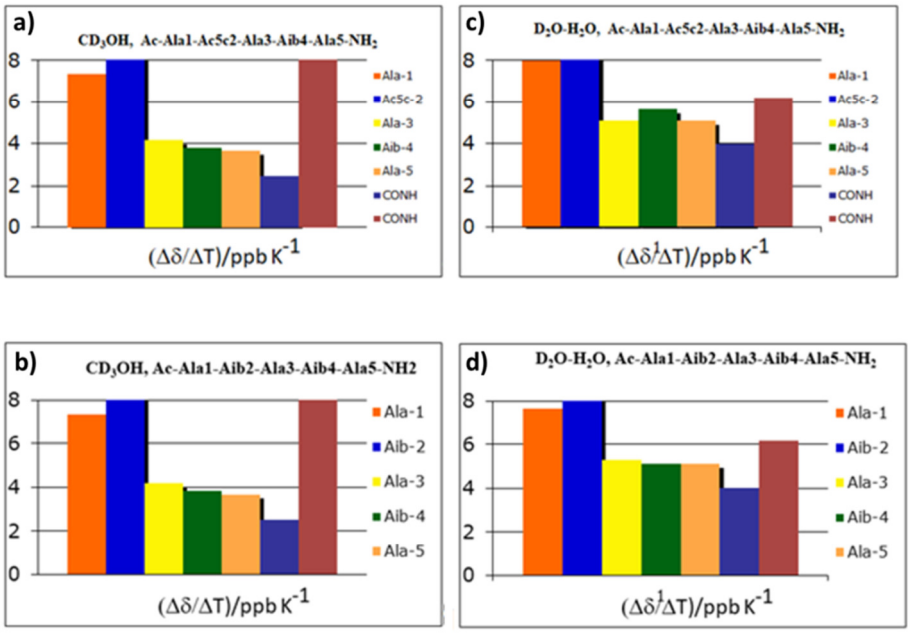

Figure 1.1.13. Temperature dependence of amide chemical shift (Δδ/ΔT 273–300 K) of peptide **3** in a) CD_3OH and b) H_2O/D_2O and of peptide **4** in c) CD_3OH and d) H_2O/D_2O

The evaluation of the ^{13}C-magnetic non-equivalence (MNE) of the signals related to the diastereotopic methyl groups of Aib4 was performed by HSQC experiments in CD_3CN, CD_3OD and D_2O as shown in table 1.1.4. This analysis, as said above, highlights the different coupling relationships that occur between two chemically equivalent spins, so can gives information about the complexity of the molecular structure.

Solvent	Peptide 2'		Peptide 2''	
	Aib4 δ	MNE δ	Aib4 δ	MNE δ
CD_3CN	26.24-22.83	3.41	26.49-22.74	3.75

Solvent	Peptide 3		Peptide 4	
	Aib4 δ	MNE δ	Aib4 δ	MNE δ
CD_3CN	26.384-22.894	3.49	26.79-23.31	3.48
CD_3OD	25.237-23.112	1.125	25.65-23.50	2.15
D_2O	24.300-23.943	0.36	24.65-24.24	0.41

Table 1.1.4. Chemical shift in ppm of Aib-4 in peptide **2'/2''**, **3**, and **4** and MNE

The values reported largely demonstrate how in CD_3CN (peptides **2'/2''**, **3** and **4**) and in CD_3OD (peptides **3** and **4**) all peptides present a stable secondary structure that fits perfectly with the 3_{10}-helix previously described for peptides **1'**and **1''**. The same analysis in D_2O gave very low Δδ values. According to literature data previously described,[22] these results confirm the absence of a stable helix structure for peptides **3** and **4**.

The helical conformation of peptide **4** was confirmed by the single crystal X-ray analysis. Suitable needle-shape crystals were obtained from slow evaporation of H_2O/CH_3CN (10:0.5) solution at 25°C (Fig. 1.1.14).

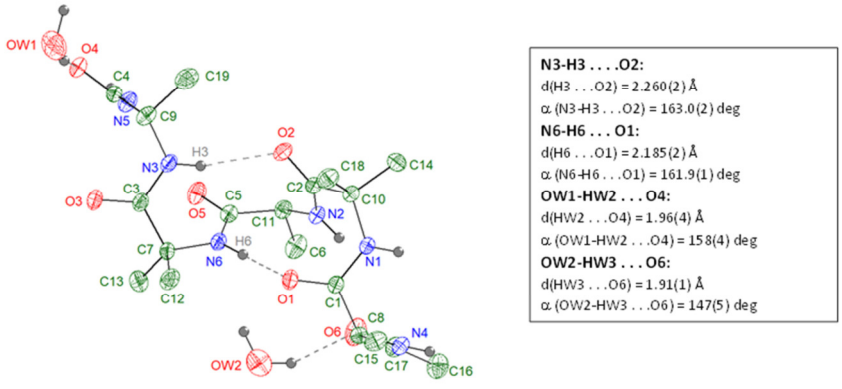

Figure 1.1.14. Intramolecular interactions (hydrogen bonds) in compound **4** as obtained from X-ray diffraction on a single crystal at 293 K. Asymmetric unit: 1 compound **4** molecule + 2 hydration water molecules

The crystallographic analysis proved that compound **4** is involved in four H bonds (dash in the figure). The solid state data are comparable with data in liquid (NMR in CD_3OH). In fact, in solid state, intramolecular H bonds involve Ala4 (N6-H6 · · ·O1) and Ala5 (N3-H3 · · ·O2), which have low $\Delta\delta/\Delta T$ values in methanol solution (fig. 1.1.13). Moreover, also in solid state amide N-terminus seems to be involved in additional H bond with a water molecule (OW1-HW2 · · ·O2), underline its important in the conformation stability. Further H bond in solid state involves acetyl group at C-terminus and another water molecule (OW2-HW3 · · ·O6). This H bond wasn't found in liquid state experiments but the importance of acetyl group in conformational stabilization is already reported in the literature [20].

The secondary structure of peptides **2'**, **2''**, **3** and **4** were also studied with circular dichroism and FT-IR.

Circular dichroism spectra were acquired in 2,2,2-trifluoroethanol (TFE), MeOH and water at 25°C with a peptides concentration of 0.1 mM (Fig. 1.1.15). In TFE peptides **3** and **4** showed a positive Cotton effect at 190 nm and two negative Cotton effects at 202 nm and 227 nm. The R ratios ($\theta_{227}/\theta_{202}$) suggest the 3^{10}-helix as the dominant structure, since R ≤ 0.5 (**3**: R= 0.5; **4**: R=0.37). Also the spectrum of peptide **2'** exhibited the typical Cotton effects of helical structure (R=0.5), but the two negative signals are less obvious than in peptides **3** and **4**. On the other hand, the spectrum of peptide **2''** was not attributable to a helical conformation. The analysis in MeOH for peptides **3** and **4** was similar to that in TFE, although the band at 227 was weaker. In this solvent, also both peptides **2'** and **2''** showed a trend which was attributable to a 3^{10}-helix as dominant structure.

Finally in H_2O, peptides **2'**, **3** and **4** showed a prevalent random conformation, supported by a strong signal at 190 nm and a less evident band at 222 nm. The spectrum of peptide **2''** is unusual but it could be attributed to a non-ordered structure.

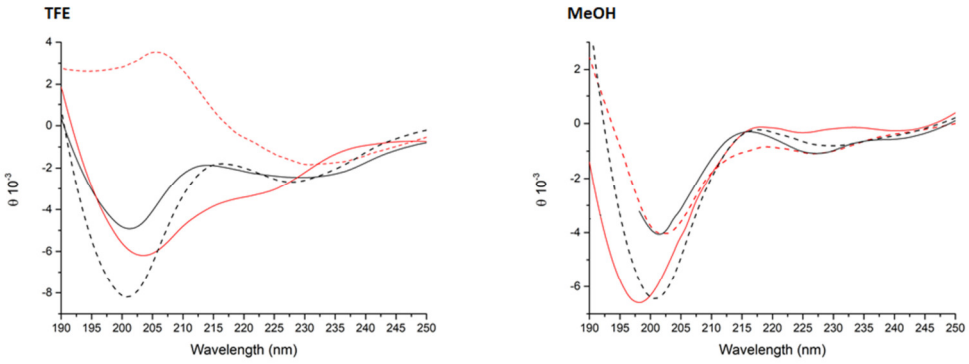

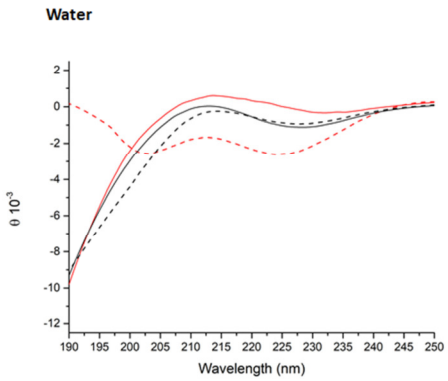

Figure 1.1.15. CD spectra in TFE, MeOH and water (0.1 mM) of peptides **2'** (straight red), **2''** (dash red), **3** (straight black) and **4** (dash black)

IR spectra were recorded for all peptides in the solid state (Table 1.1.5) and, after deconvolution, the N-H stretching vibration region of the amides was analysed to figure out peptide secondary structure.[32] The typical α-helix IR-band at 1656± 2 cm^{-1} is evident in all peptides. Due to this signal, we could suppose that all peptides have an intrinsic helical behaviour, but the number of amino acids in these compounds is too low to allow a univocal structure. In fact, in all spectra is evident the band at 1648 ± 2 cm^{-1} indicating random conformation, while there wasn't any typical 3_{10}-helix band at 1663±3 cm^{-1}, as we expected from CD and NMR data. Peptide **2''** also showed an IR-band at 1678 cm^{-1}, a typical signal of β-turn: this suggests also the minimal presence of β-component and this could explain why the CDs were unclear.

peptide	α-helix IR-band (1656 ± 2 cm^{-1})	Random coil IR-band (1648 ± 2 cm^{-1})	β-turn IR-band (1680 ± 2 cm^{-1})
2'	1654	1648	
2''	1655	1648	1678
3	1657	1648	
4	1654	1648	

Table 1.1.5. IR signals after deconvolution of N-H stretching vibration region of the amides

Summarizing, NMR, CD and IR data confirmed that peptides **3** and **4** have similar conformational structures with a predominant helical structure in MeOH while in water a prevalent random conformation is observed. The conformational studies of peptides **2'**

and **2''** turned out to be more difficult, so an accurate analysis of their structures wasn't possible.

Chemical characterization- conformational analysis of C-terminus modified peptides

NMR analysis of previous amidate peptides showed that the C-terminus is the most stable part of the structure. Furthermore, slightly modifications of this part could influence a lot not only the stability of the secondary structure but also the self-assembly ability of the molecule.[15] For this reason, peptides **5**, **6**, **7** have been synthesized. They are analogues of peptide **4**, with different C-termini.

Preliminary analyses were performed by circular dichroism. The spectra were acquired in 2,2,2-trifluoroethanol (TFE), MeOH and water at 25°C with a peptides concentration of 0.1 mM (Fig. 1.1.16).

In TFE only peptide **4** showed the 3^{10}-helix as the dominant structure with the positive Cotton effect at 190 nm and two negative Cotton effects at 202 nm and 227 nm, while in MeOH also peptide **6**, which has a non-ordered structure in TFE, seemed to have a helical conformation. Peptides **5** and **7** spectra were attributed to a non-ordered structures both in TFE and MeOH. Finally, in H_2O, all peptides showed a prevalent random conformation, supported by the strong signal at 190 nm and a less evident band at 222 nm.

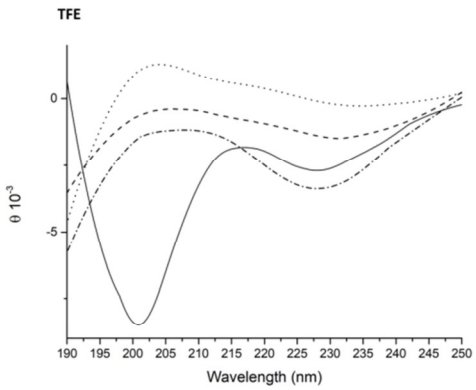

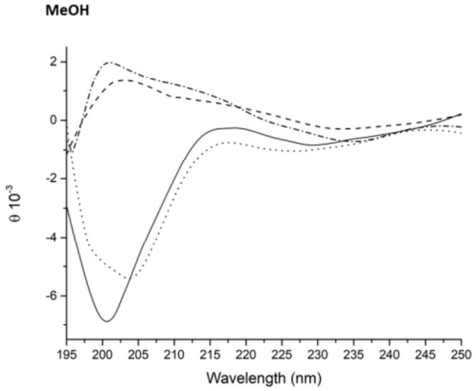

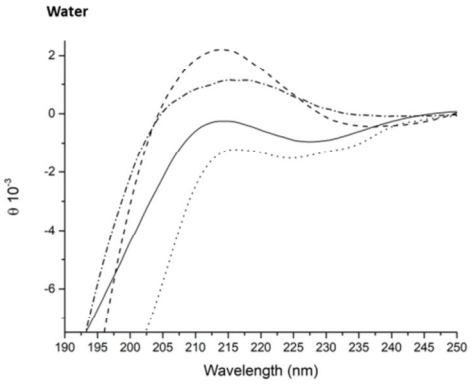

Figure 1.1.16. CD spectra in TFE, MeOH and water (0.1 mM) of peptides **4** (straight), **5** (dash), **6** (dot) and **7** (dash dot)

IR spectra were recorded for all peptides in the solid state (Table 1.1.6). The typical α-helix IR-band at 1656± 2 cm^{-1} is evident in all peptides except in peptide **6**. We could suppose that peptides **5**, **6** and **7** didn't show a univocal structure because more than one band is present in all peptides and this could explain the unstable structures found in CD spectra. Peptide **6** and **7** showed the presence of β-component, as peptide **2''**, and, as in the previous in case, this fact could explain why the CDs were unclear.

peptide	α-helix IR-band (1656 ± 2 cm^{-1})	Random coil IR-band (1648 ± 2 cm^{-1})	β-turn IR-band (1680 ± 2 cm^{-1})
4	1654	1648	
5	1655	1650	
6	1654		1682
7	1659	1647	1682

Table 1.1.6. IR signals after deconvolution of N-H stretching vibration region of the amides

In order to better understand the conformational differences highlighted in CD and IR spectra, a complete NMR characterization on peptides **5**, **6** and **7** were performed in CD_3OH in order to compare their secondary structures with that of peptide **4**, previously described. As shown in figure 1.1.18, a complete set of NH_i,NH_{i+1} NOE cross peaks were observed for all peptides. On the other hand, the analysis of $C^{\alpha}H$-NH region didn't show any significant signals for peptides **5** and **7**. Only in peptide **6**, it was possible to distinguish a $C^{\alpha}H_i$-NH_{i+2} signal between Ala3 and Aib4-NH and a $C^{\alpha}H_i$-NH_{i+1} signal between

Ala5 and CONH, confirming the importance of C-terminus amide for the stabilization of the conformational structure. However, unlike the peptide **4** and, in general, all peptides described above which assumed a stable helical conformation in methanol, NMR analysis of peptides **5**, **6** and **7** didn't show any ordered structures and these results can explain better CD and IR data.

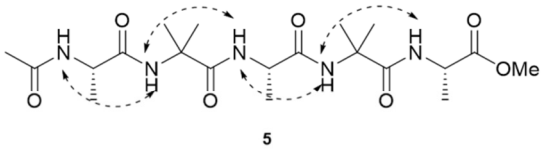

5

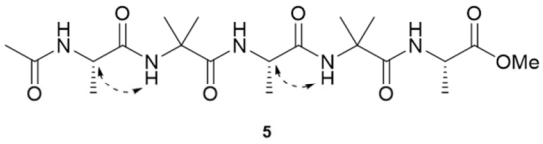

5

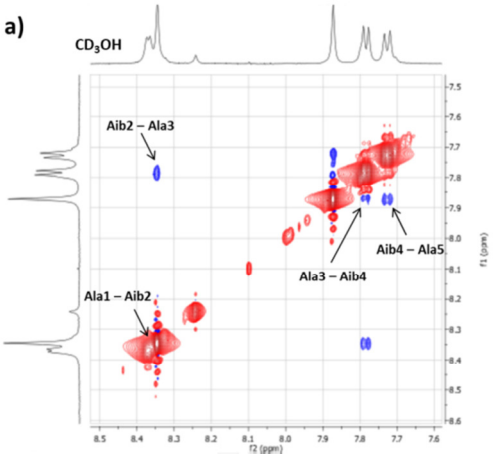

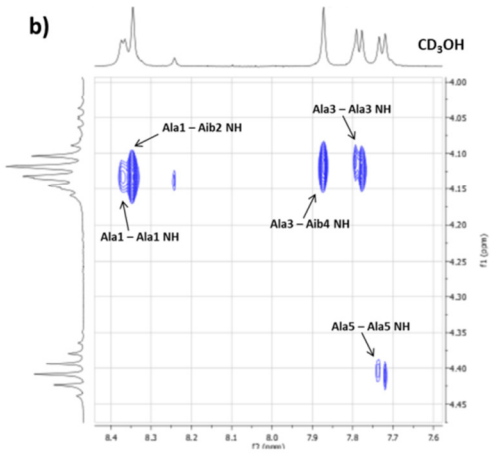

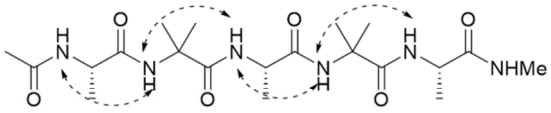

6

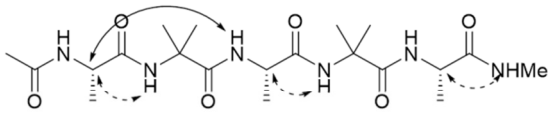

6

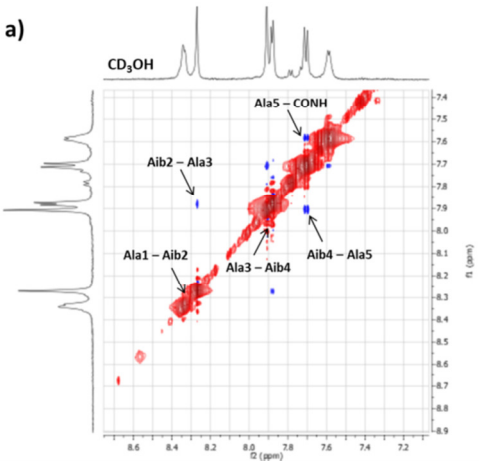

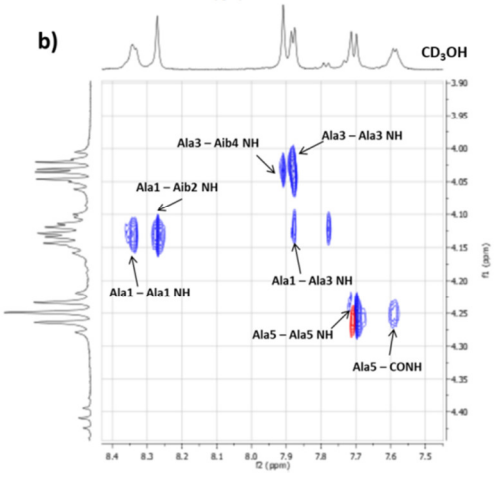

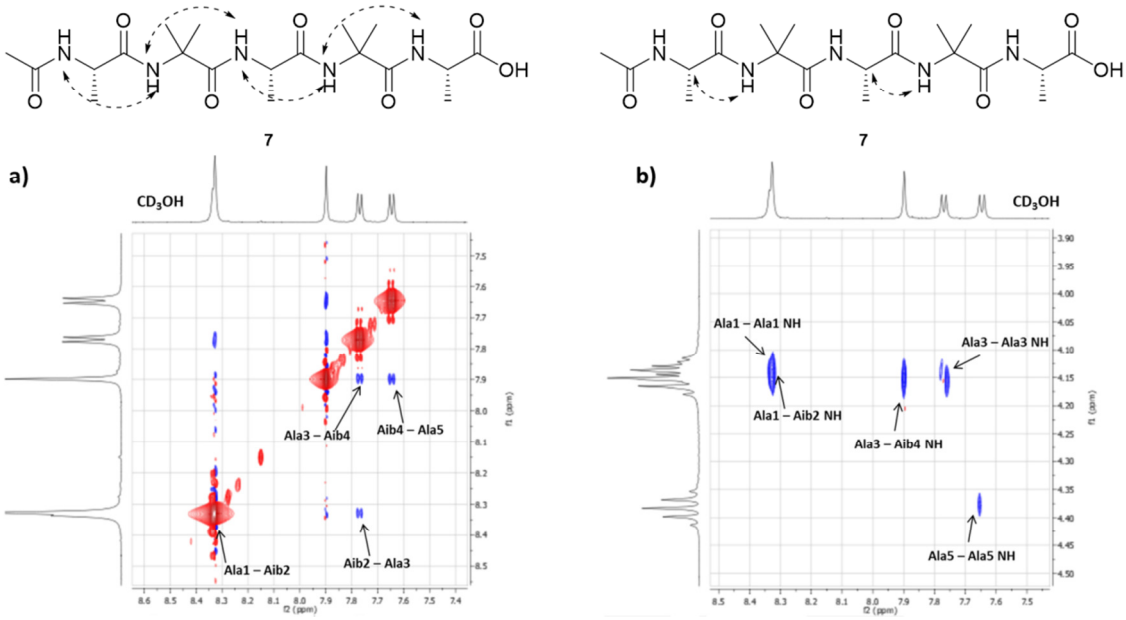

Figure 1.1.18. NOESY experiments analysis of a) N_i, N_{i+1} region and b) $C^{\alpha}H$-NH region in CD_3OH for peptides **5**, **6** and **7**

The variable temperature experiments (273-323 K) gave a further confirmation of a less stable secondary structure. In fact peptide **5** showed only one Δδ/ΔT NH value lower than 4 ppm/K which is NH of Ala in position 3. As expected from NMR experiments, the lowest Δδ/ΔT NH value for peptide **6** is attributed to NH at C-terminus, which we think being the most stable part of the molecule, but the value is still too high to hypothesized an H-bonded. Finally, in peptide **7**, all the NHs showed Δδ/ΔT NH values of around 4 ppb/K (Fig. 1.1.19).

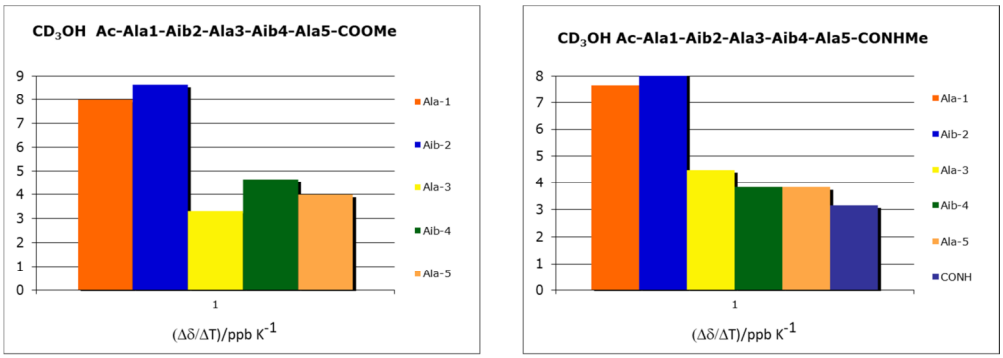

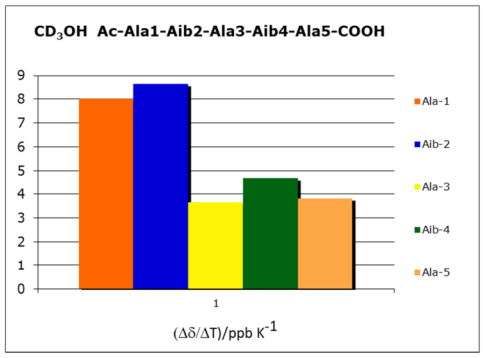

Figure 1.1.19. Temperature dependence of amide chemical shift (Δδ/ΔT 273–300 K) of peptides **5**,**6** and **7** in CD_3OH

All these data indicate that only with amide function at C- terminus, Ala-Aib pentapeptide **4** can assume a stable helical conformation in methanol, while with the other C-termini (COOMe, CONHMe and COOH) random coil conformation is the predominant structures.

Self-assembly studies

The self-assembly ability of peptides **1'** and **1''** in aqueous environment (MilliQ, Millipore) at the concentration of 5.0 mg/ml was investigated [14] individually or in 1:1 mixture using Dynamic Light Scattering (DLS), which represents a valuable tool to measure the particles size in the sub-micron region (Fig. 1.1.20a). The particle size measurements were repeated for three runs at room temperature (rt) and the data reported as the average hydrodynamic diameter. All the three samples showed the capability to self-assemble in aqueous environment and form aggregates whit hydrodynamic diameter values (i.e. mean size) ranged from about 320 to 370 nm. Although the measured size values were quite similar, **1'** formed supramolecular structures (357.0 nm) slightly bigger than **1''** (322.9 nm) with polydispersity index (pdI) of 0.117 and 0.195 respectively. When oligopeptides **1'** and **1''** were mixed together, monodisperse structures were still detected by DLS (pdI 0.185), whose size (369.1 nm) was similar to that obtained by individual oligopeptides.
The stability of the oligopeptide assemblies (mixture of **1'** and **1''**) in foetal bovine serum (FBS) mimicking the in vivo conditions, was also tested (Fig. 1.1.20b) in order to evaluate if the self-assembly system could be used as a drug carrier. The DLS analysis exhibited that the peak of the supramolecular assemblies in pure FBS was clearly visible. This suggested that the interaction with FBS proteins did not affect the overall structure of the

supramolecular assemblies which appeared stable under physiological mimicking conditions without substantial changes in their size.

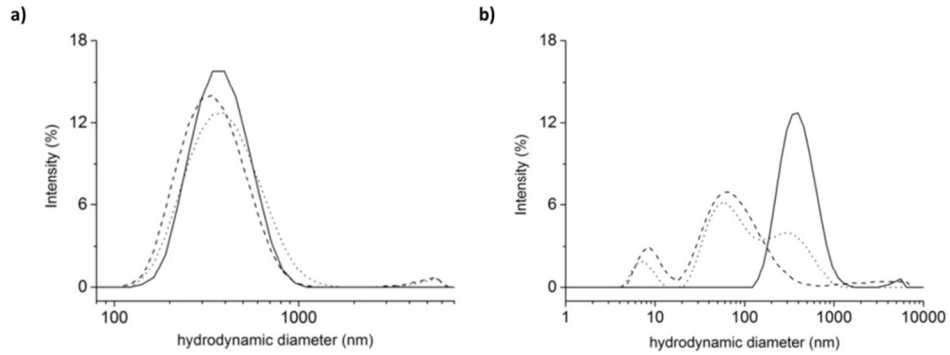

Figure 1.1.20. a) Size distribution by intensity in water of **1'** (straight) and **1''** (dash) oligopeptides, as well as their 1:1 mixture (dot). b) Size distribution by intensity of the mixture of **1'** and **1''** suspended in FBS (dot). As a control, FBS (dash) and the mixture of **1'** and **1''** in water (straight) were analysed. Mean results are given for three different measurements

To further investigate the morphology of the supramolecular assemblies, the mixture of **1'** and **1''** was analysed by TEM. The assemblies showed spherical shape with diameters ranging from 30 to 60 nm (Fig. 1.1.21). The discrepancy between TEM and DLS data could arise from the formation of agglomerates (i.e. weakly bound aggregates) of the assemblies in suspension to minimize interfacial energy.

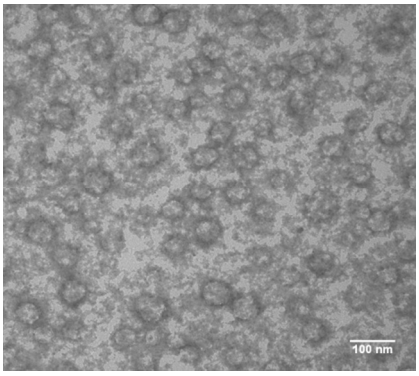

Figure 1.1.21. TEM micrograph of the 1:1 mixture of oligopeptides **1'** and **1''**. The suspension of peptides (5mg/ml) was deposited on a copper grid, then negative staining was performed using saturated uranyl acetate in 20% ethanol

Finally, the critical aggregation concentrations (CACs) of **1'** and **1''** in aqueous solution were determined by DLS. Different samples with increasing concentration of either **1'** and **1''** were prepared and their intensity of scattered light was monitored. The experimental

data showed that samples with concentration higher than 5.0 and 26.0 mg/mL for **1'** and **1''**, respectively, led to a decrease in the count rate value. This suggested that the assemblies' concentration increased up to an optimal value and then decreased, probably due to altered interactions between the involved oligopeptides.

Since the conformational studies of peptides **2'**, **2''**, **3** and **4** have showed high similarity in the secondary structures compared to peptides of **1'** and **1''**, DLS analysis in water was also performed (Fig. 1.1.22). All peptides are able to self-assemble at the concentration of 5.0 mg/ml in reproducible way but slightly differences in the dimensions of aggregates were observed. The smallest assemblies were obtained with peptide **4** with measured size value of 232 nm and PdI of 0.42. On the other hand, peptide **2''** gave the biggest aggregates (average size: 470 nm; PdI: 0.33). Peptides **2'** and **3**, instead, have formed supramolecular assemblies of comparable dimensions with measured size values of 326 and 314 nm and PdI of 0.28 and 0.20 respectively.

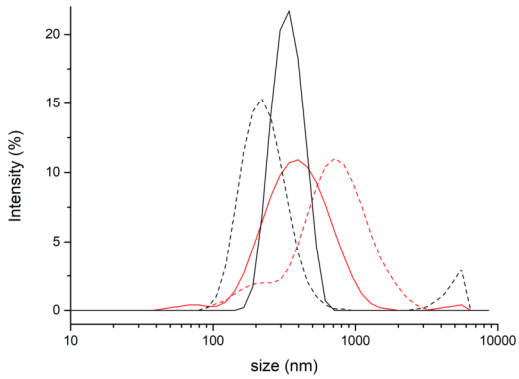

Figure 1.1.22. Size distribution by intensity in water of peptides **2'** (straight red), **2''** (dash red), **3** (straight black) and **4** (dash black). Mean results are given for three different measurements.

The self-assembly ability in water of C-terminus modified peptides **5**, **6** and **7** at the concentration of 5.0 mg/ml, was investigated using DLS (Fig. 1.1.23). Peptides **5** and **7** are able to self-assemble in reproducible way and they form supramolecular aggregates with similar hydrodynamic diameter values (**5**: 275 nm PdI 0.26; **7**: 282 nm PdI 0.21). Peptide **6**, instead, did not give reproducible data. As shown in figure 16b, repeated analyses showed, in some cases, a monomodal distribution with measured size values of 212 nm (PdI 0.38), in other cases, two different populations of aggregates with dimensions of 381 nm and 83 nm (PdI 0.58).

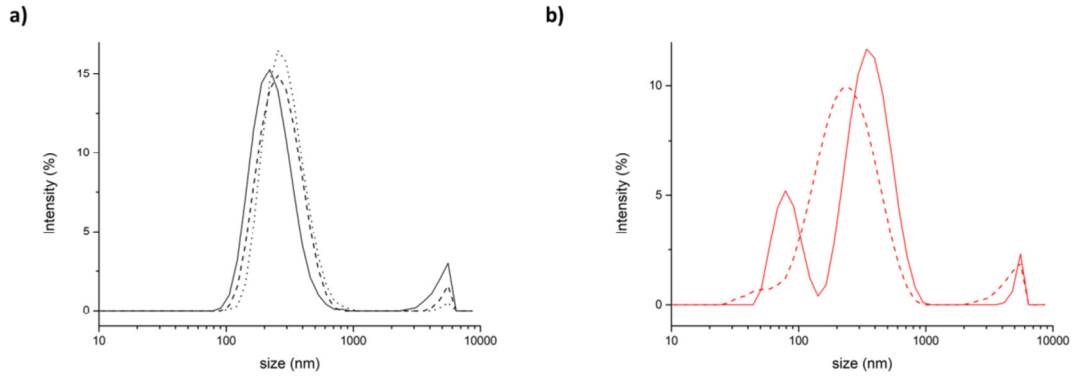

Figure 1.1.23. Size distribution by intensity in water of peptides a) **4** (straight black), **5** (dash black), **7** (dot black) and b) **6** (straight and dash red). Mean results are given for three different measurements (black)

Summarizing, DLS results highlighted that all synthesized peptides are able to form supramolecular assemblies in water. In aqueous environment all these compounds show the same non-ordered secondary structure, so the high or less propensity to give helical structure in methanol doesn't affect the self-assembly ability. Modifying amino acid in position 2, aggregates with different hydrodynamic diameter have been obtained, probably due to a different packaging of the molecules. Regarding modifications on C-terminus, only peptide **6** (CONHMe) shows a different behaviour since its aggregates are not stable but in a dynamic equilibrium. The hydrophobic nature of peptide molecules may suggest that the aggregates have a hydrophobic core. This hypothesis is verified with the work described in Part II, where a hydrophobic molecule (curcumin) has been encapsulated within aggregates of peptide **4**.

Conclusion

In this work, several pentapeptides containing different C^{α} tetra substituted amino acid in position 2 were synthesized and the experimental data were collected in CD_3CN and in CD_3OD confirmed a conformational preference toward a stable 3_{10}-helical structure for all of them. Conformational studies were performed also in H_2O/D_2O where, instead, a helix/random coil transition is still observed. Then, starting from the simplest pentapeptide **4**, some analogues with different C-termini were synthesized, aiming to evaluate any possible influence of the C-terminus substitution. A stable helical conformation in methanol was established only for the peptides with carboxamide group at C terminus. This is a confirmation that amide plays a central role in secondary structure stabilization and carboxyamide pentapeptides seem to be the best helix inducers among the other pentapeptides with different C-termini.

The most interesting aspect of these ultrashort peptides is their ability to form supramolecular assemblies of spherical shape in water, allowing the availability of these peptides for several applications.

Part II

Introduction

Self-assembly mechanism in Drug Delivery

Self-assembly of small molecules in complex supramolecular structures provides a new strategy in the development of materials in drug delivery applications. The low aqueous solubility is the major problem linked to the formulation of new chemical entities since more than 40% of these molecules developed in pharmaceutical industry are practically insoluble in water. The consequences of a low solubility are slow drug absorption that leads to insufficient bioavailability and possible gastrointestinal mucosal toxicity. For oral drugs, solubility is the most important parameter to achieve the desired concentration in systemic circulation for pharmacological response. Various techniques are used to increase the solubility of poorly soluble molecules which include physical and chemical modifications of drug, particle size reduction, salt formation, solid dispersion, use of surfactant, complexation, and so forth.[33] In recent years, research about self-assembled systems has gained increasing attention as they have demonstrated potential application in drug delivery due to their many advantages including improving solubility of drugs, biocompatibility, biodegradability, high efficiency for drug loading, reducing drug toxicity, controlling drug release rate and protection against biochemical degradation.[34] Several types of self-assembled structures have been studied to develop new drug carriers involving micellar, hydrogels, vesicles, polymers, microcapsules, lipoproteins, liposomes, cubosomes, colloidosomes, etc.[35] Among different biomaterials that can be used to fabricate ordered structures, peptides remain one of the most promising for many reasons.[36] They are easily synthesized using solid-phase methods where the peptide sequence could be specifically modified at molecular levels.[37] In this way, naturally occurring structures such as α-helices and β-sheets can be easily stabilized and exploited for driving the self-assembly processes and modulating the shape and dimension of the aggregates.[38]

In literature, there are many examples of self-assembled peptides that found application in several fields of drug delivery [39] and some of them are here summarized. Recent studies reported the ability of the Fmoc-FFRGDF peptide to self-assemble into transparent hydrogel consisting in beta sheet fibrils with a width of 20 nm, which exhibit biocompatibility in rabbit eyes as an implantable delivery system for the treatment of ocular anterior diseases such as glaucoma and keratopathy.[40] In another study, a peptide-

based system was designed attaching the heparin-binding sequence domain to a self-assembled motif in order to obtain nanofibers that act as drug carriers for cardiovascular diseases.[41] Sadatmousavi et al. showed that the peptide AC8 (FEFQFNFK) self-assembles in aqueous solution to form 100 nm particles and can encapsulate ellipticine (0.05 mg/ml). This complex showed evidence in killing both human breast cancer cells (MCF-7) and adenocarcinomic human alveolar basal epithelial cells (A549) after 48 h.[42] Furthermore, self-assembled peptide hydrogels have been modified by adding phosphoserine or RGD residues to improve mineralization and cell adhesion, respectively.[43]

Curcumin: water insoluble drug model

Curcumin [1,7-bis(4-hydroxy-3-methoxyphenyl)-1,6-heptadiene-3,5-dione] is a yellow orange polyphenol. It is the main curcuminoid in the rhizome of Turmeric (*Curcuma longa)*, which is a member of the ginger family, *Zingiberaceae.* Curcumin possesses two isomers, enol form and β-diketone form due to the presence of α,β-unsaturated β-diketone moiety. Enol form has a strong internal hydrogen bond and an extended conjugation of the molecular backbone compared with the diketone form (Fig. 1.2.1). The enol form is more stable in solution and the enolic proton is the most easily dissociated;[44] this evidence explains the radical-scavenging mechanisms of curcumin in Alzheimer's diseases where it blocks amyloid-β aggregation.[45]

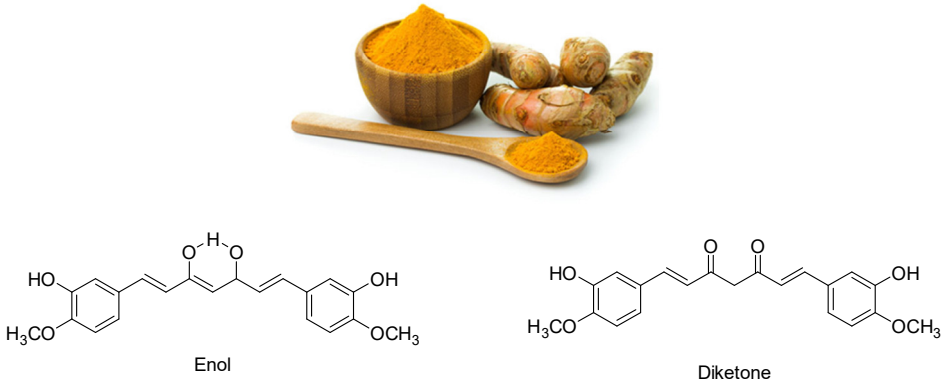

Figure 1.2.1. Curcumin powder from rhizome of Turmeric and molecular structure of curcumin (enol and diketone forms)

In recent years, the interest toward this pigment has considerably increased due to its several biological and pharmacological properties, including antioxidant, antitumor, anti-inflammatory, antibacterial, antifungal, antiviral and anticoagulant activities.[46] Moreover, curcumin is toxicologically relatively inert even at high doses, in fact it was found that it is non-toxic for humans up to the dose of 10 g/die.[46c, 47] Despite all these advantages, its clinical use is limited by its extremely poor bioavailability, which is a consequence of a poor solubility and high instability in aqueous solution, in particular in alkaline pH. It has been found that in aqueous solution the absorption intensity of curcumin rapidly decreases in a time period of 30 minutes, reflecting its high degradation level. In phosphate buffer (pH=7.4) the level of degradation is reported to be more than 80% after 1 h.[48]

Several attempts have been made to increase its aqueous solubility and stability through encapsulation of curcumin in supramolecular structures. Most methods imply the use of surfactant micelles formed by the common non-ionic surfactants like Tween (TW) 20, TW80 or the cetyltrimethylammonium bromide (CTAB).[49] Sarkar and co-workers proposed a delivery system consisting of noisomes formed from TW20 and cholesterol which seem more effective than the conventional surfactants forming micelles.[50] In another work, a comparison between the chitosan-TW80 system and the chitosan-CTAB system was carried out evaluating the binding constant between chitosan and curcumin.[51] Other standard methods regard the use of polymeric nanoparticles,[52] hydrogel,[53] liposomes,[54] cyclodextrines.[55]

In recent years, peptide-based self-assembled structures have emerged as a powerful approach for developing curcumin delivery systems due to their biocompatibility, biodegradability and easily tuning properties of the final structure. However, still few works regarding the use of peptides as curcumin delivery vehicles have been reported until now. Pochan and co-workers exploited the hydrogel technology to develop injectable drug delivery vehicle,[56] while Alam and Panda studied the formation of peptide nanoparticles from a dipeptide containing dehydrophenylalanine to enhance the cellular uptake of curcumin.[57] Chatterjee and co-workers reported the concentration-dependent self-assembly mechanism of a tripeptide containing Trp residue which forms nanospheres exploited to encapsulate the drug. They demonstrated that upon forming the nanospheres, in the presence of curcumin, the encapsulation occurs. On the other hand, when curcumin is added to nanospheres, it is intercalated on the surface instead of being encapsulated in the spheres.[58]

Aim of the project

I performed this part of the project at Fondazione Unimi, in collaboration with Dr. Simona Argentiere and Prof. Cristina Lenardi.

The goal is to propose a peptide-based carrier system for water insoluble molecules. On the basis of the chemical studies reported in part I, peptide **4** (Fig. 1.2.2) was selected because it is easy to synthesize in solid phase, with low costs of production and it is completely characterized both in liquid and in solid state. Moreover, the Ala-Aib oligomers are a very well-known and consolidated self-assembly system which is metabolic stable due to the presence of the non-natural residues Aib.

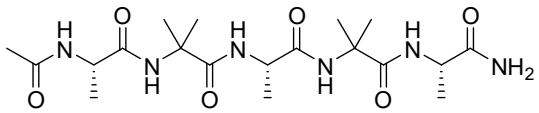

Figure 1.2.2. Molecular structure of peptide **4**

As water insoluble drug model, curcumin was used for its safety, pharmacological activities and fluorescence properties easily detectable using standard techniques. Two different approaches were used to study the interaction between curcumin and peptide aggregates. In the first approach peptide aggregates are formed in the presence of curcumin (physical entrapment), while in the second approach curcumin is added to the already formed peptide aggregates (Partitioning) (Scheme 1.2.1).

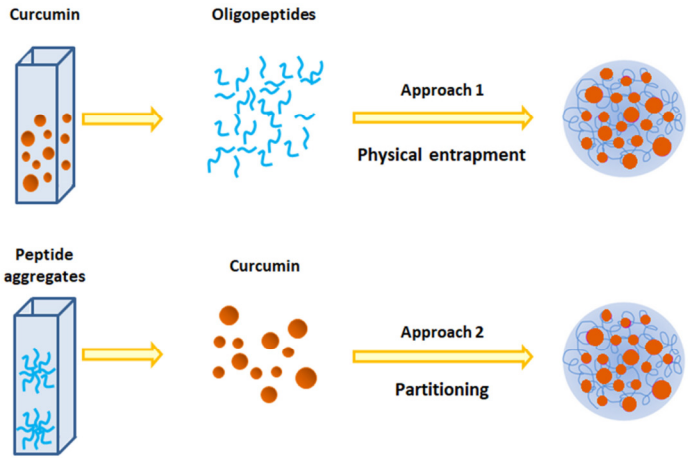

Scheme 1.2.1. Schematic representation of the two different approaches

The morphology of aggregates was studied using DLS and TEM. The interaction of the drug molecules with the peptide aggregates was studied using the absorption and the intrinsic fluorescence emission of the drug.

Results and discussion

Morphology characterization of peptide aggregates

The morphology of the peptide **4** assembly at the concentration of 5.0 mg/ml was deeper investigated using DLS and TEM in aqueous solution. All DLS measurements were run on freshly prepared peptide solutions and the formation of self-assembled supramolecular structures was found to be fully reproducible.
DLS analysis (Fig. 1.2.3) showed that peptide **4** aggregates both in water and in 10 mM phosphate buffer (PBS). Although the measured size values were quite similar, in PBS the supramolecular assemblies (290 nm) were slightly bigger than in water (232 nm).

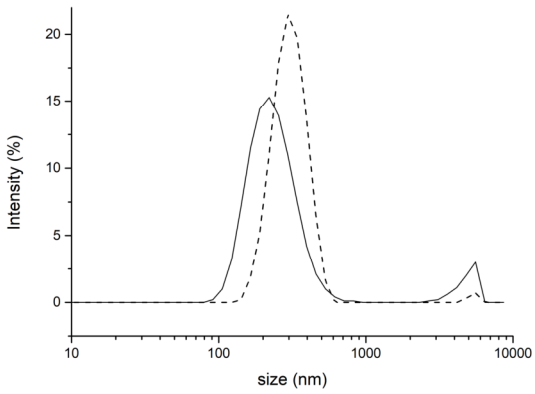

Figure 1.2.3. DLS results. Size distribution by intensity of peptide **4** in water (straight) and in PBS (dash). Mean results are given for three different measurements

Transmission Electron Microscopy (TEM) confirmed that peptide **4** self-assembled in the aqueous medium into highly ordered aggregates of spherical shape with nanometric dimensions (Fig. 1.2.4). The average aggregate diameter (255 nm) was obtained by measuring about 150 particles by using Image-J software. The average size measured with TEM is perfectly in line with the data obtained with DLS.

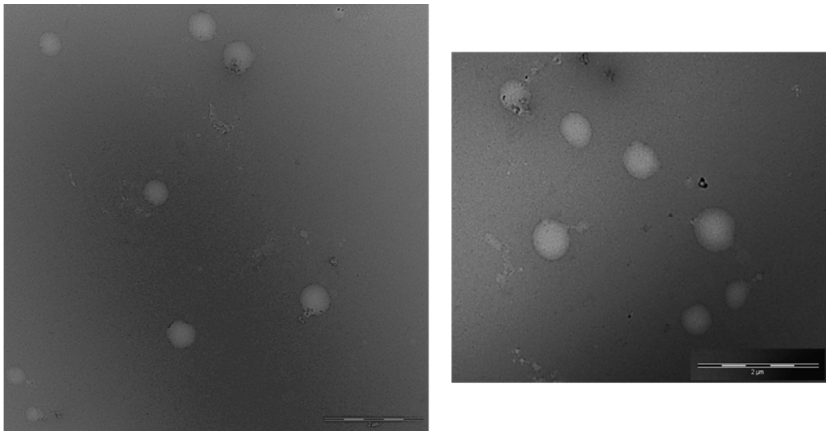

Figure 1.2.4. TEM micrographs of the self-assembled structures formed by peptide **4** in water (scale bar 2 μm). The suspension of peptide **4** (5mg/ml) was deposited on a copper grid, then negative staining was performed using saturated uranyl acetate in 20% ethanol

Encapsulating system formulation

Curcumin was dissolved in DMSO (1 mg/ml) and then was diluted in 10 mM PBS (pH=7.4) or in water until reaching a concentration of 9.6 μM. Both aqueous solutions, containing minimum amount of DMSO (0.34%), showed the maximum absorption band at 428 nm and a shoulder at 348 nm, while the fluorescence spectrum exhibited a fluorescence band at 554 nm after excitation at 430 nm (Fig. 1.2.5).

The band at 428 nm of the absorbance spectrum is assigned to the π-π* transitions in the enolic form in solution while the shoulder at 348 nm is due to the nonplanar diketo form and it appears in aqueous solution as a result of a strong interaction between water molecules and curcumin.[44, 59]

On the other hand, the position of the emission spectrum peak is found to be largely affected by the polarity and hydrogen bonding ability of the surrounding microenvironments. It has been reported that in hydrophobic macromolecular environment, the fluorescent intensity significantly increases with a blue-shift of about 80 nm.[53] This means that the greater is the interaction with water, the lesser will be the extent of blue-shift and the emission quantum yield.[50, 60]

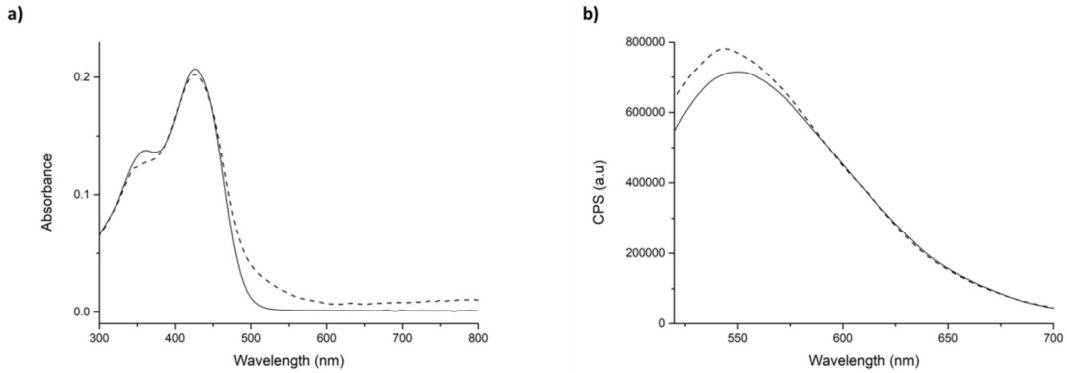

Figure 1.2.5. a) Absorption and b) fluorescence spectra of curcumin (9.6 μM) in water (straight) and PBS (dash) with 0.34% of DMSO

The position of the peak in the absorption and emission spectra of curcumin are completely independent from the concentration and pH of the aqueous solution (Fig. 1.2.6). This is an important point since the intrinsic acidity of peptide **4** reduces of one unit the pH in water.

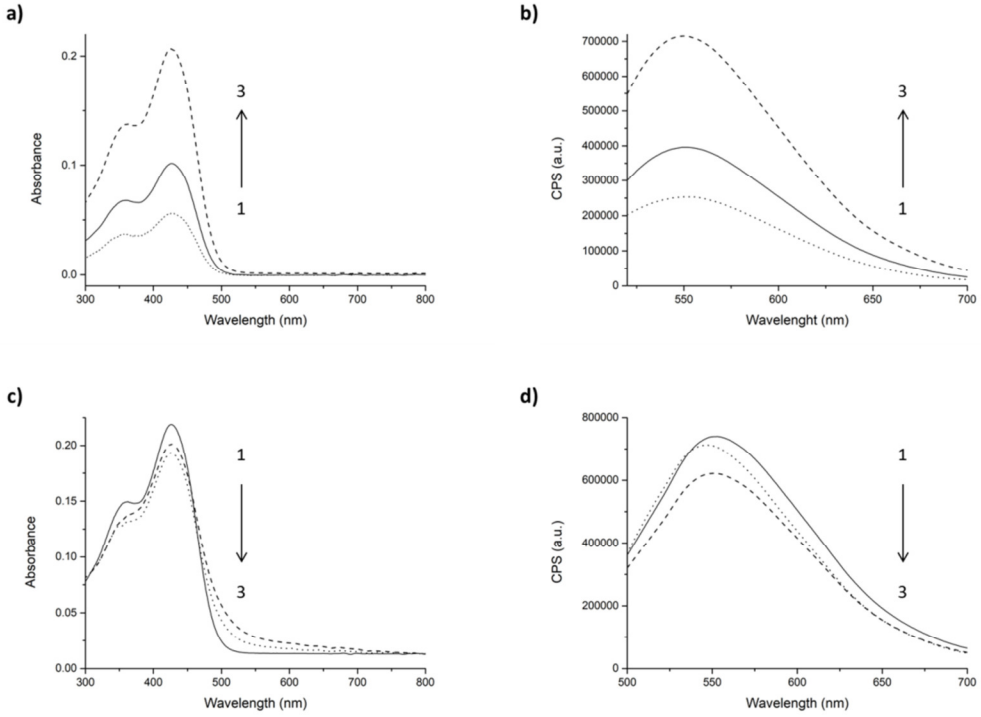

Figure 1.2.6. a) Absorption and b) fluorescence spectra at different concentrations of curcumin: (1) 2.4 μM (dot), (2) 4.8 μM (straight), (3) 9.6 μM (dash) in water with 0.34% of DMSO. c) Absorption and d) fluorescence spectra of curcumin at decreasing pH in water with 0.34% of DMSO

Since the curcumin solution contains a minimum amount of DMSO which is 0.34%, before starting the encapsulation experiments, the behaviour of peptide aggregates in the presence of such amount of DMSO was studied, to exclude any variation. The DLS analysis (Fig. 1.2.7) showed that this tiny amount of DMSO doesn't affect the average dimensions of aggregates which were 270 nm with a PdI of 0.45. Also the ζ potential was measured with and without DMSO but we any significant differences were observed. In fact the ζ potential of peptide suspension in PBS is -22.8 mV, while for the peptide suspension in PBS with 0.34% of DMSO is -19.3 mV.

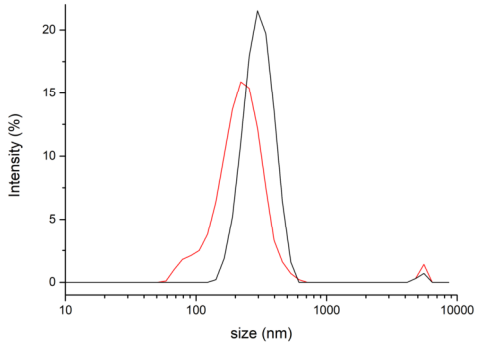

Figure 1.2.7. Size distribution by intensity of peptide **4** in PBS (black) and in PBS with 0.34% of DMSO (red). Mean results are given for three different measurements

According to all these results, the following experiments were conducted using 10 mM solution of PBS for both the peptide and curcumin since the buffer helps to maintain a constant pH also in presence of the peptide; moreover, the osmolality and ion concentrations are isotonic with the solutions in the human body. The final concentration of peptide suspension is 5 mg/ml while the final concentration of curcumin is 9.6 μM and it contains 0.34% of DMSO which is an amount that affects neither the PBS solution osmolality nor the self-assembly of the peptide.

Encapsulation approaches

In the first approach (physical entrapment), peptide aggregates were formed in the presence of curcumin solution (Scheme 1.2.2).

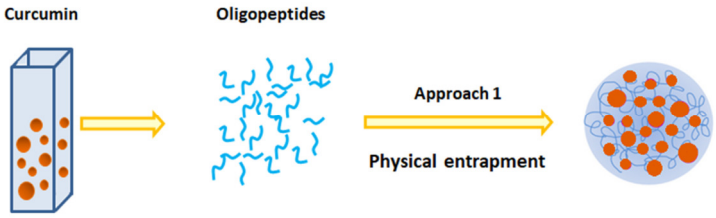

Scheme 1.2.2. Scheme of physical entrapment approach

Peptide **4** (5mg/ml) was added to 9.6 μM curcumin solution. The mixture was stirred for 1 hour at 25°C, and then the absorption and the intrinsic fluorescence emission of curcumin were measured. Figure 1.2.8 shows the absorption and fluorescence spectra of curcumin upon being incubated with the peptide. After the addition of peptide, the absorbance of curcumin decreased a lot and both the peaks at 428 and 348 nm were detected. The fluorescence emission instead was quenched. In fact it was measured a blue-shift of 20 nm, which indicated the interaction of the drug with the peptide. However, in this approach, the interaction between curcumin and the aqueous environment seems to be still high.

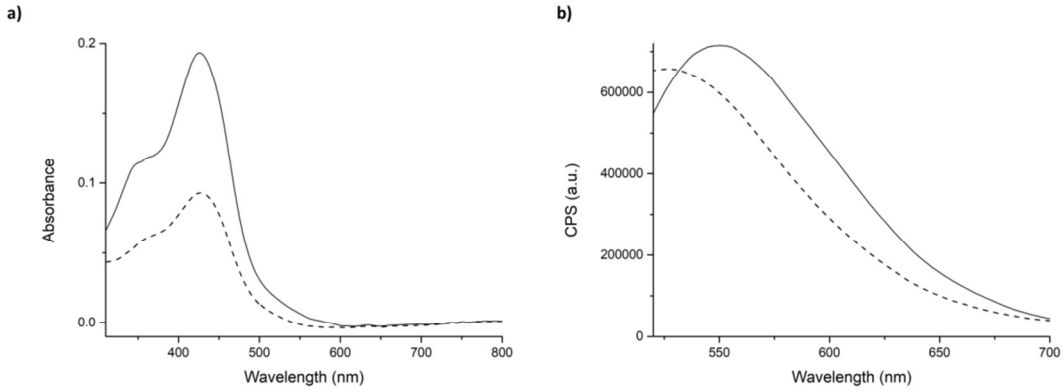

Figure 1.2.8. Physical entrapment approach. a) Absorption and b) fluorescence spectra of curcumin (9.6 μM) in PBS (straight) and in presence of 5mg/ml of peptide **4** (dash)

The DLS measurements exhibited relevant differences with respect to the control peptide (Fig. 1.2.9). The hydrodynamic diameter of aggregates in presence of curcumin increased until reaching size value of 560 nm with a PdI of 0.35. Also the ζ potential was measured but only a slight increase was observed (from - 19.3 to - 15.3 mV).

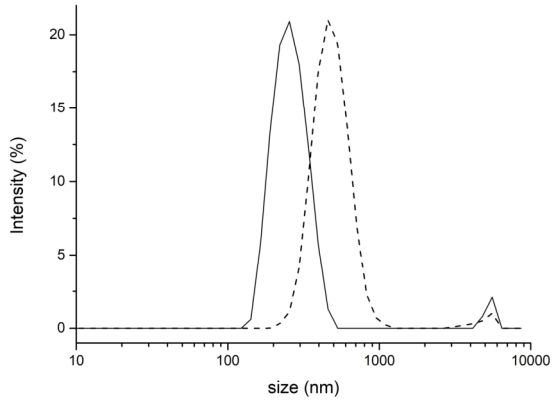

Figure 1.2.9. Physical entrapment approach. Size distribution by intensity of peptide **4** alone (straight) and in presence of curcumin (dash). Mean results are given for three different measurements

In the second approach (partitioning) curcumin is added to the peptide aggregates (Scheme 1.2.3).

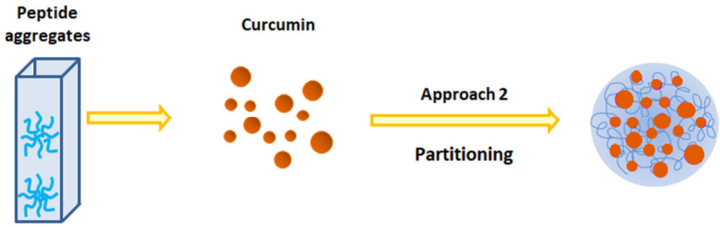

Scheme 1.2.3. Scheme of partitioning approach

Curcumin solution in DMSO (1mg/ml) is added to pre-formed peptide **4** aggregates in order to have a final curcumin concentration of 9.6 μM. The mixture was stirred for 1 hour at 25°C, and then the absorption and the intrinsic fluorescence emission of curcumin were measured. Figure 1.2.10 shows the absorption and fluorescence spectra of curcumin upon being incubated with the peptide. In this case, the absorbance spectrum showed a slightly increase of intensity of the peak at 428 nm, while the shoulder at 348 nm was barely visible, suggesting stronger binding of the hydrogen bond cis-enol with the peptide rather than with water molecules. The fluorescence emission confirmed that curcumin less

interacted with water since its surrounding environment was more hydrophobic. In fact, the fluorescence intensity significantly increased with a blue shift of 20 nm.

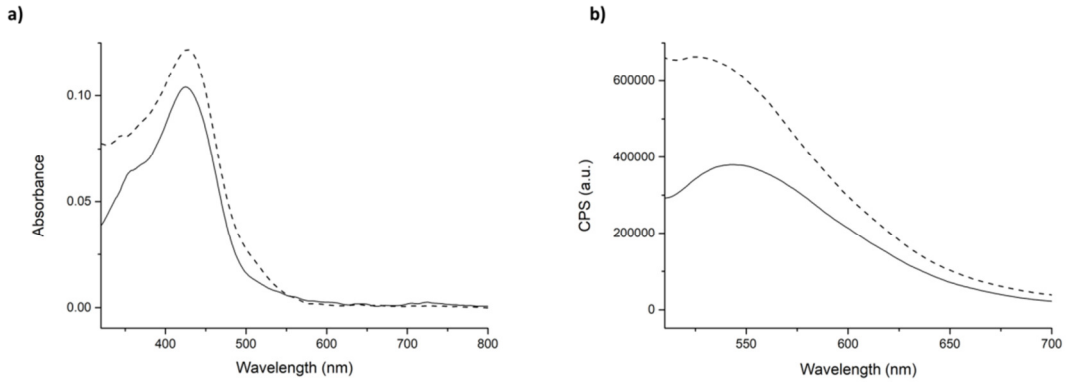

Figure 1.2.10. Partitioning approach. a) Absorption and b) fluorescence spectra of curcumin (9.6 μM) in PBS (straight) and in presence of 5mg/ml of peptide **4** (dash)

DLS analysis exhibited differences with respect to the previous approach. In the presence of curcumin the peptide formed aggregates slightly bigger than the control with hydrodynamic diameter value of 340 nm and a PdI of 0.24 (Fig. 1.2.11). The ζ potential is a bit more negative than the control (- 24.7 rather than – 19.3 mV).

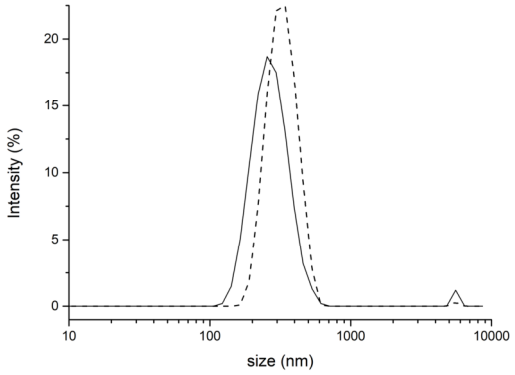

Figure 1.2.11. Partitioning approach. Size distribution by intensity of peptide **4** alone (straight) and in presence of curcumin (dash). Mean results are given for three different measurements

Based on the results obtained with the two different approaches, the following hypothesis has been put forward: i) with partitioning approach (approach 2), curcumin seems to be

encapsulated within the peptide aggregates. For this reason, the fluorescence and absorption intensity enhanced, suggesting an increase of curcumin stability due to a poor interaction with water molecules. The hydrophobic environment around curcumin is proved by the decrease in absorbance of the shoulder at 348 nm and by the increase of the fluorescence emission, ii) with the physical entrapment approach (approach 1), the appreciable decrease of the absorbance which, however, maintained the shoulder at 348 nm, suggested that curcumin wasn't entrapped within the aggregates, but that only slight superficial interaction with peptide aggregates occurred. This might be proved by the enhancement of the hydrodynamic diameter which is influenced by the presence of curcumin on the surface. Figure 1.2.12 gives a schematic representation of our hypothesis.

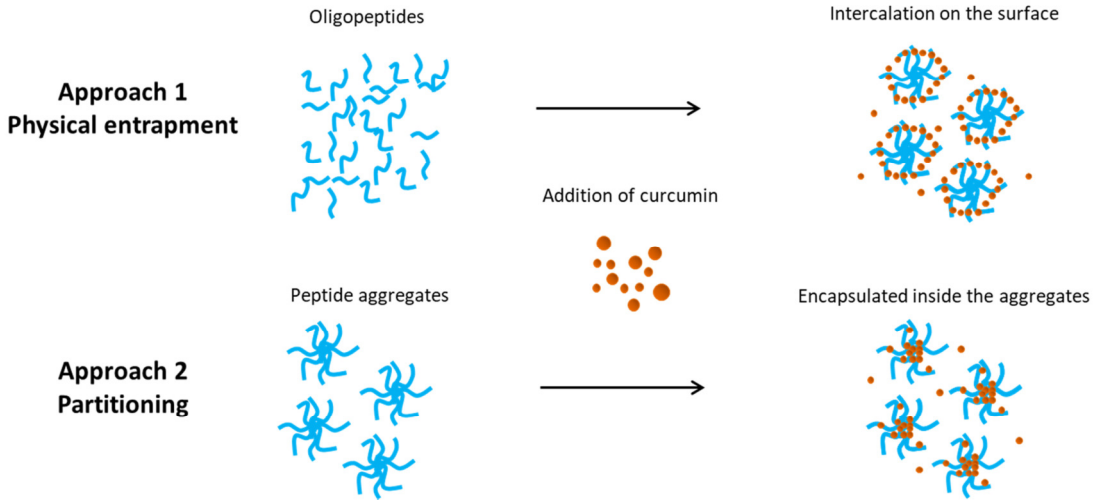

Figure 1.2.12. Schematic representation of interaction between curcumin and peptide aggregates in physical entrapment and partitioning approaches.

In order to verify our hypothesis, Tween 20 (TW20) was added to the mixtures. TW20 is a non-ionic surfactant which is an important constituent in pharmaceutical formulation since it allows maintaining good sink condition.[50] The strong interaction between TW20 (0.005%) and curcumin induced an intense enhancement of fluorescence intensity along with the blue-shift in the emission spectra. In the absorbance spectrum the shoulder at 348 nm completely disappeared (Fig. 1.2.13).

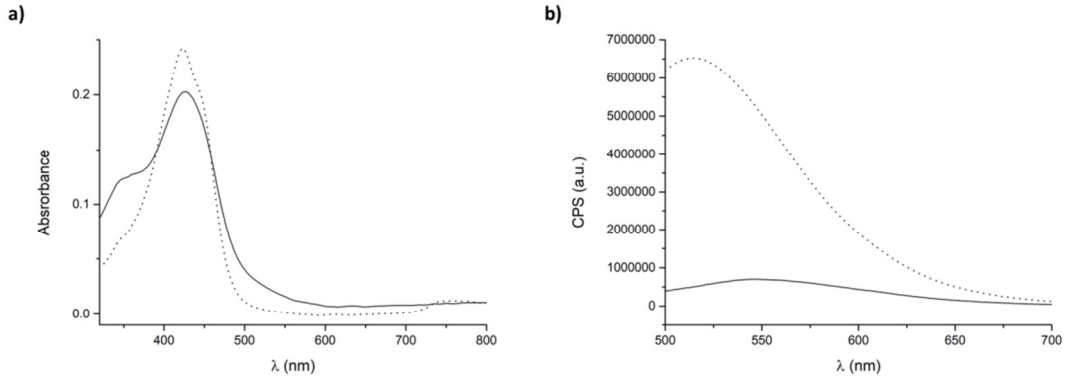

Figure 1.2.13. a) Absorption and b) fluorescence spectra of curcumin (9.6 μM) in PBS (straight) and in presence of 0.005% of TW20 (dot)

In our experiments, we prepared the mixture of peptide and curcumin using the two different approaches and, after 1 hour of incubation, we added 0.005% of TW20.

In the first approach, the physical entrapment, the addition of TW20 to the mixture induced huge fluorescence amplification and a blue-shift of the emission peak of about 30 nm. The absorbance, instead, has slightly been reduced (Fig. 1.2.14).

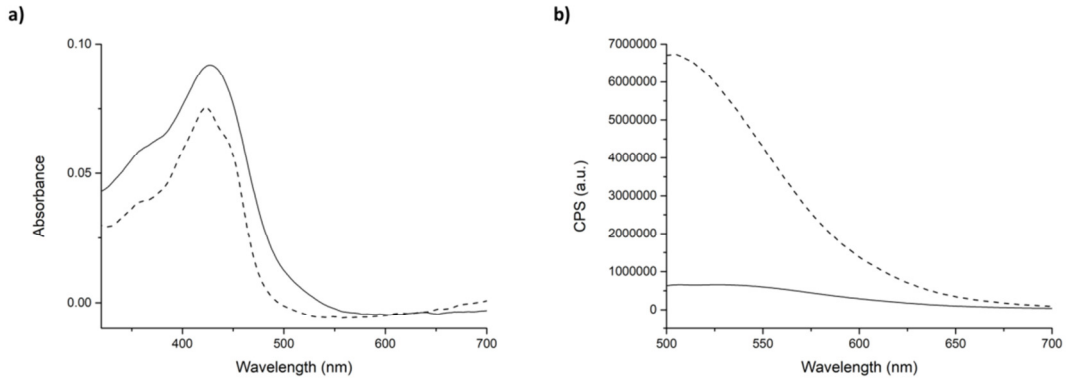

Figure 1.2.14. Physical entrapment. a) Absorption and b) fluorescence spectra of curcumin (9.6 μM) in presence of 5 mg/ml of peptide **4**, before (straight) and after (dash) the addition of 0.005% of TW20

DLS analysis showed that after the addition of TW20, the average hydrodynamic diameter of peptide aggregates was reduced until the normal value of 270 nm (Fig. 1.2.15). This could mean that curcumin interacts stronger with TW20 rather than with peptide. In fact the fluorescence emission of curcumin after the addition of surfactant is exactly the same

with or without peptide. As the curcumin interacted with TW20, the surface of peptide aggregates was released and the average size returned to the initial values.

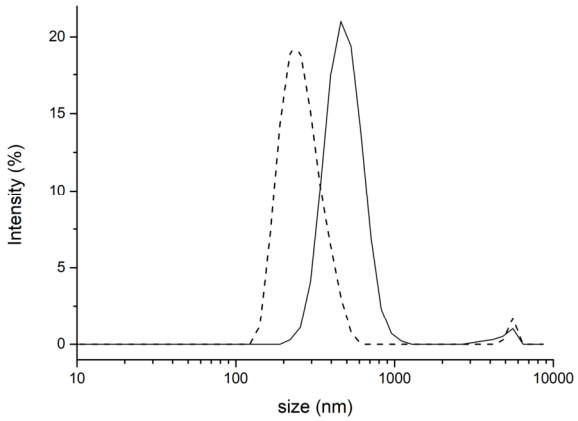

Figure 1.2.15. Physical entrapment approach. Size distribution by intensity of peptide **4** in presence of curcumin before (straight) and after (dash) addition of TW20. Mean results are given for three different measurements

In the second approach, partitioning, the enhancement of fluorescence intensity after the addition of TW20 to the mixture was much less intense than in the previous case (Fig. 1.2.16). Our hypothesis is that only the curcumin, which hasn't been encapsulated within the peptide aggregates, interacted with TW20.

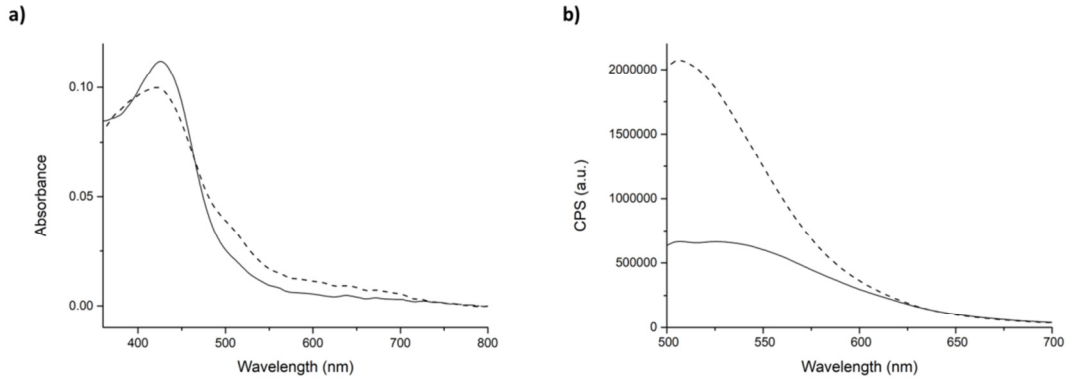

Figure 1.2.16. Partitioning. a) Absorption and b) fluorescence spectra of curcumin (9.6 μM) in presence of 5 mg/ml of peptide **4**, before (straight) and after (dash) the addition of 0.005% of TW20

The average hydrodynamic diameter with the second approach didn't change also after the addition of TW20 (Fig. 1.2.17).

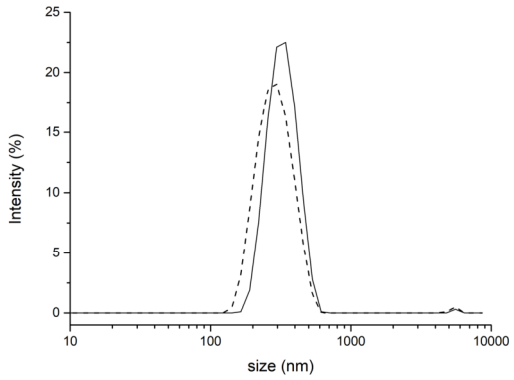

Figure 1.2.17. Partitioning. Size distribution by intensity of peptide **4** in presence of curcumin before (straight) and after (dash) addition of TW20. Mean results are given for three different measurements

A further proof of curcumin encapsulation is given by confocal microscopy. Before the acquisition of the images, the samples were washed by Amicon Ultra® system (0.5 ml, 10K). After washing (0.8 rpm, 30 min), only the sample prepared with approach 2 gave fluorescent signals (fig. 1.2.18). No signals were detected with approach 1 since all curcumin was washed away with Amicon filtration. Once the encapsulation with approach 2 has been verified, the percentage of curcumin within the aggregates was measured by comparing fluorescence emission at 430 nm before and after washing. Peptide aggregates seem to be able to encapsulate around 50% of added curcumin.

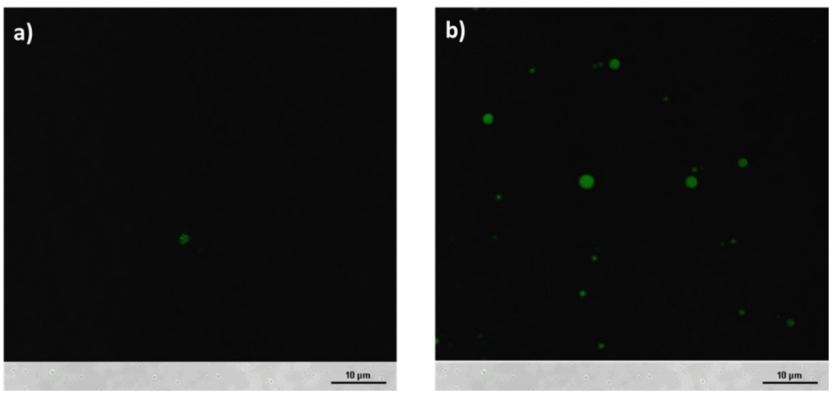

Figure 1.2.18. Confocal micrographs of sample prepared according a) approach 1 and b) approach 2.

Conclusion

In conclusion, peptide **4** is able to self-assemble in hydrophobic aggregates of spherical shape and their potential use for encapsulating water insoluble drugs was demonstrated. The results allowed hypothesizing that when curcumin interacts with peptide aggregates, the encapsulation occurs. On the other hand, when peptide aggregates were formed in presence of curcumin, the drug interacts with peptide molecules during the self-assembly process and remains exposed on the surface of the aggregates instead being encapsulated. This hypothesis has been verified using TW20 as sequestrate of free curcumin and by confocal microscopy. It is found that with approach 2 around 50% of added curcumin is encapsulated in the peptides aggregates. Further experiments about the quantification of encapsulated curcumin and the release studies are ongoing.

Part III

Gold Nanoparticles (AuNPs)

Nanotechnology is the science of materials and systems on a molecular scale. The aim is to create materials, devices, and systems with new properties and functions by engineering their small structure. This is the ultimate frontier to economically change materials properties, and the most efficient length scale for manufacturing and molecular medicine.[61]

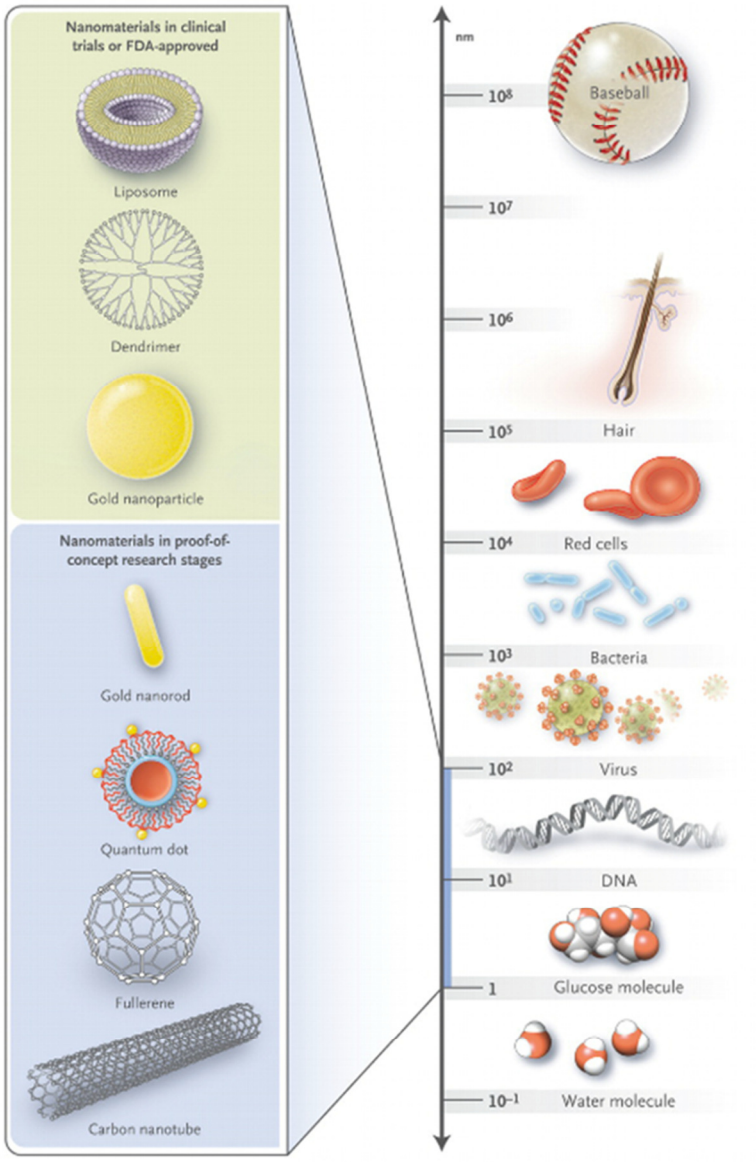

Figure 1.3.1. Object scale and nanomaterials in clinical trials or FDA-approved[62]

For the International System of Unit (SI), the metric prefix "nano" is added to indicate one billionth of a metre (10^{-9}), which is about 1/100000 of the thickness of a paper sheet. According to the U.S. National Nanotechnology Initiative (NNI), the size of a nanoparticle spans the range between 1 and 100 nm, including particles that are found in smoke or volcanic ash and that derive from anthropological sources. In biology, it is the scale of important cellular components such as DNA (about 2.5 nm of diameter), proteins (the diameter of haemoglobin is about 5 nm) and biological barriers (Fig. 1.3.1). Metallic nanoparticles have different physical and chemical properties from bulk metals (e.g., lower melting points, higher specific surface areas, specific optical properties, mechanical strengths, and specific magnetizations), properties that might prove attractive in various industrial applications. Since nanoparticles have the same scale of biological molecules, they also find important applications in medical field such as biosensors,[63] imaging agents,[64] drug carriers.[65]

The optical property is one of the fundamental attractions and an important characteristic of nanoparticles. For example, 20 nm AuNPs have a characteristic wine red colour, silver nanoparticles are yellow, while platinum and palladium nanoparticles are black. Not surprisingly, the optical characteristics of nanoparticles have been used from immemorial time in sculptures and glass painting. The most famous example is the dichroic glass of Lycurgus cup (4th century AD), that changes colour when held up to the light thanks to the presence of a small amount of metal crystals of Ag and Au with a diameter of about 70 nm.[66] The modern era of AuNPs began in 1857 with the work of Michael Faraday, who was possibly the first to observe that colloidal gold solutions have properties that differ from bulk gold.[67] The first ultramicroscopy experiments about size distribution of AuNPs were, instead, performed by Zsigmondy (Chemistry Nobel Prize 1925). Figure 1.3.2 shows his size classification of AuNPs. The different colour of suspension is a consequence of the different shape. Later, in 1951, Turkevich developed one of the most popular approach for preparing citrate-capped spherical AuNPs on a relatively large scale and with high degree of monodispersity. The citrate acts at first as reducing agent for gold (Au^{3+} is reduced to Au^0), then as stabilizer: citrate ions negatively charged are electrostatically adsorbed on the AuNP surface in order to prevent the nanoparticles aggregation.[68] Further studies conducted by Frens have shown the possibility to control nucleation and the particle size, varying the ratio between sodium citrate and $HAuCl_4$, synthesizing nanoparticles with diameters ranging from 5 to 250 nm.[69]

Figure 1.3.2. Size distribution of AuNPs performed Zsigmondy. The μμ notion is referred to nm. The particles range is from 0.2 to 2 nm (left) to 100-130 nm (right)

Many properties of nanoparticles arise from their large surface-area-to-volume ratio and the spatial confinement of electrons and electric fields in and around these particles. The large surface-area-to-volume ratio in nanoparticles may cause deviations from the usual bulk atomic arrangements and, consequently, greater chemical reactivity, greater tendency to reflect and refract light and greater conductivity are observed.[70] Among the numerous properties of AuNPs, a fundamental role is attributed to the surface plasmon resonance (SPR). SPR is an optical phenomenon arising from the interaction between an electromagnetic wave and the conductive electrons in a metal. This phenomenon occurs since the diameter of AuNPs is smaller than the light's wavelength; for this reason, under the irradiation of the light at a resonant frequency relative to the lattice of positive ions, the incident light is absorbed by the nanostructure. Some of this light is released with the same frequency in all directions and this process is known as scattering. At the same time, some of this light is converted into vibrations of the lattice and this process is referred to as absorption. In general, the SPR peak of a gold nanostructure should include both scattering and absorption components. The resonance is detectable due to the intense colour that is generated.[71]

The position and width of the gold SPR absorption maxima strongly depends on the size, shape and composition of AuNPs, as shown in figure 1.3.3, but depends also on the dielectric constant of the solvent, as described in the Mie's theory.[72]

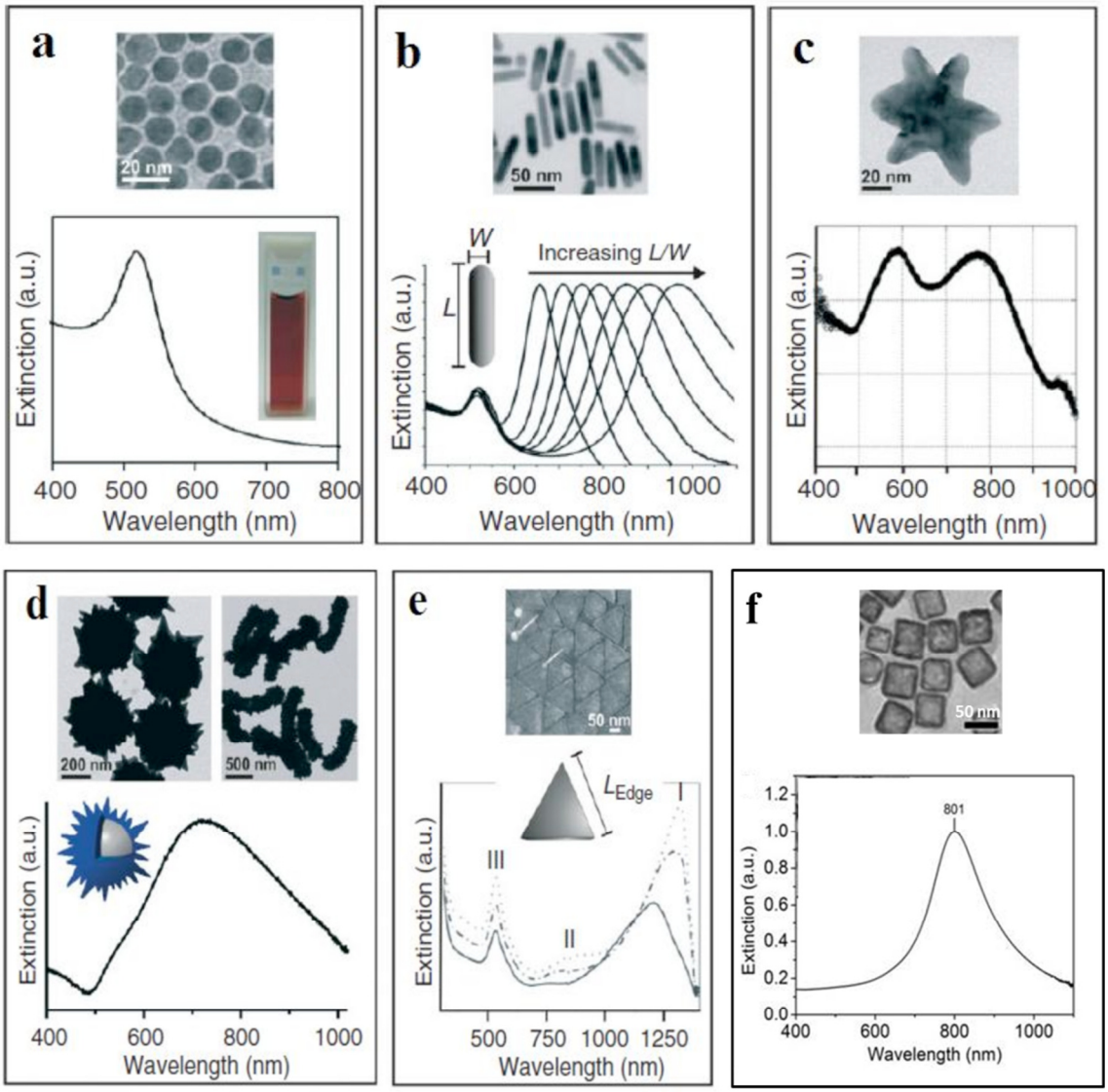

Figure 1.3.3. TEM micrographs and UV-vis absorption spectra of: a) spherical AuNPs of 13 nm; b) gold nanorods with different sizes; c) gold nanostars; d) gold nanoshells with spherical and rod core; e) nanoprisms with different sizes; f) gold nanocages

Moreover, the functionalization of AuNPs modifies the position and width of SPR absorption since this reaction changes the chemical and physical environment of the particle and consequently, its optical properties. The monitoring of the SPR signal is considered an easy method to control the functionalization reaction and the stability of AuNPs.[73]

Applications of AuNPs

Biological sensing. AuNPs, thanks to their optical-electronics properties and to the fact that they are amenable to the attachment of biomolecules or ligands through the well-known thiol chemistry, have become a very attractive tool for biological sensing. One example is the glucose sensing system studied by Geddes which is based on the aggregation and disassociation of 20-nm gold particles and the changes in plasmon absorption induced by the presence of glucose. The sensing platform could potentially be used to monitor μM → mM glucose levels in many physiological fluids, such as tears, blood, and urine, where the glucose concentrations are significantly different.[74] AuNPs have also been used as efficient sensors for the detection of different analytes such as metal ions, anions, and molecules like, saccharides, nucleotides,[75] proteins[76] and toxins.[77]

Imaging. Emerging nanotechnologies promise new approaches to early detection of metastatic cancer. El-Sayed and co-workers conjugated AuNPs with monoclonal anti-epidermal growth factor receptor (anti-EGFR) antibodies and, after incubation in cell cultures with a non-malignant epithelial cell line and malignant oral epithelial cell lines, they demonstrated that functionalized-AuNPs bind to the surface of the cancer type cells with 6 times greater affinity than to the non-cancerous cells.[78] The latest research achievements have developed bio-affinity probes based on AuNPs for molecular and cellular imaging and for early cancer detection. These technologies would have the ability to identify cancers that are much smaller than those detected with conventional imaging techniques.[79]

Selective targeting and hyperthermia. AuNPs provide a highly multifunctional platform not only for imaging, but also for diagnosis diseases and for selectively delivery. During my master thesis and in the first months of my PhD I was involved in a project about the use of gold nanoparticles for diagnosis and treatment of prostate cancer, published on *Bioconjugate Chemistry* [80] in collaboration with Prof. Romeo and Prof. Magni (University of Milan) and Dr. Svetlana Avvakumova and Prof. Prosperi (University of Milan-Bicocca). In this study, AuNPs were used for selective targeting of prostate cancer cells (PC3) via specific interaction between neuropeptide Y (NPY) receptor and three different NPY analogues conjugated to nanoparticles. Among numerous nanoparticles, gold nanocages (AuNCs) were chosen, which are versatile nanostructures characterized by hollow interiors and ultrathin porous walls, thanks to their unique optical properties associated

with a tuneable surface plasmon resonance (SPR). Moreover, AuNCs have been used as promising agents for non-invasive photothermal therapy taking advantage of the large absorption cross section in the near-infrared (NIR) region of the optical spectrum. Finally, their easy functionalization with thiol-containing molecules through Au–S covalent interaction make them excellent nanoconjugates for use as tumour targeting agents. Combined together, these features give rise to an efficient multifunctional nanotheranostics system able to label and detect cancer cells via specific targeting of molecular receptors and to induce their irreversible death through NIR-assisted hyperthermia (Fig. 1.3.4).

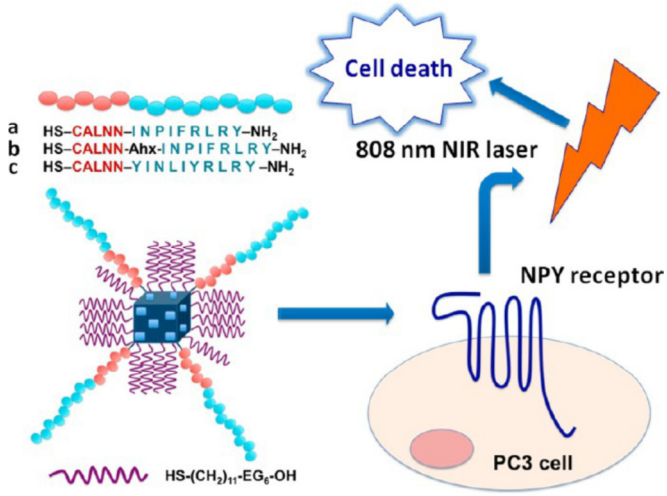

Figure 1.3.4.[80] Schematic representation of NPYR targeting on prostate cancer cells by peptide-functionalized gold nanocages and subsequent hyperthermia by NIR irradiation. Three kinds of AuNCs are considered, deriving from the surface functionalization with selected peptides, namely, a) Au-CALNN-INP, b) Au-CALNN-Ahx-INP, and c) Au-CALNN-YIN, respectively. Peptide sequences are sketched in the figure. The available surface of AuNCs was saturated by short PEG molecules, HS-$(CH_2)_{11}$-EG_6-OH

Peptide sequences contain a nanoparticle-binding motif (CALNN) and a NPY-binding motif. NPY-binding motifs were derived from the C-terminus NPY 25–36 fragment common recognition site for the receptor according to the results reported in the literature.[81] To prepare the three different batches of functionalized AuNCs, AuNCs were reacted with a mixture of each peptide and thiolated PEG to allow the capping-ligand exchange and Au–S bond formation. AuNCs functionalization resulted in a large shift of UV–vis plasmon absorption from 802 to 860 nm, slightly increased of hydrodynamic diameter and a less negative value of zeta potential compared to non-functionalized AuNPs.

To study receptor–ligand interactions, the assessment of signal transduction activation upon receptor binding approach was used. It was found that when peptide-conjugated nanoparticle binds to NPY receptor on PC3 cell, signalling cascade activation takes place. In particular, the experiment focused on the phosphorylation of the extracellular signal-regulated kinase (ERK), which is a pivotal step of the cytosolic signalling pathway associated with NPYR activation and we found that all Au-peptide NCs were indeed able to stimulate ERK activation, especially Au-CALNN-YIN NPs showed extremely high pERK/ERK ratios at short incubation time and a prolonged effect up to 60 min after incubation (Fig. 1.3.5).

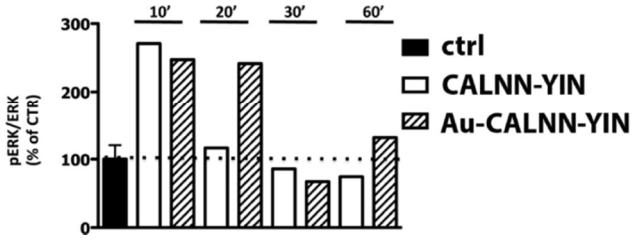

Figure 1.3.5. Time dependence of ERK phosphorylation in PC3 cells in response to specific NPYR targeting by nanocages decorated with CALNN-YIN peptide. Number of replicates, n = 3 (adapted from [80])

Then, the confocal scanning microscopy and TEM techniques were applied to investigate the internalization kinetics of NPY-conjugated AuNCs into PC3 cells and, as expected Au-CALNN-YIN NPs have the fastest internalization kinetics and they preferentially accumulated in lysosomes.

Then, the efficiency of targeted AuNCs inducing prostate cancer cell death via photothermal treatment was investigated. Once loaded with AuNCs, cancer cells were irradiated with NIR laser at ca. 800 nm wavelength showing a heating enhancement dependent on both the irradiation intensity and nanoparticle uptake. Cells treated with Au-peptide NCs were irradiated at 10 W/cm^2 showing extensive necrosis after 20 min. Not surprisingly, cell viability was mostly compromised in the case of Au-CALNN-YIN NPs even after 30 s of irradiation. By contrast, the irradiation of the untreated cells with the same laser power did not lead to cell death, confirming the safety of our experimental conditions. Morphological changes of cell cytoskeleton upon laser treatment were studied with SEM in order to have an idea of the cellular damage (Fig. 1.3.6).

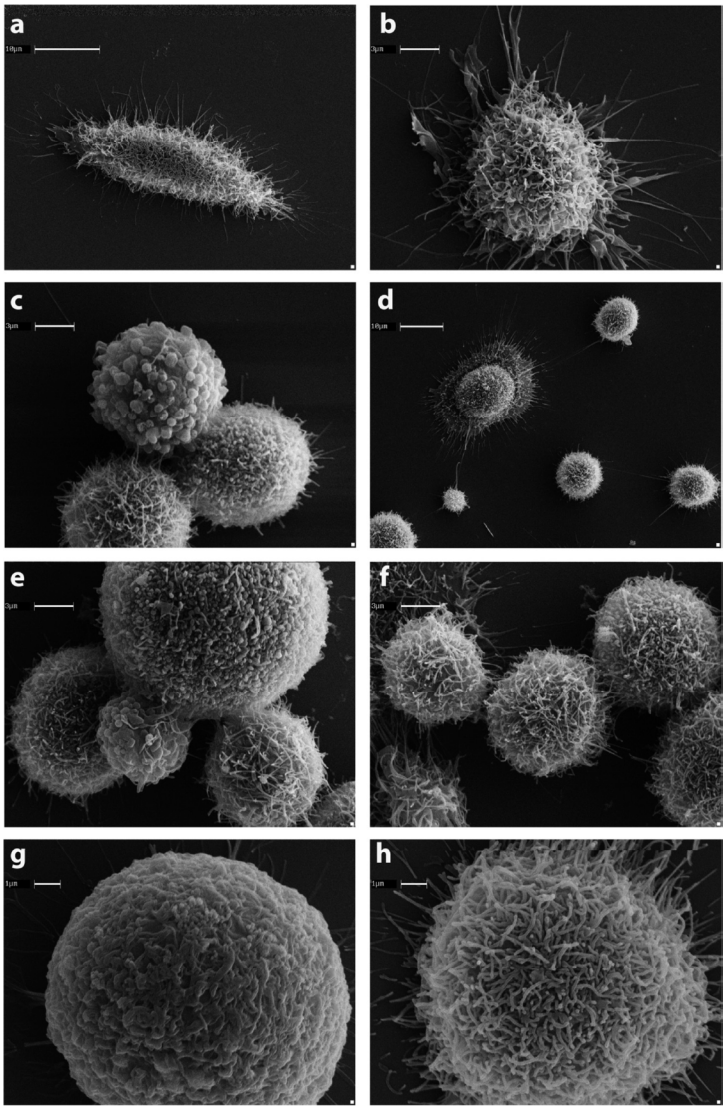

Figure 1.3.6.[80] SEM images showing PC3 cell morphology changes pre- and post-hyperthermia treatment with AuNCs: a) untreated PC3 cells, b) PC3cells irradiated with laser, c) PC3 cells incubated with Au-PVP NCs and irradiated with laser, d) PC3 cells incubated with Au-PVP NCs without laser irradiation, e) PC3 cells incubated with Au-CALNN-INP NCs and irradiated with laser, f) PC3 cells incubated with Au-CALNN-INP NCs without laser irradiation, g) PC3 cells incubated with Au-CALNN-YIN NCs and irradiated with laser, and h) PC3 cells incubated with Au-CALNN-YIN NCs without laser irradiation. Scale bars: (a,d) 10 μm; (b,c,e,f) 3 μm; (g,h) 1 μm

As shown in figure 1.3.6a,b untreated PC3 cells showed the presence of numerous characteristic microvilli on the cell surface both before and after exposure to NIR laser irradiation. In contrast, cells treated with Au-PVP NCs and exposed to NIR radiation (Fig 1.3.6c) showed some morphological changes, such as membrane blebbing and partial reduction in microvilli exposure which were indicative of apoptosis occurring. On the other hand, cells treated with Au-PVP NCs but not exposed to the laser did not exhibit

evidence of damage or apoptosis (Fig 1.3.6d). Finally, cells treated with Au-CALNN-YIN NPs (Fig. 1.3.6g) revealed a complete loss of surface microvilli and a different morphological aspect compared to both Au-PVP NCs and Au-CALNN-INP NPs, suggesting, as expected, a more relevant effect of hyperthermia on the cytoskeleton organization. In conclusion, Au-peptide NCs proved to be an efficient theranostic nanosystem for targeted detection and activation of killing of prostate cancer cells.

Toxicity of AuNPs

Despite the huge potential benefit of nanomaterials for biomedical and industrial applications, very little is known about potential short- and long-term toxicity effects on human and environmental health. There are two different types of toxicity linked to AuNPs: on one hand the toxicity deriving from the material, in this case gold, on the other hand, the common cellular impact of nanomaterials in vivo. Wyatt and co-workers studied the in vivo toxicity of a library of spherical AuNPs with different sizes and they found that although some precursors of nanoparticles, in particular gold-salts, might cause toxicity, the nanoparticles themselves are not necessarily harmful to cellular functions.[82]

Cationic AuNPs are positively charged nanoaggregates that are able to penetrate the cells in a non-endocytotic way,[83] featuring fast and large uptake and they could find applications in drug delivery. Rotello and co-workers, however, demonstrated that at higher nanoparticle concentrations, transfection efficiency decreases due to cytotoxicity. The cytotoxicity of AuNPs is related to the positive charge of cationic nanoparticles that induces a strong electrostatic interaction with cellular membranes which are negatively charged. Anionic AuNPs, otherwise, have been demonstrated to be quite non-toxic thanks to their negative charge.[84]

Poor stability in physiological environments remains one of the major limitations that contribute to poor translation of nanoparticle formulations from bench to clinic. Physiological environments abundant with proteins and salts can influence the stability and interaction of AuNPs with biological systems. The high ionic strength of physiological media can cause their aggregation, thus reducing their cellular internalization. For instance, AuNPs capped with common stabilizing agents such as citrate and cetyltrimethylammonium bromide (CTAB) have been found to be unstable in buffers of pH 4, 7, 8, or 10. Thus, the stabilization of GNPs with capping agents are often required to enable any biological applications of AuNPs.[85] So, an active field of research is finding a

biomolecule able to stabilize AuNPs in physiological environments, considering the various applications that they can have on the basis of their unique properties (Fig.1.3.7).

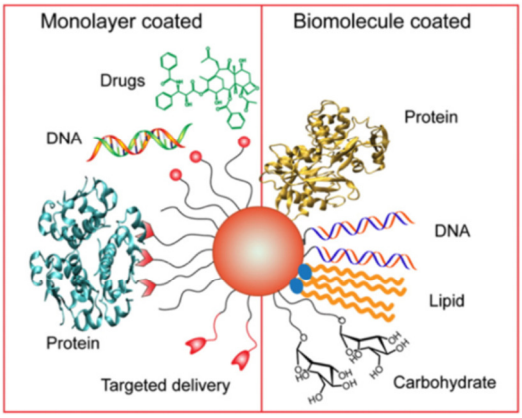

Figure 1.3.7. AuNPs functionalization with biomolecules

Aim of the project

Synthetic peptides are gaining an increased interest as an alternative to the use of biomolecules for the AuNPs functionalization, due to their easy synthesis and their pharmacokinetic profiles that can be easily improved by making appropriate changes in the peptide sequence. On the other hand, few peptide sequences able to stabilize AuNPs are known from the literature. One of the few example is the binding CALNN motif, designed by Levy et al.[86] (Fig. 1.3.8) One of the most interesting aspects of this work is that CALNN-AuNPs remain stable even when decorated with longer peptides or proteins which opens the option to develop biological applications for this system.

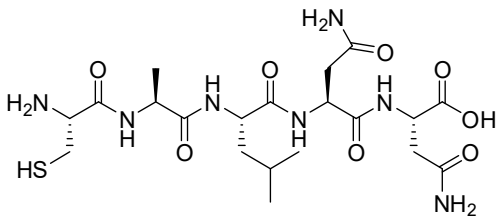

Figure 1.3.8. Molecular structure of CALNN

This sequence is characterized by a strong affinity for gold, thanks to the N-terminal cysteine which is able to make a covalent bond to the gold surface. Alanine and Leucine in positions 2 and 3 possess hydrophobic side chains and were chosen to promote the self-assembly of the peptide to form monolayer through hydrophobic interactions. Asparagine in positions 4 and 5 form the hydrophilic part due to the amide group that increases the stability and solubility in water. Considering the great potential of this kind of system in different fields, the aim is to increase the choice of short peptides that could be used as binding motif for AuNPs. On this purpose, Ala-Aib oligopeptides seem to possess all the features required for their stabilization. In fact, they have hydrophobic structure but are able to form stable self-assemblies in water, as described in the previous part. Moreover, they are easily functionalized with a thiol which make a covalent bond with gold. For this reason, analogues of pentapeptides **3** and **4,** previously described, were synthesized, and used to functionalize spherical AuNPs with 20 nm diameter, using ligand exchange method. The aim is to study their ability to form a self-assembled monolayer on nanoparticles and then, their potential use as binding motif. Moreover, the effect of variations of the peptide sequence on stability was investigated. The variation criteria were the anchor (at C- or N-terminus), the peptide core (position 2) and the peptide length. The tested peptides are listed on table 1.3.1.

Compound	Sequence
8	Ac-A-Aib-A-Aib-A-**C**-$CONH_2$
9	Ac-**C**-A-Aib-A-Aib-A-$CONH_2$
10	**HS-CH_2CH_2CO**-A-Aib-A-Aib-A-$CONH_2$
11	Ac-A-Ac_5c-A-Aib-A-**C**-$CONH_2$
12	**HS-CH_2CH_2CO**-A-Ac_5c-A-Aib-A-$CONH_2$
13	**HS-CH_2CH_2CO**-A-Aib-A-$CONH_2$
14	**HS-CH_2CH_2CO**-A-Ac_5c-A-$CONH_2$

Table 1.3.1. Synthetized compounds

Peptides containing Ala and Aib residues have been already used for functionalizing AuNPs. Schade functionalized very small AuNPs (1-2nm) with the two octapeptides Trt-S-$(CH_2)_2$-O-CO-Aib-Ala-$(Aib)_6$-OMe and Trt-S-$(CH_2)_2$-O-CO-$(Aib)_3$-Ala-$(Aib)_4$-OMe labelled on Ala with $^{13}C{=}O$ isotope for using them as local thermometer.[87] Longo and co-workers

passivated AuNPs with diameter of 2 nm with Ala-Aib oligopeptides in order to induce chiroptical properties in nanoparticles.[88]

Results and discussion

AuNPs characterization

Citrate-stabilized AuNPs were prepared by modified Turkevich-Frens method[67-68] and were characterized by observing their absorbance. According to the Mie Theory, in fact, different-sized AuNPs exhibit unique light properties. This allows measuring the average size of synthesized AuNPs with UV-vis spectroscopy through the ratio of the absorbance at the surface plasma resonance peak (A_{spr}) to the absorbance at 450 nm (A_{450}), that is the wavelength at which the majority of the absorption signal comes from the interband transitions of the metal.[89]

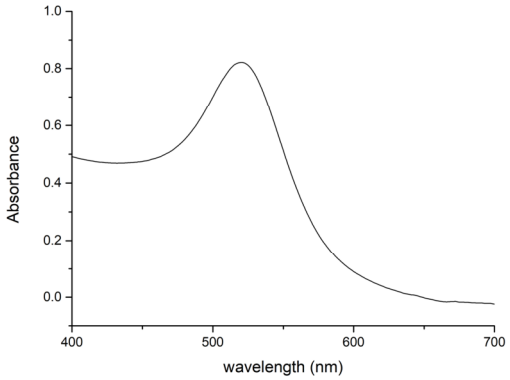

Figure 1.3.9. Absorption spectrum of synthesized AuNPs in water

Figure 1.3.9 showed the absorption spectrum in water of synthesized AuNPs. SPR peak occurred at 518 nm and the calculated A_{spr}/A_{450} value is 1.73 which corresponds to an average size of 20 nm.[90] This value was also confirmed by DLS (22.75 nm, PdI 0.18) and TEM (16 ± 1.8 nm, obtained by measuring about 150 particles by using Image-J software) as shown in figure 1.3.10.

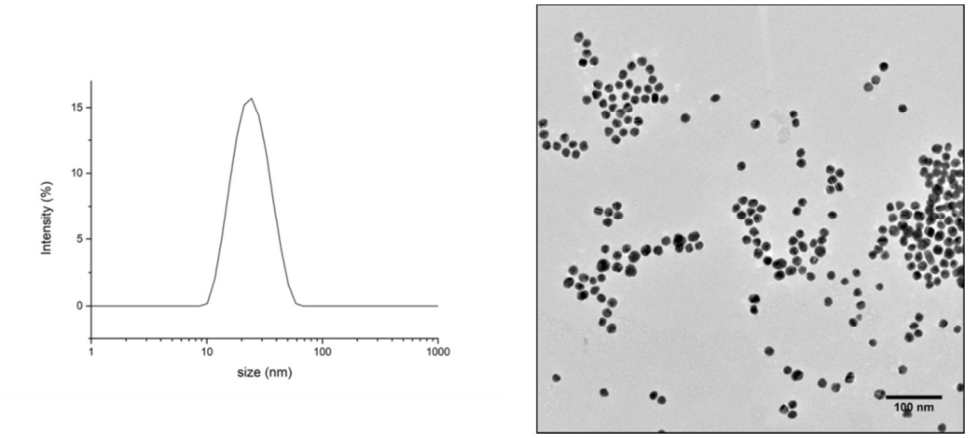

Figure 1.3.10. Size distribution by intensity and TEM micrograph of synthesized AuNPs. Mean DLS results are given for three different measurements

The concentration *c* of AuNPs in solution (0.9 nM) was calculated from absorption A at 450 nm for a standard path length *l* of 1 cm according to Lambert-Beer Law (eq.1.3.1).

$$\boldsymbol{c} = \mathbf{A_{450}}/\boldsymbol{\varepsilon_{450}} \cdot \boldsymbol{l} \qquad (1.3.1)$$

ε_{450} is the molar extinction coefficient of AuNPs at 450 nm in water and it depends on the size of nanoparticles. The theoretical value for AuNPs with diameter of 20 nm is 5.41E+08 M·cm according to the literature data.[90] From the concentration, it is possible to calculate the number of particles in solution. All experiments were performed on 2 ml of AuNPs dispersion ($\boldsymbol{V}$), which contains 1.08 x 10^{13} particles according to the following equation:

$$\mathbf{N_{AuNPs}} = \boldsymbol{c} \cdot \boldsymbol{N_{AV}} \cdot \boldsymbol{V} \qquad (1.3.2)$$

where $\boldsymbol{N_{AV}}$ is Avagadro constant (6.02×10^{23} mol^{-1}).

AuNPs functionalization

The most common approach to functionalize AuNPs is the ligand exchange method which essentially involves displacement of one ligand for another. In the presence of molecules containing thiol group such as cysteine-containing peptides, citrate-capped AuNPs undergo ligand exchange to give functionalized nanoparticles, since thiol group has a stronger interaction with gold compared to the citrate ions.[91] For this reason, analogues

of peptide **4** (Fig. 1.3.11) were synthesized, whit cysteine at C- or N-terminus (peptides **8** and **9**) and thiopropionic acid (peptide **10**) that could also act as spacer between the SH group and the peptide sequence.

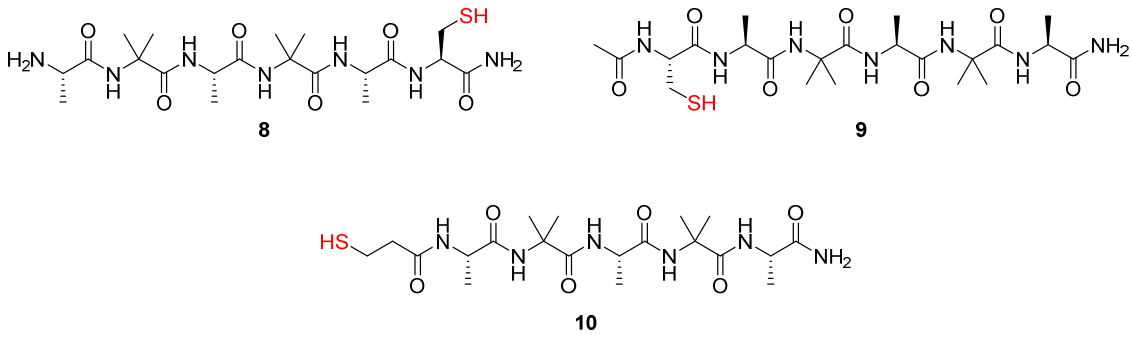

Figure 1.3.11. Molecular structure of peptides **8**, **9** and **10**. The binding site to the AuNPs is indicated in red

First of all, the circular peptide axial footprint, which is defined as the average area each peptide occupies on the nanoparticle surface, was measured. The peptide area (A_p = 0.38 nm^2) has been approximated according to the equation 1.3.3, measuring the peptide axial average diameter (d) from the crystal structure of peptide **4**, which has been found of 7 Å:

$$\mathbf{A_p = \pi\,(d/2)^2} \qquad (1.3.3)$$

The ratio between the AuNPs and the peptide areas ($K = A_{AuNPs}/A_p$) gives the average number of peptides per particle with a 20 nm radius. Some assumptions regarding surface area were made: first, nanoparticles were modelled as perfect sphere; second, the numbers of particles larger and smaller than the average particle size were assumed to be equal; third, peptides were assumed to be evenly distributed on the nanoparticle surface. In this case, according these assumptions, K is 3265 peptides/AuNP. Since 2 ml of AuNPs solution contains 1.08 x 10^{13} nanoparticles, we need 3.5 x 10^{16} ($N_{AuNPs} \cdot K$) peptide molecules (N_p), which are 117 µl of 0.5 mM solution, to exchange all citrate ions and completely cover nanoparticles. An excess of peptide has been used to facilitate the exchange reaction and to be sure to create the self-assembled monolayer.

For the AuNPs functionalization, all peptides were dissolved in DMSO to give 0.5 mM stock solution. Then, 175 µl (1.5–fold excess) were added to AuNPs dispersion under vigorous stirring and allowed to react overnight at room temperature. The excess of peptide and

citrate ions were washed by centrifugation at 14000 rpm for 15 minutes. Then, the stability of peptide-capped AuNPs were tested by UV-vis spectroscopy and DLS.

AuNPs functionalization resulted in a redshift of UV−vis plasmon absorption from 518 to 525 nm, characteristic of the dielectric constant change due to peptide and conjugation to the particle surface (Fig. 1.3.12a). This was also confirmed by changes size-distribution features of nanoparticles determined by DLS, which showed slight increase of hydrodynamic diameter (Fig. 1.3.12b).

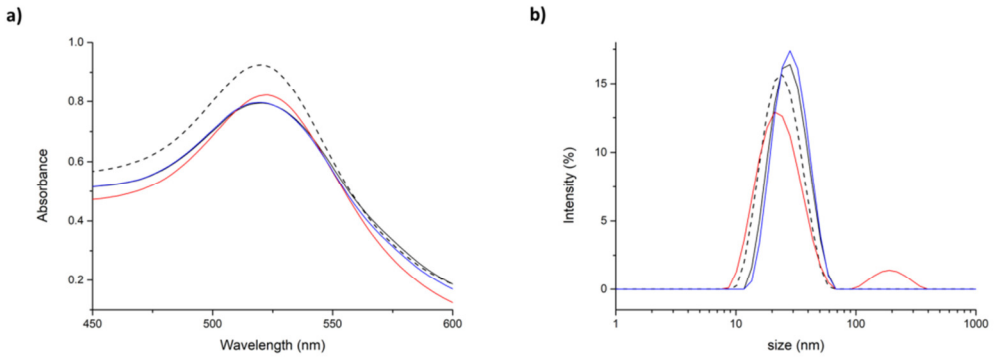

Figure 1.3.12. a) Absorption spectra and b) size distribution by intensity of citrate-capped AuNPs (dash) and functionalized-AuNPs with peptides **8** (black), **9** (red) and **10** (blue). Mean DLS results are given for three different measurements. The hydrodynamic diameter is found 22.75 nm PdI 0.18 for citrate-AuNPs, 26.64 nm, PdI 0.17 for peptide **8**-AuNPs, 25.19 nm PdI 0.3 for peptide **9**-AuNPs, 27.64nm, PdI 0.18 for peptide **10**-AuNPs

The stability of peptide-capped AuNPs after freeze-drying was also evaluated. As shown in figure 1.3.13, only peptide **10**-capped AuNPs remained perfectly stable after redispersion in water. This means that it is possible to store them as a powder for further utilization. This is an important result since very few preparations beside CALNN-capped AuNPs can be stored in dry state and redispersed in water.[86] On the other hand, peptides **9**-capped AuNPs, are the less stable since not negligible aggregation occurred after redispersion in water, which was clearly visible from changing in colour of AuNPs dispersion. This result was also confirmed by DLS analysis.

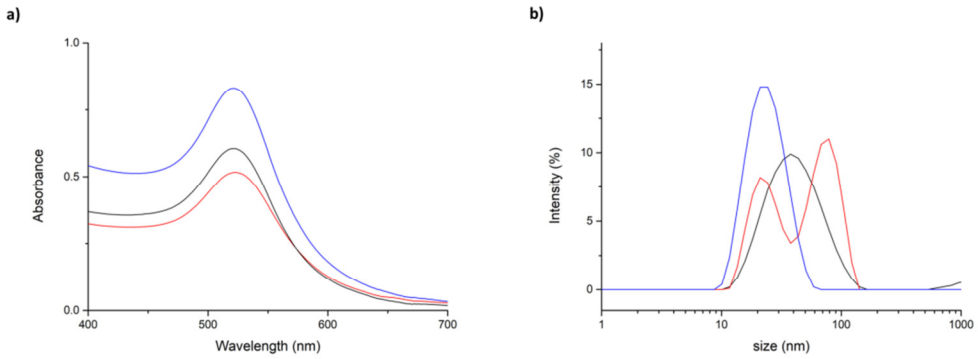

Figure 1.3.13. a) Absorption spectra and b) size distribution by intensity of functionalized-AuNPs with peptides **8** (black), **9** (red) and **10** (blue) after freeze-drying. Mean DLS results are given for three different measurements. The hydrodynamic diameter is found 38.59 nm PdI 0.32 for peptide **8**-AuNPs, 23.89 and 72.62 nm PdI 0.2 for peptide **9**-AuNPs, 24.09nm, PdI 0.27 for peptide **10**-AuNPs

In the second step, Aib in position 4 of peptides **8** and **9**, was changed into Ac_5c, which is also a hydrophobic amino acid but with a greater steric effect, to give peptides **11** and **12** (Fig. 1.3.14) and the influence on stabilization was studied.

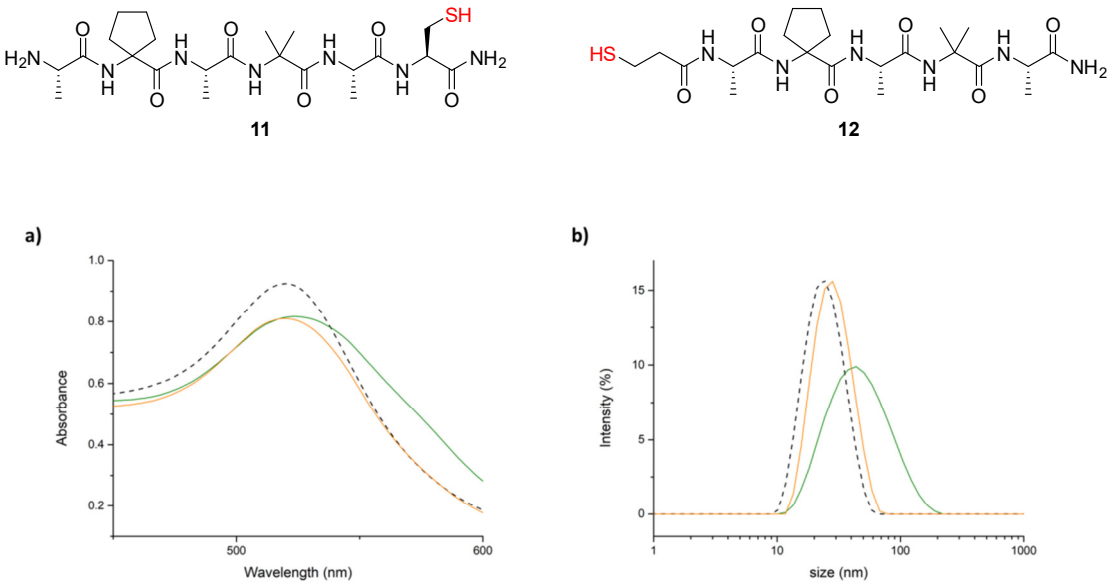

Figure 1.3.14. Molecular structures of peptides **11** and **12**. The binding site to the AuNPs is indicated in red. a) Absorption spectra and b) size distribution by intensity of citrate-capped AuNPs (dash) and functionalized-AuNPs with peptides **11** (green), **12** (orange). Mean DLS results are given for three different measurements. The hydrodynamic diameter is found 22.75 nm PdI 0.18 for citrate-AuNPs, 37.19 nm, PdI 0.28 for peptide **11**-AuNPs, 27.19 nm PdI 0.2 for peptide **12**-AuNPs

In this case, when Cys is at C-terminus (peptide **11**), AuNPs showed aggregation after centrifugation: in addition to the colour change of suspension, the plasmon absorption peak became broader and hydrodynamic diameter increases of more than 20 nm (Fig. 1.3.14a,b). On the other hand, peptide **12** with thiol group at N-terminus is able to stabilize AuNPs after freeze-drying in the same way of peptide **10**.

The above results suggested us that thiopropionic acid is a better anchor group to AuNPs than Cys, maybe because it acts as a spacer between nanoparticles and peptides.

The peptide amount per particle, after functionalization with peptides **10** and **12**, which gave the best stability results, was evaluated by analytical HPLC according to the method reported in experimental section. Washing supernatants were analysed after subtracting a reference blank. The blank was obtained as a mixture of peptide and dimethyl sulfoxide at the same amounts and conditions of the reaction, which was freeze-dried and suspended in methanol to reach a concentration of 1 mg/ml. Washing supernatant was also freeze-dried before the analysis and suspended in the same amount of methanol of blank in order to compare peak areas and obtain the unknown concentration.

	Blank		**Washing supernatant**	
Peptide **10**	Peak 1 monomer (rf: 10.34')	Peak 2 dimer (rf: 13.69')	Peak 1 monomer (rf: 10.34')	Peak 2 dimer (rf: 13.69')
Peak area (mAu*s)	855.73	1750.91	52.03	528.22
ESI-MS (m/z)	511.52 $[M+Na]^+$	997.82 $[2M+Na]^{2+}$	511.12 $[M+Na]^+$	997.62 $[2M+Na]^{2+}$

	Blank		**Washing supernatant**	
Peptide **12**	Peak 1 monomer (rf: 12.80')	Peak 2 dimer (rf: 15.70')	Peak 1 monomer (rf: 12.80')	Peak 2 dimer (rf: 15.70')
Peak area (mAu·s)	1280.58	1255.60	142.54	1462.60
ESI-MS (m/z)	537.06 $[M+Na]^+$	1050.70 $[2M+Na]^{2+}$	537.06 $[M+Na]^+$	1050.77 $[2M+Na]^{2+}$

Table 1.3.2. HPLC and mass spectroscopy results for determination of peptides **10** and **12** amount per particle.

In DMSO, thiol groups tend to form disulphide bridges, in fact for both peptides **10** and **12** the HPLC chromatogram showed two different peaks that through mass spectrometry analysis were identified as monomeric and dimeric form. In presence of gold, disulphide bridges are broken due to the high affinity of thiol group for gold The experimental data are summarized in Table 1.3.2.

The sum of peaks 1 and 2 areas gives the total area of peptide. From these values it is possible to calculate the total amount of peptide molecules bonded to AuNPs (N_{bp}) according to the following equation:

$$\mathbf{N_{bp} = N_{tot} - (A_{ws}/A_b \cdot N_{tot})} \qquad (1.3.4)$$

where N_{tot} is the total amount of peptide molecules used in all experiments (5.26×10^{16}), A_{ws} is the total area of peptide (monomer and dimer) in washing supernatant and A_b is the total area of blank (monomer and dimer). The number of peptides per single particle is found from the ration between N_{bp} and N_{AuNPs}.

As expected, for peptide **12** the number of molecules per particle found (1759 peptide/AuNP), is lower than the number for peptide **10** (3703 peptide/AuNP), very likely because the steric effect of Ac_5c amino acid is much bigger than that of Aib. Peptide **10** value is perfectly in line with theoretical values measured from the crystal structure.

The stability of AuNPs functionalized with peptide **10** and **12** was evaluated on short time, while stability tests on long time are still ongoing. Figure 1.3.15 shows that after one week the nanoparticles have maintained the same SPR absorbance and DLS profiles.

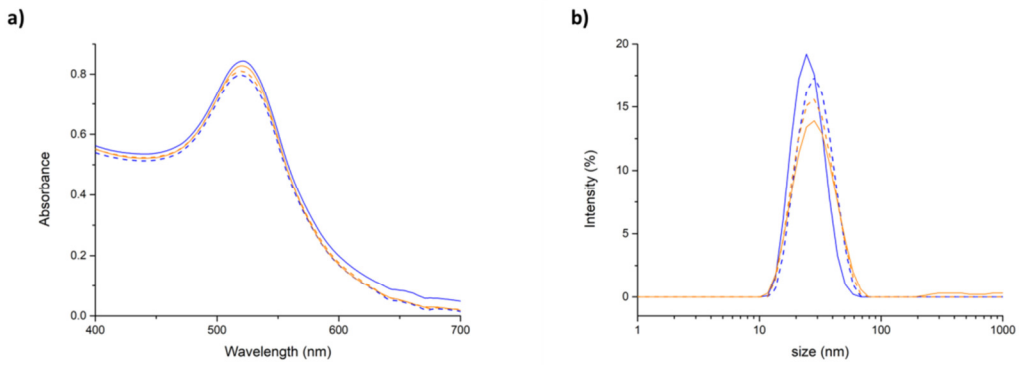

Figure 1.3.15.Short time stability studies: a) absorption spectra and b) size distribution by intensity of functionalized-AuNPs with peptides **10** (blue dash), **10** after one week (blue straight), **12** (orange dash) and **12** after one week (orange straight). Mean DLS results are given for three different measurements. The hydrodynamic diameter is found 27.64nm, PdI 0.18 for peptide **10**-

AuNPs, 26.30 and PdI 0.22 for peptide **10**-AuNPs after one week, 29.37nm, PdI 0.29 for peptide **12**-AuNPs and 27.19nm, PdI 0.2 for peptide **12**-AuNPs after one week

Finally, the effect of peptide length on nanoparticle stability was studied and peptides **13** and **14** were synthesized (Fig. 1.3.16).

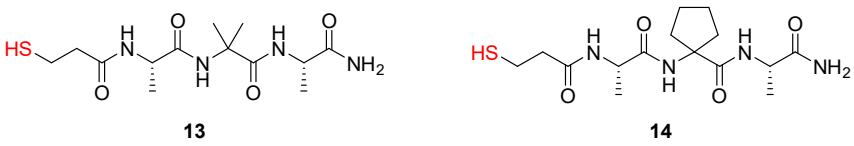

Figure 1.3.16. Molecular structure of peptides **13** and **14**. The binding site to the AuNPs is indicated in red

Peptides **13** and **14** capped-AuNPs were stable after purification by centrifuge and they displayed a redshift of UV–vis plasmon absorption and an increase of hydrodynamic diameter of very few nm, probably due to the short length of peptides (Fig. 1.3.17). The stability tests on short and long time are, instead, still ongoing.

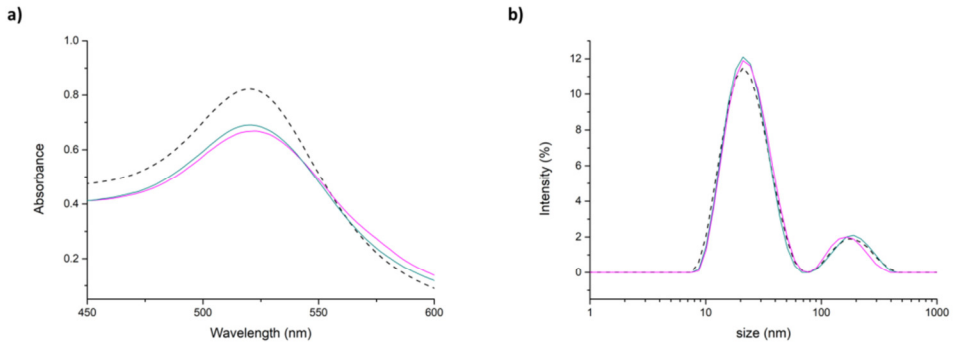

Figure 1.3.17. a) Absorption spectra and b) size distribution by intensity of citrate-capped AuNPs (dash) and functionalized-AuNPs with peptides **13** (cyan) and **14** (magenta). Mean DLS results are given for three different measurements. The hydrodynamic diameter is found 24.22 nm PdI 0.34 for citrate-AuNPs, 25.85 nm PdI 0.35 for peptide **13**-AuNPs, 26.39nm, PdI 0.34 for peptide **14**-AuNPs

The possibility for peptides **13** and **14** capped-AuNPs to be stored as a powder was studied after freeze-drying, but, as shown in figure 1.3.18, only peptide **13**-AuNPs appeared stable after resuspension in water.

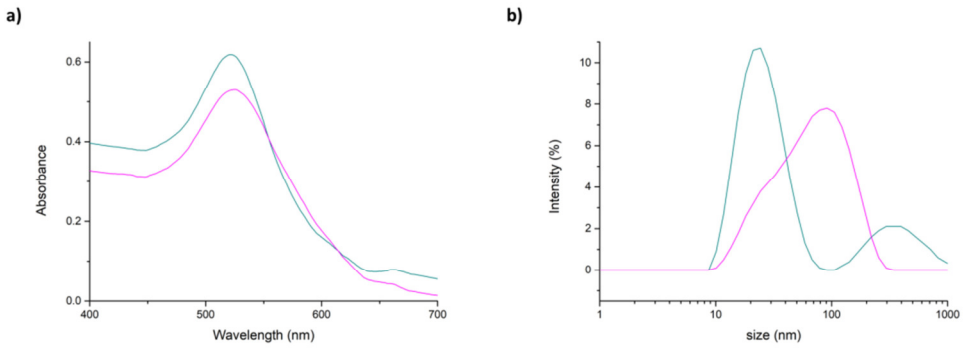

Figure 1.3.18. a) Absorption spectra and b) size distribution by intensity of functionalized-AuNPs with peptides **13** (cyan) and **14** (magenta) after freeze-drying. Mean DLS results are given for three different measurements. The hydrodynamic diameter is found 27.09 nm PdI 0.36 for peptide **13**-AuNPs, 59.22 PdI 0.39 for peptide **14**-AuNPs

Summarizing, it was observed that when thiol group is at N-terminus instead at C-terminus, the peptide self-assembled monolayer stabilized better AuNPs. Moreover, a greater stabilization occurred when thiol group is bearded on linear molecules like thiopropionic acid instead on Cys, maybe due to steric effects. The substitution of Aib in position 2 with cyclic C^{α}-tetrasubstituted amino acid (Ac_5c) didn't drastically affect the stability of nanoparticles, but the number of peptides in the self-assembled monolayer decreased probably because, also in this case, steric repulsion effects took over. In fact in peptide **10**-AuNPs the number of linked peptides is the 77% of the total added peptide molecules, while in peptide **12**-AuNPs, the number of linked peptide is 37%. Finally, peptide length influenced the stability only in presence of Ac_5c amino acid but not with Aib.

Conclusion

In conclusion, three different peptides (**10**, **12** and **13**) have been identified as possible AuNPs stabilizers through the formation of self-assembled monolayer (Fig. 1.3.19). All these peptide-capped AuNPs can be stored as a powder and once they are redispersed in water, they display exactly the same SPR absorption spectrum and DLS profile as before.
The next step of this work is to evaluate the use of these peptides as AuNPs binding motif by decorating them with longer peptides and studying how the stability of AuNPs is affected. Another interesting aspect that we would like to investigate is the stability of

these AuNPs in biological medium and study a system that is able to reduce plasma protein adsorption. To achieve this goal, AuNPs could be covered with a mixture of described peptides, since it is known from the literature that when nanoparticles are decorated with a layer consisting of conformational random PEG chains, the surface is protected against adsorbing proteins because of the unfavourable entropy change that results in compression of this coating layer.[92] In this way it is possible to open the opportunity to use our system, among other fields, also in biomedical area.

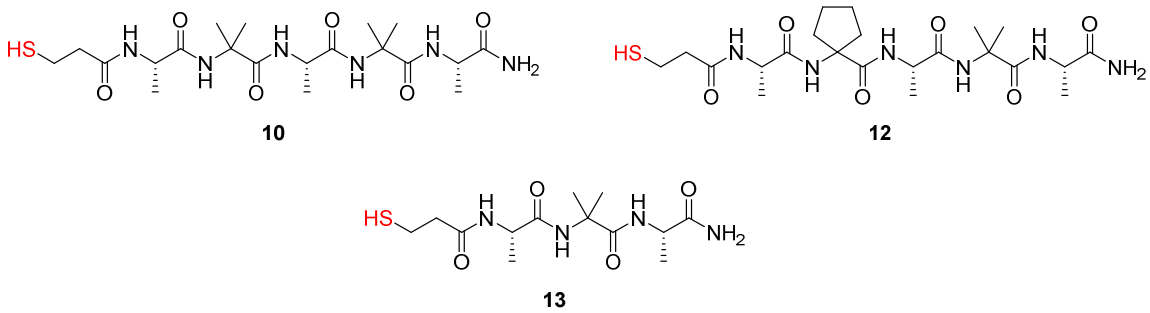

Figure 1.3.19. Molecular structure of peptides **10**, **12** and **13**, which are the peptides that give the best results in terms of AuNPs stabilization. The binding site to the AuNPs is indicated in red

Experimental Section

Materials

All reagents were purchased from Sigma-Aldrich, Iris Biotech or Fluka. All solvents were of ACS grade or higher and were obtained from Sigma-Aldrich. Reactions were monitored by thin-layer chromatography carried out on 0.25 mm Merck silica gel plates (60F-254) with UV light as the visualizing agent and ninhydrin as developing agents. Chromatographic separation was performed using Silicycle 60 Å SiO_2 (230-400 mesh). NMR spectra were recorded on Varian Gemini 300 or Bruker Avance 500 using appropriate deuterated solvents. Mass spectra were acquired on Fisons MD800 spectrometer and electrospray ion trap on a Finnigan LCQ advantage Thermo-spectrometer. IR spectra were recorded in KBr pellet in ParkinElmer FTIR spectrometer. Melting point were measured on SMP3 apparatus, Stuart Scientific. $[\alpha]_D$ were measured on ParkinElmer model 343 plus polarimeter. Chromatographic separation was performed using a DENALI C-18 column (10 mm, 250_22 mm). Purity was analysed by HPLC VWR Hitachi Pump L2130. The Loading of peptides on AuNPs was measured using LUNA 5µ C-8. CD spectra were recorded with JASCO spectropolarimeter, J-810 model, using quartz cuvette with 1.0 cm path length. Measurement are performed at room temperature, using wavelength from 250 to 190 nm, a bandwidth of 1.0 nm, sensitivity is 20 mdeg and scansion speed is 50 nm/min. (Department of Pharmaceutical Sciences, University of Milan). Regarding part II, the Dynamic Light Scattering (DLS) and ζ-potential measurements were performed in low volume disposable cuvettes using a Malvern Zetasizer Nano ZS90 instrument at 25°C, equipped with 633 nm solid state He–Ne laser at a scattering angle of 90°. Analyses were performed in water (viscosity: 0.8872 Cp, refractive index: 1.33). The size and charge measurements were averaged from at least three repeated measurements. Fluorescence spectra were performed on Horiba Scientific fluoromax_4 spectrofluorometer using a cuvette of path 1 cm, in the spectral region 350-450 nm using an excitation wavelength of 430 nm. Absorption spectra were carried on Agilent Technologies, cary 100 UV-vis spectrophotometer using a cuvette of path 1 cm, in the spectral region 300-800 nm at 25°C (Fondazione Unimi, Milan). Transmission Electron Miscroscopy (TEM) and confocal micrographs were acquired by Unitech NOLIMITS. For TEM analysis, measurements were run with a FEI Tecnai G2 (FEI, Eindhoven, NL) instrument with an accelerating voltage of 200kV. The suspension of peptide (5mg/ml) was deposited on a copper grid, then negative

staining was performed using saturated uranyl acetate in 20% ethanol. Regarding part III, the Dynamic Light Scattering (DLS) measurements were performed using a Malvern Zetasizer Nano ZS90 instrument at 25°C, equipped with a 633 nm solid state He–Ne laser at a scattering angle of 173°. Analyses were performed in water (viscosity: 0.8872 Cp, refractive index: 1.33). The size measurements were averaged from at least three repeated measurements. UV–vis absorption spectra were acquired on an Agilent model 8543 spectrophotometer at room temperature and using standard quartz cells with 1.0 cm path length. (Department of Chemistry, University of Milan)

Methods

Peptide purity was measured by reverse phase HPLC according to the method described below:

Time (min)	% A	% B	Flow (ml/min)
0	100	0	0
1	100	0	1
18	50	50	1
22	0	100	1
23	0	100	1
25	100	0	1
31	100	0	0

- phase A: H_2O/CH_3CN/TFA 97:3:0.1
- phase B: H_2O/CH_3CN/TFA 30:70:0.1

The peptide amount per particle after functionalization with peptides **10** and **12**, was evaluated by analytical HPLC according to the method described below:

Time (min)	% A	% B	Flow (ml/min)
0	95	5	0.8
1	95	5	0.8
20	50	50	0.8
28	5	95	0.8

- phase A: H_2O/CH_3CN/TFA 95:5:0.1
- phase B: H_2O/CH_3CN/TFA 95:5:0.1

Purification of compounds was performed using preparative HPLC, according to the methods described below:

a) for peptides **1'/1''**

Time (min)	% A	% B	Flow (ml/min)	Gradient
0	95	5	1	linear
1	95	5	14	linear
30	80	20	14	linear
35	50	50	14	linear
40	0	100	14	linear
41	0	100	14	linear
45	95	5	14	linear
46	95	5	0	linear

- phase A: H_2O/CH_3CN/TFA (95:5:0.1)
- phase B: CH_3CN/H_2O/TFA (95:5:0.1)

b) for other peptides

Time (min)	% A	% B	Flow (ml/min)	Gradient
0	100	0	20	linear
1	100	0	20	linear
20	50	50	20	linear
28	0	100	20	linear
29	0	100	20	linear
33	100	0	20	linear
34	100	0	0	linear

- phase A: H_2O/CH_3CN/TFA (95:5:0.1)
- phase B: CH_3CN/H_2O/TFA (95:5:0.1)

General Synthetic Procedure

Procedure 1: (1R*,2R*,4R*)-and (1R*,2S*,4R*)-ethyl 2-nitrobicyclo[2.2.1]hept-5-ene-2-carboxylate synthesis[14]

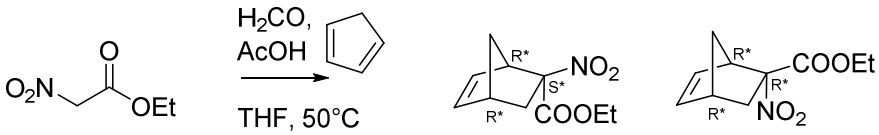

Ethyl 2-nitroacetate is dissolved in THF (0.1M). Then, freshly distilled cyclopentadiene (5 eq), formaldehyde (5 eq) and acetic acid (5 eq) are added. The mixture is heated to 50°C and is refluxed for 12 hours. The reaction is monitored by TLC (ethyl acetate/hexane 1:4, detected by Pancaldi reagent:$(NH_4)_6MoO_4$, $Ce(SO_4)_2$, H_2SO_4, H_2O) and then the solvent is evaporated under reduced pressure. The residue is dissolved in water and extracted three times with ethyl acetate. The combined organic phases are dried over Na_2SO_4 , filtered and evaporated under reduced pressure. The crude product is purified by silica gel column chromatography (hexane/ethyl acetate, from 100:0 to 10:1).

Procedure 2: (1R*,2S*,4R*)- and (1R*,2R*,4R*)-ethyl 2-aminobicyclo[2.2.1]hept-5-ene-2-carboxylate synthesis[14]

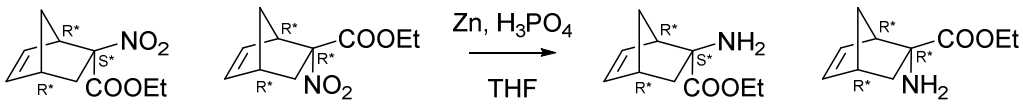

NRB nitroesters are dissolved in THF (0.1M) and Zn powder (20 eq) is added under vigorous stirring. The mixture is cooled to 0°C before adding 1M aqueous phosphoric acid (20 eq) dropwise. The mixture is stirred for 12 hours at rt and is monitored by TLC (ethyl acetate/hexane 1:1, detected by ninhydrin). The resulting suspension is filtered under vacuum and the solvent is evaporated under reduced pressure. The remaining aqueous phase is basified to pH 8 with solid $NaHCO_3$ and then extracted three times with ethyl acetate. The combined organic phases are dried over Na_2SO_4 , filtered and evaporated under reduced pressure. The crude product is purified by silica gel column chromatography (hexane/ethyl acetate 6:1 + 0.8% TEA) affording the two separated amines as yellow oil.

Procedure 3: (1R*,2R*,4R*)-2-((tert-butoxycarbonyl)amino)bicyclo[2.2.1]hept-5-en-2-carboxylic acid synthesis[14]

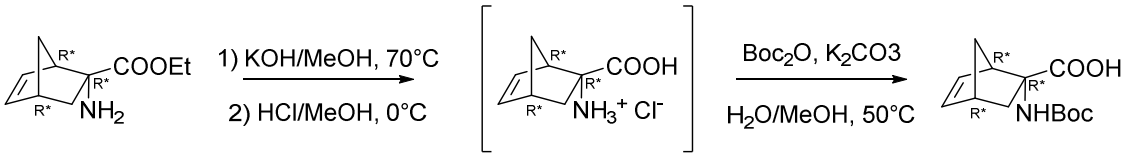

(1R*,2R*,4R*)-NRB amine is dissolved in KOH saturated MeOH solution and heated to 70°C for 4 hours. The reaction is monitored by TLC (MeOH/DCM 1:5, detected by ninhydrin) and the solvent is evaporated under reduced pressure. The dry solid is treated with HCl saturated MeOH solution at 0°C until pH 2 The precipitate (KCl) is filtered under vacuum and the solvent is evaporated under reduced pressure. The obtained crude product is dissolved in a mixture of H_2O/MeOH 1:1 (0.1M) then, Boc_2O (1.2eq) and K_2CO_3 (2.5 eq) are added. The mixture is heated to 50°C and monitored by TLC (MeOH/DCM 1:6). Two additions of the same equivalents of Boc_2O and K_2CO_3 are made every 6 hours. At the end of the reaction, organic solvent is evaporated at reduced pressure and the crude was

dissolved at 0°C in 1M aqueous HCl until pH 2. The precipitate is filtered under vacuum affording Boc-NRB amino acid as white solid.

Procedure 4: Tert-butyl ((1S*,2S*,4S*)-2-(((R)-1-((1-(((R)-1-amino-1-oxopropan-2-yl)amino)-2-methyl-1-oxopropan-2-yl)amino)-1-oxopropan-2-yl)carbamoyl)bicycle [2.2.1]hept-5-en-2-yl)carbamate synthesis[14]

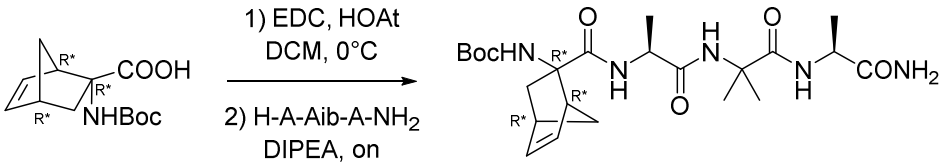

(1R*,2R*,4R*)-Boc-NRB-OH (1 eq) is dissolved in dichloromethane (10 ml/mmol) under nitrogen. The mixture is cooled at 0 °C before adding EDC (1.1 eq) and HOAt (1.1 eq) and is stirred for 1 hour. Then, the tripeptide H-A-Aib-A- $CONH_2$ (1.1 eq) and DIPEA are added until pH=7-8. The mixture is allowed to react overnight at rt. The solvent is removed under reduced pressure. The residue is dissolved in DCM and the organic phase is washed with saturated aqueous NH_4Cl, saturated aqueous $NaHCO_3$, and brine. The organic layer is dried over Na_2SO_4, filtered, and concentrated under reduced pressure. The residue is crystallized from DCM-hexane to afford the mixture of the two diasteroisomers as white solid.

Procedure 5: (1S,2S,4S)-2-amino-N-((R)-1-((1-(((R)-1-amino-1-oxopropan-2-yl)amino-2-methyl-1-oxopropan-2-yl)amino)-1-oxopropan-2-yl)bicyclo[2.2.1]hept-5-ene-2 carboxamide synthesis[14]

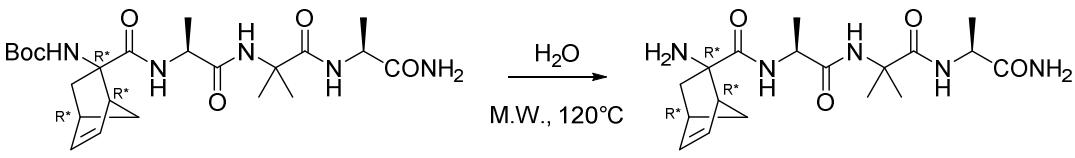

The mixture of the two Boc-protected tetrapeptides is dissolved in water in a micro waves reactor and is irradiated by microwaves for 20 minutes at 120°C. The reaction is monitored by TLC (MeOH/DCM 1:8, detected by ninhydrin). and if it necessary, another round of 20 min was performed. At the end of the reaction, the solvent is evaporated

under reduced pressure and the residue is crystallized from ether to afford the mixture of the two diasteroisomers as white solid.

Procedure 6: 3-tritylsulfanyl-propionic acid synthesis

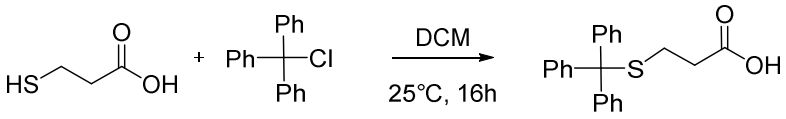

Triphenylmethyl chloride (1 eq) is dissolved in dichloromethane (0.1 M). Then a solution of 3-mercaptopropanoic acid (1 eq) in dichloromethane (0.1 M) is added dropwise. The mixture is stirred for 16 hours at room temperature, then filtered and the solvent is evaporated under reduced pressure. The residue is crystallized from ether to afford the pure product as white powder.

Procedure 7: Gold Nanoparticles (AuNPs) synthesis

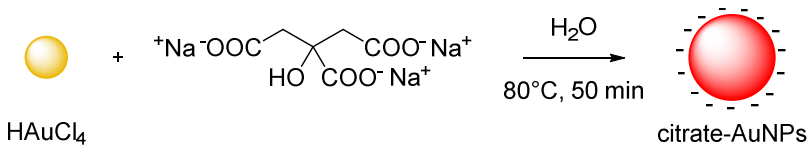

AuNPs of around 20 nm are prepared by a modified Turkevich-Frens method.[67-68] A boiling solution of $HAuCl_4$ trihydrate (15 mg, 40 µmol) in 150 mL of Milli-Q water is quickly mixed with 4.5 mL of warm (60–80°C) 1% (wt) aqueous solution of trisodium citrate, followed by reflux for 60 min. The resulted nanoparticle suspension was then allowed to cool down to room temperature and stirred overnight.

Procedure 8: Gold Nanoparticles (AuNPs) functionalization

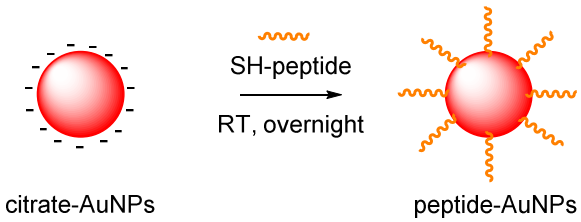

The functionalization of AuNPs with peptides is carried out following a procedure described by Levy et al.[86] Peptides are dissolved in DMSO to give 0.5 mM stock solution. Peptide solution is added to 2 mL of 0.9 nM. AuNPs dispersion under vigorous stirring. The ligands are allowed to attach to the particles overnight, followed by washing by centrifugation at 14000 rpm for 15 minutes.

General Synthetic Procedures: Solid Phase Peptide Synthesis

Procedure 1: Resin swelling

The resin (0.15 mmol) is swelled in a mixture of DCM (6.5 ml) and NMP (1 ml) for 30 minutes before use.

Procedure 2: Coupling Reaction

Method A: the Fmoc-protected amino acid (3 eq) is dissolved in 0.45M solution of HOBt (5 eq), HBTU (5 eq) and DIPEA (8 eq) in DMF. The peptidyl resin is treated with the mixture for 1 hour, drained and washed six times with DMF.

Method B: the Fmoc-protected amino acid (3 eq) is dissolved in 0.5M solution of HOBt (5 eq) and DIC (5 eq) in DMF and stirred for 20 minutes. The peptidyl resin is treated with the mixture for 1 hour, drained and washed six times with DMF and six times with DCM.

Procedure 3: Fmoc-Deprotection

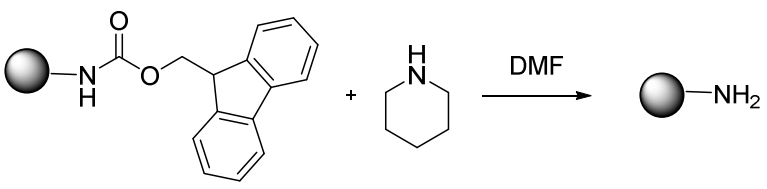

Fmoc-protected peptidyl resin is treated with 20% (v/v) piperidine in DMF for 5 minutes. Then, the resin is drained and the treatment is repeated for 15 minutes. The resin is finally washed six times with DMF.

Procedure 4: Acetylation

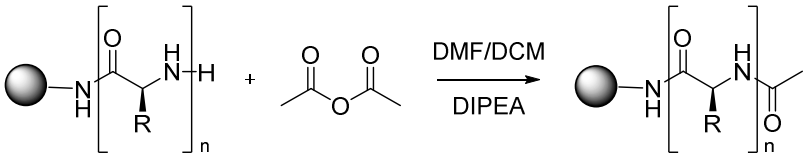

Peptidyl resin is treated with a mixture of DCM (1 ml), DMF (1 ml), acetic anhydride (0.1 ml) and DIPEA (0.2 ml) for 30 minutes. Then, the resin is drained and the treatment is repeated for another 30 minutes. The resin is finally washed six times with DMF.

Specific Synthetic Procedures for Solid Phase Peptide Synthesis

Fmoc-Rink Amide MBHA resin (100-200 mesh)

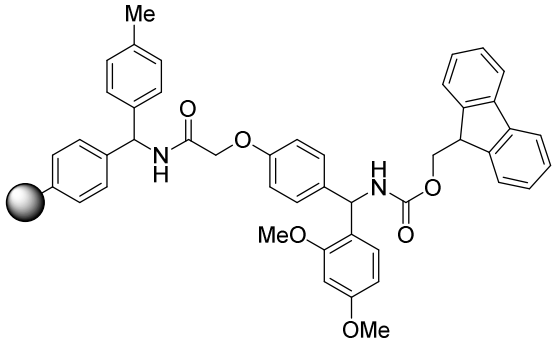

Coupling of first amino acid

Fmoc-Rink Amide MBHA resin (0.217 g, loading 0.69 mmol/g) is deprotected according genera procedure **3** of solid phase peptide synthesis before coupling the first amino acid according general procedure **2** of solid phase peptide synthesis.

Cleavage

Peptidyl resin is washed six times with DCM and dried with ether before starting the cleavage. Then, the resin is treated with a mixture (2 ml) of TFA/TIS/water (92:4.5:3.5)

for 2 hours under magnetic stirring. Subsequently, the resin is drained and washed with methanol. The filtrate is concentrated in vacuum and extruded in 40 ml of cold ether. A white fluffy precipitated is formed and collected by centrifugation (6000 rmp, 5 min). The supernatant is decanted, the residue is resuspended in 20 ml of ether and centrifuged again. This is repeated twice. The residue is finally purified by preparative HPLC (method b) and freeze-dried.

2-Chlorotritylchloride resin (100-200 mesh)

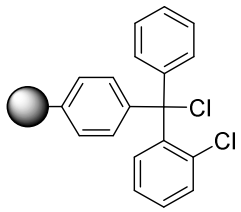

Coupling of first amino acid

The first Fmoc-protected amino acid (1 eq) is dissolved in a mixture (1 ml) of DCM/NMP 2:1 then, DIPEA (2 eq) is added. 2-chlorotritylchloride resin (0.25 g, loading 1.6 mmol/g) is treated with the mixture for 1 hour then, methanol (0.4 ml) is added to the mixture and stirred for another 5 min. Finally, the resin is drained and washed six times with DMF.

Cleavage

Peptidyl resin is washed six times with DCM and dried with ether before starting the cleavage. Then, the resin is treated with a mixture (2 ml) of TFA/TIS/water (92:4.5:3.5) for 2 hours under magnetic stirring. Subsequently, the resin is drained and washed with methanol. The filtrate is concentrated in vacuum and extruded in 40 ml of cold ether. A white fluffy precipitated is formed and collected by centrifugation (6000 rmp, 5 min). The supernatant is decanted, the residue is resuspended in 20 ml of ether and centrifuged again. This is repeated twice. The residue is finally purified by preparative HPLC (method b) and freeze-dried.

HMBA-AM resin (200-400 mesh)

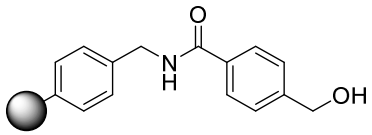

Coupling of first amino acid

The first Fmoc-protected amino acid (5 eq) is dissolved in a mixture of DCM/DMF. DIC (5 eq) is added and the mixture is stirred for 30 min at 0°C. The solvent is removed under reduced pressure, the residue is suspended in DMF (2 ml) and DMAP (0.1 eq) is added. HMBA-AM resin (0.5 g, loading 0.96 mmol/g) is treated with the mixture for 1 hour, drained and washed six times with DMF and six times with DCM. The coupling reaction is repeated twice.

Fmoc-protection is removed according general procedure **3**, the filtrate is collected and the loading is controlled by the following procedure: the filtrate is diluted first with DMF until 25 ml and then it is diluted another 30 times. The loading is calculated using the Lambert-beer equation **1** after recording the absorbance at 300.8 nm:

$$\mathbf{mmol/g = [(Abs_{solv} - Abs_{rif})/(\varepsilon \cdot b)] \times 25\ ml \times 30} \qquad (1)$$

setting the extinction coefficient (ε) at 7800 $L \cdot mol^{-1} \cdot cm^{-1}$ and optical path (b) at 1 cm. If the loading is low, the coupling should be repeat.

Cleavage

Peptidyl resin is washed six times with DCM and dried with ether before starting the cleavage. Then, the resin is treated with a mixture (25 ml) of DMF/methanol/DIPEA (45.5:45.5:9) for 1 hours at rt, for 3 hours using sonication and overnight at 50°C. Subsequently, the resin is drained and washed with methanol. The filtrate is concentrated in vacuum and extruded in 40 ml of cold ether. A white fluffy precipitated is formed and collected by centrifugation (6000 rmp, 5 min). The supernatant is decanted, the residue is resuspended in 20 ml of ether and centrifuged again. This is repeated twice. The residue is finally purified by preparative HPLC (method b) and freeze-dried.

Specific Synthetic Procedures

Peptides 1' and 1"

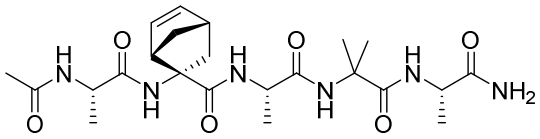

1'

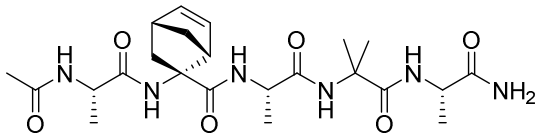

1"

The mixture of the two H_2N-tetrapeptides, previously prepared according general procedure from **1** to **5** is dissolved in THF (0.1 M) in a microwave reactor. Then, EEDQ (1.1 eq) and (L)-AcNH-Ala-OH (1 eq) were added. The mixture was irradiated by microwaves under magnetic stirring for 30 min at 60°C (80 Watt). The reaction was monitored by TLC (MeOH/DCM 1:8, detected with ninhydrin) and if it necessary, another round of 30 min was performed. The mixture is concentrated in vacuum and the residue is crystalized in 40 ml of cold ether. A white fluffy precipitated is formed and collected by centrifugation (6000 rmp, 5 min). The supernatant is decanted, the residue is resuspended in 20 ml of ether and centrifuged again. This is repeated twice. The two diasteroisomers were separated using preparative HPLC according to the reported method a. The reaction was scaled from 50 mg to 100 mg.

Peptide 1': white solid. $[\alpha]_D$: -8.3 (MeOH). IR (KBr) 3429, 3066, 2981, 2945 (NH) 1658, 1533 (CO) cm^{-1}. ^1H NMR (500 MHz, H_2O+D_2O) δ 1.25 (d, 3H, J=7.3 Hz), 1.29 (d, 3H, J=7.3 Hz), 1.31 (d, 1H, J=3.2 Hz), 1.34 (d, 3H, J=7.4), 1.39 (d, 6H, J=5.8 Hz), 1.47 (dd, 1H, J=9.2, 1.5 Hz), 1.60 (d, 1H, J=9.1 Hz), 1.93 (s, 3H), 2.29 (dd, 1H, J=13.2, 3.7 Hz), 2.87 (s, 1H), 3.33 (d, 1H, J=1.0 Hz), 4.23-4.02 (m, 3H), 6.02 (dd, 1H, J=5.8, 3.2 Hz), 6.40 (dd, 1H, J=5.7, 3.1 Hz), 6.98 (s, 1H), 7.34 (s, 1H), 7.74 (d, 1H, J=6.4 Hz), 7.90 (s, 2H), 7.97 (s, 1H), 8.14 (d, 1H, J=5. Hz). ^{13}C NMR (126 MHz, D_2O) δ 15.82, 16.21, 16.47, 21.67, 24.00, 24.35, 40.42, 41.81, 48.16, 49.04, 49.83, 50.08, 50.91, 56.70, 65.38, 133.04, 141.04, 174.03, 175.21, 175.49, 176.95, 177.11, 178.27. ESI-MS (m/z): 515.4 $[M+Na]^+$

Peptide 1": white solid. $[\alpha]_D$:+2 (MeOH). IR(KBr) 3430, 3066, 2981, 2943 (NH), 1656, 1534 (CO) cm^{-1}. ^1H NMR (500 MHz, H_2O+D_2O) δ 1.28 (d, 3H, J=7.4 Hz), 1.32 (d, 3H, J=7.4 Hz), 1.39 (d, 3H, J=7.4 Hz), 1.41-1.40 (m, 1H), 1.43 (d, 6H, J=3.8 Hz), 1.48 (d, 1H, J=9.1 Hz), 1.60 (d, 1H, J=9.2 Hz), 1.97 (s, 3H), 2.24 (dd, 1H, J=13.4, 3.7 Hz), 2.89 (s, 1H), 3.40 (s, 1H),

4.10-4.04 (m, 2H), 4.22-4.15 (m, 1H), 6.04 (dd, 1H, J=5.8, 3.1 Hz), 6.41 (dd, 1H, J=5.8, 3.1 Hz), 7.00 (s, 1H), 7.33 (s, 1H), 7.75 (d, 1H, J=6.5 Hz), 7.81 (s, 1H), 7.88 (d, 1H, J=5.2 Hz), 7.93 (s, 1H), 8.16 (d, 1H, J=5.1 Hz). ^{13}C NMR (126 MHz, D_2O) δ 15.70, 15.83, 16.35, 21.53, 23.65, 24.50, 40.21, 41.73, 48.09, 49.03, 49.96, 50.38, 51.16, 56.63, 65.05, 133.19, 140.75, 174.21, 175.44, 175.90, 177.13, 177.22, 178.25. ESI-MS (m/z): 515.4 $[M+Na]^+$

Peptides 2' and 2''

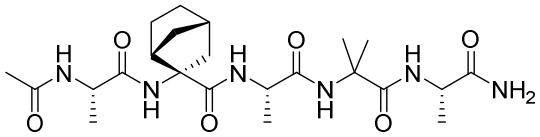

2'

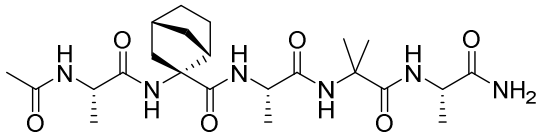

2''

Peptides **1'** or **1''** (30 mg, 0.06 mmol) was dissolved in methanol (10 ml/mmol) and then 10% Pd/C (80 mg/mmol) is added. The mixture is reacted under hydrogen at rt and atmospheric pressure overnight. The catalyst was filtered and the solvent was evaporated under reduced pressure. The residue was washed with ether and purified using preparative HPLC according to the reported method b.

Peptide 2': white solid, HPLC 97%, R_f: 22.55'. mp: 238-247°C. IR (KBr) 3309, 2988 (NH), 1674, 1534 (CO) cm^{-1}. ^{1}H NMR (500 MHz, CD_3CN) δ 1.06 (d, 1H, J=12.7 Hz, CH_2), 1.21-1.25 (m, 2H, CH_2 + CH), 1.33 (d, 3H, J=7.2 Hz, $CH_{3\ Ala}$), 1.38 (d, 3H, J=7.4 Hz, $CH_{3\ Ala}$), 1.39 (d, 3H, J=7.4 Hz, $CH_{3\ Ala}$), 1.42 (s, 3H, $CH_{3\ Aib}$), 1.45 (s, 3H, $CH_{3\ Aib}$), 1.48-1.52 (m, 1H, CH_2), 1.57-1.60 (m, 1H, CH_2), 1.71-1.76 (m, 2H, CH_2), 2.00 (s, 3H, CH_3), 2.25 (m, 1H, CH), 2.65 (m, 1H, CH), 3.96 (s, 1H, CH_{Ala}), 4.06-4.13 (m, 2H, CH_{Ala}), 5.90 (bs, 1H, NH), 7.04 (d, 2H, J=17.3 Hz, NH), 7.27-7.47 (m, 3H, NH). ^{13}C NMR (500 MHz, CD_3CN) δ 15.86, 16.65 ($CH_{3\ Ala}$), 22.04 (CH_3), 22.83 ($CH_{3\ Aib}$), 23.21(CH_2), 26.24 ($CH_{3\ Aib}$), 27.95 (CH_2), 36.06 (CH), 36.37 (CH_2), 41.06 (CH), 45.19 (CH_2), 49.72, 51.15, 52.21 (CH_{Ala}), 56.40, 64.44 (C), 172.17, 174.53, 174.60, 175.67, 176.22 (CO). ESI-MS (m/z): 517.55 $[M+Na]^+$

Peptide 2'': white solid, HPLC 86%, R_f: 23.27'. mp: 172-186°C. IR (KBr) 3413, 3073, 2986 (NH), 1675, 1536 (CO) cm^{-1}. ^{1}H NMR (500 MHz, CD_3CN) δ 1.23 (m, 1H, CH_2), 1.31-1.36 (m, 2H, CH_2), 1.37 (d, 3H, J=7.2 Hz, $CH_{3\ Ala}$), 1.38 (d, 3H, J=7.2 Hz, $CH_{3\ Ala}$), 1.41 (d, 3H, J=7.4 Hz, $CH_{3\ Ala}$), 1.41 (m, 1H, CH_2), 1.44 (s, 3H, $CH_{3\ Aib}$), 1.47 (s, 3H, $CH_{3\ Aib}$), 1.49-1.52 (m, 1H, CH_2), 1.57-1.59 (m, 1H, CH_2), 1.96-1.98 (m, 2H, CH_2), 2.01 (s, 3H, CH_3), 2.21 (m, 1H, CH), 2.94 (m,

1H, CH), 3.91 (m, 1H, CH_{Ala}), 4.05-4.13 (m, 2H, CH_{Ala}), 5.75 (bs, 1H, NH), 7.04 (d, 2H, J=18.5 Hz, NH), 7.33-7.37 (m, 2H, NH), 7.48 (s, 1H, NH). ^{13}C NMR (500 MHz, CD_3CN) δ 15.96, 16.00, 13.64 ($CH_{3\ Ala}$), 21.97 (CH_3), 22.74 ($CH_{3\ Aib}$), 23.15 (CH_2), 26.49 ($CH_{3\ Aib}$), 27.08 (CH_2), 35.54 (CH), 38.92 (CH_2), 43.68 (CH), 43.80 (CH_2), 49.70, 51.66, 52.26 (CH_{Ala}), 56.44, 63.97 (C), 174.77 (CO). ESI-MS (m/z): 517.55 $[M+Na]^+$

Peptide 3

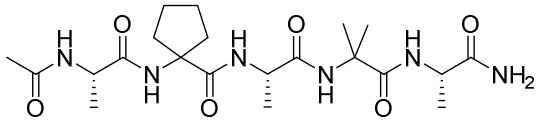

Compound **3** was synthesized using Fmoc Rink Amide resin, according to general SPPS procedure and purified using preparative HPLC according to the reported method b.
White solid, HPLC 97%, R_f: 17.78'. mp: 129.8°C. $[\alpha]_D$: -50 (H_2O). IR (KBr) 3430(NH), 1658, 1534 (CO) cm^{-1}. ^1H NMR (500 MHz, H_2O+D_2O) δ 1.30 (d, 6H, J=7.4 Hz, $CH_{3\ Ala1,Ala3}$), 1.35 (d, 3H, J=7.4 Hz, $CH_{3\ Ala5}$), 1.41 (s, 6H, $CH_{3\ Aib}$), 1.67-1.71 (m, 4H, CH_2), 1.82-1.86 (m, 2H, CH_2), 1.97 (s, 3H, CH_3), 2.04-2.10 (m, 2H, CH_2), 4.10 (m, 1H, CH_{Ala3}), 4.16 (m, 1H, CH_{Ala1}), 4.20 (m, 1H, CH_{Ala5}), 6.99 (s, 1H, CONH), 7.33 (s, 1H, CONH), 7.73 (d, 1H, J=6.5 Hz, NH_{Ala5}), 7.77 (d, 1H, J=5.6 Hz, NH_{Ala3}), 7.90 (s, 1H, NH_{Aib}), 8.18 (d, 1H, J=5.1 Hz, NH_{Ala1}), 8.43 (s, 1H, NH_{AC5C}). ^{13}C NMR (500 MHz, D_2O) δ 15.78 ($CH_{3\ Ala3}$), 15.95 ($CH_{3\ Ala1}$), 16.39 ($CH_{3\ Ala5}$), 21.53 (CH_3), 23.86, 23.93 (CH_2), 24.30 ($CH_{3\ Aib}$), 36.03, 36.64 (CH_2), 49.88 (CH_{Ala5}), 50.23 (CH_{Ala1}), 50.78 (CH_{Ala3}), 56.62 (C_{Aib}), 66.66 (C_{AC5C}), 174.22 (COOMe), 175.10 (CO_{Ala3}), 175.61 (CO_{Ala1}), 176.72 (CO_{AC5C}), 177.02 (CO_{Aib}), 178.17 (CO_{Ala5}). ESI-MS (m/z): 491.4 $[M+Na]^+$

Peptide 4

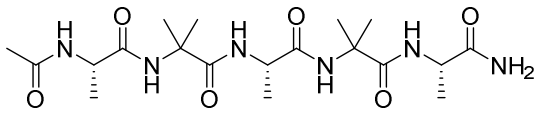

Compound **4** was synthesized using Fmoc Rink Amide resin, according to general SPPS procedure and purified using preparative HPLC according to the reported method b.

White solid, HPLC 95%, R_f: 14.12'. mp: 73.2°C. $[\alpha]_D$: +7.6 (CH_3OH). IR (KBr) 3429, 3276 (NH), 1683, 1658, 1543 (CO) cm^{-1}. ^1H NMR (500 MHz, H_20+D_2O) δ 1.30 (d, 6H, J=7.4 Hz, $CH_{3\ Ala1,Ala3}$), 1.33 (d, 3H, J=7.5 Hz, $CH_{3\ Ala5}$), 1.37 (d, 6H, J=5.6 Hz, $CH_{3\ Aib2}$), 1.40 (s, 6H, $CH_{3\ Aib4}$) 1.95 (s, 3H, CH_3), 4.08 (m, 1H, CH_{Ala3}), 4.13 (m, 1H, CH_{Ala1}), 4.17 (m, 1H, CH_{Ala5}), 6.98 (s, 1H, CONH), 7.33 (s, 1H, CONH), 7.73 (d, 1H, J=6.6 Hz, NH_{Ala5}), 7.75 (d, 1H, J=5.7 Hz, NH_{Ala3}), 7.90 (s, 1H, NH_{Aib4}), 8.18 (d, 1H, J=5.4 Hz, NH_{Ala1}), 8.35 (s, 1H, NH_{Aib2}). ^{13}C NMR (500 MHz, D_2O) δ 16.17 ($CH_{3\ Ala3}$), 16.51 ($CH_{3\ Ala1}$), 16.78 ($CH_{3\ Ala5}$), 21.96 (CH_3), 24.24, 24.35 ($CH_{3\ Aib4}$), 24.53, 24.64 ($CH_{3\ Aib2}$), 50.24 (CH_{Ala5}), 50.57 (CH_{Ala1}), 51.05 (CH_{Ala3}), 56.81 (C_{Aib4}), 57.01 (C_{Aib2}), 174.56 (COOMe), 175.37 (CO_{Ala3}), 175.45 (CO_{Ala1}), 177.41 (CO_{Aib2}), 177.67 (CO_{Aib4}), 178.55 (CO_{Ala5}). ESI-MS (m/z): 466.4 $[M+Na]^+$

Peptide 5

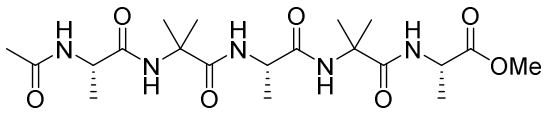

Compound **5** was synthesized using HMBA-AM resin, according to general SPPS procedure and purified using preparative HPLC according to the reported method b.

White solid, mp: 70-73°C. IR (KBr) 3347, 3320(NH), 1673, 1671, 1655, 1651, 1644 (CO) cm^{-1}. ^1H NMR (500 MHz, H_20+D_20) δ 1.34 (d, 3H, J=7.4 Hz, $CH_{3\ Ala3}$), 1.35 (d, 3H, J=7.2 Hz, $CH_{3\ Ala1}$), 1.38 (d, 3H, J=7.3 Hz, $CH_{3\ Ala5}$), 1.43 (d, 6H, J=4.7 Hz, $CH_{3\ Aib2}$), 1.44 (d, 6H, J=12 Hz, $CH_{3\ Aib4}$) 2.01 (s, 3H, CH_3), 3.74 (s, 3H, $COOCH_3$), 4.15 (m, 1H, CH_{Ala3}), 4.20 (m, 1H, CH_{Ala1}), 4.36 (m, 1H, CH_{Ala5}), 7.75 (d, 1H, J=6.0 Hz, NH_{Ala5}), 7.88 (d, 1H, J=6.6 Hz, NH_{Ala3}), 7.93 (s, 1H, NH_{Aib4}), 8.22 (d, 1H, J=5.3 Hz, NH_{Ala1}), 8.38 (s, 1H, NH_{Aib2}). ^{13}C NMR (500 MHz, D_2O) δ 16.06 ($CH_{3\ Ala3}$), 16.10 ($CH_{3\ Ala1}$), 16.24 ($CH_{3\ Ala5}$), 21.68 (CH_3), 23.57, 23.78 ($CH_{3\ Aib4}$), 24.45, 24.94 ($CH_{3\ Aib2}$), 49.05 (CH_{Ala5}), 50.35 (CH_{Ala1}), 50.36 (CH_{Ala3}), 52.89 ($COOCH_3$), 56.58 (C_{Aib4}), 56.62 (C_{Aib2}), 174.22 (COOMe), 174.23 (CO_{Ala3}), 174.27 (CO_{Ala1}), 175.05 ($COOCH_3$) 176.59 (CO_{Ala5}), 176.88 (CO_{Aib4}), 177.20 (CO_{Aib2}). ESI-MS (m/z): 457.9 $[M+H]^+$, 480.2 $[M+Na]^+$

Peptide 6

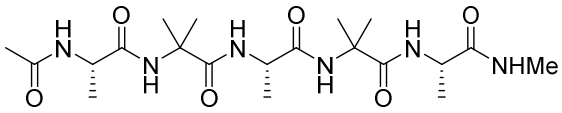

Compound **5** (50 mg, 0.11 mmol) is dissolved in 33 wt % methylamine solution in ethanol (1.25 ml) at 0°C. The mixture is allowed to react overnight at rt. The solvent is removed under reduced pressure and the residue is crystallized from ether and purified using preparative HPLC according to the reported method b.

White solid, mp: 276°C dec. (CH_3OH). IR (KBr) 3362, 3297, 3272(NH), 1673, 1654 (CO) cm^{-1}. ^1H NMR (500 MHz, CD_3OH) δ 1.37 (d, 3H, J=7.3 Hz, $CH_{3\ Ala1}$), 1.41 (d, 3H, J=2.6 Hz, $CH_{3\ Ala3}$), 1.43 (d, 3H, J=2.8 Hz, $CH_{3\ Ala5}$), 1.45 (d, 6H, J=14 Hz, $CH_{3\ Aib2}$), 1.54 (s, 6H, $CH_{3\ Aib4}$) 2.02 (s, 3H, CH_3), 2.76 (d, 3H, J=4.8 Hz, $CONHCH_3$), 4.03 (m, 1H, CH_{Ala3}), 4.13 (m, 1H, CH_{Ala1}), 4.25 (m, 1H, CH_{Ala5}), 7.58 (d, 1H, J=4.9 Hz, NH_{CONHMe}), 7.70 (d, 1H, J=7.4 Hz, NH_{Ala5}), 7.88 (d, 1H, J=5.2 Hz, NH_{Ala3}), 7.91 (s, 1H, NH_{Aib4}), 8.27 (s, 1H, NH_{Aib2}), 8.34 (s, 1H, NH_{Ala1}). ^{13}C NMR (500 MHz, CD_3OD) δ 15.31 ($CH_{3\ Ala1}$), 15.53 ($CH_{3\ Ala1}$), 16.09 ($CH_{3\ Ala5}$), 21.04 (CH_3), 22.95, 23.35 ($CH_{3\ Aib4}$), 23.07 ($CH_{3\ Aib2}$), 24.96 ($CH_{3\ CONHMe}$), 49.71 (CH_{Ala5}), 50.79 (CH_{Ala1}), 51.59 (CH_{Ala3}), 56.12, 56.59 (C_{Aib}), 172.61, 174.09, 174.38, 174.87, 175.69, 176.49 (CO). ESI-MS (m/z): 457.37 $[M+H]^+$, 479.54 $[M+Na]^+$

Peptide 7

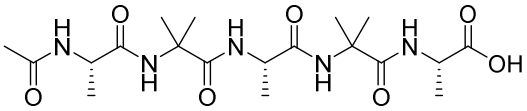

Compound **7** was synthesized using 2-Chlorotritylchloride resin, according to general SPPS procedure and purified using preparative HPLC according to the reported method b.

White solid, mp: 211-225°C. IR (KBr) 3293 (NH), 1659 (CO) cm^{-1}. ^1H NMR (500 MHz, CD_3OH) δ 1.35 (d, 3H, J=7.4 Hz, $CH_{3\ Ala3}$), 1.36 (d, 3H, J=7.4 Hz, $CH_{3\ Ala1}$), 1.40 (d, 3H, J=7.4 Hz, $CH_{3\ Ala5}$), 1.46 (d, 6H, J=11.2 Hz, $CH_{3\ Aib2}$), 1.50 (d, 6H, J=3.8 Hz, $CH_{3\ Aib4}$) 2.00 (s, 3H, CH_3), 4.13 (m, 1H, CH_{Ala1}), 4.15 (m, 1H, CH_{Ala3}), 4.38 (m, 1H, CH_{Ala5}), 7.64 (d, 1H, J=7.4 Hz, NH_{Ala5}), 7.77 (d, 1H, J=7.0 Hz, NH_{Ala3}), 7.90 (s, 1H, NH_{Aib4}), 8.33 (s, 1H, NH_{Aib2}), 8.34 (s, 1H, NH_{Ala1}). ^{13}C NMR (500 MHz, CD_3OD) δ 15.59 ($CH_{3\ Ala3}$, $_{Ala1}$), 16.37 ($CH_{3\ Ala5}$), 21.03 (CH_3), 22.85, 25.49 ($CH_{3\ Aib4}$), 23.91, 23.97 ($CH_{3\ Aib2}$), 48.21 (CH_{Ala5}), 49.74 (CH_{Ala3}), 50.71 (CH_{Ala1}), 56.31 (C_{Aib4}), 56.53 (C_{Aib2}), 172.66, 172.95, 174.24, 174.80, 175.35, 175.58 (CO). ESI-MS (m/z): 442.70 $[M-H]^-$, 466.53 $[M+Na]^+$

Peptide 8

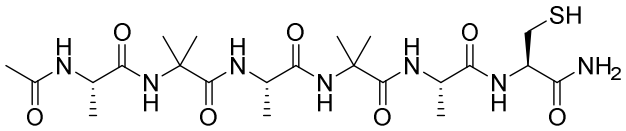

Compound **8** was synthesized using Fmoc Rink Amide resin, according to general SPPS procedure and purified using preparative HPLC according to the reported method b.
White solid, HPLC 80%, R_f: 12.5'. mp: 185°C. IR (KBr) 3311 (NH), 1659, 1536 (CO) cm^{-1}. ^1H NMR (300 MHz, CD_3OD) δ 1.36 (d, 3H, J=7.2 Hz, $CH_{3\ Ala}$), 1.41 (d, 3H, J=7.3 Hz, $CH_{3\ Ala}$), 1.43 (d, 6H, J=11.2 Hz, $CH_{3\ Aib}$), 1.47-1.50 (m, 9H, $CH_{3\ Ala,\ Aib}$), 2.04 (s, 3H, CH_3), 2.98-3.01 (m, 2H, $CH_{2\ Cys}$), 4.00-4.22 (m, 3H, CH_{Ala}), 4.31-4.36 (m, 1H, CH_{Cys}). ^{13}C NMR (300 MHz, CD_3OD) δ 15.29, 15.51, 15.81 ($CH_{3\ Ala}$), 21.04 (CH_3), 22.54, 22.89 ($CH_{3\ Aib}$), 24.87 ($CH_{3\ Aib}$), 25.17 ($CH_{2\ Cys}$), 25.34 ($CH_{3\ Aib}$), 50.80, 50.93, 51.88, (CH_{Ala}), 56.07, 56.42 (C_{Aib4}), 56.70 (CH_{Cys}), 172.65, 173.96, 174.12, 174.54, 175.06, 176.55, 176.79 (CO). ESI-MS (m/z): 545 9 $[M + H]^+$ 568.2 $[M+Na]^+$

Peptide 9

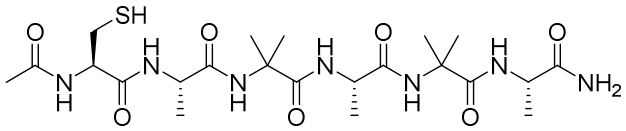

Compound **9** was synthesized using Fmoc Rink Amide resin, according to general SPPS procedure and purified using preparative HPLC according to the reported method b.
White solid. ^1H NMR (300 MHz, CD_3OD) δ 1.39-1.46 (m, 15H, CH_3), 1.49 (s, 6H, $CH_{3\ Aib}$), 2.01 (s, 3H, CH_3), 2.85 (m, 2H, $CH_{2\ Cys}$), 4.03 (m, 1H, CH_{Ala}), 4.20 (m, 1H, CH_{Ala}), 4.45 (m, 1H, CH_{Ala}), 4.85 (m, 1H, CH_{Cys}). ^{13}C NMR (300 MHz, CD_3OD) δ 15.33, 15.45, 16.21 ($CH_{3\ Ala}$), 21.04 (CH_3), 22.80, 23.08 ($CH_{3\ Aib}$), 24.96 ($CH_{3\ Aib}$), 25.06 ($CH_{2\ Cys}$), 25.27 ($CH_{3\ Aib}$), 49.49, 51.17, 51.42, (CH_{Ala}), 55.77 (CH_{Cys}), 56.26, 56.58 (C_{Aib}), 171.77, 172.16, 173.82, 174.51, 175.59, 176.25, 176.94 (CO). ESI-MS (m/z): 544.27 $[M - H]^-$, 568.10 $[M+Na]^+$

Peptide 10

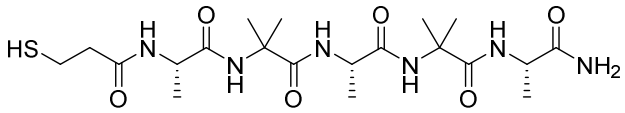

Compound **10** was synthesized using Fmoc Rink Amide resin, according to general SPPS procedure and purified using preparative HPLC according to the reported method b.
White solid, HPLC >95%, R_f: 9.5'. mp: 216°C. IR (KBr) 3311 (NH), 1658, 1535 (CO) cm^{-1}. ^1H NMR (300 MHz, CD_3OD) δ 1.38 (d, 3H, J= 7.3 Hz, $CH_{3\ Ala}$), 1.41-1.45 (m, 9H, $CH_{3\ Ala,\ Aib}$), 1.49 (d, 3H, J=1.1 Hz, $CH_{3\ Aib}$), 2.55-2.61 (m, 2H, CH_2), 2.77-2.81 (m, 2H, CH_2), 4.02-4.13 (m, 2H, CH_{Ala}), 4.18-4.25 (m, 1H, CH_{Ala}). ^{13}C NMR (300 MHz, CD_3OD) δ 15.33, 15.41, 16.16 ($CH_{3\ Ala}$), 19.56 (CH_2), 22.81, 23.01 ($CH_{3\ Aib}$), 25.09, 25.32 ($CH_{3\ Aib}$), 38.65 (CH_2), 49.53, 51.31, 51.47, (CH_{Ala}), 56.19, 56.59 (C_{Aib4}), 173.41, 174.21, 174.65, 175.65, 176.36, 177.00 (CO). ESI-MS (m/z): 511.7 $[M+Na]^+$

Peptide 11

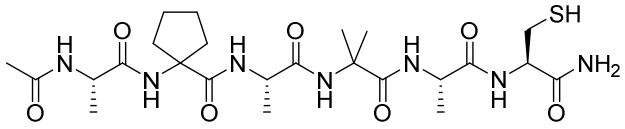

Compound **11** was synthesized using Fmoc Rink Amide resin, according to general SPPS procedure and purified using preparative HPLC according to the reported method b.
White solid, HPLC >97%, R_f: 11.3'. mp: 216°C. IR (KBr) 3430, 3345 (NH), 1651, 1535 (CO) cm^{-1}. ^1H NMR (300 MHz, CD_3OD) δ 1.36 (d, 3H, J=7.3 Hz, $CH_{3\ Ala}$), 1.39 (d, 3H, J= 7.4 Hz, $CH_{3\ Ala}$), 1.47 (s, 3H, $CH_{3\ Aib}$), 1.48 (d, 3H, J= 7.4 Hz, $CH_{3\ Ala}$), 1.51 (s, 3H, $CH_{3\ Aib}$), 1.72-1.83 (m, 5H, $CH_{2\ Ac5c}$), 1.96-1.99 (m, 2H, $CH_{2\ Ac5c}$), 2.01 (s, 3H, CH_3), 2.41-2.50 (m, 1H, CH_2), 2.98-3.00 (m, 2H, $CH_{2\ Cys}$), 4.04-4.12 (m, 2H, CH), 4.17-4.20 (m, 1H, CH), 4.32-4.37 (m, 1H, CH), 7.89, 8.27 (s, NH). ^{13}C NMR (300 MHz, CD_3OD) δ 15.26, 15.43, 15.84 ($CH_{3\ Ala}$), 21.03 (CH_3), 22.53 ($CH_{3\ Aib}$), 23.94, 24.02 (CH_2), 25.19 ($CH_{2\ Cys}$), 25.33 ($CH_{3\ Aib}$), 35.92, 36.89 (CH_2), 50.81, 50.90, 51.55 (CH), 56.43 (C_{Aib}),56.68 (CH_{Cys}) 66.33 (C_{AC5C}), 172.73, 173.93, 174.51, 174.62, 175.04, 176.11, 176.70 (CO). ESI-MS (m/z): 594.2 $[M+Na]^+$

Peptide 12

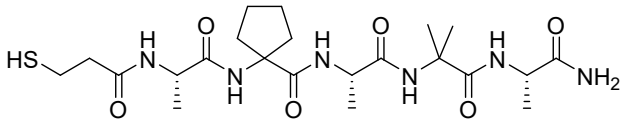

Compound **12** was synthesized using Fmoc Rink Amide resin, according to general SPPS procedure and purified using preparative HPLC according to the reported method b.
White solid, HPLC 92%, R_f: 12.8'. mp: 191°C. IR (KBr) 3452, 3319 (NH), 1649, 1536 (CO) cm^{-1}. ^1H NMR (300 MHz, CD_3OD) δ 1.36-1.39 (d, 3H, J= 7.2 Hz, $CH_{3\ Ala}$), 1.41-1.43 (d, 3H, J= 7.3 Hz, $CH_{3\ Ala}$), 1.41-1.44 (d, 3H, J=7.3 Hz, $CH_{3\ Ala}$), 1.48 (s, 3H, $CH_{3\ Aib}$), 1.49 (s, 3H, $CH_{3\ Aib}$), 1.72-1.77 (m, 4H, $CH_{2\ Ac5c}$), 1.85 (m, 1H, $CH_{2\ Ac5c}$), 1.94-1.98 (m, 2H, $CH_{2\ Ac5c}$) 2.45 (m, 1H, $CH_{2\ Ac5c}$), 2.55-2.61 (m, 2H, CH_2), 2.76-2.82 (m, 2H, CH_2), 4.01-4.15 (m, 2H, CH), 4.18-4.25 (m, 1H, CH). ^{13}C NMR (300 MHz, CD_3OD) δ 15.30, 15.40, 16.16 ($CH_{3\ Ala}$), 19.63 (CH_2), 23.06 ($CH_{3\ Aib}$), 24.07, 24.21 (CH_2), 25.30 ($CH_{3\ Aib}$), 36.13, 37.21, 38.69 (CH_2), 49.57, 51.17, 51.48 (CH), 56.57 (C_{Aib}), 66.34 (C_{AC5C}), 172.41, 173.45, 174.59, 175.59, 175.93, 176.96 (CO). ESI-MS (m/z): 537.2 $[M+Na]^+$

Peptide 13

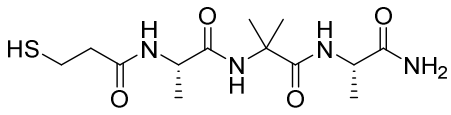

Compound **13** was synthesized using Fmoc Rink Amide resin, according to general SPPS procedure and purified using preparative HPLC according to the reported method b.
White solid. ^1H NMR (300 MHz, CD_3OD) δ 1.37 (d, 3H, J=7.2 Hz, $CH_{3\ Ala}$), 1.42 (d, 3H, J=7.3 Hz, $CH_{3\ Ala}$), 1.47 (d, 6H, J=7.4 Hz, $CH_{3\ Aib}$), 2.56 (m, 2H, CH_2), 2.78 (m, 2H, CH_2), 4.16-4.20 (m, 1H, CH_{Ala}), 4.23-4.29 (m, 1H, CH_{Ala}), 7.75, 8.11, 8.35 (NH). ^{13}C NMR (300 MHz, CD_3OD) δ 15.54, 16.25 ($CH_{3\ Ala}$), 19.53 (CH_2), 23.62, 24.53 ($CH_{3\ Aib}$), 38.89 (CH_2), 49.42, 50.53, (CH_{Ala}), 56.44 (C_{Aib4}), 173.00, 174.13, 175.20, 176.76 (CO). ESI-MS (m/z): 332.15 $[M+Na]^+$

Peptide 14

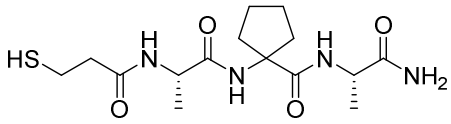

Compound **14** was synthesized using Fmoc Rink Amide resin, according to general SPPS procedure and purified using preparative HPLC according to the reported method b.
White solid. ^{1}H NMR (300 MHz, CD_3OD) δ 1.37 (d, 3H, J=7.2 Hz, $CH_{3\ Ala}$), 1.42 (d, 3H, J=7.2 Hz, $CH_{3\ Ala}$), 1.76-1.79 (m, 4H, $CH_{2\ Ac5c}$), 1.90-2.02 (m, 2H, $CH_{2\ Ac5c}$), 2.06-2.13 (m, 1H, $CH_{2\ Ac5c}$), 2.30-2.34 (m, 1H, $CH_{2\ Ac5c}$), 2.55-4.59 (m, 2H, CH_2), 2.75-2.80 (m, 1H, CH_2), 4.13-4.21 (m, 1H, CH_{Ala}), 4.25-4.30 (m, 1H, CH_{Ala}). ^{13}C NMR (300 MHz, CD_3OD) δ 15.47, 16.34 ($CH_{3\ Ala}$), 19.58, 24.12, 24.13, 36.58, 36.79, 38.87 (CH_2), 49.59, 50.46, (CH_{Ala}), 66.62 (C_{Ac5c}), 173.06, 174.59, 174.81, 176.78 (CO). ESI-MS (m/z): 357.12 $[M-H]^-$, 581.04 $[M+Na]^+$

References

[1] C. Toniolo, M. Crisma, F. Formaggio, C. Peggion, *Biopolymers* **2002**, *60*, 396-419.

[2] M. Aschi, G. Lucente, F. Mazza, A. Mollica, E. Morera, M. Nalli, M. Paglialunga Paradisi, *Organic & Biomolecular Chemistry* **2003**, *1*, 1980-1988.

[3] X. Gao, Y.-H. Chooi, B. D. Ames, C. T. Walsh, Y. Tang, *Abstracts of Papers, 243rd ACS National Meeting & Exposition, San Diego, CA, United States, March 25-29, 2012* **2012**, BIOT-129.

[4] L. D. Roberts, P. Bostrom, J. F. O'Sullivan, R. T. Schinzel, G. D. Lewis, A. Dejam, Y.-K. Lee, M. J. Palma, S. Calhoun, A. Georgiadi, M.-H. Chen, V. S. Ramachandran, M. G. Larson, C. Bouchard, T. Rankinen, A. L. Souza, C. B. Clish, T. J. Wang, J. L. Estall, A. A. Soukas, C. A. Cowan, B. M. Spiegelman, R. E. Gerszten, *Cell Metabolism* **2014**, *19*, 96-108.

[5] a) M. Ohuchi, H. Murakami, H. Suga, *Current Opinion in Chemical Biology* **2007**, *11*, 537-542; b) E. S. Iqbal, K. K. Dods, M. C. T. Hartman, *Organic & Biomolecular Chemistry* **2018**, *16*, 1073-1078.

[6] M. Crisma, C. Toniolo, *Biopolymers* **2015**, *104*, 46-64.

[7] G. N. Ramachandran, C. Ramakrishnan, V. Sasisekharan, *Journal of Molecular Biology* **1963**, *7*, 95-99.

[8] E. Benedetti, A. Bavoso, B. Di Blasio, V. Pavone, C. Pedone, M. Crisma, G. M. Bonora, C. Toniolo, *Journal of the American Chemical Society* **1982**, *104*, 2437-2444.

[9] C. Toniolo, F. Formaggio, M. Crisma, H. E. Schoemaker, J. Kamphuis, *Tetrahedron: Asymmetry* **1994**, *5*, 507-510.

[10] a) C. Toniolo, *International Journal of Peptide & Protein Research* **1990**, *35*, 287-300; b) M. Saviano, R. Iacovino, E. Benedetti, V. Moretto, A. Banzato, F. Formaggio, M. Crisma, C. Toniolo, *Journal of Peptide Science* **2000**, *6*, 571-583; c) C. Cativiera, M. D. Dìaz-de-Villegas, *Tetrahedron: Asymmetry* **2000**, *11*, 645-732; d) A. Moretto, F. Formaggio, M. Crisma, C. Toniolo, M. Saviano, R. Iacovino, R. M. Vitale, E. Benedetti, *Journal of Peptide Research* **2001**, *57*, 307-315.

[11] aS. Pellegrino, A. Bonetti, F. Clerici, A. Contini, A. Moretto, R. Soave, M. L. Gelmi, *Journal of Organic Chemistry* **2015**, *80*, 5507-5516; bF. Caputo, F. Clerici, M. L. Gelmi, S. Pellegrino, D. Pocar, *Tetrahedron: Assymmetry* **2006**, *17*, 1430-1436; cS. Pellegrino, F. Clerici, M. L. Gelmi, *Tetrahedron* **2008**, *64*, 5657-5665; dA. Ruffoni, A. Casoni, S. Pellegrino, M. L. Gelmi, R. Soave, F. Clerici, *Tetrahedron* **2012**, *68*, 1951-1962; eM. L. Gelmi, C. Cattaneo, S. Pellegrino, F. Clerici, M. Montali, C. Martini, *Journal of Organic Chemistry* **2007**, *72*, 9811-9814.

[12] N. Zhou, X. Gao, Y. Lv, J. Cheng, W. Zhou, K. Liu, *Journal of Peptide Science* **2014**, *20*, 868-875.

[13] E. Gatto, A. Porchetta, M. Scarselli, M. De Crescenzi, F. Formaggio, C. Toniolo, M. Venanzi, *Langmuir* **2012**, *28*, 2817-2826.

[14] A. Ruffoni, M. V. Cavanna, S. Argentiere, S. Locarno, S. Pellegrino, M. L. Gelmi, F. Clerici, *RSC Advances* **2016**, *6*, 90754-90759.

[15] S. J. Pike, V. Diemer, J. Raftery, S. J. Webb, J. Clayden, *Chemistry - A European Journal* **2014**, *20*, 15981-15990.

[16] E. K. S. Vijayakumar, P. Balaram, *Tetrahedron* **1983**, *39*, 2725-2731.

[17] V. Pavone, E. Benedetti, B. Di Biasio, C. Pedone, A. Santini, A. Bavoso, C. Toniolo, M. Crisma, L. Sartore, *Journal of biomolecular structure & dynamics* **1990**, *7*, 1321-1331.

[18] E. Benedetti, B. Di Blasio, V. Pavone, C. Pedone, A. Santini, A. Bavoso, C. Toniolo, M. Crisma, L. Sartore, *Journal of the Chemical Society, Perkin Transactions 2: Physical Organic Chemistry (1972-1999)* **1990**, 1829-1837.

[19] K. Otoda, Y. Kitagawa, S. Kimura, Y. Imanishi, *Biopolymers* **1993**, *33*, 1337-1345.

[20] G. Jung, H. Brueckner, R. Bosch, W. Winter, H. Schaal, J. Straehle, *Liebigs Annalen der Chemie* **1983**, 1096-1106.

[21] R. Schweitzer-Stenner, W. Gonzales, G. T. Bourne, J. A. Feng, G. R. Marshall, *Journal of the American Chemical Society* **2007**, *129*, 13095-13109.

[22] E. Longo, A. Moretto, F. Formaggio, C. Toniolo, *Chirality* **2011**, *23*, 756-760.

[23] E. Longo, M. Crisma, F. Formaggio, C. Toniolo, A. Moretto, *Polymer Journal (Tokyo, Japan)* **2013**, *45*, 516-522.

[24] P. A. Wade, J. K. Murray, S. Shah-Patel, P. J. Carroll, *Tetrahedron Letters* **2002**, *43*, 2585-2588.

[25] A. Ruffoni, A. Contini, R. Soave, L. Lo Presti, I. Esposto, I. Maffucci, D. Nava, S. Pellegrino, M. L. Gelmi, F. Clerici, *RSC Advances* **2015**, *5*, 32643-32656.

[26] K. Wuthrich, *NMR of Proteins and Nucleic Acids*, **1986**.

[27] a) G. L. Millhauser, C. J. Stenland, K. A. Bolin, F. J. M. van de Ven, *Journal of Biomolecular NMR* **1996**, *7*, 331-334; b) G. W. Vuister, A. Bax, *Journal of the American Chemical Society* **1993**, *115*, 7772-7777.

[28] R. Oekonomopulos, G. Jung, D. Leibfritz, *Tetrahedron* **1982**, *38*, 2157-2164.

[29] I. Maffucci, S. Pellegrino, J. Clayden, A. Contini, *Journal of Physical Chemistry B* **2015**, *119*, 1350-1361.

[30] S. Pellegrino, A. Contini, F. Clerici, A. Gori, D. Nava, M. L. Gelmi, *Chemistry - A European Journal* **2012**, *18*, italy8705-8715, S8705/8701-S8705/8712.

[31] a) J. D. Augspurger, V. A. Bindra, H. A. Scheraga, A. Kuki, *Biochemistry* **1995**, *34*, 2566-2576; b) N. J. Baxter, M. P. Williamson, *Journal of Biomolecular NMR* **1997**, *9*, 359-369; c) G. M. Bonora, C. Mapelli, C. Toniolo, R. R. Wilkening, E. S. Stevens, *International Journal of Biological Macromolecules* **1984**, *6*, 179-188.

[32] J. Kong, S. Yu, *Acta Biochimica et Biophysica Sinica* **2007**, *39*, 549-559.

[33] K. T. Savjani, A. K. Gajjar, J. K. Savjani, *ISRN Pharmaceutics* **2012**, 195727, 195710 pp.

[34] J. Shi, Z. Xiao, N. Kamaly, O. C. Farokhzad, *Accounts of Chemical Research* **2011**, *44*, 1123-1134.

[35] G. Verma, P. A. Hassan, *Physical Chemistry Chemical Physics* **2013**, *15*, 17016-17028.

[36] L. Sun, Z. Fan, Y. Wang, Y. Huang, M. Schmidt, M. Zhang, *Soft Matter* **2015**, *11*, 3822-3832.

[37] M. Rubert Perez Charles, N. Stephanopoulos, S. Sur, S. Lee Sungsoo, C. Newcomb, I. Stupp Samuel, *Annals of biomedical engineering* **2015**, *43*, 501-514.

[38] a) L. Zhang, J. Zhong, L. Huang, L. Wang, Y. Hong, Y. Sha, *Journal of Physical Chemistry B* **2008**, *112*, 8950-8954; b) Z. Yu, Z. Cai, Q. Chen, M. Liu, L. Ye, J. Ren, W. Liao, S. Liu, *Biomaterials Science* **2016**, *4*, 365-374; c) J. B. Matson, R. H. Zha, S. I. Stupp, *Current Opinion in Solid State & Materials Science* **2011**, *15*, 225-235.

[39] S. Eskandari, T. Guerin, I. Toth, R. J. Stephenson, *Advanced Drug Delivery Reviews* **2017**, *110-111*, 169-187.

[40] L. Liang, X.-D. Xu, C.-S. Chen, J.-H. Fang, F.-G. Jiang, X.-Z. Zhang, R.-X. Zhuo, *Journal of Biomedical Materials Research, Part B: Applied Biomaterials* **2010**, *93B*, 324-332.

[41] H.-d. Guo, G.-h. Cui, J.-j. Yang, C. Wang, J. Zhu, L.-s. Zhang, J. Jiang, S.-j. Shao, *Biochemical and Biophysical Research Communications* **2012**, *424*, 105-111.

[42] P. Sadatmousavi, *University of Waterloo* **2009**.

[43] a) A. M. Smith, R. J. Williams, C. Tang, P. Coppo, R. F. Collins, M. L. Turner, A. Saiani, R. V. Ulijn, *Advanced Materials (Weinheim, Germany)* **2008**, *20*, 37-41; b) S. Sutton, N. L. Campbell, A. I. Cooper, M. Kirkland, W. J. Frith, D. J. Adams, *Langmuir* **2009**, *25*, 10285-10291.

[44] L. Shen, H.-F. Ji, *Spectrochimica Acta, Part A: Molecular and Biomolecular Spectroscopy* **2007**, *67A*, 619-623.

[45] a) K. Ono, K. Hasegawa, H. Naiki, M. Yamada, *Journal of Neuroscience Research* **2004**, *75*, 742-750; b) F. Yang, G. P. Lim, A. N. Begum, O. J. Ubeda, M. R. Simmons, S. S. Ambegaokar, P. P. Chen, R. Kayed, C. G. Glabe, S. A. Frautschy, G. M. Cole, *Journal of Biological Chemistry* **2005**, *280*, 5892-5901.

[46] a) D. A. Dickinson, A.-L. Levonen, D. R. Moellering, E. K. Arnold, H. Zhang, V. M. Darley-Usmar, H. J. Forman, *Free Radical Biology & Medicine* **2004**, *37*, 1152-1159; b) A. J. Ruby, G. Kuttan, K. D. Babu, K. N. Rajasekharan, R. Kuttan, *Cancer Lett.* **1995**, *94*, 79-83; c) B. B. Aggarwal, A. Kumar, A. C. Bharti, *Anticancer Res.* **2003**, *23*, 363-398; d) E. Skrzypczak-Jankun, N. P. McCabe, S. H. Selman, J. Jankun, *International Journal of Molecular Medicine* **2000**, *6*, 521-526; e) N. Sreejayan, M. N. A. Rao, K. I. Priyadarsini, T. P. A. Devasagayam, *International Journal of Pharmaceutics* **1997**, *151*, 127-130.

[47] N. Chainani-Wu, *Journal of alternative and complementary medicine (New York, N.Y.)* **2003**, *9*, 161-168.

[48] a) T. Harada, D.-T. Pham, M. H. M. Leung, H. T. Ngo, S. F. Lincoln, C. J. Easton, T. W. Kee, *Journal of Physical Chemistry B* **2011**, *115*, 1268-1274; b) Y.-J. Wang, M.-H. Pan, A.-L. Cheng, L.-I. Lin, Y.-S. Ho, C.-Y. Hsieh, J.-K. Lin, *Journal of Pharmaceutical and Biomedical Analysis* **1997**, *15*, 1867-1876.

[49] a) M. O. Iwunze, *Journal of Molecular Liquids* **2004**, *111*, 161-165; b) X. Wang, Y. Gao, *Food Chemistry* **2018**, *246*, 242-248.

[50] S. Mandal, C. Banerjee, S. Ghosh, J. Kuchlyan, N. Sarkar, *Journal of Physical Chemistry B* **2013**, *117*, 6957-6968.

[51] B. Boruah, P. M. Saikia, R. K. Dutta, *Journal of Photochemistry and Photobiology, A: Chemistry* **2012**, *245*, 18-27.

[52] a) M. M. Yallapu, B. K. Gupta, M. Jaggi, S. C. Chauhan, *Journal of Colloid and Interface Science* **2010**, *351*, 19-29; b) R. K. Das, N. Kasoju, U. Bora, *Nanomedicine (Philadelphia, PA, United States)* **2010**, *6*, 153-160.

[53] C. P. Shah, B. Mishra, M. Kumar, K. I. Priyadarsini, P. N. Bajaj, *Current Science* **2008**, *95*, 1426-1432.

[54] K. Letchford, R. Liggins, H. Burt, *Journal of Pharmaceutical Sciences* **2007**, *97*, 1179-1190.

[55] K. N. Baglole, P. G. Boland, B. D. Wagner, *Journal of Photochemistry and Photobiology, A: Chemistry* **2005**, *173*, 230-237.

[56] A. Altunbas, S. J. Lee, S. A. Rajasekaran, J. P. Schneider, D. J. Pochan, *Biomaterials* **2011**, *32*, 5906-5914.

[57] S. Alam, J. J. Panda, V. S. Chauhan, *International Journal of Nanomedicine* **2012**, *7*, 4207-4222.

[58] G. Pandit, K. Roy, U. Agarwal, S. Chatterjee, *ACS Omega* **2018**, *3*, 3143-3155.

[59] a) M. H. M. Leung, T. W. Kee, *Langmuir* **2009**, *25*, 5773-5777; b) D. Ke, X. Wang, Q. Yang, Y. Niu, S. Chai, Z. Chen, X. An, W. Shen, *Langmuir* **2011**, *27*, 14112-14117; c) Z. Wang, M. H. M. Leung, T. W. Kee, D. S. English, *Langmuir* **2010**, *26*, 5520-5526.

[60] R. Ghosh, J. A. Mondal, D. K. Palit, *Journal of Physical Chemistry B* **2010**, *114*, 12129-12143.

[61] M. C. Roco, *Journal of Nanoparticle Research* **2011**, *13*, 427-445.

[62] B. Y. S. Kim, J. T. Rutka, W. C. W. Chan, *New England Journal of Medicine* **2010**, *363*, 2434-2443.

[63] A. Jakhmola, N. Anton, T. F. Vandamme, *Advanced Healthcare Materials* **2012**, *1*, 413-431.

[64] J. B. Haun, N. K. Devaraj, S. A. Hilderbrand, H. Lee, R. Weissleder, *Nature Nanotechnology* **2010**, *5*, 660-665.

[65] J. Song, J. Zhou, H. Duan, *Journal of the American Chemical Society* **2012**, *134*, 13458-13469.

[66] S. Horikoshi, N. Serpone, **2013**.

[67] D. A. Giljohann, D. S. Seferos, W. L. Daniel, M. D. Massich, P. C. Patel, C. A. Mirkin, *Angewandte Chemie, International Edition* **2010**, *49*, 3280-3294.

[68] J. Turkevich, P. C. Stevenson, J. Hillier, *Discussions of the Faraday Society* **1951**, *No. 11*, 55-75.

[69] G. Frens, *Nature (London), Physical Science* **1973**, *241*, 20-22.

[70] T. K. Sau, A. L. Rogach, F. Jaeckel, T. A. Klar, J. Feldmann, *Advanced Materials (Weinheim, Germany)* **2010**, *22*, 1805-1825.

[71] M. Hu, J. Chen, Z.-Y. Li, L. Au, G. V. Hartland, X. Li, M. Marquez, Y. Xia, *Chemical Society Reviews* **2006**, *35*, 1084-1094.

[72] J. Lv, L. Jiang, C. Li, X. Liu, M. Yuan, J. Xu, W. Zhou, Y. Song, H. Liu, Y. Li, D. Zhu, *Langmuir* **2008**, *24*, 8297-8302.

[73] Z. Krpetic, S. Saleemi, I. A. Prior, V. See, R. Qureshi, M. Brust, *ACS Nano* **2011**, *5*, 5195-5201.

[74] K. Aslan, J. R. Lakowicz, C. D. Geddes, *Analytical Chemistry* **2005**, *77*, 2007-2014.

[75] a) C. S. Thaxton, D. G. Georganopoulou, C. A. Mirkin, *Clinica Chimica Acta* **2006**, *363*, 120-126; b) Y. C. Cao, R. Jin, C. S. Thaxton, C. A. Mirkin, *Talanta* **2005**, *67*, 449-455; c) J. Li, X. Chu, Y. Liu, J.-H. Jiang, Z. He, Z. Zhang, G. Shen, R.-Q. Yu, *Nucleic Acids Research* **2005**, *33*, e168/161-e168/169.

[76] a) M. B. Thygesen, K. K. Soerensen, E. Clo, K. J. Jensen, *Chemical Communications (Cambridge, United Kingdom)* **2009**, 6367-6369; b) Y.-J. Chuang, X. Zhou, Z. Pan, C. Turchi, *Biochemical and Biophysical Research Communications* **2009**, *389*, 22-27; c) C.-C. You, R. R. Arvizo, V. M. Rotello, *Chemical Communications (Cambridge, United Kingdom)* **2006**, 2905-2907.

[77] D.-Z. Lin, P.-C. Chuang, P.-C. Liao, J.-P. Chen, Y.-F. Chen, *Biosensors & Bioelectronics* **2016**, *81*, 221-228.

[78] I. H. El-Sayed, X. Huang, M. A. El-Sayed, *Nano Letters* **2005**, *5*, 829-834.

[79] M. Z. Ahmad, S. Akhter, Z. Rahman, S. Akhter, M. Anwar, N. Mallik, F. J. Ahmad, *Journal of Pharmacy and Pharmacology* **2013**, *65*, 634-651.

[80] S. Avvakumova, E. Galbiati, L. Sironi, S. A. Locarno, L. Gambini, C. Macchi, L. Pandolfi, M. Ruscica, P. Magni, M. Collini, M. Colombo, F. Corsi, G. Chirico, S. Romeo, D. Prosperi, *Bioconjugate Chemistry* **2016**, *27*, 2911-2922.

[81] C. Cabrele, A. G. Beck-Sickinger, *Journal of Peptide Science* **2000**, *6*, 97-122.

[82] E. E. Connor, J. Mwamuka, A. Gole, C. J. Murphy, M. D. Wyatt, *Small* **2005**, *1*, 325-327.

[83] P. Nativo, I. A. Prior, M. Brust, *ACS Nano* **2008**, *2*, 1639-1644.

[84] C. M. Goodman, C. D. McCusker, T. Yilmaz, V. M. Rotello, *Bioconjugate Chemistry* **2004**, *15*, 897-900.

[85] Y. Y. Foo, V. Periasamy, L. V. Kiew, G. G. Kumar, S. N. Abd Malek, *Nanomaterials* **2017**, *7*, 123/121-123/114.

[86] R. Levy, N. T. K. Thanh, R. C. Doty, I. Hussain, R. J. Nichols, D. J. Schiffrin, M. Brust, D. G. Fernig, *Journal of the American Chemical Society* **2004**, *126*, 10076-10084.

[87] M. Schade, A. Moretto, P. M. Donaldson, C. Toniolo, P. Hamm, *Nano Letters* **2010**, *10*, 3057-3061.

[88] E. Longo, A. Orlandin, F. Mancin, P. Scrimin, A. Moretto, *ACS Nano* **2013**, *7*, 9933-9939.

[89] S. Rahman, *Undergraduate Journal of Mathematical Modeling: One + Two* **2016**, *7*.

[90] W. Haiss, N. T. K. Thanh, J. Aveyard, D. G. Fernig, *Analytical Chemistry (Washington, DC, United States)* **2007**, *79*, 4215-4221.

[91] J. Zong, S. L. Cobb, N. R. Cameron, *Biomaterials Science* **2017**, *5*, 872-886.

[92] R. Gref, M. Luck, P. Quellec, M. Marchand, E. Dellacherie, S. Harnisch, T. Blunk, R. H. Muller, *Colloids and Surfaces, B: Biointerfaces* **2000**, *18*, 301-313.

Chapter 2

Antifouling material

Introduction

Antifouling material

Biofouling is a contamination of surfaces by microbes that includes bacteria (prokaryotes), fungi and viruses. The process starts with the absorption of bioorganic molecules onto a substrate, and proceeds with the attachment of organisms to the bioorganic layer.[1] This is a complex, dynamic problem that globally impacts both the economy and environment and it is relevant in a wide range of applications, including surgical equipment and protective apparel in hospitals, medical implants, biosensors, textiles, food packaging and storage, water purification systems, marine and industrial equipment.[2] In hospital, microbial contamination and the consequent risk of infection, biosensor failure and implant rejection is a mayor driven in developing efficient antifouling strategies. In marine environments, the accumulation of bioorganic material have impacts on the powering of the ship.[1] Since biofouling is a widespread phenomenon in many areas, there is a high demand for materials that resist fouling, namely antifouling materials.

Historically, the term antifouling was synonymous of biocidal but the accumulation of biocides negatively affects non-target organisms and surrounding environment.[3] The need for nontoxic and environmental-friendly antifouling coatings led to development of many approaches. These strategies also include creating self-cleaning surfaces to prevent the attachment of the organisms and imparting of protein resistance to a surface in order to avoid biofilm formation. Nature appears to have developed a combination of these approaches.[4] One example is the superhydrophobic self-cleaning surface of leaves of some plants, such as that of Lotus (Fig. 2.1).

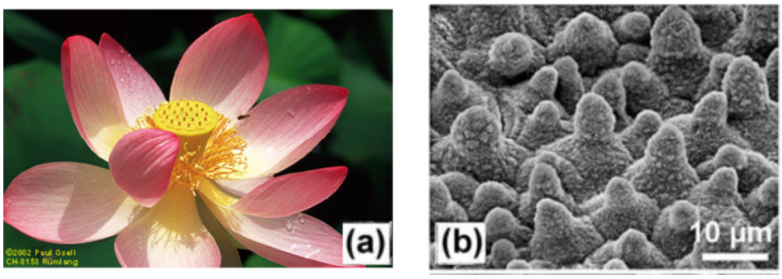

Figure 2.1. (a) Nelumbo nucifera (Lotus) flower. (b) SEM images of the papillose leaf surfaces of Nelumbo nucifera (Lotus). (Adapted from ref. [5b])

These characteristics originate from the structure of the leaves surface which is covered with micro-scale mound like structures decorated with nano-scale hair-like structures (Fig. 2.1b). The combination of micro-cones and nano-structures makes the surface superhydrophobic with contact angle between 90 and 150°, resulting in lower adhesion of the proteins to the surface.[5]

Another interesting example of self-cleaning and low-adhesion surface is the shark skin.[6] The morphology of this skin consists of patterned dermal denticles covered by anisotropic riblets aligned in the swimming direction (Fig. 2.2b) which prevent adhesion of microorganisms on the skin due to the formation of small vorticles along the body of the shark and reducing the cross-stream motion of fluid.

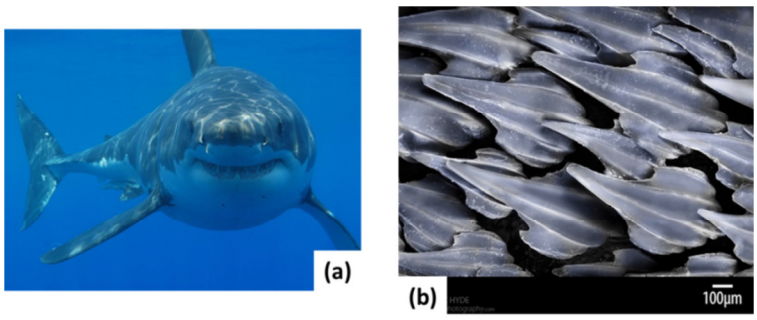

Figure 2.2. (a) shark. (b) SEM images of shark skin.

The researchers aim to mimic these types of topography in order to fabricate surfaces with antifouling activities. Carman at al. fabricated a surface in a polydimethylsiloxane elastomer that mimic the shark skin (Sharklet AF™).[7] While, inspired by lotus leaves, Pokroy and co-workers created superhydrophobic and self-cleaning surface by thermal deposition of paraffin and fluorinated waxes on various surfaces.[5a, 8]

Bixler and Bhushan reported that rice leaves and butterfly wings (Fig. 2.3) combine the anisotropic flow typical of the shark skin and superhydrophobic and self-cleaning effects of the Lotus leaves. This combination is reported to reduce drag and facilitate antifouling.[9] Rice leaves contain the longitudinal grooves with a transverse sinusoidal pattern and it is found that the hierarchical structure consists of micropapillae superimposed by waxy nanobumps. This particular structure allows rice to grow in humid and swampy environments avoiding the adhesion of unwanted fouling, which may inhibit photosynthesis.[10] Butterfly wings, instead, contain microgrooves aligned in single-like

scales, that are self-cleaning and maintain structural coloration and flight control, since butterflies are fragile and unable to clean their wings.[11]

Figure 2.3. Rice and butterfly wings effect. Shown are water droplets resting atop their superhydrophobic and low adhesion surfaces. (Adapted from[9])

As far as concerned the formation of a coating that impart protein resistance to a surface, one of the most common approach is immobilizing PEG.[12] This method is based on the postulation that the bacterial attachment on a substrate can occur after the presence of a protein adsorbed layer. Surfaces that resist to protein folding adhesion should also resist to bacteria adsorption.[13] Other materials that reduce protein adhesion are based on chitosan, hydroxyapatite or biological molecules (e.g. albumin, heparin).[14] Also many peptide-based materials are used as antifouling agents since they possess the protein resistant ability including toward bovine serum albumin, fibrinogen, fibronectin, lysozyme and streptavidin.[15] Chelmowski et al., for example, used peptides that are able to form a self-assembly monolayer to develop antifouling material for gold-coated surfaces based on protein resistance.[16] While, Messersmith and co-workers designed for the first time a pentapeptide containing DOPA and Lysine as alternating amino acids which can be functionalized with several polymers and side chains, in order to create a library of antifouling compounds that can adhere to many surfaces.[17]

3,4-Dihydroxy-L-phenyalanine (DOPA) is the main component of the glue proteins secreted by marine mussels that strongly bind to various inorganic and organic surfaces also in harsh conditions such as aqueous environments and high concentration of salt.[18]

The discovery of the role of DOPA in immobilization mechanism on different substrates induced the development of many dopamine and DOPA-based materials.

Aim of the project

This work is performed in collaboration with Prof. Meital Reches research group (University of Jerusalem, Israel).
In a previous work, her group reported a tripeptide containing DOPA amino acid (Fig. 2.4) that is able to interfere in the first step of the biofouling through formation of a functional coating.[19]

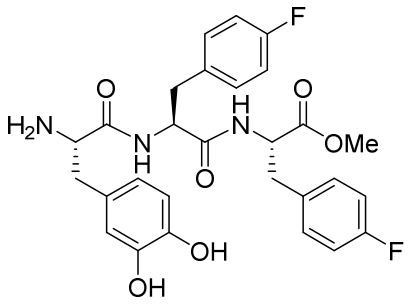

Figure 2.4. Molecular structure of the tripeptide Dopa-(F)-Phe-(F)-Phe-OMe[19]

The advantages in using peptides backbone for the design of this type of materials derive from the biocompatibility, stability and self-assemble ability which allows spontaneously forming ordered structures. In this peptide the motif that promote the self-assembly into the film is the fluorinated diphenylalanine residue which forms supramolecular structures as fibers or tubes due to aromatic interactions. Moreover, thanks to the presence of the fluorine atom, this peptide is able to form a "Teflon-like" film and prevent the protein adhesion onto a surface acting as antifouling motif. Finally, the N-terminus amino acid DOPA is exploited to immobilize the peptide on different surfaces (e.g. gold, silicon, titanium, glass).
The aim of this project concerns the exploitation of a fluorinated Phe-Phe derivative, in particular the β-amino acid showed in figure 2.5, **3b**-(**D2**), to develop antifouling coating from unnatural small peptide.

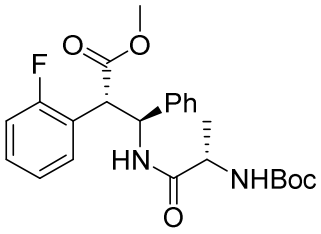

3b-(D2)

Figure 2.5. Molecular structure of **3b**-(**D2**)

This compound belongs to the class of *syn*-S*,S*-β^{2,3}-diarylamino acids, whose diasteroselective synthesis is recently reported by our research group.[20] The idea of using **3b**-(**D2**) was born from observation that it has similar properties with respect to the compound shown in figure 2.4, such as the presence of fluorine atom and the self-assembly ability of the molecule in nanotubes.[21] The advantage in using small-molecules containing unnatural amino acid residues is the remarkable impact in R&D process especially in pharmaceutical companies since they induce proteolytic resistance compared with natural peptides and they could be easily modified in order to modulate and increase the performance of the molecule.

As in the case of Reches' peptide, DOPA was added at the N-terminus of **3b**-(**D2**) to afford compound **4** (Fig. 2.6) in order to direct the adhesion of the molecule to various surfaces.

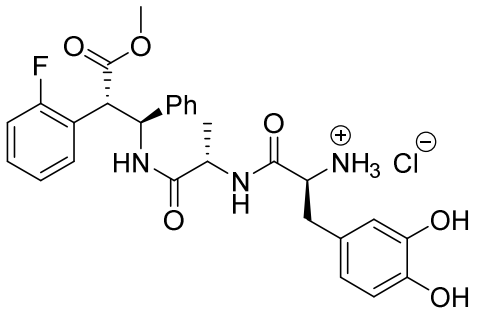

Figure 2.6. Molecular structure of compound **4**

To date, some promising results were obtained about the ability of this peptide to form a "Teflon like" film on titanium bars. However, further experiments are required in order to identify the quality of the coating and the antifouling activity. With this work, a nice

example of hybrid self-assembled material that could find applications in several fields is given.

In the following paragraph a quick overview is reported, regarding β-amino acids and in particular *syn* 3-amino-2-(2-fluorophenyl)-3-phenylpropanoic acid, whose synthesis is recently reported by our group.[21]

2-3-Diaryl-β-amino acid

β-Amino acids differ from α-amino acids for the position of the amino group, linked to the α-carbon instead of the β-carbon (Fig. 2.7).

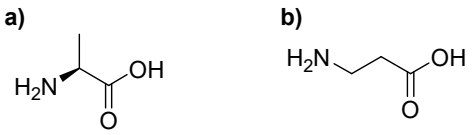

Figure 2.7. Molecular structure of (a) α and (b) β alanine

β-amino acid motif is recurrent in several biologically active compounds such as β-lactam antibiotics,[22] Taxol derivatives and β-peptides.[23] It is also considered an important starting material for the design of self-assembled nanostructures such as fibers and dendritic assemblies.[24] The apex number of β symbol, proposed by Seebach and co-workers,[25] indicates the position of the side chain substitution with respect to the carboxylic function. These terms allow distinguishing positional isomers (Fig. 2.8).

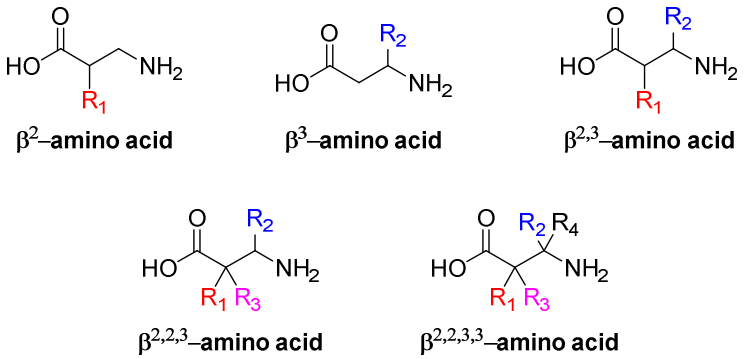

Figure 2.8. Nomenclature of β-amino acids

Furthermore, according to the position of the substituents, a particular conformation is preferred. Among the acyclic β-amino acids, the $\beta^{2,3}$-amino acids have the most constrained conformation. *Anti* diasteroisomer promotes *gauche* conformation, while *syn* diasteroisomer promotes *trans* conformation. [26]

Among the series of *syn*-S*,S*-$\beta^{2,3}$-diarylamino acids, *syn* 3-amino-2-(2-fluorophenyl)-3-phenylpropanoic acid is selected, since it possesses all the features that could be exploited for the preparation of self-assembled structures: first, the aryl groups inducing π-stacking interactions; second the fluorine atom increasing lipophilicity; third, due to its extended conformation, the potential to favour β-sheet tapes. Moreover, as a non-natural amino acid, it appears resistant to proteolysis.

Starting from compound **1**, dipeptides **3a**-(**D1**) and **3b**-(**D2**), containing L-Ala, (Fig. 2.9) were efficiently synthesized on a gram scale and fully characterized by NMR. [21]

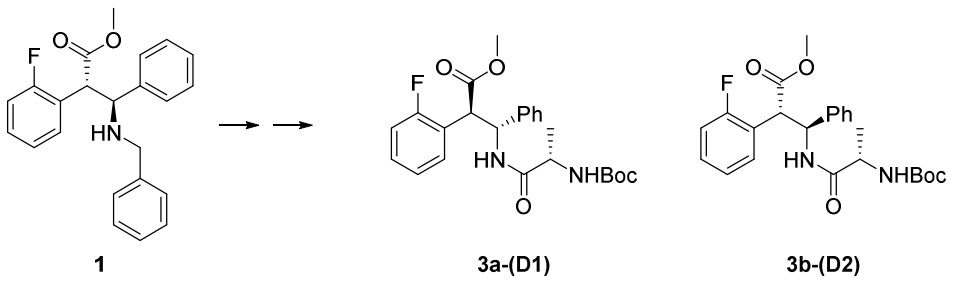

Figure 2.9. syn 3-amino-2-(2-fluorophenyl)-3-phenylpropanoic acid (compound **1**) and compounds **3a**-(**D1**) and **3b**-(**D2**)

This work is focused on diasteroisomer **3b**-(**D2**) because it is the only one that gives supramolecular structures. Indeed, it is able to self-assemble into proteolytic stable nanotubes due to the presence of intermolecular hydrogen bonds and Van der Waals interactions leading mainly to hydrophobic constructs. These architectures were also able to enter in the cell locating in the cytoplasmic/perinuclear region, representing interesting candidates for biomedical applications. [21]

Compound **3b**-(**D2**) was fully characterized by NMR 500 MHz (1H, 13C, HMBC, HSQC, NOESY) to study its secondary structures. As expected, this β-amino acid is characterized by a trans conformation according to $^{3}J_{C\beta H-C\alpha H}$ values (10 Hz) that are typical of *syn* $\beta^{2,3}$-amino acids. [26] This conformation is confirmed by the single-crystal X-Ray analysis. The crystal also provided the establishment of the S,S-stereochemistry of the β-residue (Fig. 2.10).

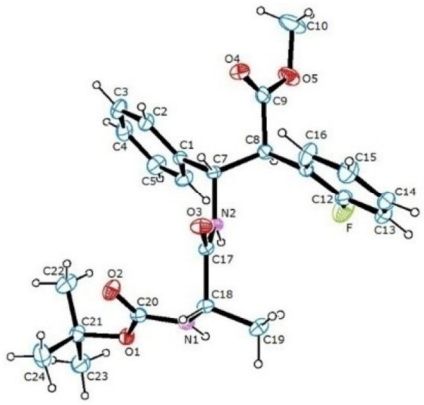

Figure 2.10. ORTEP view of the compound **3b**-(**D2**) showing atom-labelling scheme. Displacement is at the 40% probability level

The solid state analysis showed the formation of strong hydrogen bonds which seem the prevalent force involved in the self-assembly. On the other hand, the NMR solution studies didn't confirm the NH involvement in hydrogen bond, indicating a different behaviour in solution and in solid state. Moreover, NMR data suggested that **3b**-(**D2**) do not possess a preferred conformation in solution.[21]

Results and discussion

Synthesis

Compound **1** is synthesized in racemic form through an efficient $TiCl_4$/TEA-catalyzed Mannich-like reaction.

Dipeptides **3a**-(**D1**) and **3b**-(**D2**) were efficiently synthesized in gram scale from racemic *syn*-**1** (Scheme 2.1).[20]

Compound **1** was firstly deprotected at nitrogen atom by catalytic reduction (H_2, Pd/C, MeOH, 25 °C, 1 atm, 24 h) affording S*,S*-$\beta^{2,3}$-diarylamino acids **2** in quantitative yield. The condensation reaction of **2** with N-Boc-(L)-AlaOH was studied following different reaction conditions. The best result (94% yield) is obtained using EDC (1.1 eq) and Oxyma Pure (1.1 eq) for the activation of the carboxylic acid of L-Ala in DCM (0°C, 1h). Then, compound **2** and DIPEA are added and the stirring is continued overnight at 25°C. The two diasteroisomers **3a**-(**D1**) and **3b**-(**D2**) were separated by flash chromatography.

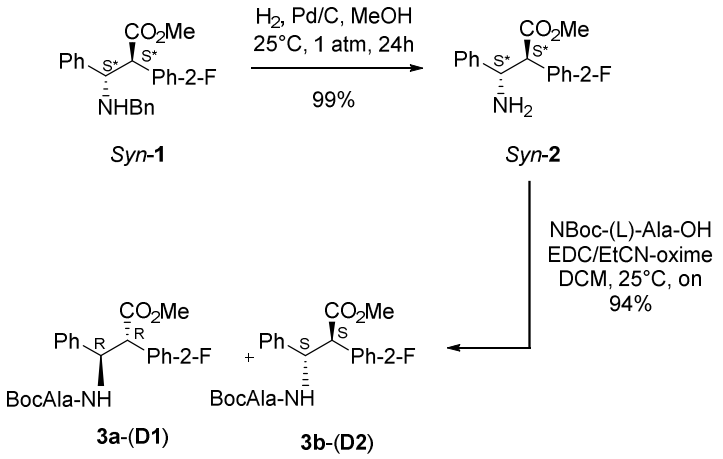

Scheme 2.1. Synthetic scheme of compounds **3a**-(**D1**) and **3b**-(**D2**)

The deprotection of compound **3b**-(**D2**) is performed in a mixture of TFA/DCM (1:1, 3h, 25°C) to give intermediate **5b**-(**D2**) in quantitative yield. Intermediate **5b**-(**D2**) is coupled with Boc-(L)-DOPA-OH according the coupling procedure previously described to afford intermediate **6** which is Boc-deprotected without any purification, using a mixture of TFA/DCM (1:1, 3h, 25°C). The resulting compound **4** is purified by HPLC and fully characterized by NMR (scheme 2.2).

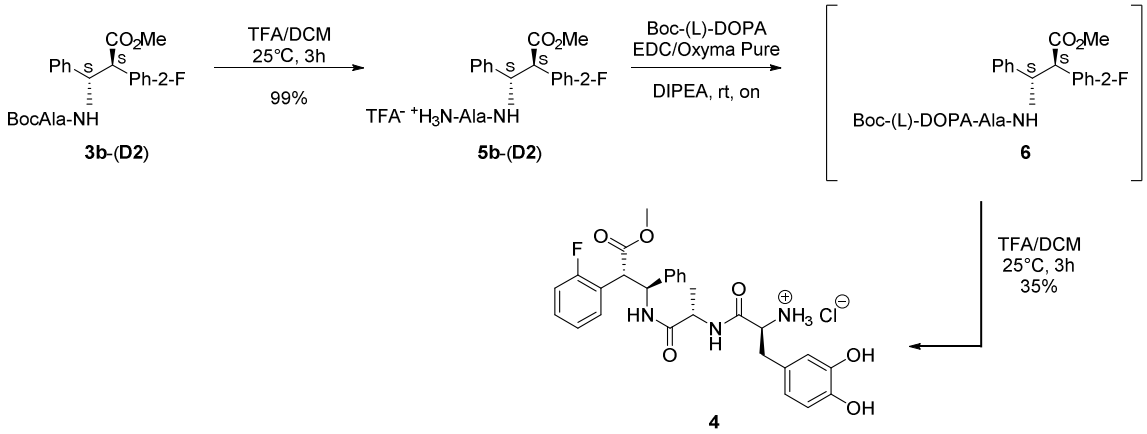

Scheme 2.2. Synthetic scheme of compounds **4**

NMR characterization

Compound **4** was characterized by NMR 300 MHz in $CDCl_3$ (^1H, ^{13}H, HMBC, HSQC, NOESY) to study its secondary structure. Compound **4** is present in solution as a single extended conformer, in which the $\beta^{2,3}$-diarylamino acid is characterized by a trans configuration according to $^3J_{C\beta H}$–$C_{\alpha H}$ values (11.3 Hz).

A complete set of $C^{\alpha}H_i$-NH_{i+1} is detected by NOESY experiments, but no NH_i,NH_{i+1} NOEs typical of helical structure were observed, so it was hypothesized that it assumes an extended conformation (Fig. 2.11).

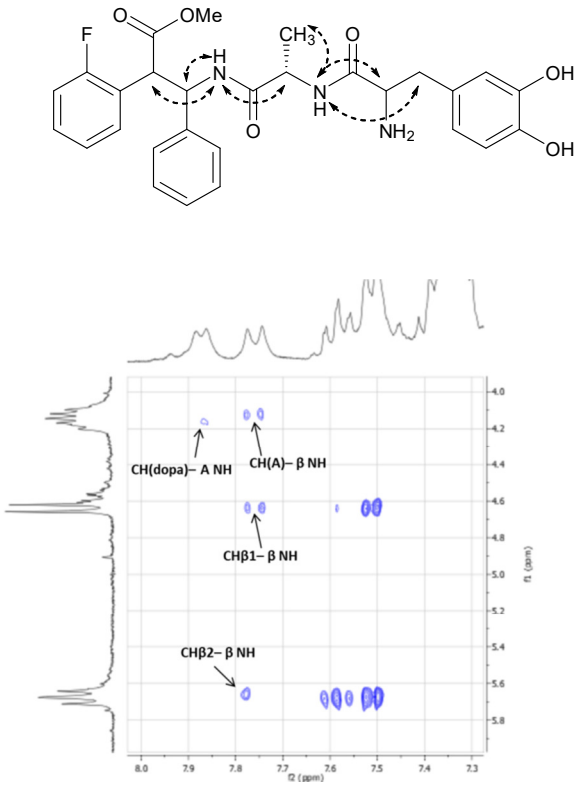

Figure 2.11. NOESY experiments analysis of $C^{\alpha}H$-NH region in $CDCl_3$ for compound **4**

The hypothesis was confirmed estimating the temperature dependence of amide chemical shift (Δδ/ΔT, 273–300 K) in $CDCl_3$ In fact, only the amide of Ala has a Δδ/ΔT NH value close to 4 ppb/K as shown in figure 2.12, providing a slight intramolecular hydrogen bond.

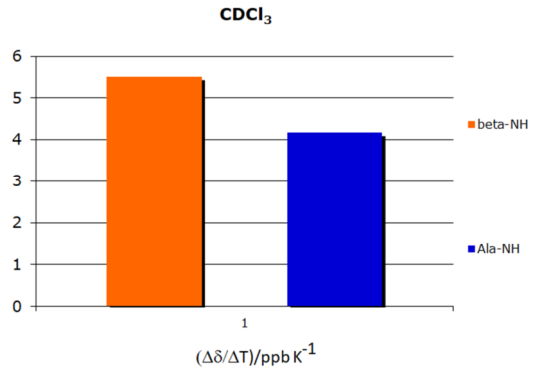

Figure 2.12. Δδ/ΔT values of β.amino acid amide (orange) and Ala amide (blue) of compound **4**

Coating characterization

To evaluate if compound **4** generated a "Teflon-like" layer on titanium surfaces, their contact angles were measured. As shown in figure 2.13, the coating of compound **4** makes the surface more hydrophobic, but not as hydrophobic as the Dopa-(F)-Phe-(F)-Phe-OMe peptide[19] since it increases the contact angle. Furthermore, the differences between the various concentrations are not significant.

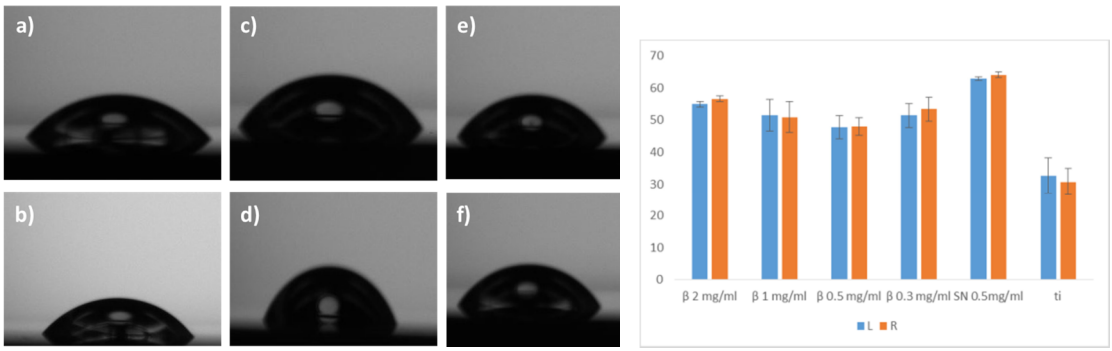

Figure 2.13. a-f) Contact angle measurements of a) bare titanium b) coated titanium with Dopa-Phe-Phe-OMe c) coated titanium with 0.3 mg/ml compound **4** d) coated titanium with 0.5 mg/ml compound **4** e) coated titanium with 1 mg/ml compound **4** f) coated titanium with 2mg/ml compound **4**

The real-time adhesion of the peptides to titanium substrates was studied using Quartz Crystal Microbalance with Dissipation monitoring (QCM-D). Peptide **4** was injected into a flow cell containing a titanium-coated sensor. The injection of compound **4** resulted in

changes both in frequency (ΔF) and dissipation (ΔD). This suggests that the peptide bonded to the sensor (Fig. 2.14)

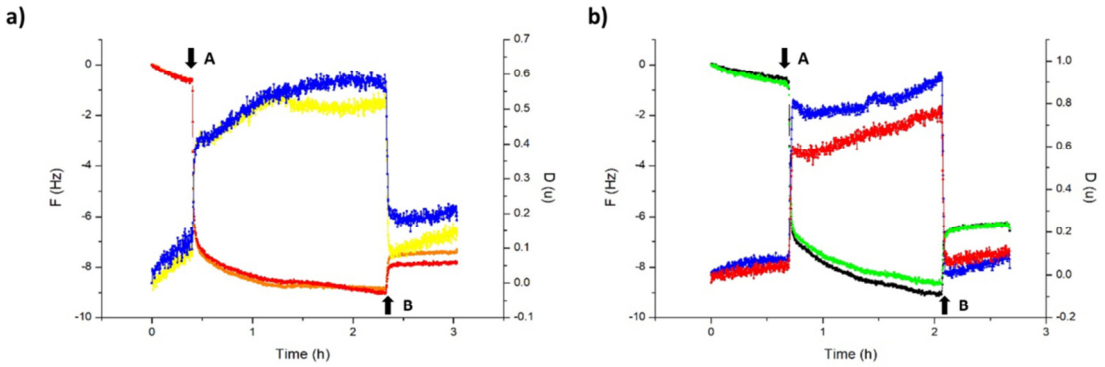

Figure 2.14. Real-time QCM-D measurements of a) 1 mg/ml peptide **4** and b)0.5 mg/ml peptide **4**. Frequency overtones 5 and 7 are presented in a) orange and red respectively and in b) black and green respectively. Dissipation overtones 5 and 7 are presented in a) blue and yellow respectively and in b) blue and red respectively. Arrow A indicates peptide addition, arrow B washing with ethanol.

As it seemed from figure 2.14 the coating spread across the entire surface. It can be assumed this phenomenon, because the frequency and the dissipation of the sensor are similar in various frequencies. Furthermore, two conclusion can be deduced from the frequency curves. First of all, the coating is bonded to the surface strongly: after rinsing the sensor with ethanol only small amount of the peptide has washed away from the surface. Moreover, Since QCM-D is a mass dependent technique, a change in frequency is expected, that would be linearly dependent on mass. In this case, there are negligible differences in the mass of the peptide that coats the surface, between different concentrations. This result is in line with the contact angle measurements. The magnitudes of changes in dissipation are also very informative. The changes in dissipation observed for peptides **4** were around 0.1 x 10^6, characteristic of a rigid film.

According to the contact angle and QCM-D measurements, concentration of 0.5 mg/ml is enough to get a sufficient coating.

The evaluation of antifouling activity of peptide-based film (0.5 mg/ml) is still ongoing.

Conclusion

In conclusion, a new antifouling material based on the self-assembly of an unnatural tripeptide, is suggested. The peptide design includes the amino acid DOPA as the adsorption motif, the dipeptide that contains the $\beta^{2,3}$-diarylamino acid as the element that directs the self-assembly process and fluorine atoms as the antifouling agents. The application of the peptide on the surface occurs spontaneously, so it is a very simple process. The formation of a coating on titanium surface was demonstrated. Further characterization analyses of the film on titanium and also on various substrates have been already planned, as well as the antifouling activity tests. The peptide presented here can be useful in several applications such as the coating of medical devices and hospital equipment in order to prevent possible infections or, in marine environment, to preserve the powering of the ship and the marine equipment.

Experimental Section

Materials

All reagents were purchased from Sigma-Aldrich, Iris Biotech or Fluka. All solvents were of ACS grade or higher and were obtained from Sigma-Aldrich. Reactions were monitored by thin-layer chromatography carried out on 0.25 mm Merck silica gel plates (60F-254) with UV light as the visualizing agent and ninhydrin as developing agents. Chromatographic separation was performed using Silicycle 60 Å SiO_2 (230-400 mesh). NMR spectra were recorded on Varian Gemini 300 or Bruker Avance 300 using appropriate deuterated solvents. Mass spectra were acquired on Fisons MD800 spectrometer and electrospray ion trap on a Finnigan lcq advantage Thermo-spectrometer. IR spectra were recorded in KBr pellet in ParkinElmer FT-IR spectrometer. Melting points were measured on SMP3 apparatus, Stuart Scientific. $[\alpha]_D$ was measured on ParkinElmer model 343 plus polarimeter. Chromatographic separation was performed using a DENALI C-18 column (10 mm, 250_22 mm). (Department of Pharmaceutical Sciences, University of Milan). Contact angle measurements were carried out using a Theta Lite optical tensiometer (Attension, Finland). Each experimental measurement consisted of three repeats. QCM-D measurements (Q-sense, Biolin Scientific) were performed in a flow module E1 system. Ti sensors with a fundamental resonant frequency of 5MHz (Q-sense) are used as supplied. Before each experiment, Ti sensors were cleaned with Oxygen/Plasma (Atto, Diener Electronic), followed by rinsing with 2% SDS and TDW and finally dried under nitrogen. All QCM-D experiments were performed under flow-through conditions using a digital peristaltic pump (IsmaTec Peristaltic Pump, IDEX). The studied solutions were injected to the sensor crystal chamber 0.1 mL/min rate. A tube and an O-ring compatible with organic solvent were used for the flow system. Peptides were dissolved in EtOH to a concentration of 0.5 mg/mL. (The Institute of Chemistry and the Center for Nanoscience and Nanotechnology. The Hebrew University of Jerusalem, Israel)

Methods

Purification of compound **6** was performed using preparative HPLC, according to the method described below:

Time (min)	% A	% B	Flow (ml/min)	Gradient
0	95	5	20	linear
1	95	5	20	linear
20	0	100	20	linear
26	0	100	20	linear
30	95	5	20	linear
31	95	5	0	linear

- phase A: $H_2O/CH_3CN/TFA$ (95:5:0.1)
- phase B: $CH_3CN/H_2O/TFA$ (95:5:0.1)

General Synthetic Procedures

Procedure 1: Mannich Reaction

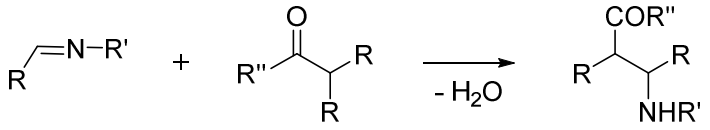

An enolizable carbonyl compound (1.05 eq) is dissolved in anhydrous dichloromethane (10 ml/mmol) under nitrogen. The imine is added and the mixture is cooled at -78 °C before adding a $TiCl_4$ solution in anhydrous dichloromethane (2.2 eq in 0.6 ml/mmol) in 15 minutes. The mixture is stirred for 30 minutes then, TEA (2.2 eq) is added and the stirring is continued for further 15 minutes. A saturated aqueous K_2CO_3 is dropped and the temperature is raised at 25°C. The white solid is filtered through celite®, the organic layer is separated and the organic phase is extracted with dichloromethane. The combine organic layers are washed with brine, dried over Na_2SO_4, filtered, and concentrated under reduced pressure.

Procedure 2: Coupling Reaction

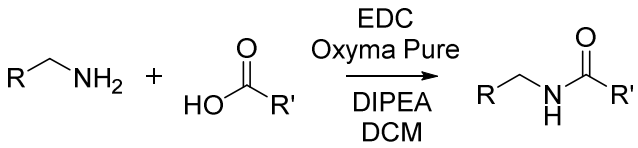

The carboxylic acid (1.1 eq) is dissolved in dichloromethane (10 ml/mmol) under nitrogen. The mixture is cooled at 0 °C before adding EDC (1.1 eq) and Oxyma Pure (1.1 eq) and is stirred for 1 hour. Then, the amide (1 eq) and DIPEA are added until pH=7-8. The mixture is allowed to react overnight at rt. The solvent is removed under reduced pressure. The residue is dissolved in DCM and the organic phase is washed with 5% w/v aqueous $KHSO_4$, saturated aqueous $NaHCO_3$, and brine. The organic layer is dried over Na_2SO_4, filtered, and concentrated under reduced pressure.

Procedure 3: Benzyl-Deprotection by catalytic reduction

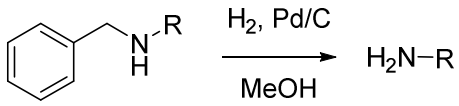

Benzyl-protected compound is dissolved in methanol 20 ml/mmol). 10% Pd/C (80 mg/mmol) is added and the mixture is stirred under H_2 atmosphere at rt for 24 hours. Then, the mixture is filtered through celite® and the filtered solution is evaporated under reduced pressure.

Procedure 4: Boc-Deprotection

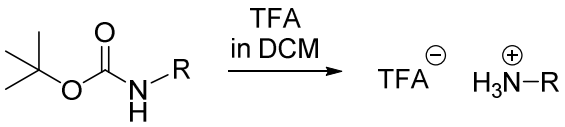

Boc-protected compound is dissolved in dichloromethane (10 ml/mmol) and cooled to 0°C before adding trifluoroacetic acid (10 ml/mmol) dropwise. The mixture is stirred for 3 hours at rt, then the solvent is evaporated under reduced pressure and the residue is

washed three times with ethyl ether. The deprotected product is used in the following step without further purification.

Procedure 5: Boc- L-3,4-dihydroxyphenylalanine synthesis

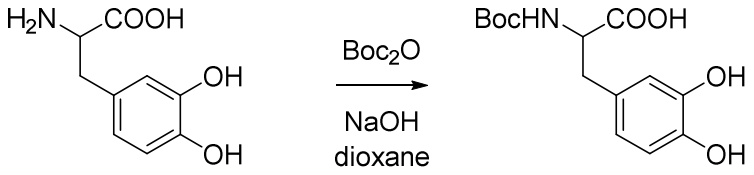

L-3,4-dihydroxyphenylalanine (1 g, 5 mmol) is dissolved in a mixture of dioxane (8 ml) and water (5 ml). Then, a solution of di-tert-butyl dicarbonate (1.22 g, 5.6 mmol) in dioxane (1.6 ml) and 1M NaOH (5.6 ml) is dropped into the mixture. After 30 minutes, 1 hour and 7 hours the pH is adjusted to 10 by the addition of 1M NaOH. The reaction is allowed to react overnight. The solvent is evaporated under reduced pressure and the pH is adjusted to 2 with 1M HCl at 0°C. The residue is extracted three times with ethyl acetate, the organic layer is washed with water and brine, dried over Na_2SO_4 , filtered and evaporated under reduced pressure. The product is used in the following step without further purification.

Specific Synthetic Procedures

Compound 1

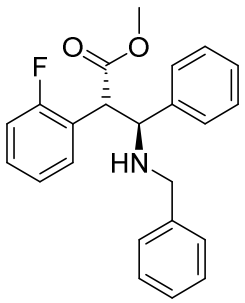

Compound **1** was synthesized following general procedure **1** from methyl (2-F-phenyl)-acetate (0.315 g, 1.9 mmol) and N-benzylidene-1-phenylmethanamine (0.353 g, 1.8

mmol). The reaction is monitored by TLC (hexane/ethyl acetate, 20:1) and the crude product is purified by silica gel column chromatography (hexane/ethyl acetate, 9:1).

White solid, yield 86%. mp: 78.3°C. IR (KBr) 1738, 1490, 1155 cm^{-1}. ^{1}H NMR (300 MHz, $CDCl_3$) δ 1.65 (bs, 1H), 3.38 (s, 3H), 3.55 (AB system, 2H, J=13.9 Hz), 4.30 (AB system, 2H, J=9.5 Hz), 7.48-7.00 (m, 9H). ^{13}C NMR (300 MHz, $CDCl_3$) δ 50.7, 50.9, 52.0, 63.6, 115.7 (d, J=22.9 Hz), 123.5, 124.5, 124.6, 127.1, 127.9, 128.2, 128.4, 128.6, 129.4, 129.5, 129.7, 143.4, 161.5 (d, J=246 Hz), 171.98.19. F NMR (282 MHz, $CDCl_3$): δ -117.4. ESI-MS (m/z): 364.1 $[M+H]^+$

Compound 2

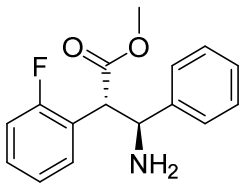

Compound **2** (6.02 g, 16.6 mmol) was benzyl-deprotected by catalytic reduction according general procedure **3**.

White solid, yield >98%. mp: 81.2°C. IR (KBr) 1735, 1491, 1153, 758 cm^{-1}. ^{1}H NMR (200 MHz, $CDCl_3$) δ 1.50 (s, 2H), 3.46 (s, 3H), 4.45(AB system, 2H, J=9.2 Hz), 7.62-7.00 (m, 9H). ^{13}C NMR ($CDCl_3$, 200 MHz) δ 52.0, 58.4, 115.7 (d, J=22.9 Hz), 123.4, 123.7, 124.4, 127.3, 127.9, 128.7, 129.5, 143.2, 161.5 (d, J=246.5 Hz), 172.3. ESI-MS (m/z): 274.1 $[M+H]^+$

Compound 3a (D1) and 3b (D2)

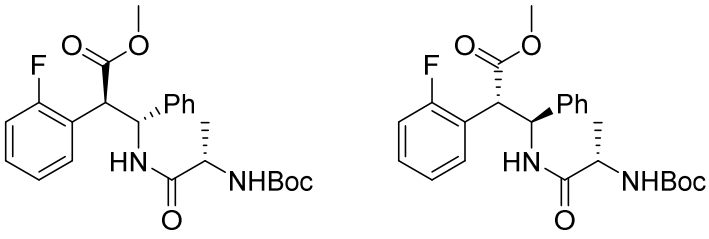

Compounds **3a** and **3b** were synthesized by coupling (general procedure **2**) compound **2** (4 g, 14.7 mmol) and Boc-L-Ala-OH (3.1 g, 16.3 mmol). The reaction is monitored by TLC (ethyl acetate/hexane 1:1) and the two diasteroisomers were separated by silica gel column chromatography (hexane/ethyl acetate 5:1).

(2R, 3R)-(D1): white solid, yield 45%. $[\alpha]_D$ = +34.5 ($CHCl_3$). IR (KBr) 3372 (NH), 1737, 1672 (CO) cm^{-1}. ^1H NMR (500 MHz, $CDCl_3$) δ 0.81 (d, 3H, J=6.7 Hz), 1.35 (s, 9H), 3.46 (s, 3H), 3.82-3.78 (m, 1H), 4.50 (d, 1H, J=10.9 Hz), 5.38 (bs, 1H), 5.69 (dd, 1H, J=10.9, 10.7 Hz), 7.07 (d, 1H, J=10.8 Hz), 7.15-7.10 (m, 3H), 7.20 (ddd, 1H, J=8.3, 1.3 Hz), 7.31 (ddd, 1H, J=7.6, 1.3 Hz), 7.44-7.31 (m, 3H), 7.54 (ddd, 1H, J=7.6, 1.5 Hz). ^{13}C NMR ($CDCl_3$, 500 MHz) δ 17.8, 27.9 (x 3C), 49.6, 50.1, 52.2, 54.1, 79.1, 115.7, 117.7, 124.8, 124.9, 127.8, 128.2, 128.9, 129.8, 130.1, 130.2, 140.9, 155.5, 161.2, 171.3, 172.2. ESI-MS (m/z): 467.4 $[M+Na]^+$

(2S, 3S)-(D2): white solid, yield 43%. $[\alpha]_D$ = +53.6 ($CHCl_3$). ^1H NMR (500 MHz, $CDCl_3$) δ 0.92 (d, 3H, J=6.7 Hz), 1.37 (s, 9H), 3.46 (s, 3H), 3.80-3.74 (m, 1H), 4.52 (d, 1H, J=10.5 Hz), 5.38 (brs, 1H), 5.68 (dd, 1H, J=10.5, 9.9 Hz,), 7.07 (d, 1H, J=9.9 Hz,), 7.15-7.10 (m, 3H), 7.19 (ddd, 1H, J=9.6, 8.3 Hz), 7.30 (ddd, 1H, J=7.6, 1.2 Hz), 7.58-7.30 (m, 3H), 7.54 (ddd, 1H, J=7.6, 1.4 Hz,). ^{13}C NMR ($CDCl_3$, 500 MHz) δ 17.6, 27.9 (x 3C), 49.6, 51.1, 52.1, 53.9, 79.4, 115.7, 117.7, 124.8, 124.9, 127.7, 128.2, 128.6, 128.8, 130.1, 130.3, 140.9, 155.5, 161.2, 171.4, 172.5.. ESI-MS (m/z): 467.4 $[M+Na]^+$

Compound 4

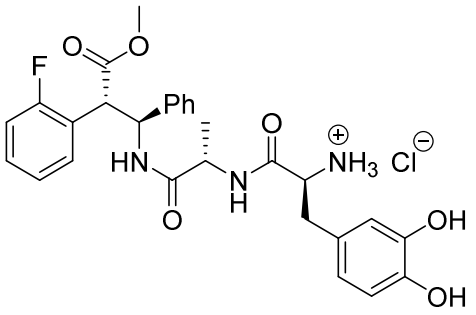

Compound **5** (0.13 g, 0.2 mmol) was Boc-deprotected according general procedure **4**. The residue is purified using preparative HPLC according to the reported method.

Gray solid, yield 35%. mp: 139.8-140.3°C. $[\alpha]_D$ = -53 (CH_3OD). IR (KBr) 3232, 3065 (NH), 1739, 1666 (CO) cm^{-1}. ^1H NMR (300 MHz, CD_3CN) δ 0.96 (d, 3H, J=7.1 Hz, $CH_{3(A)}$), 2.93 (m, 2H, CH_2), 3.42 (s, 3H, CH_3), 4.12-4.17 (m, 2H, $CH_{(A)}$ + $CH_{(dopa)}$), 4.64 (d, 1H, J=11.3, CHCOOMe), 5.68 (t, 1H, J=10.7 Hz, CH), 6.64 (s, 1H, ArylH), 6.75 (s, 1H, ArylH), 7.1-7.6 (m, 10H, ArylH + NH_2), 7.76 (d, 1H, J=9.5, $NH_{(\beta)}$), 7.87 (d, 1H, J=6.4 Hz, $NH_{(A)}$). ^{13}C NMR (300 MHz, CD_3CN) δ 17.0 ($CH_{3(A)}$), 29.1 (CH_2), 49.4 (CHCOOMe), 49.8 ($CH_{(A)}$), 51.7 (CH_3), 52.1

($CH_{(dopa)}$), 53.8 ($CH_{(\beta)}$), 111.9, 115.1, 115.5 (ArCH), 124.4, 127.4-130.2 (ArCH), 140.5, 144.5, 144.6, 159.3, 162.6, 167.3, 170.9, 171.1 (C). ESI-MS (m/z): 525.26 $[M+H]^+$, 523.03 $[M-H]^-$

Intermediate 5b (D2)

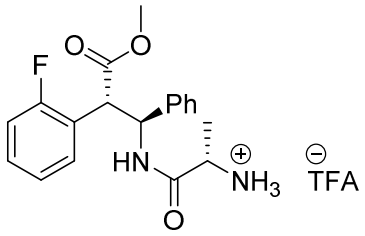

Compound **4b** (0.1 g, 0.3 mmol) was Boc-deprotected according general procedure **4**. White solid, yield >98%. mp: 87.7°C. $[\alpha]_D$ = +76.8 ($CHCl_3$). IR (KBr) 1736, 1671, 1592, 1495 cm^{-1}. ^1H NMR (200 MHz, $CDCl_3$) δ 0.84 (d, 3H, J=6.88 Hz), 3.40-3.80 (m, 2H), 3.49 (s, 3H), 4.52 (d, 1H, J=10.48 Hz), 5.67 (t, 1H, J=10.11 Hz), 7.41-6.98 (m, 9H), 7.57 (ddd, 1H, J=1.47, 7.33 Hz), 8.02 (d, J=9.53 Hz, 1H). ^{13}C NMR (200 MHz, $CDCl_3$) δ 19.6, 49.0 (d, J=3.0), 50.0, 52.2, 54.3, 115.2 (d, J=21.8), 122.5 (d, J=13.82), 124.5 (d, J=3.46), 127.4, 127.9, 128.6, 129.5 (d, J=8.06), 129.8 (d, J=3.45), 139.6, 161.1 (d, J=245.3), 171.0, 172.1. ESI-MS (m/z): 345.3 $[M+H]^+$

Intermediate 6

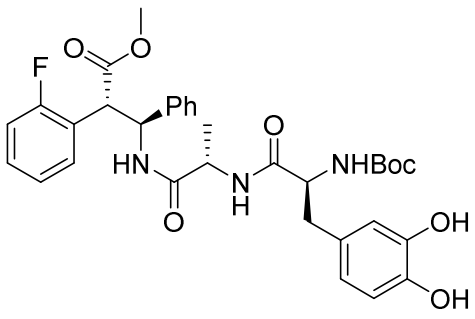

Compound **5** was synthesized by coupling (general procedure **2**) compound **4b** (0.1 g, 0.3 mmol) and Boc-L-Dopa-OH (0.1 g, 0.35 mmol) previously synthetized according general procedure **5**. The reaction is monitored by TLC (DCM/methanol 10:0.3) and the residue is used in the following step without further purification.

IR (KBr) 3402 (NH), 1740, 1673 (CO) cm-1. ^{1}H NMR (300 MHz, CD_3OD) δ 1.00 (d, 3H, J=6.9 Hz, $CH_{3(A)}$), 1.45 (s, 9H, CH_3), 2.81-2.89 (m, 2H, CH_2), 3.42 (s, 3H, CH_3), 4.01-4.11 (m, 2H, $CH_{(A)}$ + $CH_{(dopa)}$), 4.55 (d, 1H, J=11.2, CHCOOMe), 5.67 (d, 1H, J=11.3 Hz, CH), 6.48-7.57 (m, 12H, ArylH). ESI-MS (m/z): 646.41 $[M+Na]^+$

References

[1] C. M. Kirschner, A. B. Brennan, *Annual Review of Materials Research* **2012**, *42*, 211-229.

[2] I. Banerjee, R. C. Pangule, R. S. Kane, *Advanced Materials (Weinheim, Germany)* **2011**, *23*, 690-718.

[3] S. Sonak, P. Pangam, A. Giriyan, K. Hawaldar, *Journal of environmental management* **2009**, *90 Suppl 1*, S96-108.

[4] a) V. B. Damodaran, N. S. Murthy, *Biomaterials Research* **2016**, *20*, 18/11-18/11; bS. Nir, M. Reches, *Current Opinion in Biotechnology* **2016**, *39*, 48-55.

[5] a) S. Pechook, B. Pokroy, *Advanced Functional Materials* **2012**, *22*, 745-750; b) H. J. Ensikat, P. Ditsche-Kuru, C. Neinhuis, W. Barthlott, *Beilstein Journal of Nanotechnology* **2011**, *2*, 152-161.

[6] a) M. Salta, J. A. Wharton, P. Stoodley, S. P. Dennington, L. R. Goodes, S. Werwinski, U. Mart, R. J. K. Wood, K. R. Stokes, *Philosophical Transactions of the Royal Society, A: Mathematical, Physical & Engineering Sciences* **2010**, *368*, 4729-4754; b) A. V. Bers, M. Wahl, *Biofouling* **2004**, *20*, 43-51.

[7] M. Carman, T. Estes, A. Feinberg, J. Schumacher, W. Wilkerson, L. Wilson, M. Callow, J. Callow, A. Brennan, *Biofouling* **2006**, *22*, 11-21.

[8] S. Pechook, N. Kornblum, B. Pokroy, *Advanced Functional Materials* **2013**, *23*, 4572-4576.

[9] G. D. Bixler, B. Bhushan, *Critical Reviews in Solid State and Materials Sciences* **2015**, *40*, 1-37.

[10] *Marine Fouling and Its Prevention*, **1952**.

[11] T. Wagner, C. Neinhuis, W. Barthlott, *Acta Zoologica* **1996**, *77*, 213-225.

[12] a) K. L. Prime, G. M. Whitesides, *Science (Washington, D. C., 1883-)* **1991**, *252*, 1164-1167; b) J. P. Bearinger, S. Terrettaz, R. Michel, N. Tirelli, H. Vogel, M. Textor, J. A. Hubbell, *Nature Materials* **2003**, *2*, 259-264; c) J. H. Lee, J. Kopecek, J. D. Andrade, *Journal of Biomedical Materials Research* **1989**, *23*, 351-368; d) V. A. Liu, W. E. Jastromb, S. N. Bhatia, *Journal of Biomedical Materials Research* **2002**, *60*, 126-134; e) K. L. Prime, G. M. Whitesides, *Journal of the American Chemical Society* **1993**, *115*, 10714-10721.

[13] E. Ostuni, R. G. Chapman, M. N. Liang, G. Meluleni, G. Pier, D. E. Ingber, G. M. Whitesides, *Langmuir* **2001**, *17*, 6336-6343.

[14] C. R. Arciola, F. I. Alvi, Y. H. An, D. Campoccia, L. Montanaro, *The International journal of artificial organs* **2005**, *28*, 1119-1125.

[15] S. Chen, Z. Cao, S. Jiang, *Biomaterials* **2009**, *30*, 5892-5896.

[16] R. Chelmowski, S. D. Koester, A. Kerstan, A. Prekelt, C. Grunwald, T. Winkler, N. Metzler-Nolte, A. Terfort, C. Woell, *Journal of the American Chemical Society* **2008**, *130*, 14952-14953.

[17] a) A. R. Statz, R. J. Meagher, A. E. Barron, P. B. Messersmith, *Journal of the American Chemical Society* **2005**, *127*, 7972-7973; b) K. H. A. Lau, T. S. Sileika, S. H. Park, A. M. L.

Sousa, P. Burch, I. Szleifer, P. B. Messersmith, *Advanced Materials Interfaces* **2015**, *2*, 1400225/1400221-1400225/1400210.

[18] H. Lee, N. F. Scherer, P. B. Messersmith, *Proceedings of the National Academy of Sciences of the United States of America* **2006**, *103*, 12999-13003.

[19] S. Maity, S. Nir, T. Zada, M. Reches, *Chemical Communications (Cambridge, United Kingdom)* **2014**, *50*, 11154-11157.

[20] A. Bonetti, F. Clerici, F. Foschi, D. Nava, S. Pellegrino, M. Penso, R. Soave, M. L. Gelmi, *European Journal of Organic Chemistry* **2014**, *2014*, 3203-3209.

[21] A. Bonetti, S. Pellegrino, P. Das, S. Yuran, R. Bucci, N. Ferri, F. Meneghetti, C. Castellano, M. Reches, M. L. Gelmi, *Organic Letters* **2015**, *17*, 4468-4471.

[22] a) D. Seebach, A. K. Beck, S. Capone, G. Deniau, U. Groselj, E. Zass, *Synthesis* **2009**, 1-32; b) Z. Szakonyi, F. Fulop, *Amino Acids* **2011**, *41*, 597-608; c) K. Mikami, S. Fustero, M. Sanchez-Rosello, J. L. Acena, V. Soloshonok, A. Sorochinsky, *Synthesis* **2011**, 3045-3079; d) D. J. Hart, D. C. Ha, *Chemical Reviews (Washington, DC, United States)* **1989**, *89*, 1447-1465.

[23] a) S. H. Gellman, *Accounts of Chemical Research* **1998**, *31*, 173-180; b) D. Seebach, S. Abele, K. Gademann, G. Guichard, T. Hintermann, B. Jaun, J. L. Matthews, J. V. Schreiber, L. Oberer, U. Hommel, H. Widmer, *Helvetica Chimica Acta* **1998**, *81*, 932-982; c) J. L. Goodman, E. J. Petersson, D. S. Daniels, J. X. Qiu, A. Schepartz, *Journal of the American Chemical Society* **2007**, *129*, 14746-14751; d) D. Balamurugan, K. M. Muraleedharan, *Chemistry - A European Journal* **2012**, *18*, 9516-9520, S9516/9511-S9516/9546; e) K. Gademann, T. Hintermann, J. V. Schreiber, *Current Medicinal Chemistry* **1999**, *6*, 905-925.

[24] a) R. S. Seoudi, M. G. Hinds, D. J. D. Wilson, C. G. Adda, M. D. Borgo, M.-I. Aguilar, P. Perlmutter, A. Mechler, *Nanotechnology* **2016**, *27*, 135606/135601-135606/135609; b) F. Clerici, E. Erba, M. L. Gelmi, S. Pellegrino, *Tetrahedron Letters* **2016**, *57*, 5540-5550.

[25] T. Hintermann, D. Seebach, *Chimia* **1997**, *51*, 244-247.

[26] R. P. Cheng, S. H. Gellman, W. F. DeGrado, *Chemical Reviews (Washington, D. C.)* **2001**, *101*, 3219-3232.

Chapter 3

Electrospinning

Introduction

Electrospinning

Electrospinning is a simple and versatile technique used for the fabrication of continuous ultrafine fibers, having diameters from tens of nanometers to a few microns, commonly known as nanofibers. It seems the only technique that can produce nanofibers on an industrial scale with a length up to several meters. This procedure uses an electrical field to create nanofibers from a conductive solution prepared mainly from polymeric or composite solutions. The structural and functional versatility of these submicron fibers has allowed a wide range of applications, such as membranes and filters[1], biomaterials[2], electrical and optical components and sensors[3]. It has been reported they are important also in pharmaceutical industry thanks to their chemical composition and physicochemical characteristics. In particular, they find applications in wound dressing[4], tissue engineering[5] and drug delivery systems[6]. Among the advantages of electrospun nanofibers as drug carriers, the high surface-to-volume ratio accelerates the aqueous solubility and therefore can improve the efficiency of the drug, especially for highly porous fibers. Moreover, it is a convenient technique with low operating cost and the fiber diameter and directions can be controlled depending on materials, instrument setup and process parameters. The principle is based on applying a high voltage (kV range) to a high viscosity fluid, which forms a jet that can be collected in dry form on a grounded substrate. The electrospinning process can be divided in two phases: in the first phase the solution droplet is charged above a critical high voltage, resulting in the formation of Taylor cone shape 0.1-1 mm of diameter by electric force. In the second phase, a jet is ejected and travels to the grounded collector. Further away from the cone, the solution jet has an instability, and whipping occurs in which the jet travels and rapidly elongates on its way to and the collector (Fig. 3.1). It undergoes thinning (diameter of nanometre range), and very rapid bending ("whipping"), generating structures appearing as if it were a cone of spraying droplets from a faucet to the human eyes (Fig. 3.1 "rapid acceleration"). In fact, only one single fiber is ejected. The solvent evaporates, leaving behind a charged fiber deposited on a collector.

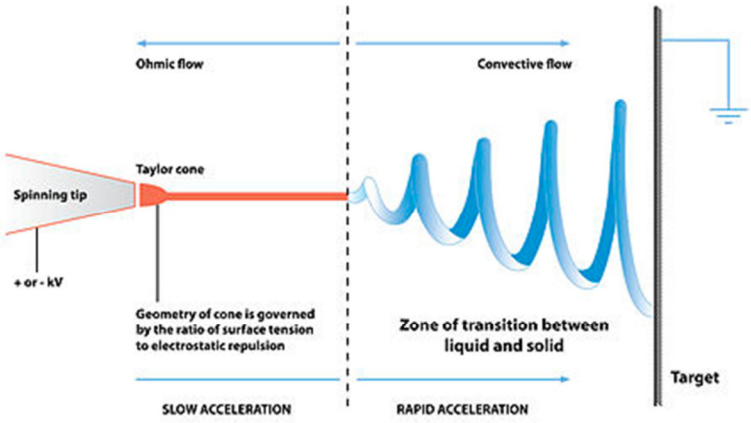

Figure 3.1. The two phases of the electrospinning process

Working parameters (solution, process and ambient parameters) can affect the fibers morphologies and by a proper control of them, it is possible to produce electrospun fibers with desired morphologies and diameters (Fig. 3.2).[7] The resulting fibers are typically disorganized but oriented fibers are produced by controlling the geometry of the collector.

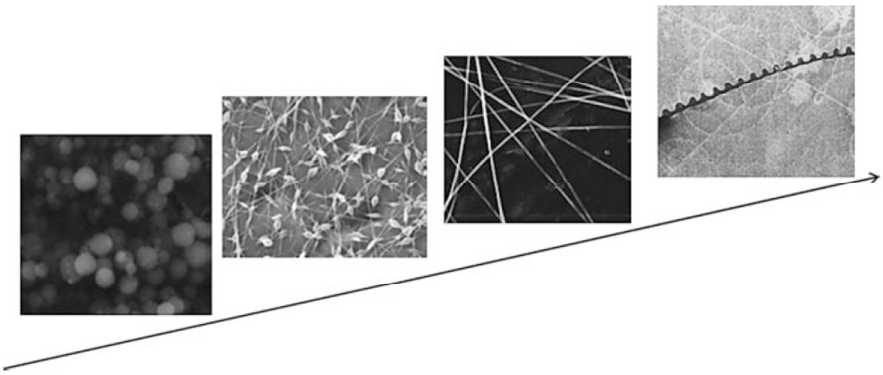

Figure 3.2. SEM micrographs of the evolution of the products with different concentrations from low to high during the electrospinning. (adapted from [7])

Non-polymeric molecules can usually not be electrospun, because only polymer solutions or melts are sufficiently viscous and provide the required degree of molecular entanglement.[8] However, recent studies have demonstrated that high molar mass polymers are not essential for production of uniform electrospun fibers and that the

presence of sufficient intermolecular interactions that effectively act as chain entanglements is the primary criterion.[9]

Heterocycles

Heterocycles are an important class of compounds with a wide range of physical, chemical and biological properties, making up more than half of all known organic compounds. Heterocycles play an important role in nature, in particular they have been frequently found as a key structural units in many natural products, including vitamins, hormones, antibiotics and alkaloids, and biomolecules such as DNA, RNA and proteins. In addition, a large number of synthetic heterocyclic compounds with pharmacological and physiological properties are also known. Many of these compounds are used as pharmacophore to arrange potent and selective drugs since they display suitable properties such as high membrane permeability and metabolic stability, low flexibility and numerous binding sites toward hydrophobic pockets or hydrogen bond acceptors and donors. Among heterocyclic compounds, nitrogen-containing heterocycles are the building block of life due to their central role in the chemical reactions that occur in all organisms.[10] In recent years, numerous isothiazole derivatives, containing sulphur and nitrogen atoms, obtained patent as agrochemicals and medical agents thanks to their antifungal and antibacterial properties. In particular, compounds containing the 3(2H)-isothiazole skeleton are potent antimicrobials and are suggested for use in circulating water apparatus for industry, rubber latex and paints. Moreover, many isothiazole derivate are useful to prevent fungal growth in a wide range of manufactured goods.[11] One of the most important and best-known isothiazole derivative is Saccharin, which is an artificial sweetener about 300-400 times as sweet as sucrose, with effectively no food energy. The isothiazole ring is also incorporated into pharmaceutical drugs such as Ziprasidone and Perospirone (Fig.3.3), two atypical antipsychotics approved by the FDA in 2001 for the treatment of schizophrenia, acute mania and bipolar disorder.

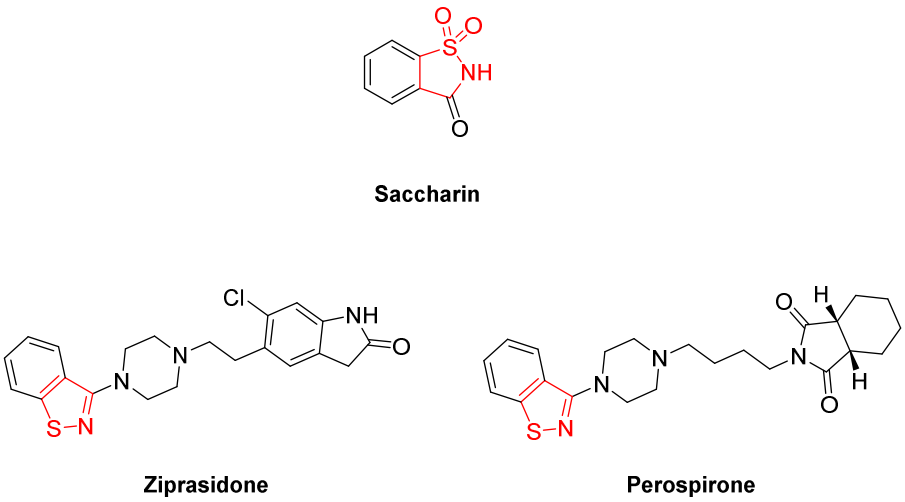

Figure 3.3. Drug molecules containing isothiazole structure

For several years, my research group worked on a particular class of isothiazole, the 3-amino-isothiazole oxides[12], describing a simple method for the synthesis of isothiazole mono and dioxides unsubstituted or mono/disubstituted with halogen atoms, both with a substituted amino group in C-3 (Fig. 3.4).[13]

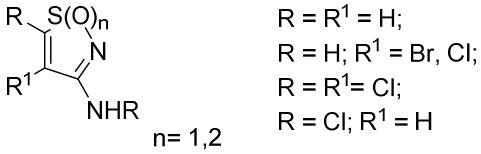

Figure 3.4. 3-Amino-isothiazole derivatives

Starting from these compounds, many bicyclic systems were prepared by cycloaddition reaction, exploiting the C-4 C-5 double bond reactivity toward several 1,3-dipoles.[14] This thesis is focused on bicyclic compounds containing the pyrazole-isothiazole system (Fig. 3.5).

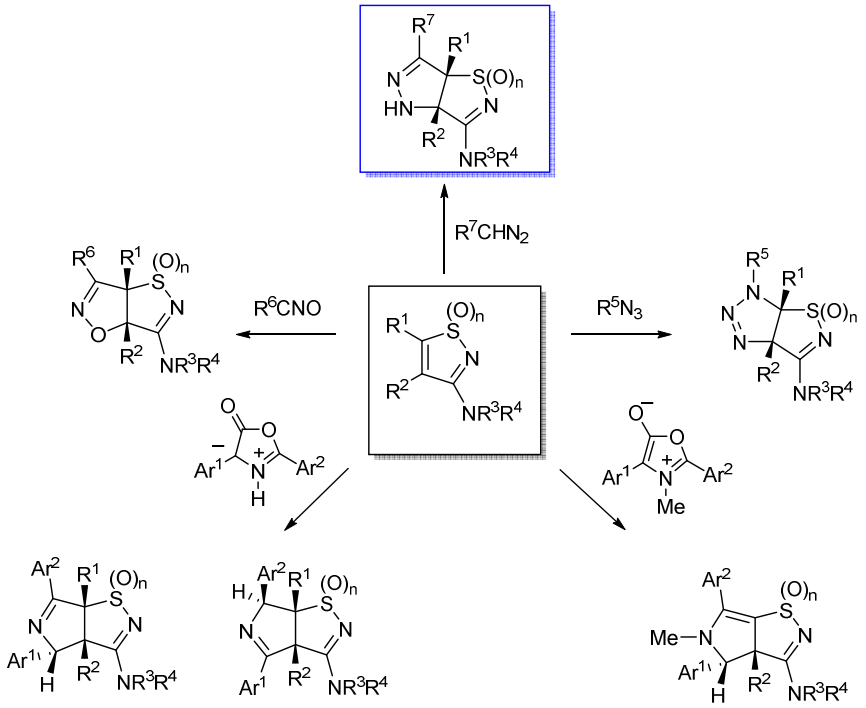

Figure 3.5. Heterocyclic systems prepared by cycloaddition reaction

Pyrazole-isothiazole possesses many interesting chemical properties. First of all, it is a versatile building block for the synthesis of peptidomimetics, indeed, it is possible to functionalize it with carboxylic substituent in C-6 which, in the same way as the pyrazole NH group, can be exploited for coupling reaction with amino acids. Moreover, starting from isothiazole dioxide or 4-bromoisothiazole dioxide, two different bicyclic systems are obtained by cycloaddition reaction: in the first case two enantiomers of a chiral compound with C3a-C6a single bond are formed, in the second case, a completely planar system with C3a-C6a double bond is formed after spontaneous elimination of HBr (Fig. 3.6). The interesting aspect is that the different geometry of the two bicyclic systems could also influence the conformation and the secondary structure of the peptide sequence linked to the heterocycle. 3-Amino isothiazole derivatives possess also many non-covalent interaction points. In particular, the sulfonyl and the NH group at C-3 can stabilize intra and intermolecular interactions since they behave respectively as hydrogen bond acceptor and donor. Moreover, the introduction of aromatic ring on the nitrogen atom at C3 induces additional π-stacking interactions. Hydrogen bonding and π-stacking are able to stabilize the folding of molecules and provide key energetic contribution in the self-assembly.

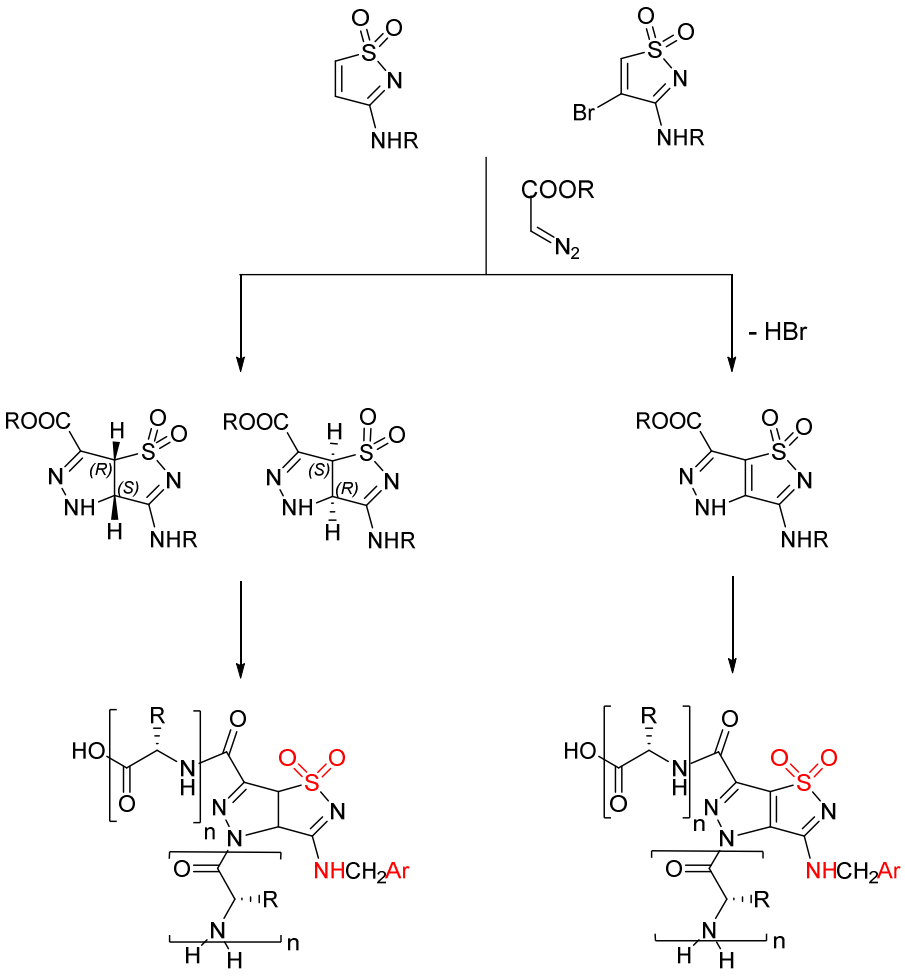

Figure 3.6. Bicyclic systems obtained from isothiazole dioxide derivatives. Non-covalent interaction points are indicated in red: the sulfonyl and the NH group at C-3 behave respectively as hydrogen bond acceptor and donor; aromatic ring on the nitrogen atom at C3 induces additional π-stacking interactions

Aim of the project

Recently it has been reported on the electrospinning of the dipeptide phenylalanine-phenylalanine (FF), and of two Fmoc derivatives, Fmoc glycine (Fmoc-Gly), and Fmoc-phenylalanylglycine (Fmoc-Phe-Gly).[15] In spite of their small size, they can assemble by electrospinning to nanofibers and these structures are based on noncovalent interactions only. On the other hand, information about electrospinning of non-natural small molecules, at our knowledge, is not reported in the literature. For this reason, we decided to exploit the chemical properties of the pyrazole-isothiazole system and its possibility to

give intermolecular interactions to develop electrospun nanofibers from a non-natural small molecules, in order to better understand the forces that play important role in electrospun fiber assembly, taking into account that the chemical characterization of a small molecule is easier than that of a polymer. The aim is indeed increasing the choice of substances for electrospinning.

The preparation and characterization of the fibres were performed in the laboratory of Prof Bittner at CIC NanoGUNE (Donostia, Spain).

For these studies, starting from the works reported in the literature, different model compounds containing the bicyclic systems linked to single amino acids or inserted in a short peptide chain (table 3.1) were designed. As amino acids it was chosen first, Fmoc-Gly, in line with other reported electrospinning peptides; second, Fmoc-Ala because it is the simplest chiral amino acid and it generates two diasteroisomers; third, the dipeptide Leu-Val, which is very well known to adopt an extended conformation, and which could be used to evaluate the role of the pyrazole-isothiazole system in the peptide folding.

Bicyclic system	**Sequence**
Pyrazoleisothiazole scaffold **1b** 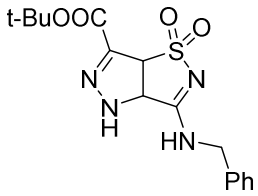	Fmoc-Gly-pyrazoleisothiazole-O-tBu Fmoc-Ala-pyrazoleisothiazole-O-tBu Fmoc-Gly-pyrazoleisothiazole-Leu-Val-NH_2
Pyrazoleisothiazole scaffold **2b** 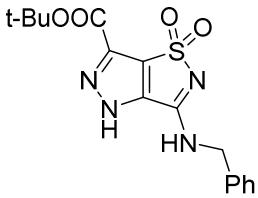	Fmoc-Gly-pyrazoleisothiazole-O-tBu Fmoc-Ala-pyrazoleisothiazole-O-tBu Fmoc-Gly-pyrazoleisothiazole-Leu-Val-NH_2

Table 3.1. Designed model compounds

Results and discussion

Synthesis

3-Benzylamino isothiazole 1,1-dioxide is produced using a synthetic strategy already developed in our group.[14b] Then, a cycloaddition reaction is performed with different diazoacetates, taking advantage of the reactivity of the C-4 C-5 double bond toward 1,3-dipoles, affording the Δ_2-pyrazoline 1a-c through tautomerization of the primary cycloaddition product, the Δ_1-pyrazoline. (Scheme 3.1). The reaction appeared to be completely regioselective, affording only one regioisomer.

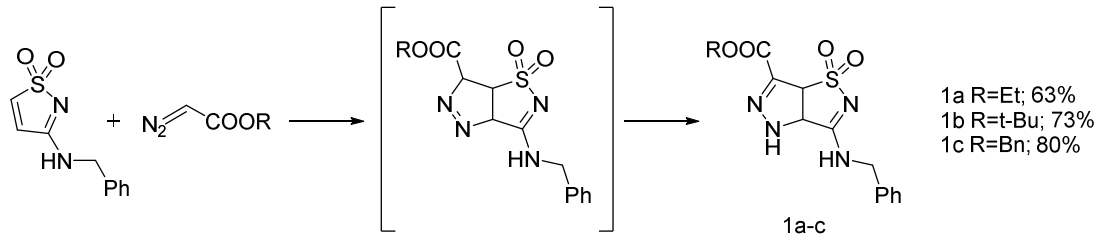

Scheme 3.1. Synthetic scheme of compounds **1a-c**

As far as concerned the planar bicyclic system, 3-benzylamino-4-bromoisothiazole 1,1-dioxide was reacted with different diazoacetates, affording compounds **2a-c** as the only reaction products, after spontaneous elimination of HBr (scheme 3.2).

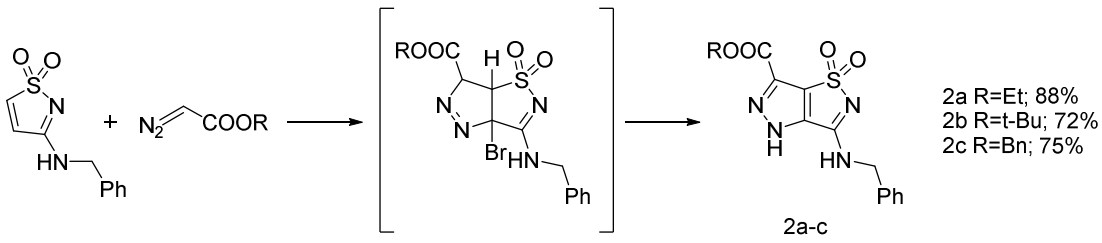

Scheme 3.2. Synthetic scheme of compounds **2a-c**

In the second step, the coupling reaction conditions have been studied in order to insert the two systems in a peptide chain. For a first series of attempts, compounds **1b** and **2b** were used since they have the t-butyl protection group which is an orthogonal group

compared to Fmoc at N-terminus, and which is easily removed under mild acidic conditions. Pyrazole NH group of compound **1b** demonstrated to be reactive toward Fmoc-Gly chloride, which is easy to prepare, in THF as the solvent, using TEA as base (32% yield). Notwithstanding the formation of the desired product was observed, the yield was unsatisfactory (< 50%); moreover the use of acyl chlorides in peptide coupling is limited by the possible hydrolysis, racemization and cleavage problems. Aiming to design a general procedure exploitable for any amino acid, several attempts were made modifying reagents and conditions: the reaction is tried using DIC (1.1 eq) and HOBT (1,1 eq) in DCM in presence of DIPEA but the DCU formed during the reaction was difficult to remove. The best result was achieved with the following procedure: after the activation of the carboxylic acid with HOBT (1.1 eq) and EDC (1.1 eq) in DCM (0°C, 1h), compound **1b** (1.1 eq) and DIPEA are added and the stirring is continued overnight at 25°C. This reaction is performed with Fmoc-Gly to give compound **3** (84% yield) and with Fmoc-Ala to give the two diastereoisomers **4'** and **4''** which are separated by flash chromatography affording compound **4'** and **4''** in 44% and 37% yield respectively.

The deprotection of carboxylic group in C-6 of compound **3** is performed in a mixture of TFA/DCM (1:1, overnight, 25°C) to give intermediate **6** in quantitative yield. Intermediate **6** is coupled with dipeptide Leu-Val-NH_2 according to the coupling procedure previously described, to afford compounds **5'/5''** which are separated by flash chromatography (Scheme 3.3).

Regarding compound **2b**, unfortunately the pyrazole NH group and carboxylic group in C-6 are not reactive in coupling reactions maybe due to the high aromaticity of the system. However, it is possible to obtain pyrazoleisothiazole "amino acid" after deprotection of carboxylic group with a mixture of TFA/DCM (1:1, 3h, 25°C) as shown in scheme 3.4.

All compounds prepared for this project were analysed and their structures confirmed (Mass spectrometry, ^{1}H- ^{13}C-NMR, literature comparison; see Experimental). New compounds were completely characterized (See below: Chemical Characterization).

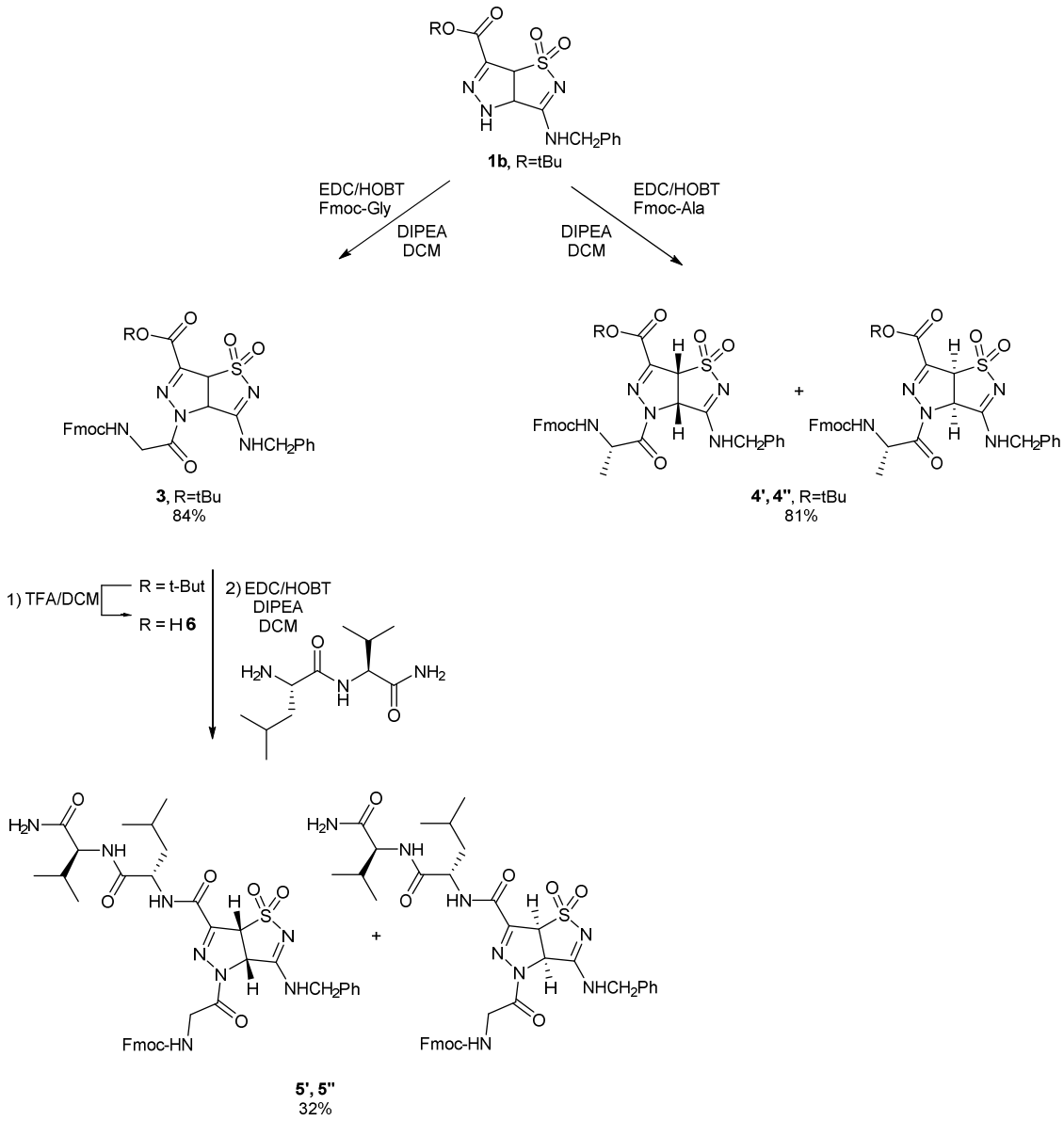

Scheme 3.3. Synthetic scheme of compounds **3**, **4'/4''** and **5'/5''**

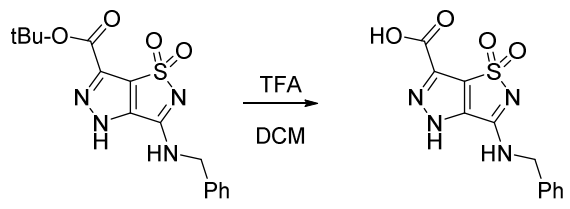

Scheme 3.4. Synthetic scheme of compound **8**

Electrospinning

The electrospinnability of the synthesized compound (**3**, **4'/4''** and **5'/5''**) has been tested. Starting from the experiments developed by Nuansing and co-workers about the electrospinnability of the short peptide Fmoc-Phe-Gly [15b], preliminary tests were performed on compound **3** containing only Fmoc-Gly as amino acid. Compound **3** is soluble in high concentration in HFIP, which is suitable solvent for electrospinning because it is highly polar, with high vapour pressure and low surface tension, so it easily evaporates after application of a high voltage. In contrast, its low viscosity can causes beads or droplets in fibres (stemming from deformation of the jet into droplets); this problem could be improved by increasing the concentration of the substance as much as possible. The concentration of the solution was calculated and prepared in percentage by weight %(wt/wt) as shown in eq. 3.1.

$$concentration\ \%(wt/wt) = \left(\frac{mass\ of\ substance}{mass\ of\ solvent + mass\ of\ substance}\right) x\ 100 \qquad (3.1)$$

The electrospinning setup is inside a closed Perspex chamber, with slow air suction to remove solvent vapours. The experiments are executed on the <5 µl scale with the microliter electrospinning technique, and on the 0,5 ml scale with a conventional setup. In the first case, the high voltage is applied to a vertically oriented platinum (Pt) wire of 0.25 mm of diameter, at 15 cm of distance from the collector. The solution is directly placed from a micropipette on the tip of the Pt wire, in this way it is possible to test the elctrospinnability of substances using µg amounts. In the second case, the high voltage is applied to a steel needle connected with a standard syringe pump to control the flow rate of solution. Best results are obtained with a mixture concentration of 30% wt/wt and applied high voltage of 15 kV. The temperature and the humidity are controlled with a hot air gun placed in the chamber, in order to have values around 30% and 27°C, respectively.
A first analysis of the electrospun nanofibers is performed depositing directly the fibers on a glass substrate and acquiring images with optical microscopy with a magnification up to 1000X. Scanning Electron Microscopy (SEM) is used to acquire high resolution images of fibers deposited on clean silicon wafer.
Figure 3.7 shows optical (Fig 3.7a,b) and SEM (Fig. 3.7c,d,e) micrographs of electrospun fibers of compound **3**: the fibers appear continuous, fairly homogenous, without any beads. This is a very satisfactory result, taking into account that compound **3** is a small

molecule and not a polymer. Their diameter (762 ± 167 nm) and their height (630 ± 84 nm) are evaluated using ImageJ software. The cross section is analysed cutting the fibers with a knife and then acquiring SEM images after tilting the sample stage of 75°; figure 7d shows that compound **3** gives fully filled fibers, not a tube, different from Phe-Phe.[15a]

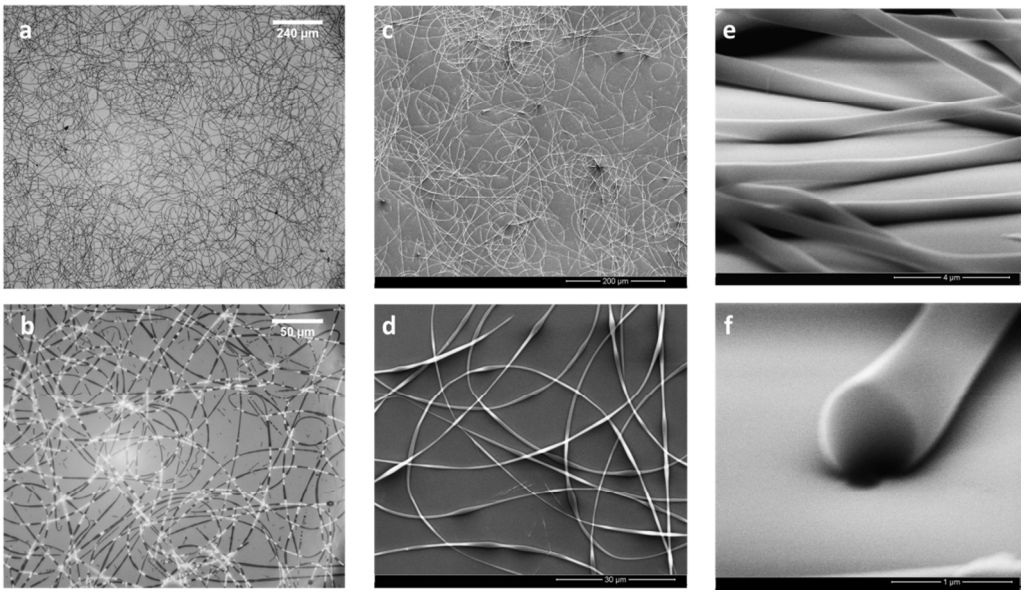

Figure 3.7. a, b) Optical micrographs of compound **3** nanofibers. c,d) SEM micrographs of compound **3** nanofibers, e) also observed under tilt of 75°. f) Cross section of the fiber. SEM images were acquired in HV (10.00 KV)

The fiber surface structure is also imaged with Atomic Force Microscopy (AFM), using silicon wafer to deposit the sample. The topography images (Fig 3.8 a) show different thicknesses. The thickness of the large fibers is in the range of 400-800 nm while the thickness of the smallest fibers found varies among 70-200 nm. The results obtained for the large fibers fit with width and diameter calculated with EM images. However, AFM can provide much finer details, as demonstrated in figure 3.8. Submicron areas, scanned exactly on the largest elevation of the fibers suffer from the high curvature. Therefore, the scans were flattened by fitting to a polynomial background. Thus treated images show a grainy structure with sizes that can vary from 7-20 nm. The grains are very compact and do not show any ordered or symmetric structure. Furthermore, the roughness of these surface is 0.8 ± 0.3 nm which demonstrates that the fibers are very smooth. This explains that other techniques show extremely smooth fibers. Some protrusions, e.g. on the right hand side of figure 3.8e, show height differences of 2 nm, which correlate with the molecular size, but due to the absence of ordering, features such as islands do not exist.

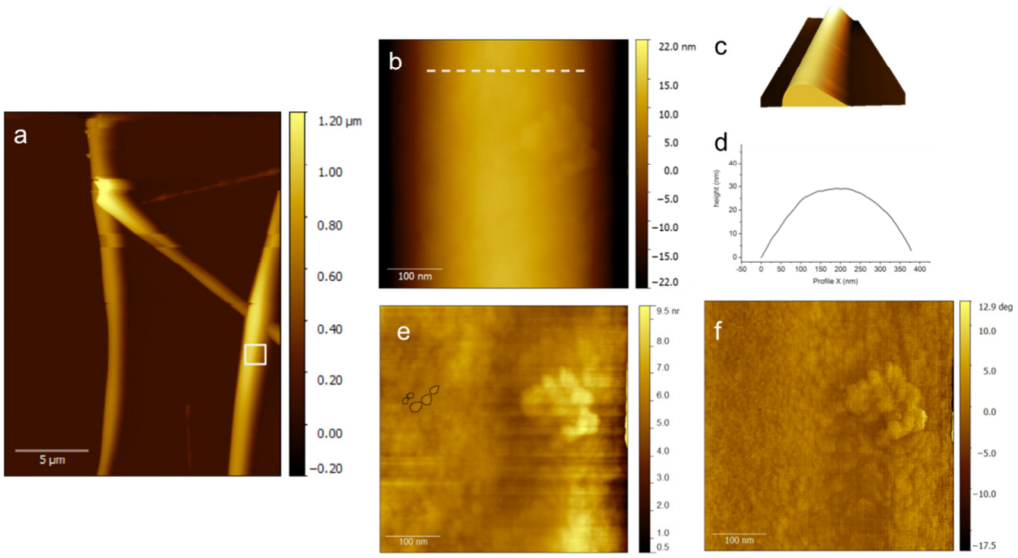

Figure 3.8. AFM micrographs of compound **3** nanofibers. a) topography image of compound **3** nanofibers on silicon substrate. b) zoom in of image a) as it is indicated in the marked area (white rectangle). c) 3D images of a part of compound **3** nanofiber. d) profile corresponding to white dashed line in b). e) filtered AFM topography image with polynomial background subtraction (2nd degree). The black marks indicate the grain boundaries on the nanofiber surface f) AFM phase image of compound **3** nanofiber

FT-IR and Raman were performed in solid state to look into the conformation of compounds **3**. The most informative frequency ranges for these molecules are 3500-3200 cm^{-1}, which corresponds to the N-H stretching vibrations of the amide and N-protecting urethane groups, and 1800-1600 cm^{-1}, which corresponds to the C=O "amide I" stretching vibrations of the amide, urethane and ester groups. [16] Figure 3.9a shows the overlapping of Raman (bottom) and IR spectra (top) of compounds **3**. N-H stretching vibrations for this molecule is calculated at around 3400 cm^{-1} and it is absent in Raman, where the "amide A" (NH stretch) vibrational signature is barely detectable as well as the "amide I" C=O stretching at around 1690 cm^{-1} which loses intensity in Raman but, however, it is still visible. On the other hand, the strong Raman signal at 1610 cm^{-1}, originating from in plane C-H bending vibrations on the fluorenyl, loses intensity in IR spectrum.

The chemical properties of the fibers have been analysed with FT-IR. IR spectra of powder and fibres (Fig 3.9b) show an overlap of the main peaks, this means they have the same chemical identity and chemical conformation and configuration, despite the application of high voltage and organic solvent. This result has been confirmed by mass spectrometry on

the fibers, since the mass (m/z) found is 666.25 $[M+Na]^+$ and 642.00 $[M-H]^-$ which correspond to the mass of monomeric form.

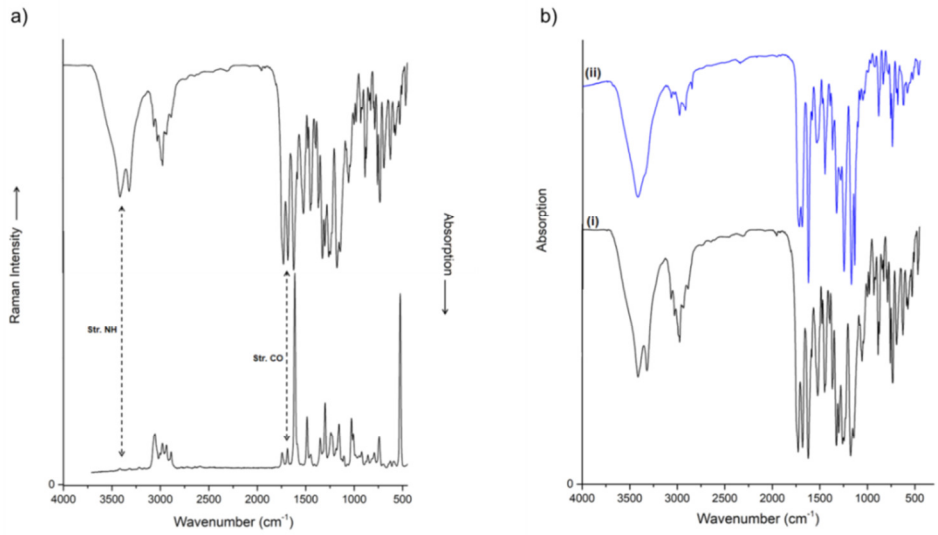

Figure 3.9. a) Raman (bottom) and IR spectra (top) compound **3**. b) IR overlapped spectra of powder (i) and fibers (ii) of compound **3**. Spectra are scaled and offset for clarity

The powerful aspect of FT-IR is that some of the most important correlations in the study of hydrogen bonding have been derived from a study of the stretching frequency of the X-H bond as observed in the mid-infrared (MIR). In particular, when the X-H group is no longer "free", its absorption is shifted to lower frequencies (red shift) and flatted to give a broad band. Since the frequency change of few wavenumbers is easily measured, IR spectroscopy is considered a sensitive method for detecting hydrogen bonds. [17]

Figure 3.10 show the enlargement of 4000-1000 IR region in order to highlight the changes in the peaks. In the case of compound **3**, the "amide A" N-H stretching band of the fibers is shifted to higher frequencies (from 3319 to 3346 cm^{-1}), while the "amide I" C=O stretching band doesn't change a lot (1682 cm^{-1} in powder and 1690 cm^{-1} in fiber). Moreover, the peak at 2940 cm^{-1}, attributed to some of the three CH groups, shows a big redshift (from 2940 to 2910 cm^{-1}). The redshift would mean that the bicyclic system interacts with neighbouring molecules more in the fiber than in the powder. Finally, the phenyl signal at 1075 cm^{-1} is clearly weaker in the fiber than in the powder so the aromatic rings should be oriented differently. From these results it seems that hydrogen bonds are not crucial for the fibers formation, but probably π-stacking of the aromatic

systems and other intermolecular interactions play the most important role in fiber-assembly.

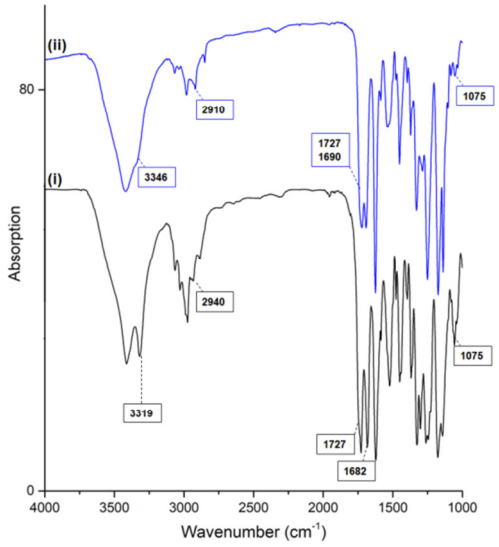

Figure 3.10. IR enlargement of 4000-1500 cm^{-1} region of powder (i) and fibers (ii) of compounds **3**. Spectra are scaled and offset for clarity

The cytotoxicity of compound **3** (powder and fibers) has also been tested on human colorectal adenocarcinoma cell line (Caco-2) at different concentrations (0, 12.5, 25, 50, 100, 200 μM), in order to open the possibility of nanofibers applications in life sciences. The cell viability has been determined by sulphorhodamine B (SRB) assay after 48 h of incubation with compounds, and the effects of the compounds vs control were analysed by two-tailed Student's t test for unpaired data. From these results it's clear that neither the powder nor fibers damage the cell vitality (Fig. 3.11).

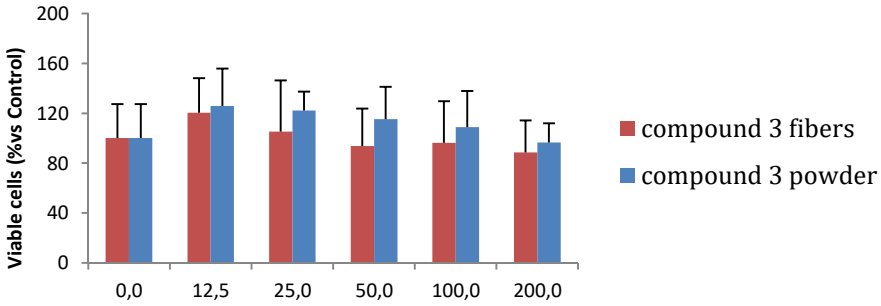

Figure 3.11. Cytotoxicity test of powder (blue) and fiber (red) of compound **3**

Electrospinning has been also performed on compounds **4'/4''** and **5'/5''**.

In case of compound **4**, containing Fmoc-Ala instead of Fmoc-Gly, diasteroisomer **4'** shows a strong decrease in the electrospinnability, while diasteroisomer **4''** is completely insoluble in HFIP. Fibers of compound **4'** appear long, but inhomogeneous and with a lot of beads (Fig. 3.12).

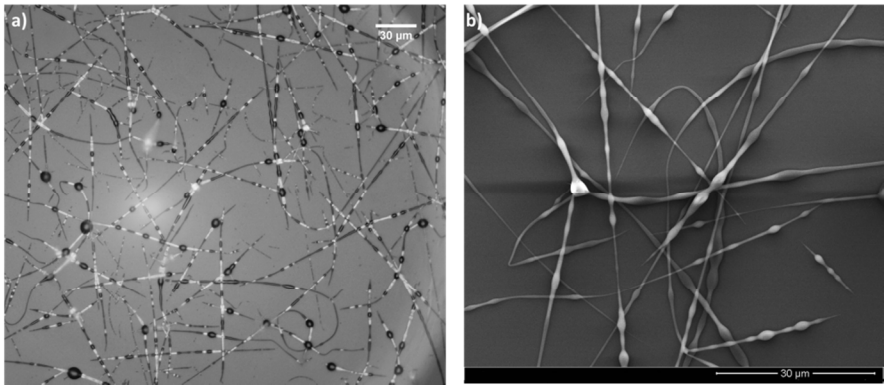

Figure 3.12. a) Optical and b) SEM micrographs of compound **4'**. SEM images were acquired in HV (10.00 KV)

Also the two diastereoisomers of compounds **5** show different behaviour: while both are well soluble in HFIP, the first one (**5'**) exhibits no electrospinnability, while the second one (**5''**) gives only short and discontinuous nanofibers, which, however, are quite homogenous with the same diameter of compound **3** (Fig. 3.13).

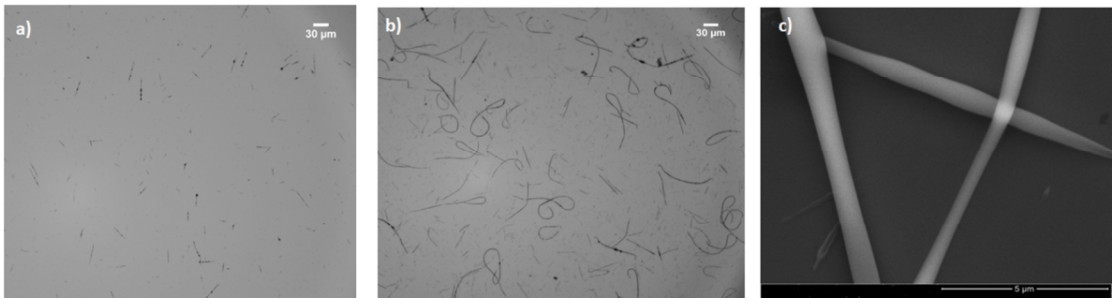

Figure 3.13. a) Optical micrographs of compound **5'**. b) Optical and c) SEM micrographs of compound **5''** nanofibers. SEM images were acquired in HV (10.00 KV)

In order to better understand the conformational differences between the diasteroisomers of the two couples which could influence their different electrospinnability, a complete

chemical characterizations of compounds has been performed, using NMR and spectroscopic techniques. With these results we would like to acquire more information about the forces that play important role in electrospinning process.

Chemical characterization

Compounds **4'** and **4''** and compounds **5'** and **5''** have been fully characterized by NMR 300 MHz (^{1}H, ^{13}H, HMBC, HSQC, NOESY) to study their secondary structures.
Unfortunately, the analysis was very tricky due to the overlapping of several important signals and, despite several attempts, we were unable to grow any suitable crystals for X-ray analysis, so it's not possible to assign the correct stereochemistry. However, some differences in the chemical shifts as well as on the NOE signals were observed for both couples of diasteroisomers. (Fig. 3.14)

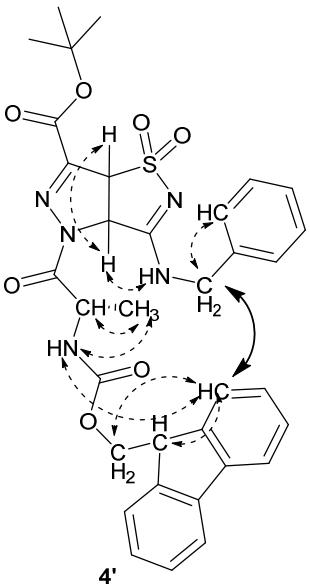

4'
Rf = 0.3 (AcOEt)

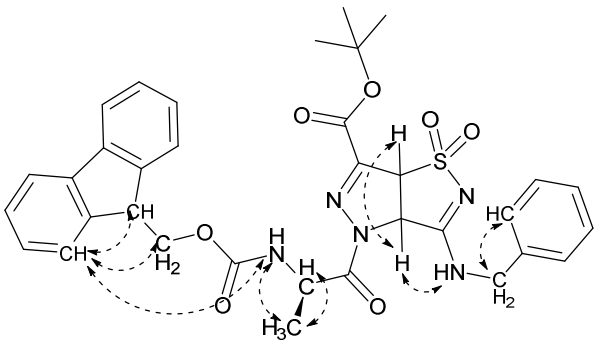

4''
Rf = 0.19 (AcOEt)

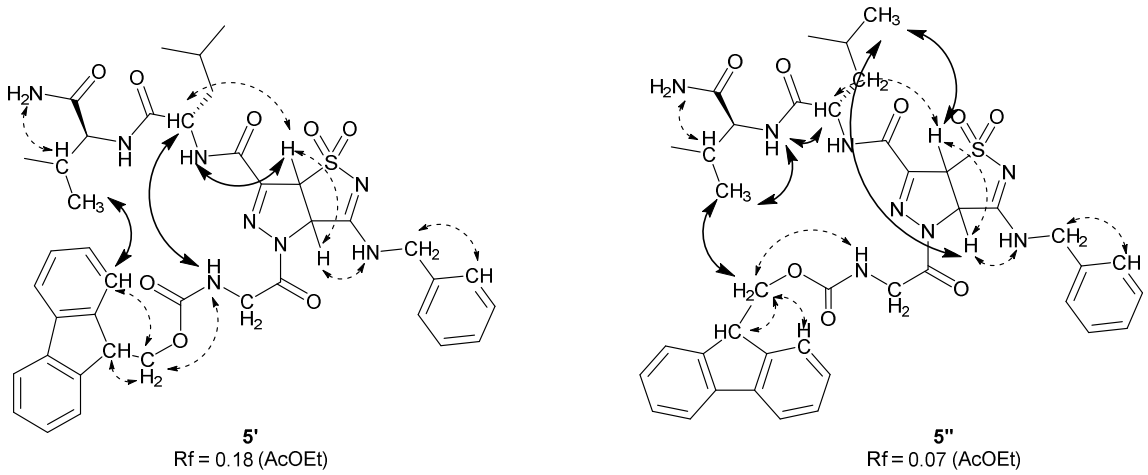

Figure 3.14. Significant Noesy (300 MHz, $CDCl_3$, 300 ms) for compounds **4'/4''** and **5'/5''**

As shown in the figure 3.14, in the case of compound **4'/4''**, the main difference between the two diastereoisomers is the NOE observed between methylene hydrogens of benzyl group and hydrogen of the aromatic moiety of Fmoc protecting group of **4'**, absent in **4''**. This finding allows to hypothesize a more extended conformation in solution for diasteroisomer **4''** than diasteroisomer **4'**, which seems to have instead stronger intramolecular interactions.

As far as concerned compounds **5'** and **5''**, spatial proximity between the two ends of the peptide chains can be observed and computational analysis proved that a "closed" end-to-end structure is thermodynamically stable in both molecules. The first diasteroisomer shows NOEs between the two peptidyl arms of the bicyclic system, in particular between the glycine amide group and leucine α-carbon, and aromatic moiety of Fmoc group and methyl group of valine side chain. On the other hand, in the second diasteroisomer NOEs are stronger between the side chain at C-terminus and the heterocyclic ring, in particular between methyl group of leucine side chain and H-3a and H-6a. This suggested a greater involvement of pyrazole-isothiazole system in intramolecular interactions in **5''** rather than **5'**.

The conformation of these compounds was also studied with Raman and FT-IR. As in the case of compound **3**, the Raman spectra don't show N-H stretching vibrations around 3400 cm^{-1}, while they have the strong Raman signal at 1610 (Fig. 3.15a,b).

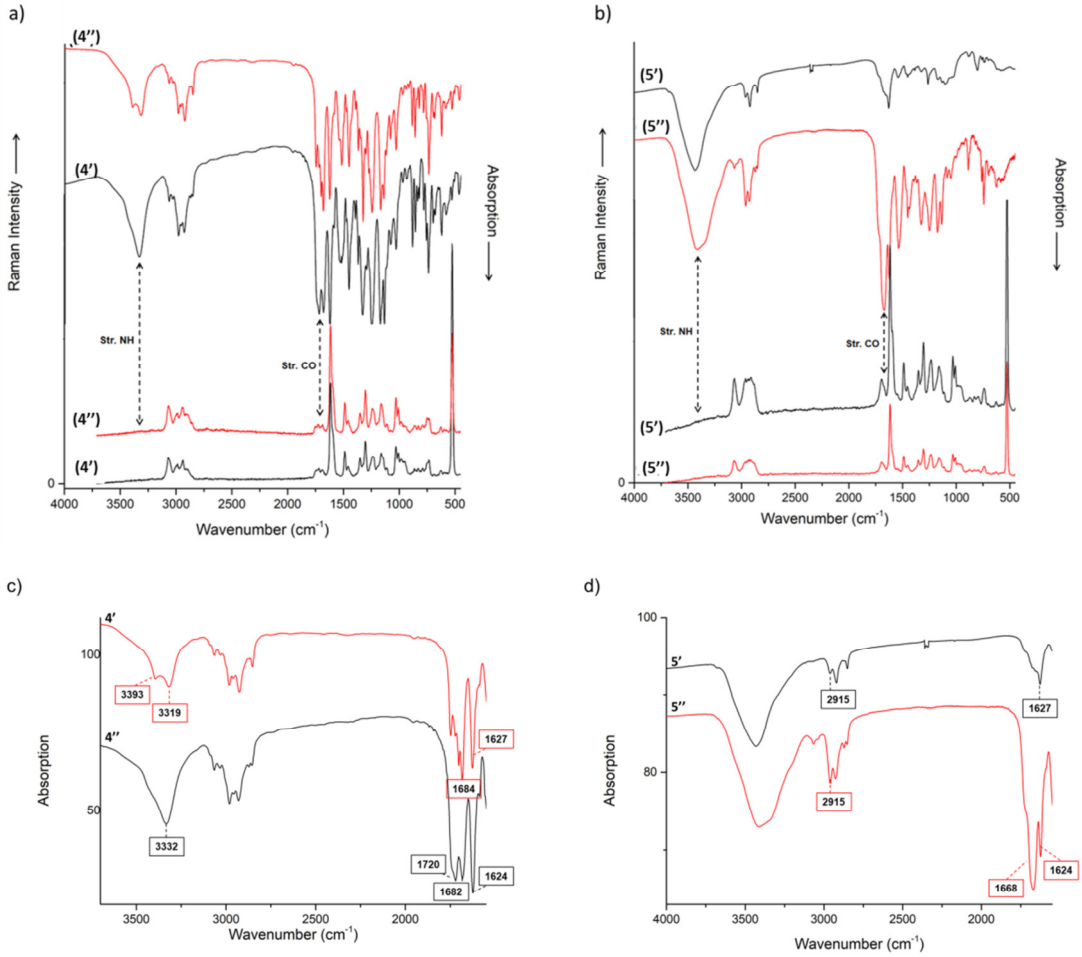

Figure 3.15. Raman (bottom) and IR spectra (top)of a) compounds **4'** (black)/**4''** (red) and b) compounds **5'** (black)/**5''** (red). c) IR enlargement of 4000-1500 cm^{-1} region of compounds **4'** (black)/**4''** (red). d) IR enlargement of 4000-1500 cm^{-1} region of compounds **5'** (black)/**5''** (red). Spectra are scaled and offset for clarity

The comparison between the IR spectra of the two diasteroisomers gives some interesting results. As far as concerned the diasteroisomers **4'/4''** (Fig. 3.15c), we didn't observe significant differences between the two diasteroisomers, despite their different configuration. In **4''** the N-H free (not H-bonded) stretching at 3393 cm^{-1} is narrower than in **4'** while the H-bonding N-H stretching band is redshifted in **4''** (from 3332 to 3319 cm^{-1}), so, considering also NMR data, it could be hypothesized that **4"** has stronger intramolecular H-bonds with NH. Moreover, the O-CO stretching band at 1720 cm^{-1} is less intensive in **4''** rather than **4'** highlighting a different orientation of the groups. As in the previous case, the presence of hydrogen bonds doesn't seem much crucial for the fibers formation.

In the case of diasteroisomers **5'/5''** (Fig. 3.15c), only IR spectra (not Raman) shown differences between the two diasteroisomers. These changes interest the intensity of the peaks, but not their shifts. This means, presumably, that the different configurations of **5'** and **5"** do not cause a very different intermolecular interaction (or crystal packing), but that some chemical groups are oriented in a different direction, such that vibrating dipoles (partially) cancel out. In detail, the C-H stretching band at 2950 cm^{-1} is much stronger in **5''** than in **5'**, suggesting a different orientation of some aliphatic groups. Moreover, the amide I stretching band at 1668 cm^{-1} is highly intensive in **5''**. The explanation could be finding in previously hypothesized "closed" end-to-end structure for both diasteoisomers, but probably in **5'** CH_2 and CONH groups point outwards. Unfortunately, the lack of crystal structures doesn't allow us to confirm the hypothesis.

Conclusion

In conclusion, two bicyclic systems obtained from isothiazole dioxide scaffold have been synthesized and conjugated with a single amino acid or inserted in a peptide chain. The obtained molecules have been used for electrospinning and it was found that compound **3** gives continuous and fairly homogenous fibers, without any beads, which are comparable with the fibres described in the literature and obtained from polymers. IR analysis shows that, probably, hydrogen bonds are less important than π-stacking interactions for the fiber formation, pointing out the key role of aromatic systems for electrospinning. The importance of intra and intermolecular interactions has been confirmed thanks to the NMR data collected from compounds **4'/4''** and **5'/5''**. These data demonstrate that diasteroisomers with lower propensity to give intermolecular interactions (**4''** and **5'**) loose completely the electrospinnability. With this work, electrospun nanofibers from a non-natural small molecule have been obtained, opening the possibility to use also such compounds in electrospinning techniques.

Experimental Section

Materials and methods

All reagents were purchased from Sigma-Aldrich, Iris Biotech or Fluka. All solvents were of ACS grade or higher and were obtained from Sigma-Aldrich. Reactions were monitored by thin-layer chromatography carried out on 0.25 mm Merck silica gel plates (60F-254) with UV light as the visualizing agent and ninhydrin as developing agents. Chromatographic separation was performed using Silicycle 60 Å SiO_2 (230-400 mesh). NMR spectra were recorded on Varian Gemini 300 or Bruker Avance 300 using appropriate deuterated solvents. Mass spectra were acquired on Fisons MD800 spectrometer and electrospray ion trap on a Finnigan LCQ ADVANTAGE Thermo-spectrometer. IR spectra were recorded in KBr pellet in ParkinElmer FTIR spectrometer. Melting points were measured on SMP3 apparatus, Stuart Scientific. $[\alpha]_D$ was measured on ParkinElmer model 343 plus polarimeter (Department of Pharmaceutical Sciences, University of Milan). Raman spectra were recorded on Alpha300, WITec confocal Raman spectra were recorded on Alpha300, WITec confocal Raman spectrometer in specular reflection. The sample was deposited on a clean silicon wafer and excited with a frequency-doubled Nd:YAG laser at 532 nm (ν1/c=18797 cm-1, green), focussed by a 100x objective with a 0.9 NA lens. Raman emission was collected through the same optics. A first analysis of the electrospun nanofibers was performed depositing directly the fibers on a glass substrate and acquiring images with optical microscopy with a magnification up to 1000X. Optical micrographs were acquired on BX50, Olympus equipped with a digital camera (D300, Nikon). SEM micrographs were acquired on QuantaTM 250FEG, FEI in high vacuum, after depositing the sample on clean silicon wafer. The beam current was limited by selecting a small aperture, thus limiting beam damage. The average fiber diameter was obtained by using Image-J software. AFM micrographs were acquired in air on AFM 5500 keysight in oscillating (AC) mode from samples deposited on clean silicon wafers. Silicon tips (with aluminum reflective back side, RTESPA from Bruker) were used with fundamental frequency of 175 kHz and a spring constant of 6 N/m. The scan speed was between 0.2-1.2 ln/s and the images have 512 x 512 points/lines. The data were processed with Gwyddion 2.3 Silicon wafers (1 x 1 cm2, Silicon Valley, SV) were cleaned by sonication with isopropanol, acetone and rinsed with Milli-Q water. Finally the substrates were treated with oxygen plasma (Diener electronics) for 8 minutes with an oxygen flow of 10 sccm and

98% of power and 0.1mbar. Then, the fibers were electrospinned directly on the cleaned silicon substrates. (CIC nanoGUNE, Donostia, Spain). For cytotoxicity tests, Eagle's minimum essential medium (MEM) was purchased from Sigma, while trypsin-EDTA, penicillin, streptomycin, sodium pyruvate, non-essential amino acid solution, fetal calf serum (FCS), plates and Petri dishes were purchased from EuroClone. The compounds were dissolved in dimethyl sulfoxide (DMSO) before performing each experiment. The concentrations utilized ranged from 200μM to 25μM. The same volume of solvent was added to control conditions and did not exceed 0.5% v/v. (University of Padua)

General Synthetic Procedures

Procedure 1: Coupling Reaction

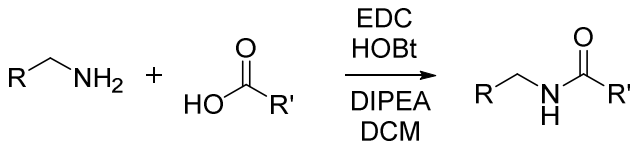

The carboxylic acid (1 eq) is dissolved in dichloromethane (10 ml/mmol) under nitrogen. The mixture is cooled at 0 °C before adding EDC (1.1 eq) and HOBt (1.1 eq) and is stirred for 1 hour. Then, the amide (1.1 eq) and DIPEA are added until pH=7-8. The mixture is allowed to react overnight at rt. The solvent is removed under reduced pressure. The residue is dissolved in DCM and the organic phase is washed with 5% w/v aqueous $KHSO_4$, saturated aqueous $NaHCO_3$, and brine. The organic layer is dried over Na_2SO_4, filtered, and concentrated under reduced pressure.

Procedure 2: Boc-Deprotection

Boc-protected compound is dissolved in dichloromethane (10 ml/mmol) and cooled to 0°C before adding trifluoroacetic acid (10 ml/mmol) dropwise. The mixture is stirred for 3 hours at rt, then the solvent is evaporated under reduced pressure and the residue is washed three times with ethyl ether. The deprotected product is used in the following step without further purification.

Procedure 3: tBu-Deprotection

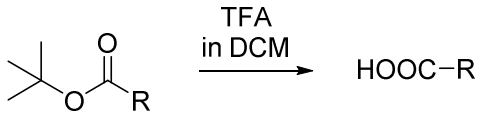

tBu-protected compound is dissolved in dichloromethane (10 ml/mmol) and cooled to 0°C before adding trifluoroacetic acid (10 ml/mmol) dropwise. The mixture is stirred overnight at rt, then the solvent is evaporated under reduced pressure and the residue is washed three times with ethyl ether. The deprotected product is used in the following step without further purification.

Procedure 4: Dithiopropionyl chloride synthesis

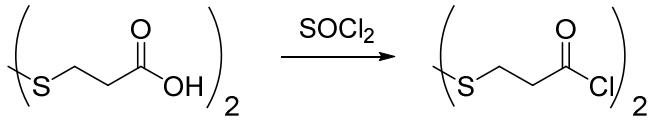

Dithiopropionic acid (10 g, 0.048 mol) is suspended in thionyl chloride (20 ml). The reaction mixture is refluxed until completely dissolution then is evaporated under reduced pressure and the product is used in the following step without further purification.

Procedure 5: N-benzyl-dithiopropionamide synthesis

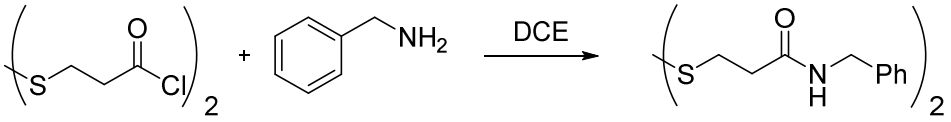

Benzylamine (21 ml, 0.19 mol) is dissolved in dichloroethane (70 ml) Then, dithiopropionic chloride (12 g, 0.048 mol) is slowly added keeping the temperature at 25°C. The resulting precipitate is filtered, washed with water and with 5% w/v aqueous citric acid and dried under reduced pressure.

Procedure 6: 2-Benzyl-isothiazol-3-one synthesis

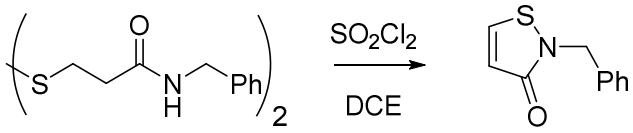

N-benzyl-dithiopropionamide (0.5 g, 1.28 mmol) is suspended in dichloethane (13 ml) and heated to 40°C then, a solution of sulfuryl chloride (0.518 g, 3.84 mmol) in dichloroethane (1 ml) is slowly dropped into the suspension. After 2 hours the reagent is usually completely dissolved giving a clear solution. The reaction is monitored by TLC (ethyl acetate/hexane 1:1) and is allowed to react at least 8 hours. The solvent is evaporated under reduced pressure and the residue is dissolved in ethyl acetate. The organic layer is washed twice with saturated aqueous $NaHCO_3$ then, the organic phase is dried over Na_2SO_4 , filtered and evaporated under reduced pressure. The residue is crystallized from ethyl acetate-hexane to afford the pure product.

Procedure 7: 3-Benzylamino isothiazole synthesis

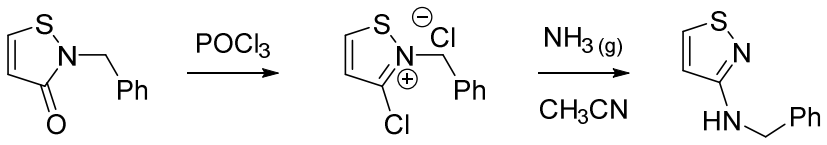

2-Benzyl-isothiazol-3-one (0.5 mg, 2 mmol) is suspended in phosphoryl chloride and stirred at rt for 16 hours. The reaction is monitored by TLC (ethyl acetate/hexane 1:1). Then, diisopropyl ether is added to the mixture and a red gum precipitates. The gum is decanted three times and is used in the following step without further purification.

The gum is suspended in acetonitrile (10 ml) and cooled to 0°C before bubbling gaseous NH_3 for about 15 minutes until the disappearance of the starting material (TLC: ethyl

acetate/hexane 3:2). The reaction mixture is filtered through celite® and evaporated under reduced pressure. The residue is dissolved in chloroform (50 ml) and washed twice with 1M aqueous NaOH and once with water. The organic phase is dried over Na_2SO_4 , filtered and evaporated under reduced pressure. The product is used in the following step without further purification.

Procedure 8: 3-Benzylamino isothiazole 1,1-dioxide synthesis

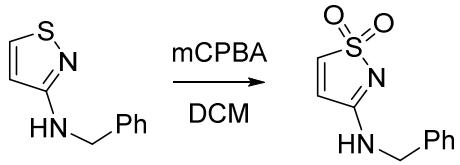

3-Benzylamino isothiazole (0.4 g, 2.1 mmol) is dissolved in dichloromethane (25 ml) and heated to 40°C. Then, metachloperbenzoic acid (0.8 mg, 4.62 mmol) is slowly added and the mixture is allowed to react overnight. The reaction is monitored by TLC (ethyl acetate/hexane 1:1) and then the solvent is evaporated under reduced pressure. The residue is dissolved in ethyl acetate (50 ml) and washed five times with a saturated aqueous $NaHCO_3$. The organic phase is dried over Na_2SO_4 , filtered and evaporated under reduced pressure. The crude product is purified by silica gel column chromatography (hexane/ethyl acetate, from 3:1 to 1:19).

Procedure 9: 3-Benzylamino-4-bromoisothiazole 1,1-dioxide synthesis

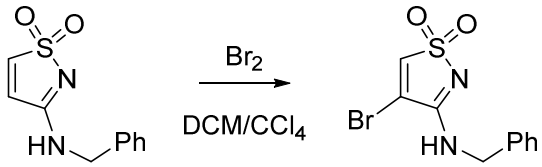

3-Benzylamino isothiazole 1,1-dioxide (0.1 g, 1.13 mmol) is dissolved in a mixture of dichloromethane (12.5 ml) and carbon tetrachloride (2.5 ml). A Br_2 solution (178 mg in 1.5 ml of CCl_4) is slowly added and the reaction is allowed to react 15 hours at rt (TLC: ethyl acetate/hexane 1:1). Then, TEA is added and the stirring continues for additional 15 hours. The reaction is quenched with 10% v/v aqueous HCl. The organic layer is washed twice with water and once with saturated aqueous $Na_2S_2O_5$ then, the organic phase is

dried over Na_2SO_4 , filtered and evaporated under reduced pressure. The residue is crystallized from dichloromethane-ether to afford the pure product.

Procedure 10: Cycloaddition reaction with 3-benzylamino isothiazole 1,1 dioxide

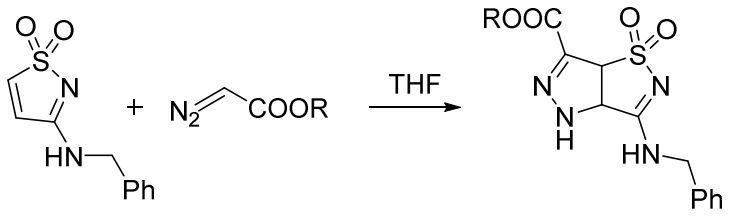

3-Benzylamino isothiazole 1,1 dioxide (1 eq) is dissolved in tetrahydrofuran (5 ml/mmol) and heated to 65°C. Then, the diazoacetate (1 eq) is added and the mixture is refluxed for 48-72 hours. The reaction is monitored by TLC (ethyl acetate/hexane 8:2) and if it is necessary, an excess of diazoacetate is added. The solvent is removed under reduced pressure and the residue is crystallized from methanol-ether to afford the pure product.

Procedure 11: Cycloaddition reaction with 3-benzylamino-4-bromoisothiazole 1,1 dioxide

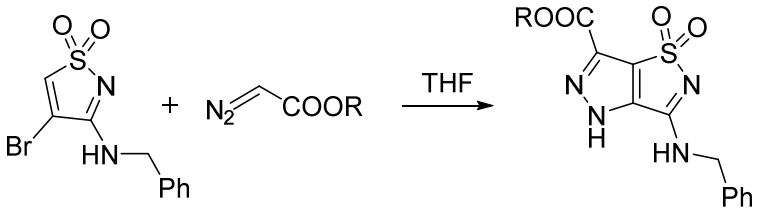

3-Benzylamino-4-bromoisothiazole 1,1 dioxide (1 eq) is dissolved in tetrahydrofuran (5 ml/mmol) and heated to 65°C. Then, the diazoacetate (1 eq) is added and the mixture is refluxed for 48-72 hours. The reaction is monitored by TLC (ethyl acetate/hexane 8:2) and if it is necessary, an excess of diazoacetate is added. The solvent is removed under reduced pressure and the residue is crystallized from methanol-ether to afford the pure product.

Specific Synthetic Procedures

Compound 1a

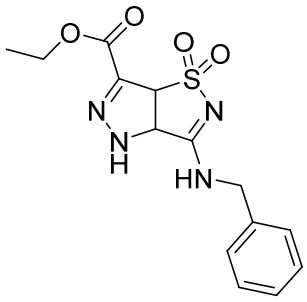

Compound **1a** was synthesized following general procedure **10** from ethyl diazoacetate (0.1 g, 0.9 mmol) and 3-benzylamino isothiazole 1,1 dioxide (0.2 g, 0.9 mmol) previously prepared according to general procedures **5**-**6**-**7**-**8**.

White solid, yield 63%. mp: 130°C dec. IR (KBr) 3334 (NH) cm^{-1}. ^{1}H NMR (300 MHz, $(CD_3)_2CO$) δ 1.30 (t, 3H, J=7.1 Hz, CH_3), 4.20-4.40 (m, 2H, CH_2), 4.58-4.60 (m, 2H, CH_2Ph), 5.01 (d, 1H; J=12 Hz, CH-6a), 5.85 (dd, 1H, J=12 Hz, CH-3a), 7.28-7.42 (m, 5H, arylH), 8.25 (bs, 1H, NH), 8.50 (bs, 1H, NH). ^{13}C NMR (300 MHz, $(CD_3)_2CO$) δ 12.85 (CH_3), 46.34 (CH_2Ph), 59.66 (CH_2), 66.54, 69.99 (CH-3a + CH-6a), 126.82, 127.13, 127.79 (ArCH), 134.57, 136.26 (C-6 + ArC), 163.32 (C-3), 200.00 (CO).

Compound 1b

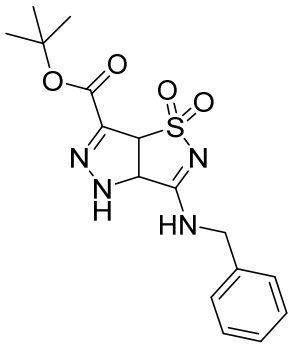

Compound **1b** was synthesized following general procedure **10** from 15% tert-butyl diazoacetate solution in toluene (0.86 ml, 0.9 mmol) and 3-benzylamino isothiazole 1,1 dioxide (0.2 g, 0.9 mmol) previously prepared according to general procedures **5**-**6**-**7**-**8**.

White solid, yield 80%. mp: 142-146°C. IR (KBr) 3355 (NH), 1687 (CO), 1615 cm^{-1}. ^{1}H NMR (300 MHz, $(CD_3)_2CO$) δ 1.53 (s, 9H, CH_3), 4.58 (d, 2H, J=5.5 Hz, CH_2), 5.00 (d, 1H, J=12 Hz, CH-6a), 5.80 (dd, 1H; J=12 Hz, CH-3a), 7.23-7.42 (m, 5H, ArylH), 8.23 (bs, 1H, NH), 8.37 (bs, 1H, NH). ^{13}C NMR (300 MHz, $(CD_3)_2CO$) δ 27.60 (CH_3), 47.35 (CH_2), 67.82, 70.90 (CH-3a + CH-6a), 81.22 (C) 127.85, 128.14, 128.82 (ArCH), 136.94, 137.31 (C-6 + ArC), 160.21 (C-3), 164.43 (CO). ESI-MS (m/z): 363.27 $[M-H]^-$

Compound 1c

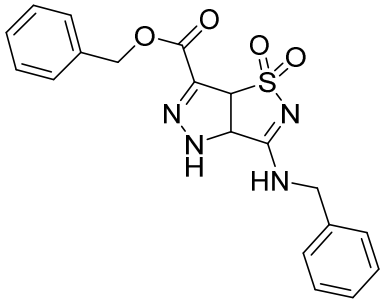

Compound **1c** was synthesized following general procedure **10** from 10% benzyl diazoacetate solution in toluene (0.883 ml, 0.45 mmol) and 3-benzylamino isothiazole 1,1 dioxide (0.1 g, 0.45 mmol) previously prepared according to general procedures **5**-**6**-**7**-**8**. White solid, yield 73%. ^{1}H NMR (300 MHz, $(CD_3)_2CO$) δ 4.68 (d, 2H, J=5.8 Hz, CH_2), 5.10 (d, 1H, J=12 Hz, CH-6a), 5.31 (s, 2H, CH_2Ph), 5.88 (d, 1H; J=12 Hz, CH-3a), 7.36-7.50 (m, 5H, ArylH), 8.31 (bs, 1H, NH), 8.63 (bs, 1H, NH).

Compound 2a

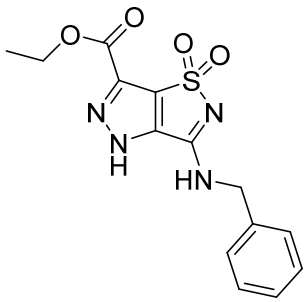

Compound **2a** was synthesized following general procedure **11** from ethyl diazoacetate (0.2 g, 1.6 mmol) and 3-benzylamino-4-bromoisothiazole 1,1 dioxide (0.5 g, 1.6 mmol) previously prepared according to general procedures **5-6-7-8-9**.

White solid, yield 88%. mp: 64-65°C. ^{1}H NMR (300 MHz, $(CD_3)_2CO$) δ 1.32 (t, 3H, J=7.1 Hz, CH_3), 4.23 (dd, 2H, CH_2), 4.37 (s, 2H, CH_2), 7.68 (s, 5H, arylH), 8.25 (bs, 1H, NH), 8.50 (bs, 1H, NH).

Compound 2b

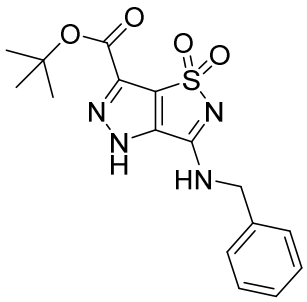

Compound **2b** was synthesized following general procedure **11** from 15% tert-butyl diazoacetate solution in toluene (0.35 ml, 0.3 mmol) and 3-benzylamino-4-bromoisothiazole 1,1 dioxide (0.1 g, 0.3 mmol) previously prepared according to general procedures **5-6-7-8-9**.

White solid, yield 72%. IR (KBr) 3296 (NH), 1733 (CO), 1628 cm^{-1}. ^{1}H NMR (300 MHz, $CDCl_3$) δ 1.62 (s, 9H, CH_3), 4.73 (s, 2H, CH_2), 6.77 (bs, 1H, NH), 7.39 (s, 5H, arylH). ^{13}C NMR (300 MHz, $CDCl_3$) δ. 27.96 (CH_3), 47.36 (CH_2), 128.39, 128.50, 129.05 (ArCH), 135.40, 135.62, 141.72, 143.72, 153.74, 156.21 (C). ESI-MS (m/z): 361.11 $[M-H]^-$

Compound 2c

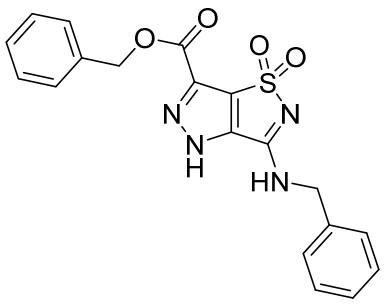

Compound **2c** was synthesized following general procedure **11** from 10% benzyl diazoacetate solution in toluene (1.44 ml, 0.7 mmol) and 3-benzylamino-4-bromoisothiazole 1,1 dioxide (0.2 g, 0.7 mmol) previously prepared according to general procedures **5-6-7-8-9**.

White solid, yield 75%. mp: 108-109°C. IR (KBr) 3370 (NH), 1738 (CO), 1624 cm^{-1}. ^{1}H NMR (300 MHz, $CDCl_3$) δ 4.65 (d, 2H, J=5.5, CH_2Ph), 5.30 (s, 2H, CH_2), 6.93 (bs, 1H, NH), 7.29-7.40 (m, 10H, arylH). ^{13}C NMR (300 MHz, $CDCl_3$) δ 47.62 (CH_2Ph), 68.77 (CH_2), 128.41-129.26 (ArCH), 134.20, 135.43, 151.67, 153.76, 157.13 (C). ESI-MS (m/z): 419.29 $[M+Na]^+$

Compound 3

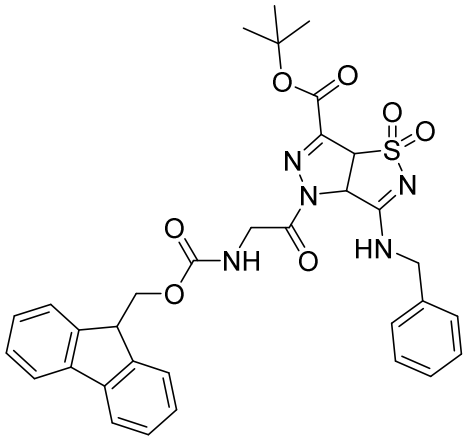

Compound **3** was synthesized by coupling (general procedure **1**) compound **1b** (0.13 g, 0.36 mmol) and Fmoc-Gly-OH (0.1 g, 0.33 mmol). The reaction is monitored by TLC (ethhyl acetate/hexane 2:1) and the pure product is afforded by crystallization from methanol-ether.

White solid, yield 84%. mp: 164-169°C. IR (KBr) 3412, 3319 (NH), 1727, 1683, 1622 (CO) cm^{-1}. ^{1}H NMR (300 MHz, $CDCl_3$) δ 1.61 (s, 9H, CH_3), 4.22 (t, 1H, J=6.7 Hz, CH), 4.34-4.66 (m, 6H, CH_2Ph + $CH_{2(G)}$ + CH_2), 5.15 (d, 1H; J=10.9 Hz, CH-6a), 5.26 (m, 1H, NH), 5.88 (d, 1H, J=10.9, CH-3a), 7.23-7.43 (m, 9H, ArylH), 7.57-7.66 (m, 3H, ArylH + NH), 7.76 (d, 2H, J=7.5 Hz, ArylH). ^{13}C NMR (300 MHz, $CDCl_3$) δ 27.88 (CH_3), 43.77 (CH_2), 47.08 (CH), 48.29 (CH_2Ph), 66.92, 67.07 (CH-3a + CH-6a), 67.30 ($CH_{2(G)}$), 85.39 (C), 120.04, 125.05, 127.10, 127.78, 127.92, 128.33, 129.04 (ArCH), 135.32, 141.30, 143.70 (ArC), 145.67 (C-6), 156.42 (COO), 157.67 (COO), 160.43 (C-3), 171.13 (CO). ESI-MS (m/z): 642.86 $[M-H]^-$, 666.13 $[M+Na]^+$

Compound 4’ and 4’’

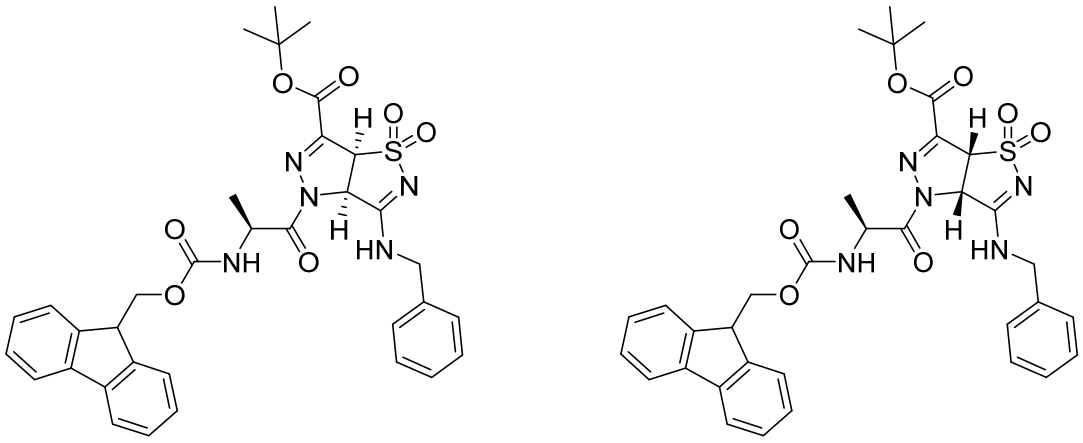

Compounds **4**’ and **4**’’ were synthesized by coupling (general procedure **1**) compound **1b** (0.1 g, 0.35 mmol) and Fmoc-L-Ala-OH (0.1 g, 0.32 mmol). The reaction is monitored by TLC (ethyl acetate/hexane 2:1) and the two diasteroisomers were separated by silica gel column chromatography (hexane/ethyl acetate 2:1).

Compound 4’: White solid, yield 44%. mp: 112°C. $[\alpha]_D$ = -60 (CH_3OH) IR (KBr) 3332 (NH), 1720, 1682, 1624 (CO) cm^{-1}. ^1H NMR (300 MHz, $CDCl_3$) δ 1.42 (d, 3H, J=6.3 Hz, CH_3), 1.63 (s, 9H, CH_3), 4.21 (t, 1H, J=6.3 Hz, CH), 4.39 (d, 2H; J=6.2 Hz, CH_2), 4.56-4.61 (m, 2H, CH_2Ph), 5.07 (t, 1H, J=6.6, CH_α), 5.17 (d, 1H, J=9.0, CH-6a), 5.30 (d, 1H, J=6.9, NH), 5.95 (d, 1H, J=8.9 Hz, CH-3a), 7.24-7.43 (m, 9H, ArylH), 7.58 (m, 2H, ArylH), 7.72 (s, 1H, NH), 7.77 (d, 2H, J=7.5, ArylH). ^{13}C NMR (300 MHz, $CDCl_3$) δ 17.91 (CH_3) 27.87 (CH_3), 47.08 (CH), 48.11 (CH_2Ph), 48.96 (CH_α), 66.90 (CH-3a + CH-6a), 67.22 (CH_2), 85.29 (C), 120.01, 124.99, 127.09, 127.71, 127.77, 128.33, 128.62, 129.03 (ArCH), 135.57, 141.30, 143.70 (ArC), 145.86 (C-6), 155.81 (COO), 157.54 (COO), 160.73 (C-3), 175.12 (CO). ESI-MS (m/z): 680.32 $[M+Na]^+$

Compound 4’’: White solid, yield 37%. mp: 191°C. $[\alpha]_D$ = +62 (CH_3OH) IR (KBr) 3393, 3319 (NH), 1747, 1720-1684, 1627 (CO) cm^{-1}. ^1H NMR (300 MHz, $CDCl_3$) δ 1.42 (d, 3H, J=6.3 Hz, CH_3), 1.63 (s, 9H, CH_3), 4.21 (m, 1H, CH), 4.40 (m, 2H; CH_2), 4.55 (m, 2H, CH_2Ph), 5.12 (m, 1H, CH_α), 5.20 (d, 1H, J=11, CH-6a), 5.31 (m, 1H, NH), 5.92 (d, 1H, J=11 Hz, CH-3a), 7.25-7.46 (m, 9H, ArylH), 7.60 (m, 2H, ArylH), 7.71 (bs, 1H, NH), 7.80 (d, 2H, J=7.4, ArylH). ^{13}C NMR (300 MHz, $CDCl_3$) δ 17.84 (CH_3), 27.89 (CH_3), 47.11 (CH), 48.30 (CH_2Ph), 49.49 (CH_α), 66.73, 66.81 (CH-3a + CH-6a), 67.14 (CH_2), 85.40 (C), 120.03, 124.98, 127.08,

127.75, 128.21, 128.94 (ArCH), 135.22, 141.32, 143.73 (ArC), 145.53 (C-6), 155.35 (COO), 157.52 (COO), 160.50 (C-3), 174.66 (CO). ESI-MS (m/z): 6565.45 $[M-H]^-$, 680.52 $[M+Na]^+$

Intermediate 6

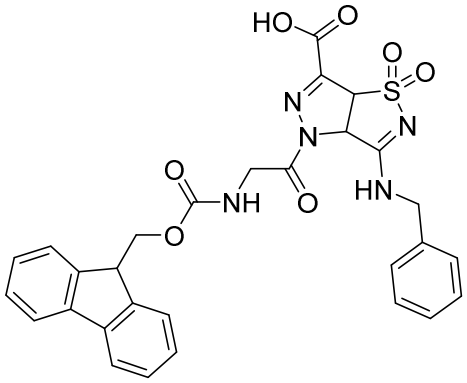

Compound **3** (0.2 g, 0.35 mmol) was tBu-deprotected according to general procedure **3**. White solid, yield >98%. mp: 208°C dec. IR (KBr) 3357, 3305 (NH), 1721, 1683, 1625 (CO) cm^{-1}. ^1H NMR (300 MHz, DMSO-d_6) δ 3.32 (bs, 1H, OH), 4.13 (d, 1H, J=6.1 Hz, CH), 4.20-4.32 (m, 6H, CH_2Ph + $CH_{2(G)}$), 4.46 (m, 2H, CH_2), 5.23 (d, 1H; J=10.6 Hz, CH-6a), 6.12 (d, 1H, J=10.6, CH-3a), 7.17-7.43 (m, 9H, ArylH), 7.70 (d, 2H, J=7.5 Hz, ArylH), 7.80 (m, 1H, NH), 7.88 (d, 2H, J=7.5 Hz, ArylH), 8.35 (t, 1H, J=6.0 Hz, NH). ^{13}C NMR (300 MHz, DMSO-d_6) δ 43.38 (CH_2), 45.97 (CH), 47.21 (CH_2Ph), 66.31 ($CH_{2(G)}$), 67.91 (CH-6a), 68.90 (CH-3a), 120.56, 125.66, 127.52, 127.60, 128.08, 128.88 (ArCH), 137.32, 141.17 (ArC), 144.25 (C-6), 156.86 (COO), 161.30 (COO), 161.85 (C-3), 171.22 (CO). ESI-MS (m/z): 542.35 $[M-COOH]^-$.

Intermediate 7

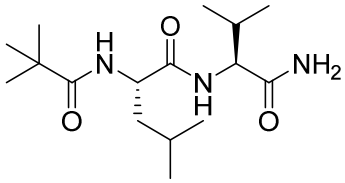

Intermediate **6** was synthesized by coupling (general procedure **1**) Boc-L-Leu-OH (0.5 g, 4.25 mmol) and L-Val-NH_2 (0.45 g, 3.86 mmol). The reaction is monitored by TLC (ethyl

acetate/hexane 2:1) and the pure product is afforded by crystallization from methanol-ether.

White solid. ^{1}H NMR (300 MHz, $CDCl_3$) δ 0.81-1.08 (m, 12H, $CH_{3\ (L,V)}$), 1.46 (s, 9H, CH_3), 1.83-1.58 (m, 3H, CH_2 + $CH_{(L)}$), 2.30 (m, 1H, $CH_{(V)}$), 4.07 (m, 1H, $CH_{\alpha(L)}$), 4.30 (m, 1H, $CH_{\alpha(V)}$), 4.89 (d, 1H, J=5.8 Hz, NH), 5.45 (bs, 1H, NH), 6.32 (bs, 1H, NH), 6.64 (d, 1H, J=8.3, NH).

Compound 5′ and 5″

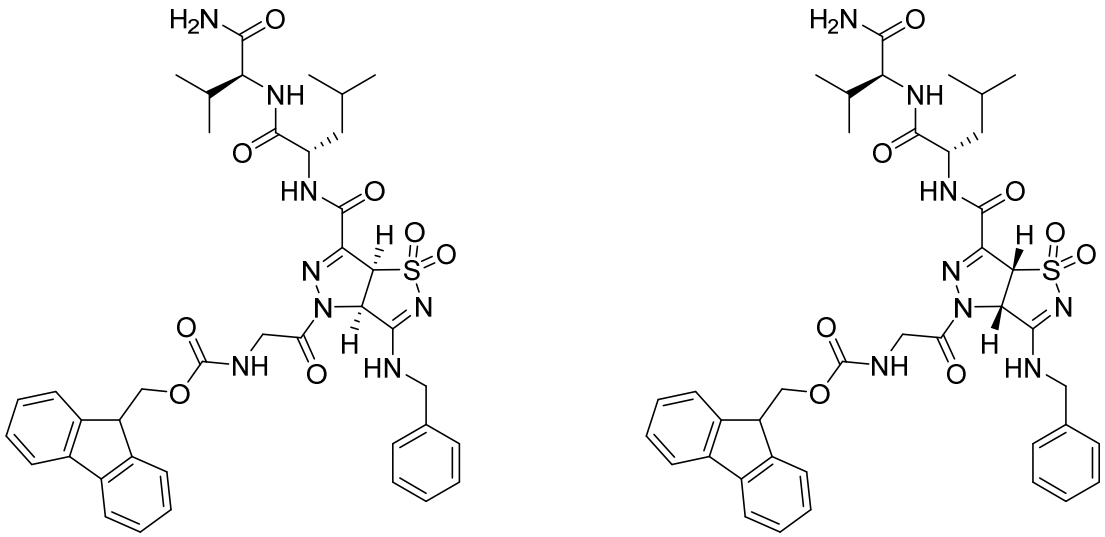

Compounds **5′** and **5″** was synthesized by coupling (general procedure **1**) intermediate **6** (0.18 g, 0.3 mmol) and intermediate **7** previously deprotected according to general procedure **2** (0.1 g, 0.33 mmol). The reaction is monitored by TLC (ethyl acetate/hexane 2:1) and the two diasteroisomers were separated by silica gel column chromatography (from hexane/ethyl acetate 2:1 to ethyl acetate).

Compound 5′: White solid, yield 16%. R_f = 0.18 (AcOEt). $[\alpha]_D$ = -4.8 (CH_3OH) IR (KBr) 3430 (NH), 1627 (CO) cm^{-1}. ^{1}H NMR (300 MHz, $CDCl_3$) δ 0.94 (m, 12H, CH_3), 1.73-1.74 (m, 3H, $CH_{(L)}$ + CH_2), 2.21 (m, 1H, $CH_{(V)}$), 4.25 (m, 2H; CH + $CH_{\alpha(V)}$), 4.40 (m, 4H, $CH_{2(G)}$ + CH_2), 4.49 (m, 1H, $CH_{\alpha(L)}$), 4.47-4.57 (m, 2H, CH_2Ph), 5.44 (d, 1H, J=10.6, CH-6a), 5.91 (m, 1H, NH), 6.0 (m, 2H, CH-3a + NH), 6.48 (s, 1H, NH), 7.00 (m, 1H, $NH_{(V)}$), 7.25-7.29 (m, 7H, ArylH), 7.40 (m, 2H, ArylH), 7.52 (m, 1H, $NH_{(L)}$), 7.62 (d, 2H, J=7.2 Hz, ArylH), 7.77 (d, 2H, J=7.2 Hz, ArylH), 7.84 (m, 1H, NH). ^{13}C NMR (300 MHz, $CDCl_3$) δ 18.18, 19.32, 21.91. 22.84 (CH_3), 24.99 ($CH_{(L)}$), 29.92 ($CH_{(V)}$), 40.83 ($CH_{2(L)}$), 43.49 (CH_2), 47.06 ($CH_{(V)}$), 48.19 (CH_2Ph), 53.60 ($CH_{\alpha(L)}$), 58.96 ($CH_{\alpha(V)}$), 66.69 (CH-6a), 67.36 ($CH_{2(G)}$), 67.41 (CH-3a), 120.00, 125.14 127.11, 127.79, 128.16, 128.94 (ArCH), 135.36, 141.28, 143.70-143-77 (ArC), 146.37 (C-

6), 156.79 (COO), 159.66 (CONH), 161.20 (C-3), 170.99 (CO), 171,52 ($CONH_2$), 173.84 (CONH). ESI-MS (m/z): 797.55 $[M-H]^-$, 821.87 $[M+Na]^+$

Compound 5″: White solid, yield 16%. R_f = 0.07 (AcOEt). $[\alpha]_D$ = -4.8 (CH_3OH) IR (KBr) 3412 (NH), 1668, 1624.37 (CO) cm^{-1}. ^1H NMR (300 MHz, $CDCl_3$) δ 0.93 (s, 12H, CH_3), 1.72 (m, 3H, $CH_{(L)}$ + CH_2), 2.11 (m, 1H, $CH_{(V)}$), 4.22-4.23 (m, 2H; CH + $CH_{\alpha(V)}$), 4.39 (m, 2H, CH_2), 4.42-4.57 (m, 4H, $CH_{2(G)}$ + CH_2Ph), 4.65 (m, 1H, $CH_{\alpha(L)}$), 5.45 (d, 1H, J=10.2, CH-6a), 5.73 (m, 1H, NH), 5.96 (d, 1H, J=10.2 Hz, CH-3a), 6.27 (s, 1H, NH), 6.62 (s, 1H, NH), 7.26-7.30 (m, 7H, ArylH), 7.40 (m, 2H, ArylH), 7.60 (m, 4H, $NH_{(L)}$ + $NH_{(v)}$ + ArylH), 7.75 (m, 3H, ArylH + NH). ^{13}C NMR (300 MHz, $CDCl_3$) δ 18.41, 19.30, 21.84. 22.85 (CH_3), 24.81 ($CH_{(L)}$), 30.49 ($CH_{(V)}$), 40.88 ($CH_{2(L)}$), 43.46 (CH_2), 47.04 ($CH_{(V)}$), 48.16 (CH_2Ph), 53.22 ($CH_{\alpha(L)}$), 58.97 ($CH_{\alpha(V)}$), 66.77 (CH-6a), 67.37 ($CH_{2(G)}$), 67.49 (CH-3a), 120.01, 125.13, 127.12, 127.79, 128.16, 128.95 (ArCH), 135.37, 141.28, 143.73-143.77 (ArC), 146.62 (C-6), 156.66 (COO), 159.17 (CONH), 161.04 (C-3), 170.99 (CO), 172,28 ($CONH_2$), 174.07 (CONH). ESI-MS (m/z): 797.25 $[M-H]^-$, 821.65 $[M+Na]^+$

Compound 8

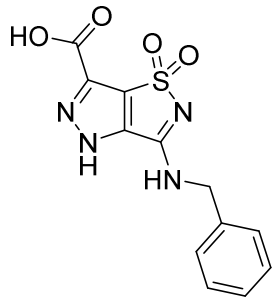

Compound **2b** (0.47 g, 0.13 mmol) was tBu-deprotected according to general procedure **3**. White solid, yield 73%. IR (KBr) 3340, 3308 (NH) 1707, 1629 (CO) cm^{-1}. ^1H NMR (300 MHz, CD_3CN) δ 4.66 (d, 2H, J=6.2, CH_2Ph), 7.39-7.42 (m, 5H, ArylH), 7.95 (bs, 1H, NH), 9.45 (bs, 1H, OH). ^{13}C NMR (300 MHz, CD_3CN) δ 45.38 (CH_2Ph), 127.45-128.64 (ArCH), 128.71, 129.20, 136.72, 151.47, 154.30, 156.84 (C). ESI-MS (m/z): 304.90 $[M-H]^-$, 261.17 $[M-COOH]^-$

Cytotoxicity tests

Cell culture

Human colorectal adenocarcinoma cell line (Caco-2) was cultured in MEM supplemented with 10% FCS, L-glutamine, sodium-pyruvate and non-essential amino acids, penicillin/streptomycin at 37°C in a humidified atmosphere of 5% CO2 and 95% air and passed every three days to maintain it in subconfluent conditions.

Cell viability assay

Cell viability was determined by sulphorhodamine B (SRB) assay.[18] Cells were seeded in a 96-well tray (8 x 103 cells/well) in octuple replicas and after 24h treated with compounds at aforementioned concentrations. SRB assay was then performed after 48h incubation.

Statistical analysis

Experimental data are expressed as mean ± S.D. The effects of the compounds vs control were analysed by two-tailed Student's t test for unpaired data. The concentration of compounds required to reduce cell viability by 50% (IC50) was calculated by nonlinear regression curve (GraphPad Prism, Version 5.01).

References

[1] a) S. Chattopadhyay, T. A. Hatton, G. C. Rutledge, *Journal of Materials Science* **2016**, *51*, 204-217; b) C. Liu, P.-C. Hsu, H.-W. Lee, M. Ye, G. Zheng, N. Liu, W. Li, Y. Cui, *Nature Communications* **2015**, *6*, 6205.

[2] X. M. Mo, C. Y. Xu, M. Kotaki, S. Ramakrishna, *Biomaterials* **2004**, *25*, 1883-1890.

[3] a) X. Wang, C. Drew, S.-H. Lee, K. J. Senecal, J. Kumar, L. A. Samuelson, *Nano Letters* **2002**, *2*, 1273-1275; b) B. Ding, M. Wang, X. Wang, J. Yu, G. Sun, *Materials Today (Oxford, United Kingdom)* **2010**, *13*, 16-27.

[4] a) T. T. Yuan, P. M. Jenkins, A. M. D. G. Foushee, A. R. Jockheck-Clark, J. M. Stahl, *Journal of Nanomaterials* **2016**, 6231040/6231041-6231040/6231010; b) D. Semnani, N. Poursharifi, N. Banitaba, A. Fakhrali, *Bull. Mater. Sci.* **2018**, *41*, 1-7.

[5] a) Q. P. Pham, U. Sharma, A. G. Mikos, *Tissue Engineering* **2006**, *12*, 1197-1211; b) W. Liu, S. Thomopoulos, Y. Xia, *Advanced Healthcare Materials* **2012**, *1*, 10-25.

[6] J. M. Cornejo Bravo, L. J. Villarreal Gómez, A. Serrano Medina, *Electrospinning - Material, Techniques, and Biomedical Applications* **2016**, *7*, 142-155.

[7] Z. Li, C. Wang, *Effects of Working Parameters on Electrospinning*, Springer, Berlin, Heidelberg, **2013**.

[8] S. L. Shenoy, W. D. Bates, H. L. Frisch, G. E. Wnek, *Polymer* **2005**, *46*, 3372-3384.

[9] M. G. McKee, J. M. Layman, M. P. Cashion, T. E. Long, *Science (Washington, DC, United States)* **2006**, *311*, 353-355.

[10] A. Ansari, A. Ali, M. Asif, Shamsuzzaman, *New Journal of Chemistry* **2017**, *41*, 16-41.

[11] F. Clerici, M. L. Gelmi, S. Pellegrino, *Isothiazoles, Vol. 4.05*, Elsevier Ltd, **2008**.

[12] a) F. Clerici, M. L. Gelmi, R. Soave, L. Lo Presti, *Tetrahedron* **2002**, *58*, 5173-5178; b) F. Clerici, M. L. Gelmi, E. Pini, M. Valle, *Tetrahedron* **2001**, *57*, 5455-5459.

[13] F. Clerici, A. Contini, M. L. Gelmi, D. Pocar, *Tetrahedron* **2003**, *59*, 9399–9408.

[14] a) F. Clerici, T. Ferrario, M. L. Gelmi, R. Marelli, *Chem. Soc. Perkin Trans* **1994**, *1*; b) F. Clerici, M. L. Gelmi, C. Monzani, D. Pocar, A. Sala, *Het. Chem* **2006**, *43*; c) P. Baggi, F. Clerici, M. L. Gelmi, S. Mottadelli, *Tetrahedron* **1995**; d) F. Clerici, F. Ferraris, M. L. Gelmi, *Tetrahedron* **1995**; e) F. Clerici, F. Galletti, D. Pocar, P. Roversi, *Tetrahedron* **1996**; f) F. Clerici, M. L. Gelmi, R. Soave, M. Valle, *Tetrahedron* **1998**.

[15] a) G. Singh, A. M. Bittner, S. Loscher, N. Malinowski, K. Kern, *Advanced Materials (Weinheim, Germany)* **2008**, *20*, 2332-2336; b) W. Nuansing, A. Rebollo, J. M. Mercero, J. Zuniga, A. M. Bittner, *Journal of Raman Spectroscopy* **2012**, *43*, 1397-1406.

[16] V. Moretto, M. Crisma, G. M. Bonora, C. Toniolo, H. Balaram, P. Balaram, *Macromolecules* **1989**, *22*, 2939-2944.

[17] M. Gorman, *J. Chem. Educ.* **1957**, *34*, 304-306.

[18] a) Y. P. Keepers, P. E. Pizao, G. J. Peters, J. Van Ark-Otte, B. Winograd, H. M. Pinedo, *European Journal of Cancer* **1991**, *27*, 897-900; b) P. Skehan, R. Storeng, D. Scudiero, A. Monks, J. McMahon, D. Vistica, J. T. Warren, H. Bokesch, S. Kenney, M. R. Boyd, *Journal of the National Cancer Institute* **1990**, *82*, 1107-1112.